6-1-2009

# Strength of Transverse Fillet Welds at Elevated and Post-Elevated Temperatures

Kathryn Conlon

James Ricles

Stephen Pessiki

# Strength of Transverse Fillet Welds at Elevated and Post-Elevated Temperatures

**by**

**Kathryn Conlon**

**James Ricles**

**Stephen Pessiki**

# Strength of Transverse Fillet Welds at Elevated and Post-Elevated Temperatures

by

**Kathryn Conlon**
**Research Associate**

**James Ricles**
**Professor of Structural Engineering**

**Stephen Pessiki**
**Professor of Structural Engineering**

# Acknowledgments

# Table of Contents

**Contents**                                                                                          **Page**

# List of Tables

# List of Figures

ix

# Abstract

Fire research has become a topic of interest over the past couple of years, specifically after the collapse of WTC 7, which was caused by exposure to fire. Research has been conducted on isolated materials, such as steel or bolts, and on whole structural systems at elevated temperatures. When steel is subjected to fire and post-fire conditions, it experiences a reduction in strength and stiffness due to the effect of elevated temperature. This behavior can compromise the integrity of the structure.

Welds are widely used in the construction of steel buildings. They are an integral part of connections. The material properties of welds at elevated temperatures are unknown. This research investigates the performance of weld metal at elevated temperatures, to evaluate how welds may perform during a fire and under post-fire conditions. This thesis focuses on the effects of elevated temperatures on weld metal subjected to shear stress.

In this thesis, fillet welds are loaded transversely under elevated temperature and cooling conditions. Design recommendations are then made for fillet welds under elevated temperature and cooling conditions. These recommendations are then compared to design procedures in the current edition of the AISC Specification and Eurocode and results found in past research. It was found that the weld metal behaves similarly to base metal, such as steel, when exposed to elevated temperatures and cooling conditions.

# Chapter 1     Introduction

## 1.1     General

This thesis presents research conducted on the performance of fillet welded lap plates subjected to tensile load at elevated temperatures in both fire and post-fire conditions, where the fillet welds are subjected to shear. This chapter discusses the motivation for this research as well as outlines the research objectives and overall scope of the thesis.

## 1.2     Motivation for Research

The behavior of materials at elevated temperatures, both during and after a fire, is a topic that has not been extensively studied. Past research, which will be discussed in Chapter 2, has shown that the properties and behavior of some widely used materials, such as steel, changes drastically at elevated temperatures. The behavior of the components and load path of a structural system also change at elevated temperatures. Forces develop in a system due to heating and cooling, which are important to understand and will be discussed further in Chapter 2.

The structural integrity of a steel frame is determined by the strength of its connections. Past research performed by Yu (2006) has shown that bolts lose strength at elevated temperatures, diminishing the strength of a connection. Due to the fact that connections can be made up of bolts or welds and either plates or angles, it is important to understand the effect of elevated temperature on the behavior of these components to fully understand the behavior of the connection.

Although welds are commonly used in connections, very little is known about their properties at elevated temperatures and post-elevated temperatures upon cooling. This provided the motivation to study the behavior of welds in fire conditions, both under fire and post-fire conditions.

Another motivation for this research is the knowledge that alternate load paths develop during exposure to elevated temperatures and during post-fire conditions. A schematic of a shear tab connection subjected to gravity loading is shown in Figure 1.1. Three cases are shown in Figure 1.1. Case (a) shows the forces the shear tab is subjected to at ambient temperature. Ambient temperature is defined as T=72°F. In this scenario, the shear force, V, acts parallel to the fillet weld on the shear tab connection. Case (b) shows the shear tab connection during a fire; therefore it is subjected to elevated temperatures. In this scenario the weld is still subjected to a shear force; however it is now also subjected to a compressive axial force as well due to the thermal expansion of the beam. Case (c) shows the shear tab connection during post-fire conditions. In this scenario the weld is subjected to a shear force and a tensile axial force due to thermal constriction, causing the beam bow up during cooling.

When the connection is not subjected to elevated temperatures or post-fire conditions, the weld behaves purely as a longitudinal weld, meaning that the load is acting parallel to the

weld. Once the connection is subjected to elevated temperatures and cooling, and an axial force develops in the beam, the weld is no longer acting purely as a longitudinal weld, due to the fact that the loading is no longer acting parallel to the weld. The resultant of the load is actually acting at some angle to the weld, and the axial force that develops is acting perpendicular to the weld. In this research, the case of the load acting perpendicular to the weld, or acting as a transverse weld, will be studied.

## 1.3     Research Objectives
The need for studying welds at elevated temperatures was identified. Welds are a critical part of structural connections which control the integrity of a structural system.
The objectives of this research are as follows:
(1) Determine the effect of elevated temperature on the strength of fillet welds loaded transversely,
(2) Determine the effect of elevated temperature followed by cooling on the strength of fillet welds loaded transversely,
(3) Develop design recommendations for transversely loaded fillet welds under elevated and elevated-cooling temperature conditions.

## 1.4     Scope of Thesis
The remainder of this thesis consists of five chapters. Chapter 2 will present relevant past fire research, including the behavior of connections at elevated temperatures. Existing fire design recommendations from Eurocode and the AISC specification will be presented. The conventional design method of welded connections will also be discussed. Chapter 3 describes the test program utilized for this research, including the test matrix, specimen design, measures material properties and dimensions of test specimens, test set up, and test protocol and procedure. Chapter 4 describes qualitative observations of specimen response during testing. The temperature and load data are also presented. Chapter 5 evaluates the test results and compares the data to existing design recommendations discussed in Chapter 2. Chapter 6 summarizes the research, conclusions, and presents recommendations for future research.
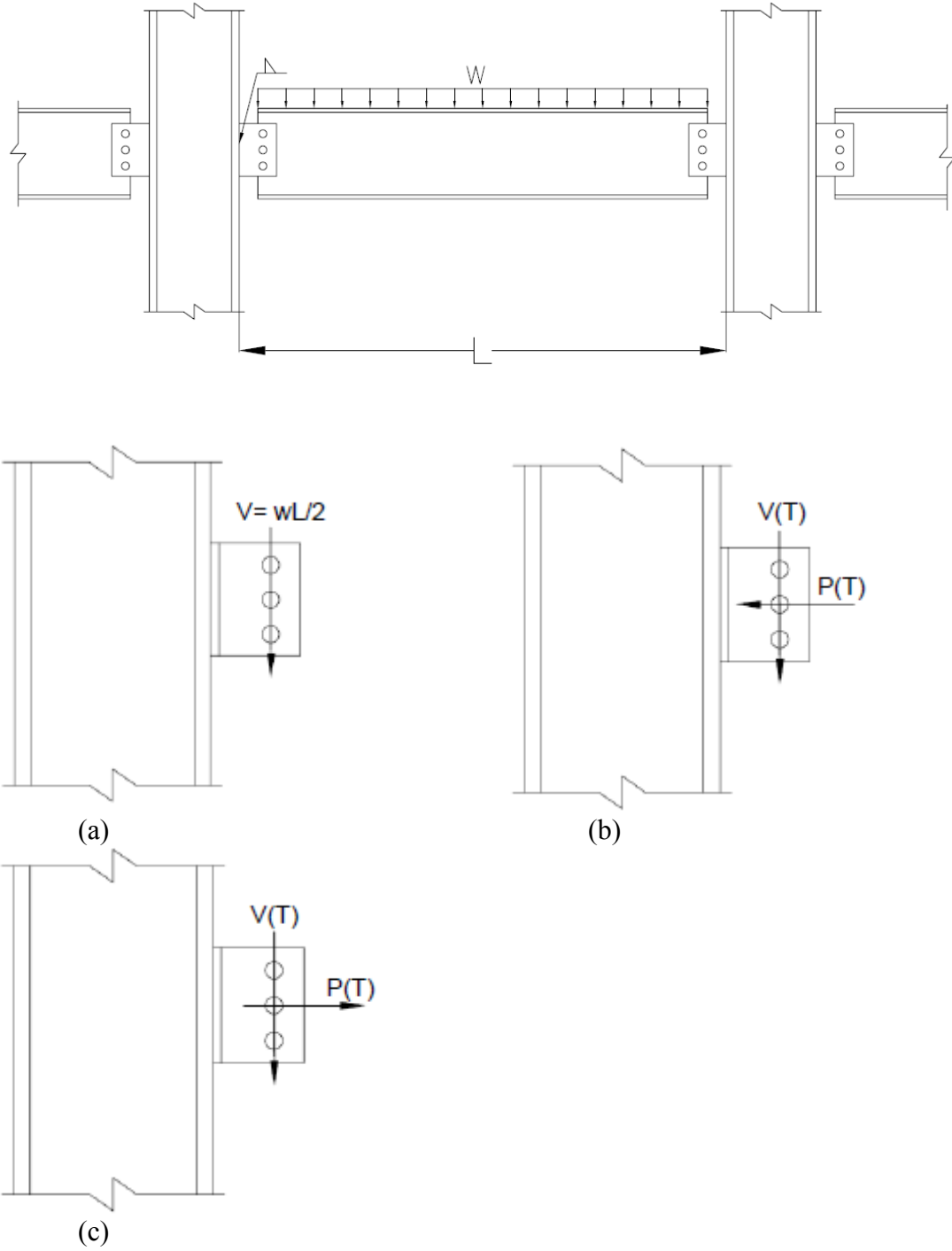
Figure 1.1  Schematic of a shear tab connection subjected to gravity loading with the shear and axial forces acting on the connection (a) At ambient temperature (b) At elevated temperatures (c) During a post-fire scenario (cooling)

**Chapter 2    Background**

## 2.1    General

This chapter presents background material relevant to this research. Information about structural fire engineering will first be presented. The behavior of connections subjected to elevated temperatures will be discussed followed by past fire research on the behavior of connections at elevated temperatures. Existing design recommendations for fire loads from Eurocode and the AISC specification will then be presented. The development of the post-fire scenario tests will then be described. Finally, the conventional design of welded connections and past research on transverse welds at room temperature, and the application of the provisions in Eurocode and the AISC Specification for elevated temperature will be discussed. This will clarify the design of the test specimen to be presented in Chapter 3.

## 2.2    Structural Fire Engineering

Elevated temperatures affect the properties of commonly used materials. For example, the material properties of structural steel degrade with increasing temperature. Figure 2.1, Figure 2.2, and Figure 2.3 show the ratios of elevated temperature to room temperature yield strength, tensile strength, and Young's Modulus, respectively. It can be observed that the material properties begin to degrade at 600°F, with a sharp decrease occurring at around 800°F. Due to the fact there is not much known about the properties of weld metal at elevated temperatures, a goal of this research is to understand if the weld strength degrades in a similar manner to the base metal.

Until recently, there have been relatively few experimental studies performed in the area of structural fire engineering. This is due mostly to the fact that many building codes are more prescriptive in their fire resistance requirements. Prescriptive design utilizes a "cook book" approach and minimizes the amount of actual engineering involved in the design.

The International Building Code Section 703.2 (IBC, 2003) requires that, "The fire-resistance rating of building elements shall be determined in accordance with the test procedures set forth in ASTM E 119." This specification, E 119 (ASTM E 119, 2005), essentially explains how all building elements, both structural and non-structural, should be tested in a furnace in order to determine their fire-resistance rating. E 119 specifies a time-temperature curve which the atmosphere of the testing furnace must match. Figure 2.4 shows the E 119 curve plotted, along with the ISO 834 standard time-temperature curve specified by Eurocode (EC3, 1995). Additionally, E 119 specifies test conditions and acceptance criteria for different building elements. A summary of those test specifications is shown in Table 2.1. The fire-resistance rating for a given member correlates to the amount of time that it can be subjected to the E 119 time-temperature curve, in addition to other pertinent test conditions, while still meeting its specific acceptance criteria. For example, if a certain building element meets its specified acceptance criteria after up to three hours of exposure to the E 119 time-temperature

curve in a furnace, then it is said to have a fire rating of three hours. The required fire ratings for different building elements are specified in Chapter 6 of the International Building Code. In order for fire protection to be adequate, it must satisfy the following:

*Required Fire-Resistance* $\leq$ *Provided Fire-Resistance* (2.1)
*Rating (Hours)*          *Rating (Hours)*

The atmospheric time temperature curve for a typical natural fire is shown in Figure 2.5. It can easily been seen that there are quite a few deviations from the specified E 119 fire curve. The most notable one being that the natural fire curve has three generalized phases: growth, fully developed fire, and decay. The natural fire curve's growth period can be more gradual than E 119's growth. It can be easily observed that the E 119 curve completely neglects the decay period of a natural fire. Note that unlike the E 119 curve, the ISO 834 curve (EC3 1995) includes a decay phase. As will be later discussed in this chapter, certain structural elements experience their most critical behavior during the decay phase of a fire. This led to the need for post-fire tests to be included in this research. The E 119 fire curve clearly does not represent a fire that would occur in a building. This is one of the problems associated with the use of the prescriptive codes and the structural fire tests associated with them. Although prescriptive fire codes are simple to follow and enforce, they result in an unknown level of safety for a given structural system's fire protection.

A limitation of the E 119 test is that it does not consider heat flux. For any given heat transfer problem, an important boundary condition to consider is the amount of heat imparted onto the element in question. E 119 attempts to use atmospheric temperature as a comparative indication of heat flux; however in order to do this accurately, the atmospheric emissivity must be constant. For furnace tests, emissivity varies with furnace dimensions, thermal properties of the furnace walls, and the chemical makeup of the gases within the furnace, among many other things. For this reason it is very difficult to exactly match the emissivities of two different furnaces. Note that it is especially difficult to match the emissivity of the furnaces used in the original E 119 tests. This is due to the fact that it was developed in the early 20th century and the furnaces that were used then are out dated today.

The concept using a limiting temperature to determine the moment capacity for structural beams and girders is shown in Figure 2.6. This concept uses the knowledge of the degrading material properties of steel with elevated temperature. Structural steel beams and girders are considered to be structurally inadequate (i.e., fail to meet performance requirements of E 119) when their material properties degrade to the point that the beam section's nominal moment capacity, Mn, cannot meet the required design moment, M$_{max}$. The temperature where this occurs is known as the beam's "limiting temperature". Commercial fire resistant coatings and sprays, such as spray-applied fire resistive materials (SFRM), can be applied to structural steel elements in order to lessen the effect of hot atmospheric temperatures. For most structural steel elements, the required fire-

resistance rating can be met simply by applying a specific thickness of fire-resistant spray. As a result, nearly all E 119 tests of structural steel beams investigate the performance of a given beam's fire protection, rather than the structural behavior of the beam itself.

### 2.2.1   Steel Connections in Fire

As mentioned previously, the structural integrity of a steel frame is often determined by the strength of its connections. If a connection in a steel frame is inadequate, then the member it connects may not perform as it is intended to. In more extreme cases, the failure of one or more connections could lead to structural instability and/or progressive collapse of the system. Although it seems that for this reason performing research on the behavior of connections in fire should have been a priority, in the past this topic has been given very little experimental or analytical attention.

Understanding the behavior of welds at elevated temperatures is very important. As weld metal cools after being subjected to elevated temperatures, it undergoes a heat treatment process. Depending on how the weld cools, it has different amounts of residual strength and ductility. The concepts of heat treatment will be discussed later in this chapter. As welds cool, a load transfer also takes place due to axial forces that develop in the beam upon cooling, which was briefly discussed previously and will be discussed in more detail later in this chapter. At elevated and post-elevated temperatures welds must carry a combination of axial and shear forces. For this reason, a longitudinal weld that was oriented parallel to its applied load may have a component of loading that is oriented perpendicular to its length, possibly making it behave like a transverse weld.

Analytically modeling steel connections in fire can be very difficult. This is due to the fact that steel connections often consist of several small parts whose interaction is very difficult to efficiently model in any finite element analysis program. Most of the models that do exist rely on simplified assumptions about connection behavior. These simplified models become excessively complicated when they are exposed to high temperatures. This is due to the fact that the material properties of the element and the nature of the interaction begin to change.

Since the joints in steel frames typically contain more material (i.e., bolts, plates, angles, welds, etc.) than the members they connect, steel joints have relatively high thermal mass. Earlier tests performed by Kruppa (1979) and British Steel (1982) supported the idea that due to the fact that connections have greater thermal mass, temperatures would become higher and increase more rapidly in their connecting members. This would lead to the conclusion that the limit state for a fire would occur in the members rather than in the connections. This theory was adopted in several codes to avoid extensive analytical or expensive experimental work.

### 2.3     Research on Steel Connections Subjected to Elevated Temperatures

There has been past research on steel connections subjected to elevated temperatures. Although most of the past research has been on bolted connections, some provides

meaningful results for the behavior of other types of connections at elevated temperatures. This research has shown much about the development of forces in a steel frame during the cooling phase of a fire. These types of scenarios are simulated in the post-fire tests.

### 2.3.1    Previous Experimental Research

As mentioned previously, conventional wisdom in structural fire engineering states that since the joints of a steel frame have more thermal mass than the structural members that they connect, the limit state for a fire will occur in members rather than connections.

Some early research was done by Kruppa (1979) and British Steel (1982) both involving testing bolted connections at elevated temperatures. Kruppa tested six different types of connections. These connections ranged from relatively flexible connections, such as single plate shear connections, to relatively rigid connections, such as flush end-plate connections. The connections were subjected to transverse gravity loading at elevated temperatures. The purpose of the study was to determine the performance of steel connections in fire. The results of the tests showed that failure of the connection, particularly the bolts, did not occur before the connecting elements had undergone considerable deformation. British Steel performed two different tests on moment-resisting "cleated" connections. The purpose of the study was also to determine the performance of a steel connection in fire. The conclusions drawn from this test also suggested that bolted connections were considerably more resistant to elevated temperatures than the connecting structural members.

### 2.3.2    Moment-Rotation Behavior of Steel Joints in Fire

Experiments on steel connections at elevated temperatures drew more interest when Lawson (1990) performed a series of tests on beam-to-column connections. Figure 2.7 illustrates the concept which Lawson studied in his experiments. Lawson proposed that additional fire resistance could be achieved in steel frames by considering the moment capacity developed by simple connections subjected to large rotations induced by exposure to fire. In the study, eight different beam-to-column connections, all end plate and cleated connections ranging from flexible to rigid, were subjected to elevated temperature prescribed from standard fire curves and transverse gravity loading. Composite and non-composite beams were tested with varying amounts of fire protection on the beams and the connections. Figure 2.8 shows the test setup. The tests led Lawson to conclude that the limiting temperature for a beam could be increased if one considered moment redistribution caused by a simple connections moment capacity at large rotations induced by elevated temperatures. This meant that the required fire protection could be decreased. In addition to this, Lawson observed, "In no case did failure of the connecting bolts or welds occur, despite relatively large deformations of the connections." Therefore, Lawson's tests seemed to further validate the conventional wisdom that connection failure is not a limit state for the steel frames subjected to fire.

### 2.3.3 Cardington Fire Tests

The Cardington Fire Tests were unique from past research in that they were system tests. Most past fire research up to that point in time consisted of testing individual materials, such as structural steel or bolts, at elevated temperatures and recording the degradation of their material properties. Although this research was important, it did not provide an understanding of how a steel frame behaves as a system at elevated and post-elevated temperatures, where for example, the development of forces and alternate load paths.

In 1990, the Broadgate building, which is a 14 story steel frame building, in London, suffered a fire while the building was still under construction. Since the building was still under construction, the structural members were not yet fire protected. Despite the fact that the fire lasted for 4.5 hours and the structural members were not fire protected, the building still managed to survive without collapse. This, in addition to observations from several other natural and experimental fires, caused many structural fire engineers to question whether the expensive practice of applying fire protection to all structural members was completely necessary. This notion provided the motivation for the Cardington Fire Tests.

From 1993 to 2003, a collaborative research project was undertaken at the Cardington Laboratories which focused on behavior of structures in fire. The laboratories at Cardington consisted of abandoned hangars that were used to house zeppelins in the early 20th century. Several full-scale test structures were constructed in the labs, including a five story timber frame building, a seven story concrete frame building, and an eight story composite steel frame building. Photographs of the composite steel frame building can be seen in Figure 2.9. Six tests were performed on the composite steel building. Four tests were carried out by British Steel (1998). Figure 2.10 shows the building floor plan and where each of those four tests took place. The two remaining tests were carried out by the Building Research Establishment (BRE, 2003). Figure 2.11 shows the building floor plan and where each of the latter two tests took place. Table 2.2 shows a summary of all tests performed in the composite steel frame building at Cardington.

Figure 2.12 shows a comparison between the atmospheric temperatures recorded for the four tests carried out at Cardington by British Steel. The ASTM E 119 curve is also shown in the figure as a reference. Figure 2.13 shows a diagram of the fire compartment used in the British Steel-4 test as described in Table 2.2, referred to as the "Office" test. Each of the thermocouple sections identified in the figure consists of a thermocouple placed on the beam's bottom flange, web, and top flange. Concrete deck temperatures were not measured in the test. Figure 2.14, Figure 2.15, and Figure 2.16 show bottom flange, web, and top flange temperature distribution throughout the test, respectively. Figure 2.17 and Figure 2.18 show diagrams of the beam's temperature gradient during the test's heating period and cooling period, respectively. Note that the temperature readings for the primary beam's south thermocouple section differed from the north and middle sections, as temperatures on the south side tended to peak approximately 25 minutes after the north and middle sections. Average bottom flange, web, and top flange temperature readings peaked after 31.5 minutes of heating at approximately 1700°F,

1600°F, and 1450°F, respectively. Also note that the temperature gradient in the beam reversed after several minutes of cooling. The gradient remained reversed until temperatures returned to the ambient temperature.

Newman (2000) summarized the results of the Cardington tests and made design recommendations for the economical fire protection of large steel framed buildings. Newman proposed that the results from the Cardington tests indicated that structural elements in a natural compartment fire have greater than expected survival time when compared to isolated tests in which elements are subjected to a standard time-temperature curve. According to Newman, this is because structural elements can derive additional strength from surrounding elements which are unaffected by the compartment fire. As discussed previously in this chapter, a beam at elevated temperature is typically considered unstable when its material properties degrade to the point where the beam's moment capacity can no longer meet the moment demand from the applied loading. Newman argued that this approach did not allow engineers to consider alternate load paths presented by the cool structure surrounding structural elements in a compartment fire.

With regards to previous research performed by Lawson et al., Newman (2000) observed that local buckling occurred in the lower flanges of beams near joints. Local buckling hindered the ability of end-plate connections to develop moments under large rotations. Since the tests performed by Lawson et al. did not consider the effect of the axial forces that develop in beams during heating and cooling, it is likely that those tests did not realistically portray the behavior of connections in fire.

Newman (2000) also made a number of observations pertaining to the performance of connections in the Cardington tests. In the building, beam-to-column connections were either flexible end-plates or were "fin plate" (i.e., shear tab), connections. A photograph of a beam-to-column connection used in the Cardington tests is shown in Figure 2.19. In general, the end-plate connections performed well with no failure occurring during the growth period of the fires. However, during the cooling period of the fire, there were two failure modes observed. In one mode, tensile forces ripped the beam web completely off of the plate. No collapse occurred in this case, as the shear force was transferred through the composite slab. In another mode, shown in Figure 2.20, one side of the plate ruptured. The shear failure took place on the plate, and not along the weld. No collapse occurred in this case either, since bolts on the side of the plate that remained intact were able to transfer shear forces to the column. Shear tab connections performed satisfactorily at elevated temperatures due to their ductility. As the fire decayed, however, unrecoverable plastic deformation caused the beams to retract as they cooled. This created large tensile axial forces in the beams and at the connections. The bolts, likely weakened by the fire, were observed to fail in several connections by shearing in every test performed at Cardington, except in BRE Test 2. A failed shear tab connection from the plane frame test (British Steel Test 2) can be seen in Figure 2.21. Note that in this case, the failure of the shear tab connection took place in the fin plate. However, no collapse occurred as a result of these failed connections. Proper overlapping of reinforcement in the floor slab

enabled the composite slab to effectively transfer the shear force to the adjacent primary beam.

The primary conclusion that Newman (2000) drew from the Cardington tests was that structural members with little conventional fire protection can achieve increased resistance to failure in a fire if the strength of the entire structure is considered, as opposed to just the strength of an isolated member. Figure 2.22 shows how catenary forces derived from the surrounding structure can increase survival time for a beam in fire. When a steel beam or girder in a compartment fire reaches its limiting temperature it can achieve additional strength if the stiffness provided by the adjacent cold structure is taken into account. In this way, a beam with inadequate flexural capacity can avoid runaway deflection and collapse by transferring the applied forces through catenary action. Additionally, Newman (2000) concluded that the use of composite floor construction adds considerable redundancy to a structure subjected to a compartment fire due to concrete's innate thermally resistant properties.

### 2.3.4　Experimentation to Study the Influence of Catenary Action in Beams

The catenary forces that develop in a beam subjected to fire exposure are important to consider when studying the behavior of steel connections. The large tensile axial forces associated with catenary action are, in general, considerably larger than the shearing forces that connections are designed to withstand (Liu et al, 2002). Through the study of catenary forces it can be seen that contrary to conventional wisdom and past experiments, the steel connection may be the component whose failure is the controlling limit state at elevated temperatures.

In 2000, a collaborative research effort was formed between the University of Manchester and the University of Sheffield with the objective of studying the influence of catenary action on the behavior of beams in fire. A furnace was constructed at Manchester's Fire Testing Laboratory which was exclusively dedicated to all of the experimental investigation carried out for the collaborative study. Schematics of the test setup in elevation view and plan view are shown in Figure 2.23 and Figure 2.24, respectively. A series of 20 tests was conducted by Liu et al (2002) in which axially restrained beams were transversely loaded and subjected to elevated temperatures. In the tests, beams were left unprotected except for the top flange, which was wrapped in ceramic fiber blanket to simulate the heat sink that would be caused by a concrete slab. The 178x102x19UB beam that was used in each test is most similar to a W8x13 AISC shape. The beam spanned approximately 6.6 ft. Axial restraint was provided by the two adjacent columns and an external axial restraint which is shown in Figure 2.23. The columns were protected by ceramic fiber blanket and were reused in each test. The external axial restraint was used in order to vary the amount of axial restraint while reusing the same columns for each test. The 152x152x30UC columns that were used in each test are most similar to a W6x20 AISC shape. Two different types of connections were used in the tests: a web-cleated connection and a flush end-plate connection. These connections can be seen in Figure 2.25.

11

The test program consisted of constant load tests, in which constant transverse loads were applied to the beam while it was subjected to the standard ISO 834 time-temperature curve (comparable to the ASTM E 119 curve). Cooling was not considered. A variety of transverse loads were utilized. Liu et al. (2000) describe transverse loading in terms of load ratio. Load ratio, *LR* is defined by British Steel (2003) as:

$$LR = \frac{\textit{Applied load or moment at fire limit state}}{\textit{Nominal load or moment capacity at 20°C}} \qquad (2.2)$$

In this case, the applied load or moment at fire limit state is similar to the limiting temperature concept that was discussed in Section 2.2. This concept helps to define a relationship between the resistance and ambient and elevated temperature.

Load ratio is often used in European structural fire engineering as a design tool or as an experimental variable. The level of axial restraint was also varied throughout testing. Liu found that catenary action only becomes significant once deflections are very large. Therefore, catenary action can only be considered as a potential load path to increase a beam's fire resistance if excessive deflection is not a failure criterion.

Research by Liu et al. (2002) helped give a better idea of the overall behavior of beams and connections subjected to fire. Initially, as a typical beam's temperature increased, compressive axial forces developed due to thermal restraint. A hogging moment also developed at the connections because the heat sink at the beam's top flange created a temperature gradient and induced curvature in the beam. The magnitude of the moment developed at cleated connections was much smaller than that developed at flush end-plate connections since cleated connections have relatively little rotational restraint. The moment, combined with the compressive forces, eventually caused buckling in the beam's lower flange and loss of rotational stiffness. As the beam's temperature continued to increase, yielding occurred at midspan and runaway deflection began. As deflection increased, catenary action took place and the axial force in the beam transitioned into tension. Liu noted that catenary action was less pronounced in the case of cleated connections due to elongation of bolt holes in the beam's web caused by the large axial compressive forces. Axial force is plotted against temperature for several of the tests conducted by Liu et al. (2002) in Figure 2.26.

### 2.3.5   Behavior of Bolted Connections in Fire and Post-Fire Conditions

A study was performed by Yu (2006) at the University of Texas (Austin) to determine the elevated temperature and post-fire properties of bolted connections. Yu performed isolated material tests at elevated temperatures to determine the strength reduction factors for bolts at elevated temperatures.

Yu's test program was designed to investigate the following properties: shear strength of A325 and A490 bolts in fire, shear strength of A325 and A490 bolts in post-fire, slip load reduction in fully-tightened connections in post-fire, bearing strength of connections in fire, and block shear strength of connections in fire. A photograph of the test setup can be

seen in Figure 2.27. The tests were conducted in an electric powered furnace at the University of Texas.  Most of the tests were constant temperature tests, meaning that the connection was heated to a specific temperature, the temperature was held, and then load was applied until failure.

In Yu's study, A325 and A490 bolts were tested in double shear from room temperature up to 800°C (1472°F). Bolts were snug-tightened. Based on the results of these tests, Yu proposed strength reduction factors which are summarized in Table 2.3. In addition to these tests, A325 and A490 bolts were tested in single shear after being exposed to varying elevated temperatures up to 800°C and then cooled to ambient temperature. Bolts were snug-tightened.  Based on the results of these tests, Yu proposed that bolts lose shear strength in post-fire if they are exposed to a temperature greater than their tempering temperature. Strength reduction factors for high strength bolts in post fire conditions which Yu proposed are summarized in Table 2.4. The concept of using reduction factors to knock down the strength at elevated temperature first appeared in Eurocode. Reduction factors (EC3, 1995) for design at elevated temperatures are used as follows:

$$Ru(T) = \theta(T) \cdot Rn(T = 20°C) \tag{2.3}$$
where:
>    Ru(T) = Capacity at elevated temperature T
>    θ(T) =  Reduction factor at elevated temperature of 20°C
>    Rn(T=20°C) = Nominal capacity at ambient temperature

A490 bolts were tested using the standard method (ASTM A325, 2004) after being heated to selected temperatures up to 800°C and then cooled to room temperature. Surfaces of steel plates were sand-blasted and bolts were tightened with an electric twist-off torque wrench. Yu proposed slip resistance reduction factors based on these tests, which are summarized in Table 2.5. Yu also tested 1/2 inch and 3/8 inch thick Grade 50 steel coupons in tension to determine their properties at elevated temperatures. Yu tested the 1/2 in thick coupons at both a high loading rate (0.1 in/min) and a low loading rate (0.01 in/min). The 3/8 inch thick coupons were only tested at the lower loading rate. The reduction factors that Yu proposed for the 1/2 inch thick coupons and the 3/8 inch thick coupons are shown in Table 2.6 and Table 2.7, respectively. While the elevated temperature properties of steel are documented in both American and European codes, Yu's testing did find that the recommended strength reduction factors for yield and ultimate strength from AISC (2001) are not conservative (both are discussed later). A comparison is shown in Figure 2.28 for the yield and ultimate strength. The reduction factors for post-fire bolt shear strength for A325 and A490 bolts are shown in Figure 2.29.

Yu also performed a series of tests to determine the effect of elevated temperatures on bearing strength in a bolted connection. Based on the results of these tests, Yu proposed the following modifications to equation J3-2a in the AISC (2001) specification for bolt bearing capacity at an elevated temperature:

13

$$R_n(T) = 1.2 \cdot L'c \cdot t \cdot F_u(T) \leq 2.4 \cdot d \cdot t \cdot F_u(T) \tag{2.4}$$

where:

$R_n(T)$ = bearing strength at temperature T (kips)

t = thickness of connected material (in)

d = nominal bolt diameter (in)

$F_u(T)$ = reduced tensile strength of connected material at temperature T (ksi)

$$L`c = \frac{Le}{\cos(\alpha)} - \frac{d + \frac{1}{16}in}{2} \tag{2.5}$$

where:

Le = distance from center of hole to edge of material (in), shown in Figure 2.30(a)

$\cos(\alpha) = P/F$

$F = \sqrt{P^2 + V^2}$

P = applied axial force to the connection (kips), shown in Figure 2.30(a)

V = applied shear force to the connection (kips), shown in Figure 2.30(a)

Yu also performed a series of tests to determine the effect of elevated temperatures on block shear strength in a bolted connection. Based on the results of these tests, Yu proposed the following modification to equation J4-3a/b in the AISC (2001) specification for block shear resistance at an elevated temperature T:

$$R_n(T) = 0.6 \cdot F_u(T) \cdot A_{nv} + F_u(T) \cdot A_{nt} \tag{2.6}$$

where:

$R_n(T)$ = block shear strength under elevated temperature T (kips)

$A_{nv}$ = net area in shear (in$^2$)

$A_{nt}$ = net area in tension (in$^2$)

Fu(T) = Rupture strength at elevated temperature, T (ksi)

Yu also proposed the following failure criteria for the block shear under orthogonal forces, as could develop during exposure to fire, as shown in Figure 2.30(b):

$$\left( \frac{1}{A1 + \frac{\sqrt{3}}{3} \cdot A2} \right)^2 \cdot T^2 + \left( \frac{1}{\frac{\sqrt{3}}{3} \cdot A1 + A2} \right)^2 \cdot V^2 \geq [Fu(T)]^2 \tag{2.7}$$

where:

A1 = net area parallel to shear force (in$^2$)

A2 = net area parallel to axial force (in$^2$)

Fu = Rupture strength (ksi)

V = applied shear force to the connection (kips), shown in Figure 2.30(b)

P = applied axial force to the connection (kips), shown in Figure 2.30(b)

### 2.3.6 Structural System Tests at Elevated Temperatures

From the study of the Cardington Fire Tests and research exploring catenary forces, it is evident that understanding the behavior of a structural system at elevated and post-elevated temperatures is important. Recent work done by Catella (2008) helps to quantify the axial forces that develop in a restrained beam under fire loading. This research also includes actual temperatures that were achieved by the steel connection, including the base material, bolts, and welds.

The structural fire test performed by Catella (2008) consisted of an unprotected composite steel beam with unprotected shear tab connections spanning between two fire-protected columns subjected to a time-temperature curve intended to simulate a natural fire. The unprotected shear tab connection is shown in Figure 2.31. No transverse gravity loading was applied for the tests due to concerns regarding the danger of using hydraulic equipment in the vicinity of high temperatures. The objectives of the test were to measure the temperature distribution in the elements of the connection members and forces that developed at the connections due to fire alone. Since no transverse loading was applied, the primary forces developed at the connections were axial forces derived from thermal restraint of the beam. These tests took place in a modular gas furnace designed by Catella (2008). A schematic diagram of the front view, side view, and top view of the assembled furnace are shown in Figure 2.32, Figure 2.33, and Figure 2.34, respectively.

Fifty-nine type K thermocouples were used to measure the atmospheric temperature, and the temperatures of the top and bottom flange, along the height of the web, the concrete deck, and the bolts, welds, and base material on the shear tab connections. The time-temperature curve used in the test is shown in Figure 2.35. A comparison of this time-temperature curve with the atmospheric temperatures recorded in the British Steel-4 test, as listed in Table 2.2, referred to as the "Office" test, performed in the series of Cardington Fire Tests, which Catella's (2008) testing most closely simulated, is shown in Figure 2.36. The atmospheric temperature of the furnace throughout the duration of the high temperature shear tab connection test is shown in Figure 2.37. The atmospheric temperature ranged from about 1200°F in the South East end to about 1500°F in the North East end of the furnace. The temperatures of the bolts, shear tabs (base material), and the welds are shown in Figure 2.38, Figure 2.39, and Figure 2.40, respectively. Note that the connection temperatures do not exceed 900°F throughout the duration of the test.

It was observed that axial forces developed in the test specimen beam throughout the heating and cooling of the beam. Figure 2.41 shows the axial forces that developed in the test specimen beam over the first 200 minutes of the fire test. Figure 2.42 shows the axial forces that developed in the test specimen beam from the start of the test until the beam cooled to ambient temperature. Note that the beam went into tension after approximately 30 minutes of cooling. At ambient temperature, a residual tensile force of 4.49 kips had developed. Had a transverse load been present in this test, the axial load developed may have been greater, resulting in a greater residual tensile force. Catella found that compressive axial forces that develop during the heating of the beam correlate with the

temperature increase of the steel section as shown in Figure 2.43. The net tensile force that develops during cooling correlates with the concrete deck's cooling with respect to time, as shown in Figure 2.44.

Therefore, this testing further verifies the development of axial forces leading to catenary action in beams during fire and post-fire conditions. This is critical for understanding welds at elevated and post-elevated temperatures. This is due to the fact that these axial forces are oriented 90° from the weld, causing a transverse load on the weld, which may be different than what the weld was initially designed for. It will be important to understand if the strength of weld metal deteriorates at elevated temperatures as steel does.

## 2.4    Existing Code
In this section, elevated temperature provisions from Eurocode and ASIC will be discussed.

### 2.4.1    Eurocode
Unlike most codes which follow a prescriptive method for accounting for fire loading, Eurocode (EC3, 1995) presents a design recommendation for structural members exposed to fire. Eurocode 3 puts forth performance requirements that are as follows:
  (1) Where mechanical resistance in the case of fire is required, steel structures shall be designed and constructed in such a way that they maintain their load bearing function during the relevant fire exposure.
  (2) Deformation criteria shall be applied where the means of protection, or the design criteria for separating members, require consideration of the deformation of the load bearing structure.

These performance criteria are carried out through the use of reduction factors for the material at elevated temperature, which are presented in Section 3 in Eurocode 3. The concept of a reduction factor was presented previously in Section 2.3.5 with Equation 2.3. This concept is used in Eurocode to develop reduction factors for various elevated temperatures. There is a detailed structural fire design procedure, which is presented in Section 4 in Eurocode 3. In this section, both a simple calculation model and an advanced calculation model are discussed.

Due to the fact that a goal of this research is to determine a reduction factor for the shear strength of weld metal at elevated temperatures, Section 3 will be discussed. Table 2.8 gives reduction factors relative to the appropriate value at ambient temperature, as developed in Eurocode 3, for the stress-strain relationship shown in Figure 2.45. In this case, ambient temperature is 20°C (68°F). The reduction factors given in Table 2.8 are defined as follows:

-effective yield strength, relative to yield strength at 20°C:  $k_{y,\theta} = f_{y,\theta}/f_y$           (2.8)
-proportional limit, relative to yield strength at 20°C:       $k_{p,\theta} = f_{p,\theta}/f_y$           (2.9)
-slope of linear elastic range, relative to slope at 20°C:    $k_{E,\theta} = E_{a,\theta}/E_a$           (2.10)

The properties on the stress-strain diagram shown in Figure 2.45 are defined as follows:

$f_{y,\theta}$ = effective yield strength

$f_{p,\theta}$ = proportional limit

$E_{a,\theta}$ = slope of the linear elastic range

$\varepsilon_{p,\theta}$ = strain at the proportional limit

$\varepsilon_{y,\theta}$ = yield strain

$\varepsilon_{t,\theta}$ = limiting strain for yield strength

$\varepsilon_{u,\theta}$ = ultimate strain

Table 2.9 provides the formulations for computing the parameters listed above.

Reduction factors for the stress-strain relationship of steel at elevated temperatures from Table 2.8 are shown plotted in Figure 2.46. Note that at a temperature a little above 400°C (approximately 800°F); there is a significant reduction in the yield strength, slope of linear elastic range, and proportional limit. Previously, it was shown in Figure 2.1 through Figure 2.3 that a significant reduction in the yield strength, tensile strength, and Young's Modulus was found to occur around this temperature. It is of particular interest in this research to determine if weld metal behaves like the base metal at elevated temperature, particularly experiencing a significant reduction in strength at approximately 800°F.

## 2.4.2   AISC

Elevated temperatures are discussed in Appendix 4, Structural Design for Fire Conditions in the AISC Specifications (2005). Appendix 4 discusses structural design for fire conditions by analysis and design by qualification testing. The material strengths at elevated temperatures are presented in Section 4.2.3 of AISC and are shown in Table 2.10. This table includes the reduction factors for Young's Modulus, yield strength, and ultimate strength at elevated temperatures. These relationships are not valid for steels with a yield strength above 65 ksi. The reduction factors shown in Table 2.10 are shown plotted in Figure 2.47. The reduction factors have a similar trend, but slightly different in values compared to those found in Eurocode. Section 4.2.3.2 presents the mechanical properties at elevated temperatures, which include the deterioration of the strength and stiffness of structural members, components, and systems, which are used for the structural analysis of a frame, subject to elevated temperatures.

Structural design requirements and methods of analysis are also presented in Appendix 4. Both advanced and simple analysis methods are discussed for tension members, compression members, flexural members, and composite floor members. Design by qualification testing is presented, which includes discussion of qualification standards which relates to the specified fire rating from ASTM E 119 (ASTM E 119, 2005), restrained construction which exists when the surrounding or supporting structure is able to resist actions caused by thermal expansion throughout the range of anticipated elevated temperatures, and unrestrained construction which includes steel beams, girders, and frames that do not support a concrete deck.

17

## 2.5 Heat Treatment

After a metal, such as steel, is heated to a certain temperature its properties begin to change. As it cools, it undergoes a heat treatment process. Different types of heat treatment vary with the way that the metal cools. Depending on the heat treatment process used, the strength and ductility of the heated material varies upon returning to ambient temperature. Weld metal, in particular, is affected by heat treatment. Three different heat treatment options were explored for the post-elevated temperature scenario tests, since the residual strength of the weld would vary with the process used.

The three heat treatment processes considered for the post-fire scenario tests were annealing, normalizing, and quenching. According to ASM (2002), all three treatment options consist of first heating the steel to slightly above the temperature $A_{c3}$, which is shown in Figure 2.48. For the heat treatment process to be properly classified as annealing, normalizing, or quenching; the heating portion must produce a homogenous austenitic phase (face-centered cubic, crystal structure) prior to cooling. Note that austenite is the non-magnetic form of iron and has the ability to dissolve carbon and alloying elements. In this research, A588 steel was used, which has a maximum carbon content between 0.15% and 0.19% (ASTM, 2008). This range is shown in Figure 2.48. Therefore, from Figure 2.48, it can be seen that heating the specimens to 1600°F for the post-fire scenario tests prior to cooling heats the metal until austenite ($A_{c3}$) forms, setting the stage for any of the three heat treatment options. Note that the duration the specimen is held at the elevated temperature prior to cooling is not of great importance. For this reason, the duration that the specimen was kept at an elevated temperature before being cooled was held constant as defined in Section 3.8.

First, annealing will be discussed. Annealing, often referred to as full annealing, consists of heating the specimen to slightly above $A_{c3}$, holding for austenite to form, then slowly cooling. This slow cooling would take place in the furnace that was used to heat the specimen, leading to the name furnace cooling. This is done to produce small grain size, softness, and good ductility. Upon cooling, the austenite transforms to ferrite and pearlite. Note that ferrite is magnetic and has very slight solid solubility for carbon. Pearlite is a mechanical mixture of ferrite and cementite (compound of iron and carbon). Annealing produces the smallest change in strength among the three heat treating processes, in turn giving the worst case scenario for strength reduction due to elevated and post-elevated temperatures.

Normalizing consists of first heating the specimen to slightly above $A_{c3}$, holding for austenite to form, and cooling the specimen in still air, often referred to as air cooling. Upon cooling, austenite transforms giving somewhat higher strength and hardness, but slightly less ductility than that of annealing. Figure 2.49 shows a comparison of time-temperature cycles for normalizing and full annealing. The slower cooling of annealing results in the formation of coarser microstructures than the more rapid cooling of normalizing does.

18

Like annealing and normalizing, quenching consists of heating the specimen to slightly above $A_{c3}$ and holding for austenite to form. Quenching refers to the process of rapidly cooling metal parts from the austenite form, typically within a temperature range of 1500°F to1600°F. This rapid cooling is usually done through the use of liquids or gases. The liquids used commonly include oil (that may contain a variety of additives), water, aqueous polymer solutions, or water that may contain salt or caustic additives. The most common gases used are inert gases, including helium, argon, and nitrogen, and are sometimes used after austenitizing in a vacuum. Quenching is often done to provide a finer grain size and often produces controlled amounts of martensite in the microstructure. The process of quenching provides the highest strength increase and least amount of ductility of these three heat treatment options.

The heat treatment process chosen for the post-fire scenario tests was annealing, or furnace cooling. This process was chosen mainly for two reasons. The first is that annealing gives the greatest reduction in strength, which leads to the most conservative results. The second reason was that annealing seemed to most closely simulate reality. When considering a natural fire, the building typically remains quite hot even after the fire dies out or is extinguished. This would cause the members to cool slowly, causing the greatest reduction in strength. Both normalizing and quenching cool too rapidly to be realistic. This will be referred to in subsequent discussion of the post-fire scenario tests.

## 2.6     Conventional Design of Welded Connections
Transverse welds will be of particular interest in this section, as they were used in the testing done in this research. Transverse welds are oriented perpendicular to the direction of the applied load. When comparing to longitudinal welds, transverse welds have greater strength and less ductility.

### 2.6.1   Past Research
Research on the strength of fillet welds as a function of the direction of load will now be presented. Even though when considering the design of welds, the strength increase found in transverse welds is sometimes neglected, it is important to study and understand the performance of longitudinal, inclined, and transverse welds. Although past research has been done at ambient temperature, it is still valuable for this study. Understanding the increase of strength of transverse welds helps to closer predict the weld failure in the testing for this research. It is also important to understand the behavior of transverse welds, because as mentioned previously in this chapter, when axial forces develop in a beam at elevated temperatures, due to the force's orientation to the weld (perpendicular), the weld will behave as if it is transverse. The failure plane of a transverse weld may be different than 45°, which is typically assumed, especially at elevated temperatures.

### 2.6.1.1 Strength of Fillet Welds as a Function of Direction of Load
Bulter and Kulak (1971) performed experimental research to determine the strength increase of welds inclined at various angles to the applied load over the strength of a longitudinal weld, with the weld axis parallel to the direction of the applied load. Butler

and Kulak also determined the decrease in ductility that a weld oriented at an angle to the applied load experiences.

Butler and Kulak conducted a series of 23 tests in order to establish a load-deformation response for elemental lengths of fillet weld. The 23 coupons were grouped into four categories. Group 1 consisted of five coupons with the weld axis parallel to the direction of the applied load, (i.e., longitudinal welds with θ=0°). Groups 2-4 had six coupons each with the welds inclined at angles of 30°, 60°, and 90° (transverse), respectively, to the direction of the applied load. A schematic drawing of the coupons is shown in Figure 2.50. Note that Figure 2.50 (a) shows the coupon with the longitudinal weld and Figure 2.50 (b) shows that coupon with the inclined weld angle. The welds were made using AWS E60XX electrode. The specimens were loaded in tension in a 440 kip testing machine. The weld deformation was recorded using two 0.001" dial gauges that were fastened to each specimen.

The load-deformation response for the longitudinal fillet weld is shown in Figure 2.51. The load-deformation response for the transverse fillet weld is shown in Figure 2.52. The load-deformation responses for 30° and 60° will not be shown, as transverse welds are of interest in this thesis. The solid lines on the plots relate to expressions that were also developed by Butler and Kulak.

The longitudinal fillet weld achieved an ultimate load of 10.9 kips/in and deformed 0.101 inches, as shown in Figure 2.51. As expected, the transverse weld achieved a higher ultimate load of 15.5 kips/in, but only deformed 0.026 inches, as shown in Figure 2.52, making its failure less ductile. Therefore, this testing concluded that transverse welds have about a 44% strength increase over longitudinal welds but show a decrease in deformation capacity in that longitudinal welds are nearly four times more ductile than transverse welds. The complete results of the experiments with mean vales and standard deviations of the ultimate loads and maximum deformation for each group are shown in Table 2.11.

Research by Fisher (1965) has shown that the load-deformation response for mechanical fasteners can be expressed by the following relationship:

$$R = R_{ult} \left(1 - e^{-\mu\Delta}\right)\lambda \tag{2.11}$$

where:
  $R$ = fastener load at a given deformation (kips)
  $R_{ult}$ = ultimate load attainable by fastener (kips)
  $\Delta$ = shearing, bending, or bearing deformation of the connected plates (in)
  $\mu, \lambda$ = regression coefficients
  $e$ = base of natural logarithms

In this expression, the constants $R_{ult}$, $\mu$, and $\lambda$ are determined for the particular fastener under investigation. Butler and Kulak proposed that this expression should be able to be used for welds as long as the direction of the applied load is taken into account.

The curve-fitting was limited by the number of specimens used in this research; therefore a trial and error procedure was used. It was important that the equation developed be a general expression valid for any angle of applied load. The following relation for the parameters for Equation 2.11 was developed for ¼" fillet welds made with E60XX electrode:

$$R_{ult} = \frac{10 + \theta}{0.92 + 0.0603\theta} \qquad (2.12)$$

$$\Delta_{max} = 0.225(\theta + 5)^{-0.47} \qquad (2.13)$$

$\Delta_{max}$ = maximum deformation of the fillet weld

$$\mu = 75e^{0.0114\theta} \qquad (2.14)$$

$$\lambda = 0.4e^{0.0146\theta} \qquad (2.15)$$

Note that the specified weld size in this testing was ¼". Nominal measurements were used, therefore, there is some error introduced by this, as the measured size of the weld was most likely slightly different.

A plot of Equation 2.12 is shown in Figure 2.53. The ultimate loads calculated from this expression are within 2% of the mean test data, validating the model. A plot of Equation 2.13 is shown in Figure 2.54.

As noted above, it was determined that transverse welds have an increase in strength of about 44% over longitudinal welds and are about 4 times less ductile than longitudinal welds. Although the electrode used in this testing was E60XX, the results can be applied to E70XX electrodes by proper consideration of the increase in electrode strength due to the fact that E60XX and E70XX electrodes have specified ultimate elongations which are nearly the same. Furthermore, these results should be able to be extended to any grade base metal due to the fact that it has been shown that the strength of welds made using electrodes of either E60XX or E70XX is not appreciably affected by the grade of base metal involved.

**2.6.1.2 Strength of Transverse Fillet Welded Joints**
Kato and Morita (1974) studied the strength of transverse fillet welds to further predict their strength increase over longitudinal fillet welds. Their work consisted of theoretical research based on a theory of elasticity approach, experimental work, and a finite element analysis.

The theory of elasticity approach which will be presented is based on the following assumptions:

21

(1) The direct stress (q) on the tensile face of the weld is uniformly distributed as shown in Figure 2.55.
(2) The pattern of the elastic stress distribution remains unchanged until the fracture of the weld occurs.
(3) Weld fracture occurs when the shear stress at a point on the fillet reaches

$$\tau_{max} = \frac{\sigma_T}{\sqrt{3}}$$ 

(2.16)

where:

$\tau_{max}$ = Von Mises shear yield stress (ksi)
$\sigma_T$ = the tensile strength of the weld metal (ksi)

Using polar coordinates ($\theta$,r) and taking the boundary conditions into account, the following stress component relationship is obtained:

$$\tau_{r\theta} = \frac{1}{r^2} \cdot \frac{\partial \Phi}{\partial \theta} - \frac{1}{r} \cdot \frac{\partial^2 \Phi}{\partial r \partial \theta}$$

$$\tau_{r\theta} = \frac{-q}{1 - \frac{\pi}{4}} \cdot \left( \sqrt{2} \cdot \sin \theta \cdot \sin(\theta - \frac{\pi}{4}) \right)$$

(2.17)

where:

q = uniformly distributed stress acting on the tensile face of a fillet weld (ksi)
$\Phi$ = stress function

Taking the derivative of Equation 2.17 and setting it equal to zero gives $\theta = \pi/8$. This coordinate yields the maximum shear stress, $\tau_{\theta max}$. Therefore, it can be concluded that $\pi/8$ is the failure plane of the weld. The following expression is then found for transverse fillet welds:

$$T_{t\,max} = \left(1 - \frac{\pi}{4}\right) \cdot \left(\sin^{-2} \frac{\pi}{8}\right) \cdot A_w \cdot \frac{\sigma_T}{\sqrt{3}}$$

(2.18)

where:

$T_{tmax}$ = external load per one transverse fillet weld (kips)
$A_w$ = throat area (in$^2$) = l*a

Note that in this case, $a = \frac{s}{\sqrt{2}}$

where:

s = size of fillet (in)

Therefore, in addition to the three assumptions mentioned previously, the throat area is based on the assumption that the weld failure plane is at 45°.
For longitudinal fillet welds, the critical section is the throat, therefore its maximum strength is:

$$T_{1\max} = A_w \cdot \frac{\sigma_T}{\sqrt{3}} \qquad\qquad\qquad (2.19)$$

where:

$T_{1\max}$ = maximum external load per one longitudinal fillet weld (kips)

Hence, the strength of a transverse weld can be written as:

$$T_{t\max} = \left(1 - \frac{\pi}{4}\right) \cdot \left(\sin^{-2} \frac{\pi}{8}\right) \cdot T_{1\max} \qquad\qquad (2.20)$$

Simplifying,

$$T_{t\max} = 1.46 \cdot T_{1\max} \qquad\qquad\qquad (2.21)$$

Therefore, the theory of elasticity predicts that transverse fillet welds are 46% stronger than longitudinal fillet welds of the same size, length, and electrode.

Experimental work was done by Kato and Morita (1974) to validate the theory of elasticity solution. Two types of specimens were manufactured and tested. The first consisted of slice-cut specimens with large size fillets and the second consisted of several sizes of fillets and a limited fillet length. Two types of electrode were used in the testing, E70XX and E110X. The test results were compared with the theoretical predications for the maximum strength and the angle of the breaking plane. These tests concluded that the specimens welded with E70XX electrode had an average ratio of strength of transverse fillet welds to longitudinal fillet welds of 1.56. The specimens welded with E110X electrode had an average ratio of strength of 1.45. Therefore, the theoretical prediction for maximum strength was quite good. The angle of the failure plane of $\pi/8$ was also found to correlate very well with what was found in the experimental results.

As stated previously, assumptions were made to use the theory of elasticity approach. A finite element analysis was conducted to account for the assumptions that were previously made. Butler and Kulak (1974) explain why the inaccuracy of the assumptions is important. In regards to assumption (1), the direct stress on the tensile face of the weld varies approximately linearly from the toe to the foot of the weld. In regards to assumption (2), the peak stress predicted by the elastic theory should be relieved by plastic deformation as soon as it exceeds the yield stress resulting in a redistribution of the stress. In regards to assumption (3), the fracture stress should be evaluated according to an appropriate failure theory. Despite these inconsistencies, the prediction from the elasticity theory has shown satisfactory agreement with previous test results.

The finite element analysis was performed on the basis of incremental strain theory and an isotropic and ductile material assumed to obey the von Mises yield criterion with the Prandtl-Reuss loading function. The specimen was modeled by triangular elements. Elastic behavior was first assumed so that the finite element results could be compared with the elasticity theory results and experimental results. The stresses found in the finite element analysis compare well to those found in the experimental and theoretical results.

Inelastic behavior was then considered in the finite element analysis. It was found that the stresses obtained from the finite element analysis compared quite well to the results based on elasticity theory. It was found that the failure plane approximately coincided with the failure plane that was predicted theoretically.

In conclusion, this research shows that the strength of transverse fillet welded joints can be estimated quite accurately from the theory of elasticity despite some theoretical shortcomings. The results from this research also agree quite well with the previous research by Butler and Kulak (1971).

## 2.6.2  AISC Design Criteria for Transverse Welds

The test specimen utilized in this research was designed according to AISC (2005). The specific details of the design will be further discussed in Section 3.3. AISC (2005) accounts for the strength increase of welds oriented at an angle to the load, as found in past research previously discussed. Equation J2-4 from AISC (2005) gives the design strength for a linear weld group loaded in-plane through the center of gravity. This equation is as follows:

$$R_n = F_w \cdot A_w \tag{2.22}$$

where:

$R_n$ = design strength (kips)

$F_w$ = nominal strength of the weld metal per unit area (ksi)

$A_w$ = effective area of the weld (in$^2$) = $\ell * a$

$\ell$ = length of weld (in)

$$a = {s}/{\sqrt{2}} \tag{2.23}$$

where:

s = size of the leg of the weld, in

Note that this assumes the failure plane is acting at 45°.

In this equation, the design strength for LRFD is $\phi R_n$ where $\phi = 0.75$ and the design strength for ASD is $R_n/\Omega$ where $\Omega = 2.00$.

When a weld is oriented at an angle, $\theta$ to the applied load, an increase of strength and loss of ductility is experienced. AISC (2005) Equation J2-5 accounts for the strength increase for any angle $\theta$ as follows:

$$F_w = 0.60 \cdot F_{EXX} \cdot (1.0 + 0.50 \cdot \sin^{1.5} \theta) \tag{2.24}$$

where:

$F_{EXX}$ = electrode classification number (ksi)

$\theta$ = angle of loading measured from the weld longitudinal axis (degrees)

For transversely loaded welds $\theta = 90°$. When this is substituted into equation 2.6, a 50% increase in weld strength is accounted for over a longitudinally loaded weld. Note that this has a slightly greater increase in strength than that found in the past research studies, as noted above.

Table 2.1  Summary of tests in ASTM E 119 (Catella, 2008)

| Element under test | Test Conditions | | | Applicable Acceptance Criteria | | | | |
|---|---|---|---|---|---|---|---|---|
| | Fire Load | Design Load | Hose Stream | Strength / Stability | Flame Passage | Opposite Surface Temp Increase | Struc. Steel. Temp Incr. | Reinf/ PS Steel Temp Incr. |
| 1. Tests of Bearing Walls and Partitions | X | X | X | X | X | | | |
| 2. Tests of Nonbearing Walls and Partitions | X | | X | | X | X | | |
| 3. Tests of Columns | X | X | | X | | | | |
| 4. Alternative Tests of Protection for Structural Steel Columns | X | | | | | X | | |
| 5. Tests of Floors and Roofs (specimens are restrained) | X | X | | X | X | X | X | X |
| 6. Tests of Loaded Restrained Beams (specimens are restrained) | X | X | | X | | | X | |
| 7. Alternative Classification Procedure for Loaded Beams (specimens are unrestrained) | X | X | | X | | | X | X |
| 8. Alternative Test of Protection for Solid Structural Steel Beams and Girders | X | | | | | | X | |

Table 2.2  Summary of tests performed on the composite steel structure at Cardington (Catella, 2008)

| Test | Researcher | Description | Fire source | Duration (min) | Max temperature (°F) Atmospheric | Steel |
|------|------------|-------------|-------------|----------------|---------------------------------|-------|
| BS-1 | British Steel | Restrained beam (connections excluded) | Gas-fired furnace | 170 | 1675 | 1607 |
| BS-2 | British Steel | Planar frame | Gas-fired furnace | 125 | 1508 | 1472 |
| BS-4 | British Steel | Corner | Timber cribs | 75 | 1868 | 1742 |
| BS-4 | British Steel | Office | Timber cribs and office furnishings | 40 | 2102 | 1940 |
| BRE – 1 | BRE | Corner | Timber cribs | 114 | 1832 | 1657 |
| BRE – 2 | BRE | Large compartment | Timber cribs | 70 | Not recorded | 1276 |

Table 2.3  Reduction factors for bolt shear strength proposed by Yu (2006)

| A325 | | A490 | |
|------|--|------|--|
| Temperature (°F) | Reduction Factor | Temperature (°F) | Reduction Factor |
| 77 | 1.00 | 89 | 1.00 |
| 209 | 0.96 | 214 | 0.91 |
| 396 | 1.00 | 393 | 0.95 |
| 572 | 1.00 | 573 | 1.00 |
| 757 | 0.61 | 752 | 0.83 |
| 943 | 0.36 | 935 | 0.60 |
| 1112 | 0.21 | 1111 | 0.34 |
| 1301 | 0.12 | 1295 | 0.16 |
| 1477 | 0.10 | 1475 | 0.14 |

Table 2.4  Reduction factors for post-fire bolt shear strength proposed by Yu (2006)

| A325 | | A490 | |
|---|---|---|---|
| Maximum Exposure (°F) | Reduction Factor | Maximum Exposure (°F) | Reduction Factor |
| 77 | 1.00 | 89 | 1.00 |
| 209 | 1.00 | 214 | 0.98 |
| 396 | 1.00 | 393 | 0.97 |
| 572 | 1.00 | 573 | 0.98 |
| 757 | 0.98 | 752 | 0.97 |
| 943 | 0.91 | 935 | 0.98 |
| 1112 | 0.81 | 1111 | 0.80 |
| 1301 | 0.67 | 1295 | 0.67 |
| 1477 | 0.58 | 1475 | 0.58 |

Table 2.5  Slip resistance reduction factors proposed by Yu (2006)

| Maximum Exposure Temperature (°F) | Slip Resistance Reduction Factor |
|---|---|
| 91 | 1.00 |
| 212 | 1.40 |
| 392 | 1.57 |
| 572 | 1.55 |
| 752 | 1.46 |
| 932 | 0.57 |
| 1166 | 0.21 |
| 1292 | 0.28 |
| 1472 | 0.11 |

Table 2.6  Summary of reduction factors for 1/2 inch thick coupons of Grade 50 steel proposed by Yu (2006)

| Temperature (°F) | Yield Strength (ksi) | Ultimate Strength (ksi) | Yield Strength Reduction Factor | Ultimate Strength Reduction Factor | Loading Rate |
|---|---|---|---|---|---|
| 84.6 | 62.41 | 74.19 | 1.00 | 1.00 | High |
| 216.9 | 56.79 | 70.23 | 0.95 | 0.91 | |
| 391.8 | 53.07 | 69.83 | 0.94 | 0.85 | |
| 572.0 | 40.90 | 73.59 | 0.99 | 0.70 | |
| 750.4 | 33.47 | 60.36 | 0.81 | 0.67 | |
| 941.7 | 26.34 | 48.32 | 0.65 | 0.57 | |
| 1094.2 | 16.84 | 28.98 | 0.39 | 0.39 | |
| 1294.9 | 13.88 | 17.21 | 0.23 | 0.26 | |
| 1485.3 | 6.23 | 8.41 | 0.11 | 0.12 | |
| 81.9 | 57.85 | 72.39 | 1.00 | 1.00 | Low |
| 217.8 | 57.11 | 70.37 | 0.99 | 0.97 | |
| 394.0 | 48.69 | 70.99 | 0.84 | 0.98 | |
| 573.4 | 40.09 | 76.16 | 0.80 | 1.05 | |
| 743.9 | 28.57 | 58.22 | 0.70 | 0.80 | |
| 932.9 | 21.98 | 42.26 | 0.59 | 0.58 | |
| 1106.2 | 11.47 | 24.32 | 0.38 | 0.34 | |
| 1283.0 | 7.19 | 13.38 | 0.22 | 0.18 | |
| 1472.9 | 3.30 | 5.29 | 0.07 | 0.07 | |

Table 2.7  Summary of reduction factors for 3/8 inch thick coupons of Grade 50 steel proposed by Yu (2006)

| Temperature (°F) | Yield Strength (ksi) | Ultimate Strength (ksi) | Yield Strength Reduction Factor | Ultimate Strength Reduction Factor |
|---|---|---|---|---|
| 84.7 | 57.07 | 78.56 | 1.00 | 1.00 |
| 212.4 | N/A | 72.78 | N/A | 0.93 |
| 390.2 | 50.37 | 74.86 | 0.88 | 0.95 |
| 568.6 | 51.06 | 80.07 | 0.89 | 1.02 |
| 753.3 | 38.74 | 74.07 | 0.68 | 0.94 |
| 931.5 | 39.23 | 60.80 | 0.69 | 0.77 |
| 1117.2 | 27.89 | 35.57 | 0.49 | 0.45 |
| 1294.2 | 18.25 | 18.53 | 0.32 | 0.24 |
| 1296.0 | 19.76 | 20.00 | 0.35 | 0.25 |
| 1473.8 | 8.02 | 9.36 | 0.14 | 0.12 |

Table 2.8  Reduction factors for stress-strain relationships of steel at elevated temperatures (EC3, 1995)

| Steel Temperature, $\theta_a$ °F[°C] | Reduction factors at temperature $\theta_a$ relative to the value of $f_y$ or $E_a$ at 20°C | | | |
|---|---|---|---|---|
| | Reduction factor (relative to $f_y$) for effective yield strength | Modified factor (relative to $f_y$) for satisfying deformation criteria | Reduction factor (relative to $f_y$) for proportional limit | Reduction factor (relative to $E_a$) for the slope of the linear elastic range |
| | $k_{y,\theta} = f_{y,\theta}/f_y$ | $k_{x,\theta} = f_{x,\theta}/f_y$ | $k_{p,\theta} = f_{p,\theta}/f_y$ | $k_{E,\theta} = E_{a,\theta}/E_a$ |
| 68 [20] | 1.000 | 1.000 | 1.000 | 1.000 |
| 212 [100] | 1.000 | 1.000 | 1.000 | 1.000 |
| 392 [200] | 1.000 | 0.922 | 0.807 | 0.900 |
| 572 [300] | 1.000 | 0.845 | 0.613 | 0.800 |
| 752 [400] | 1.000 | 0.770 | 0.420 | 0.700 |
| 932 [500] | 0.780 | 0.615 | 0.360 | 0.600 |
| 1112 [600] | 0.470 | 0.354 | 0.180 | 0.310 |
| 1292 [700] | 0.230 | 0.167 | 0.075 | 0.130 |
| 1472 [800] | 0.110 | 0.087 | 0.050 | 0.090 |
| 1652 [900] | 0.060 | 0.051 | 0.038 | 0.068 |
| 1832 [1000] | 0.040 | 0.034 | 0.025 | 0.045 |
| 2012 [1100] | 0.020 | 0.017 | 0.013 | 0.023 |
| 2192 [1200] | 0.000 | 0.000 | 0.000 | 0.000 |
| Note: For intermediate values of the steel temperature, linear interpolation may be used. | | | | |

Table 2.9  Formulations for computing stress-strain relationships at elevated temperatures (EC3, 1995)

| Strain range | Stress $\sigma$ | Tangent modulus |
|---|---|---|
| $\varepsilon \leq \varepsilon_{p,\theta}$ | $\varepsilon\, E_{a,\theta}$ | $E_{a,\theta}$ |
| $\varepsilon_{p,\theta} < \varepsilon < \varepsilon_{y,\theta}$ | $f_{p,\theta} - c + (b/a)\left[a^2 - (\varepsilon_{y,\theta} - \varepsilon)^2\right]^{0,5}$ | $\dfrac{b(\varepsilon_{y,\theta} - \varepsilon)}{a\left[a^2 - (\varepsilon_{y,\theta} - \varepsilon)^2\right]^{0,5}}$ |
| $\varepsilon_{y,\theta} \leq \varepsilon \leq \varepsilon_{t,\theta}$ | $f_{y,\theta}$ | $0$ |
| $\varepsilon_{t,\theta} < \varepsilon < \varepsilon_{u,\theta}$ | $f_{y,\theta}\left[1 - (\varepsilon - \varepsilon_{t,\theta})/(\varepsilon_{u,\theta} - \varepsilon_{t,\theta})\right]$ | $-$ |
| $\varepsilon = \varepsilon_{u,\theta}$ | $0,00$ | $-$ |
| Parameters | $\varepsilon_{p,\theta} = f_{p,\theta}/E_{a,\theta}$      $\varepsilon_{y,\theta} = 0,02$ | $\varepsilon_{t,\theta} = 0,15$      $\varepsilon_{u,\theta} = 0,20$ |
| Functions | $a^2 = (\varepsilon_{y,\theta} - \varepsilon_{p,\theta})(\varepsilon_{y,\theta} - \varepsilon_{p,\theta} + c/E_{a,\theta})$ <br> $b^2 = c(\varepsilon_{y,\theta} - \varepsilon_{p,\theta})E_{a,\theta} + c^2$ <br> $c = \dfrac{(f_{y,\theta} - f_{p,\theta})^2}{(\varepsilon_{y,\theta} - \varepsilon_{p,\theta})E_{a,\theta} - 2(f_{y,\theta} - f_{p,\theta})}$ | |

Table 2.10  AISC reduction factors for Young's Modulus, yield strength, and ultimate strength of steel at elevated temperatures (AISC, 2005)

| Table A-4.2.1 Properties of Steel at Elevated Temperatures | | | |
|---|---|---|---|
| Steel Temperature (°F) [°C] | $k_E = E_m/E$ | $k_y = F_{ym}/F_y$ | $k_u = F_{um}/F_u$ |
| 68 [20] | 1.00 | 1.00 | 1.00 |
| 200 [93] | 1.00 | 1.00 | 1.00 |
| 400 [204] | 0.90 | 1.00 | 1.00 |
| 550 [288] | 0.78 | 1.00 | 1.00 |
| 600 [316] | 0.70 | 1.00 | 1.00 |
| 800 [427] | 0.67 | 0.94 | 0.94 |
| 1000 [538] | 0.49 | 0.66 | 0.66 |
| 1200 [649] | 0.22 | 0.35 | 0.35 |
| 1400 [760] | 0.11 | 0.16 | 0.16 |
| 1600 [871] | 0.07 | 0.07 | 0.07 |
| 1800 [982] | 0.05 | 0.04 | 0.04 |
| 2000 [1093] | 0.02 | 0.02 | 0.02 |
| 2200 [1204] | 0.00 | 0.00 | 0.00 |

Table 2.11  Experimental Results with mean values and standard deviations of the ultimate loads and maximum deformation for each weld group (Butler et al, 1971)

| Group $\theta$, deg | Ultimate Load (kips/in) | | Maximum Deformation (in) | | Predicted Values | |
|---|---|---|---|---|---|---|
| | Mean | Std. Deviation | Mean | Std. Deviation | Ultimate Load (kips/in) | Max Deformation (in) |
| 0 | 10.9 | 0.67 | 0.101 | 0.008 | 10.9 | 0.105 |
| 30 | 14.6 | 0.03 | 0.049 | 0.011 | 14.6 | 0.042 |
| 60 | 14.1 | 0.51 | 0.031 | 0.004 | 15.4 | 0.031 |
| 90 | 15.5 | 0.95 | 0.026 | 0.002 | 15.7 | 0.026 |
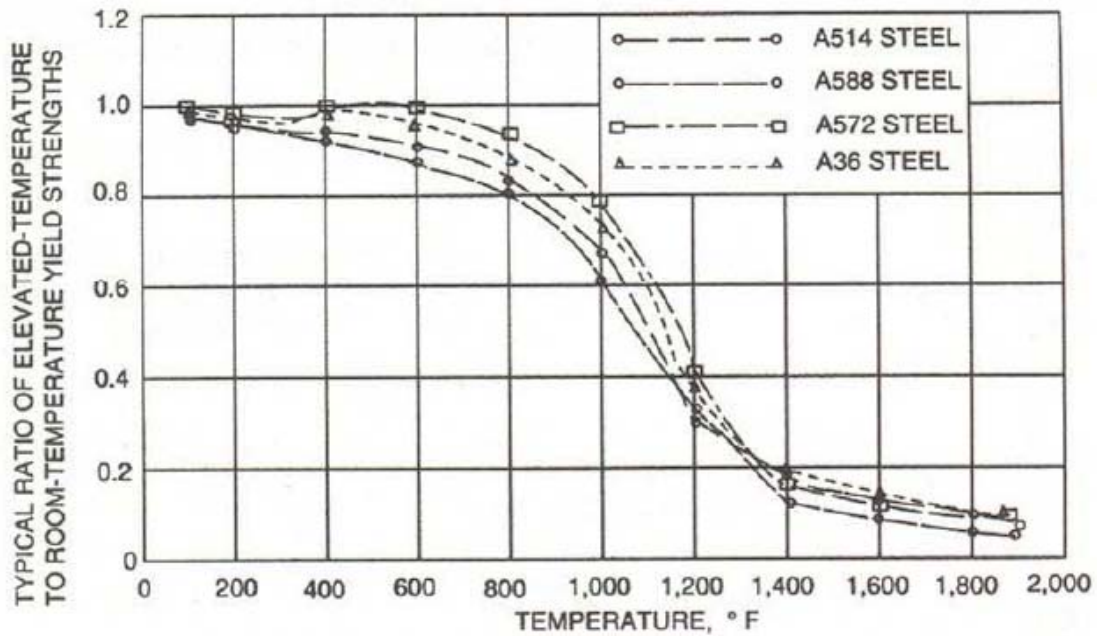
Figure 2.1 Degradation of yield strength with increasing temperature (Brockenbrough and Johnson, 1981)
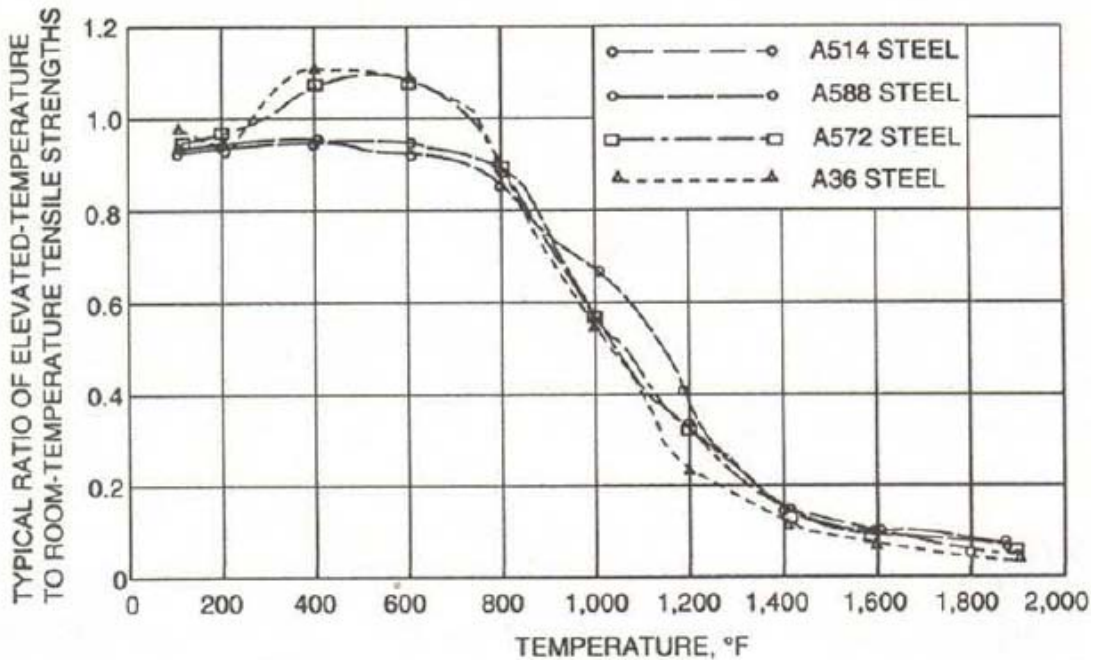


Figure 2.2 Degradation of tensile strength with increasing temperature (Brockenbrough and Johnson, 1981)

32
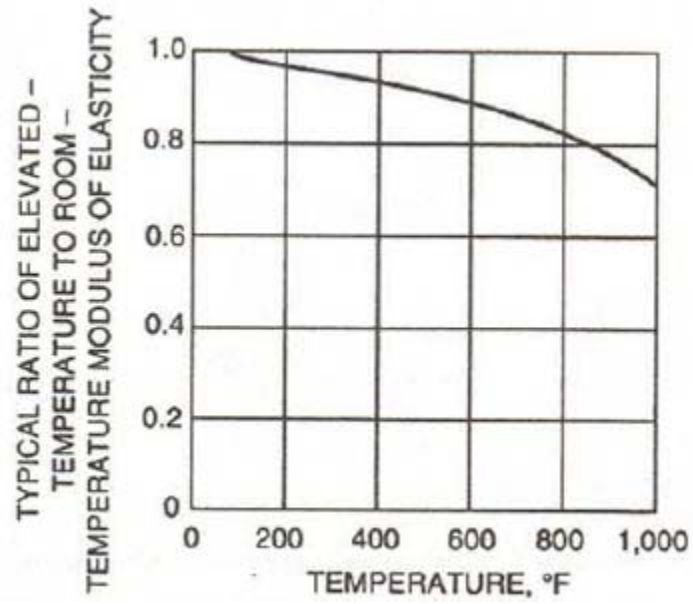
Figure 2.3  Degradation of Young's modulus with increasing temperature
(Brockenbrough and Johnson, 1981)
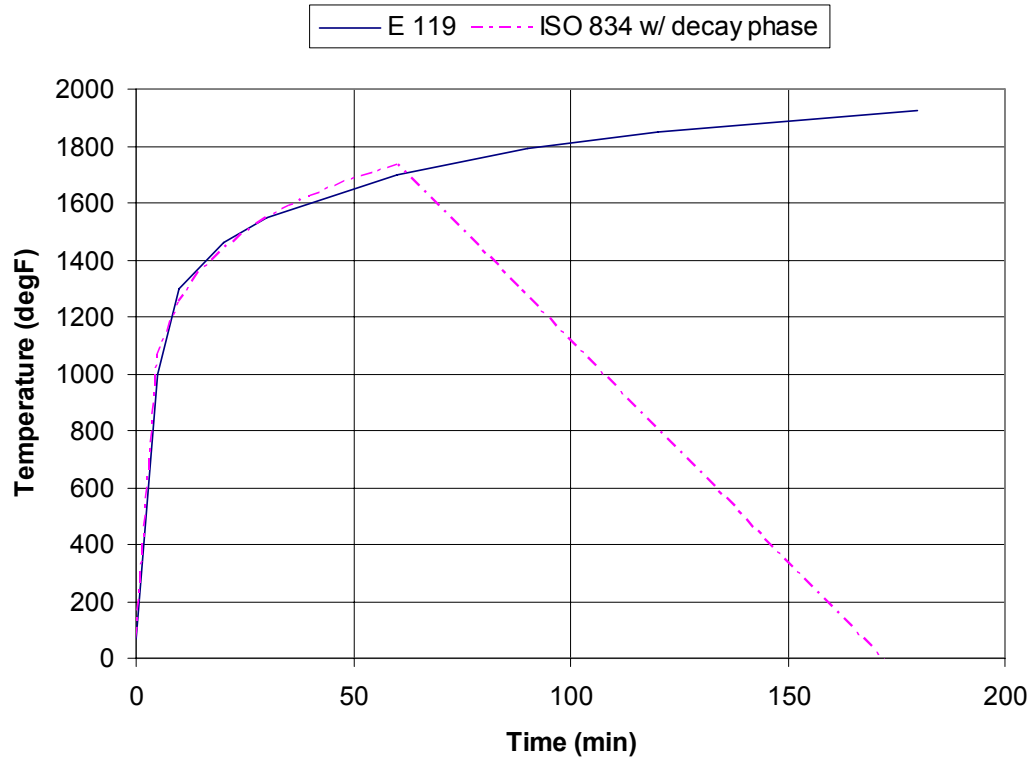
Figure 2.4  Time-temperature curve of furnace atmosphere specified in ASTM E 119
(Catella, 2008)
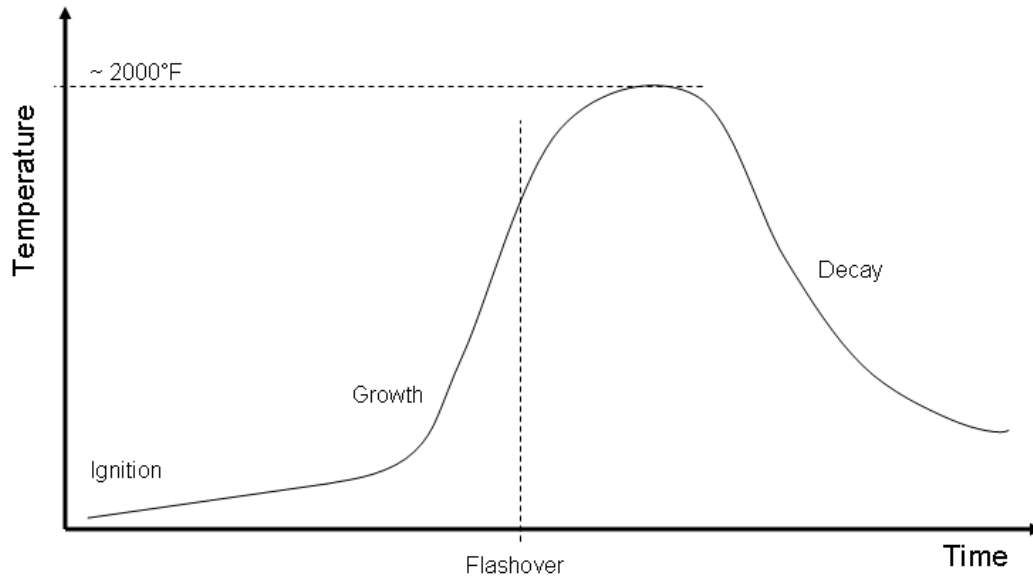
Figure 2.5  Conceptual atmospheric time-temperature curve for a typical natural fire (Catella, 2008)
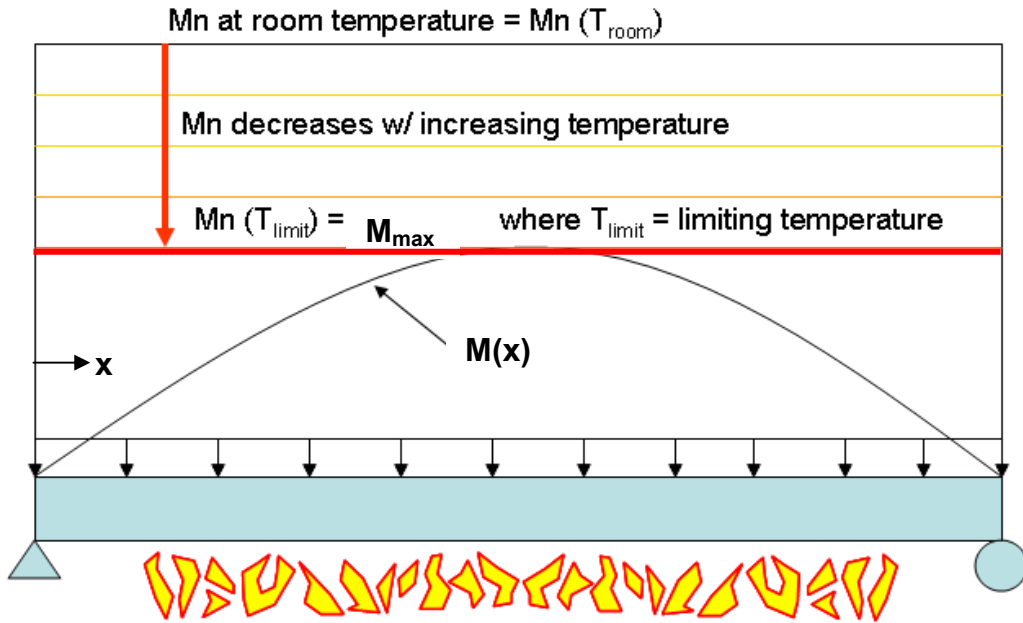
Figure 2.6  Illustration of the limiting temperature concept (Catella, 2008)
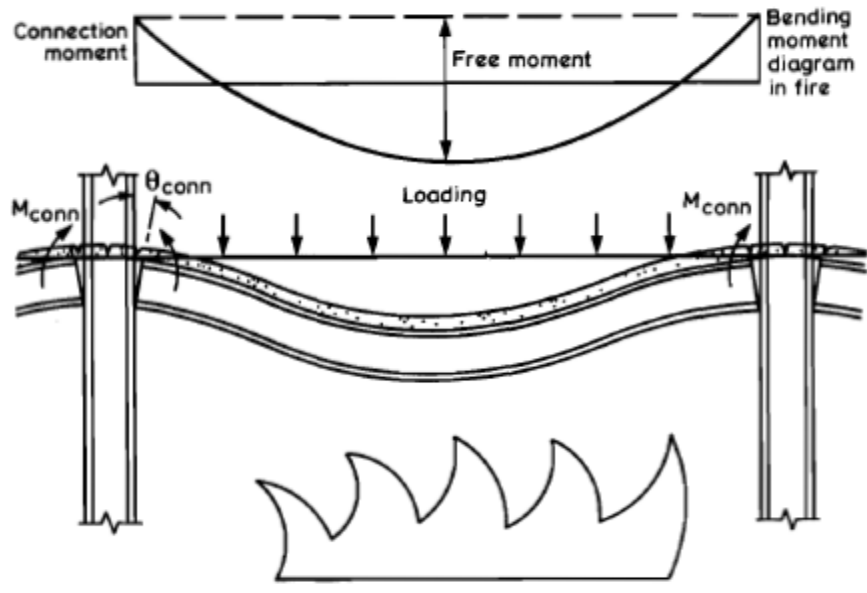


Figure 2.7  Illustration of impetus for research by Lawson (1990) [from Lawson (1990)]
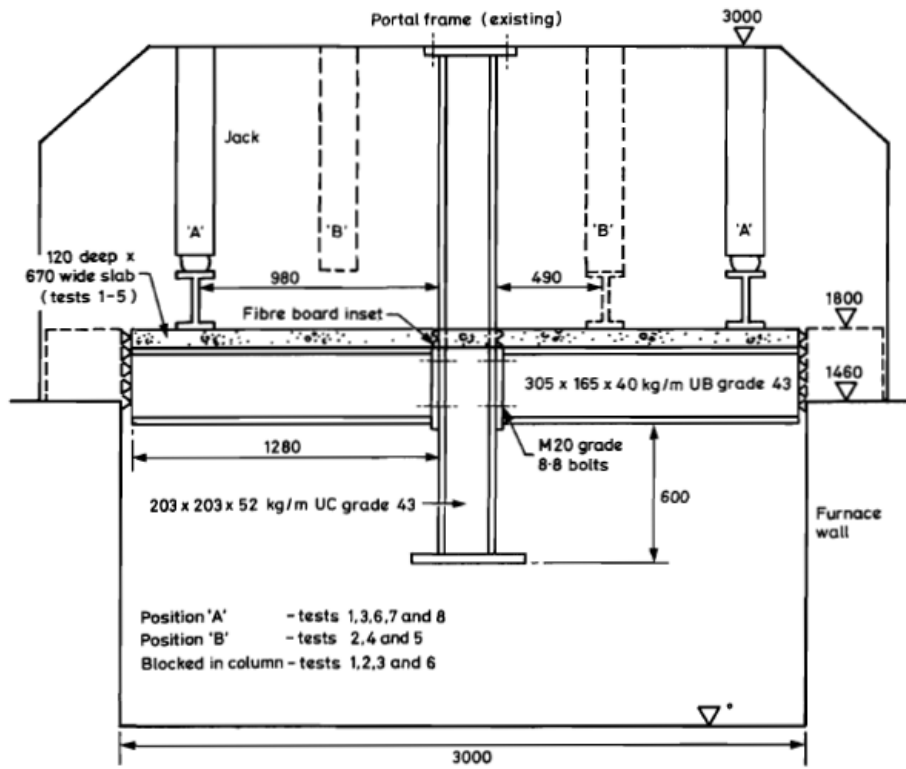
Figure 2.8  Setup for steel connection tests performed by Lawson (1990) [from Lawson (1990)]

Figure 2.9  Photographs of the composite steel frame building studied at Cardington Labs (Newman, 2000)
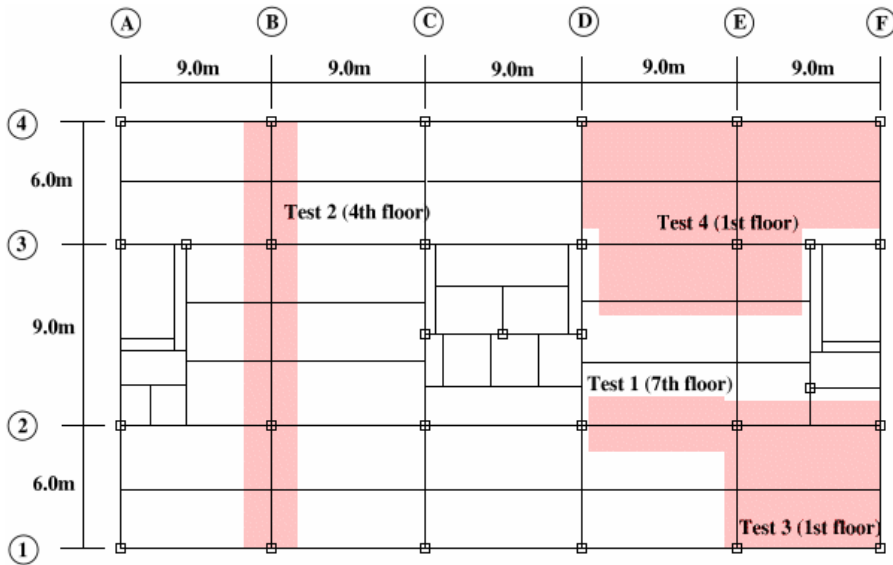
Figure 2.10  Floor plan showing where tests conducted by British Steel took place (Newman, 2000)
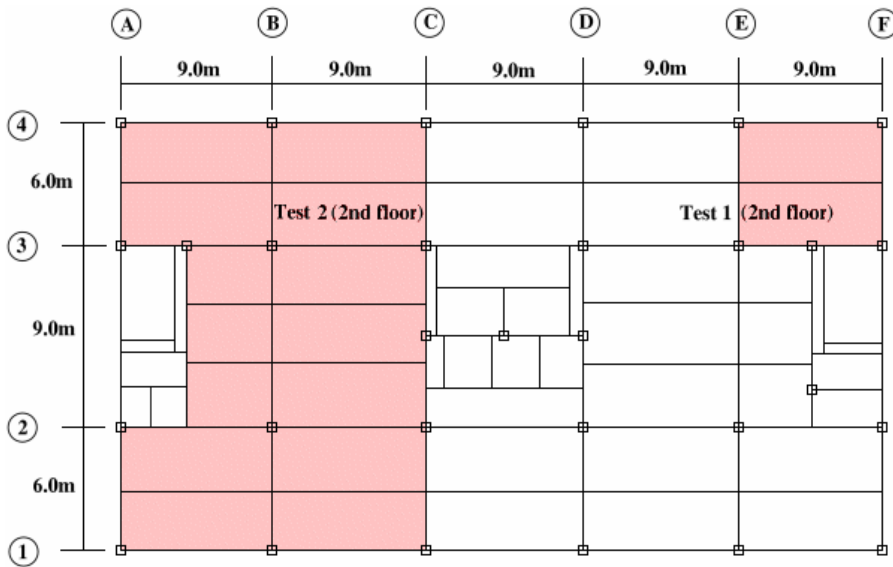


Figure 2.11  Floor plan showing where tests conducted by BRE took place (Newman, 2000)
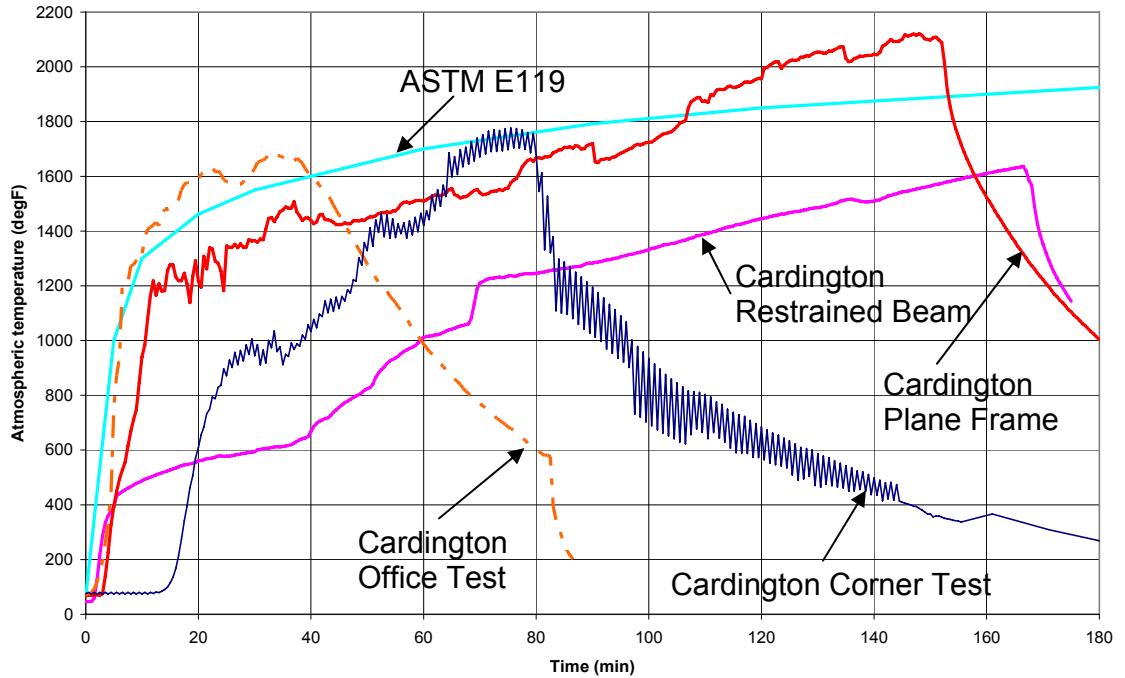
Figure 2.12  Comparison of atmospheric temperatures recorded in the four tests carried out at Cardington by British Steel (Catella, 2008)
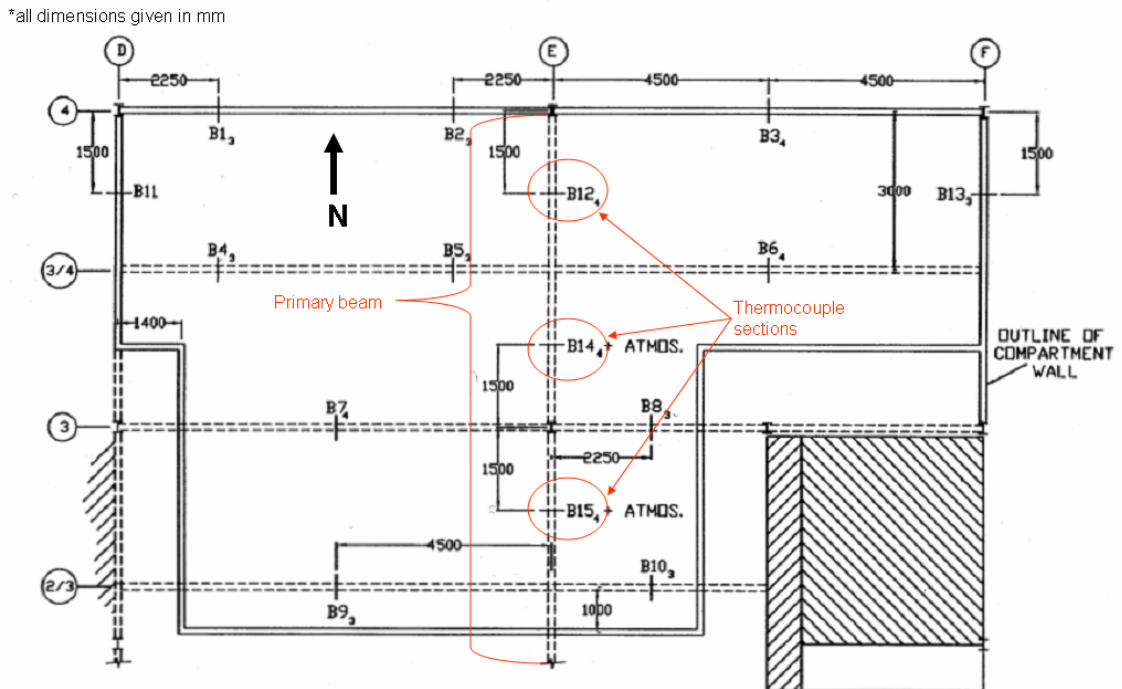


Figure 2.13  Diagram of temperature sensor locations for the Cardington Office Demonstration test (British Steel, 1998)
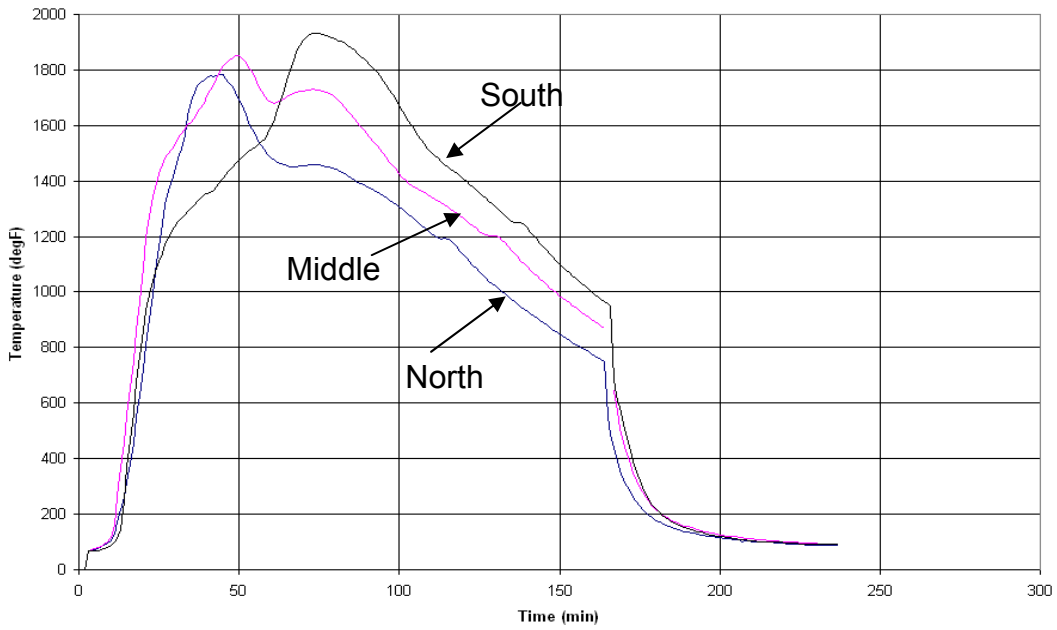
Figure 2.14  Primary beam bottom flange temperature distribution during the Cardington Office Demonstration test (British Steel, 1998)
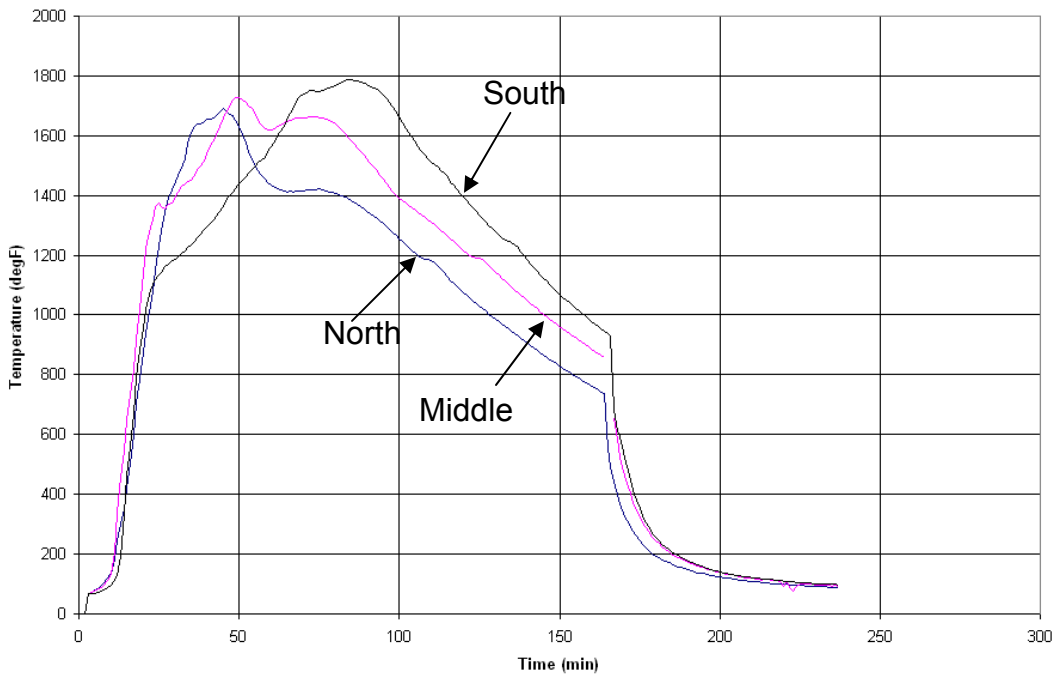


Figure 2.15  Primary beam web temperature distribution during the Cardington Office Demonstration test (British Steel, 1998)

41
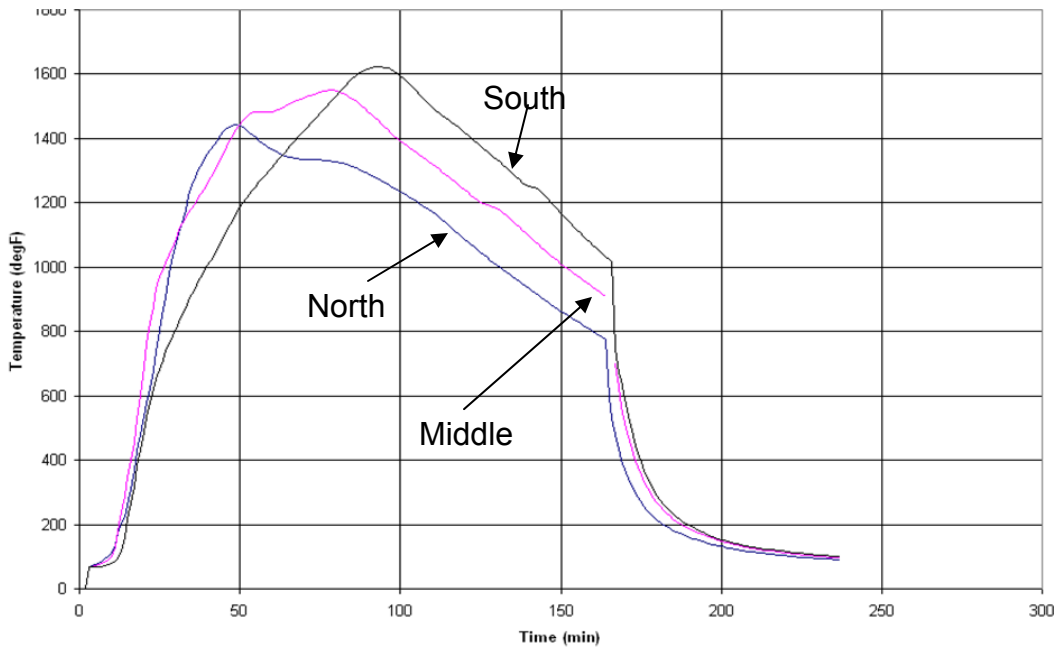
Figure 2.16  Primary beam top flange temperature distribution during the Cardington Office Demonstration test (British Steel, 1998)
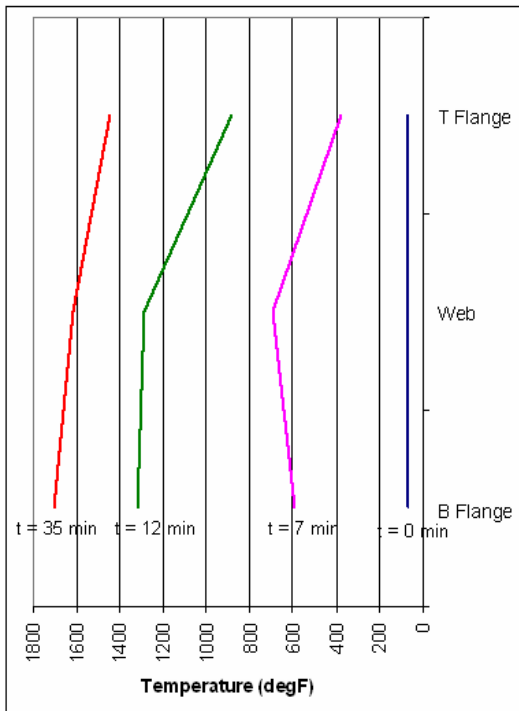


Figure 2.17  Primary beam temperature gradient during heating period of the Cardington Office Demonstration test (British Steel, 1998)
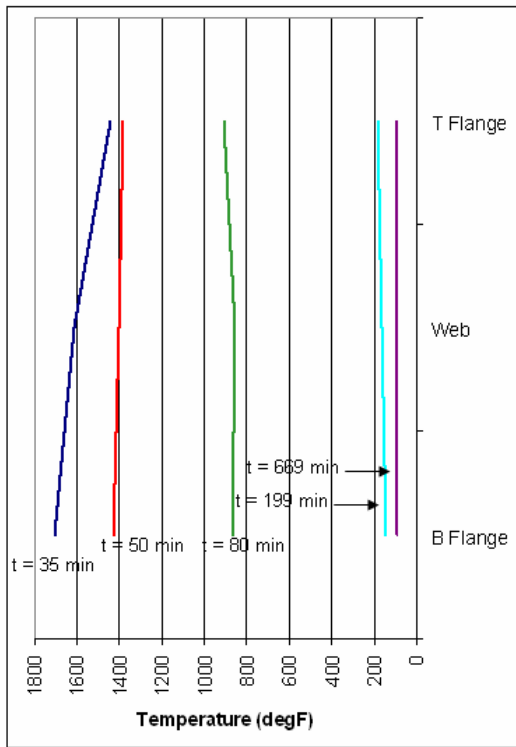
Figure 2.18 Primary beam temperature gradient during cooling period of the Cardington Office Demonstration test (British Steel, 1998)
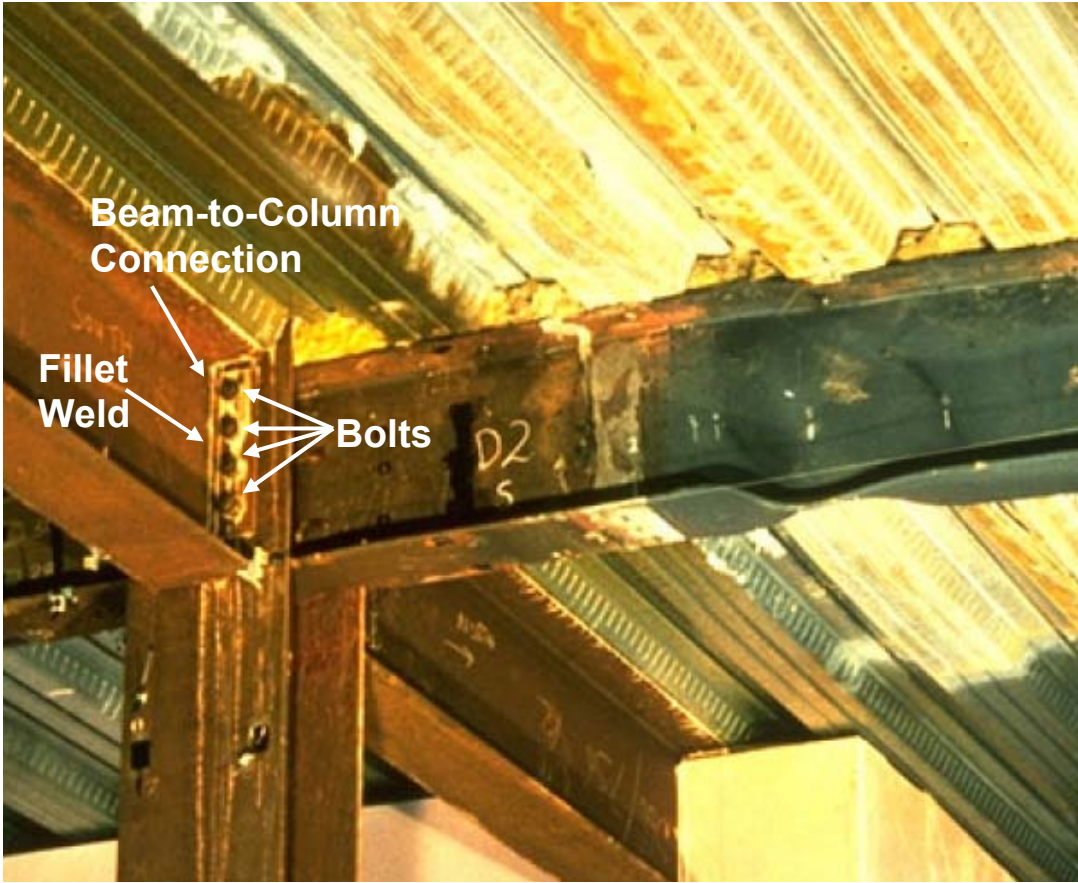
Figure 2.19  Photograph of typical beam-to-column connection used in the Cardington
Fire Tests (Newman, 2000)
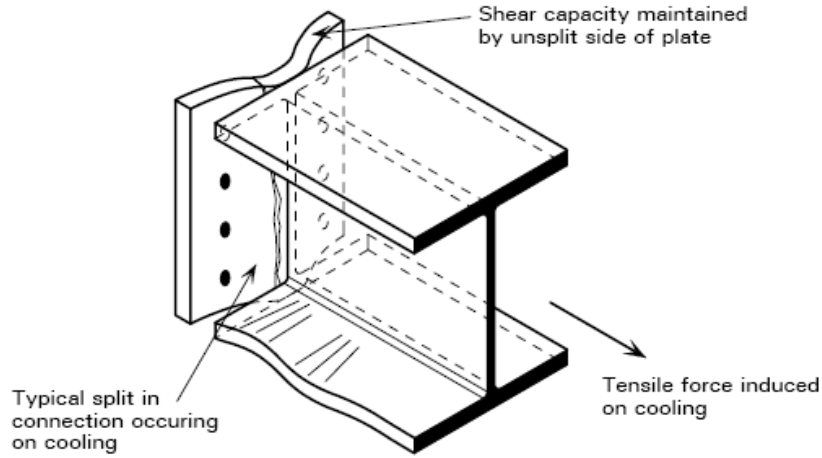
Figure 2.20  One of two failure modes observed in end plate connections during the Cardington tests (Newman, 2000)



Figure 2.21  Failure of the fin-plate on the shear tab connection in British Steel Test 2 (Newman, 2000)
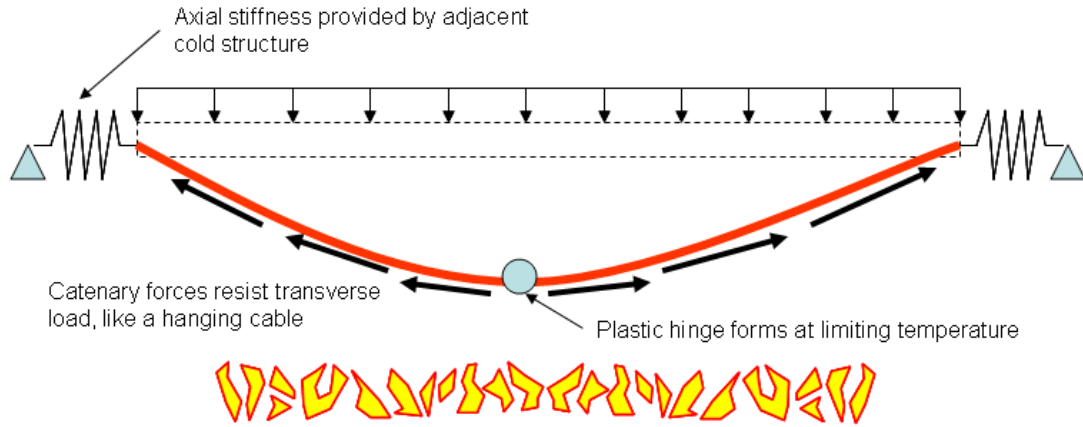
Figure 2.22  Illustration of catenary action (Catella, 2008)
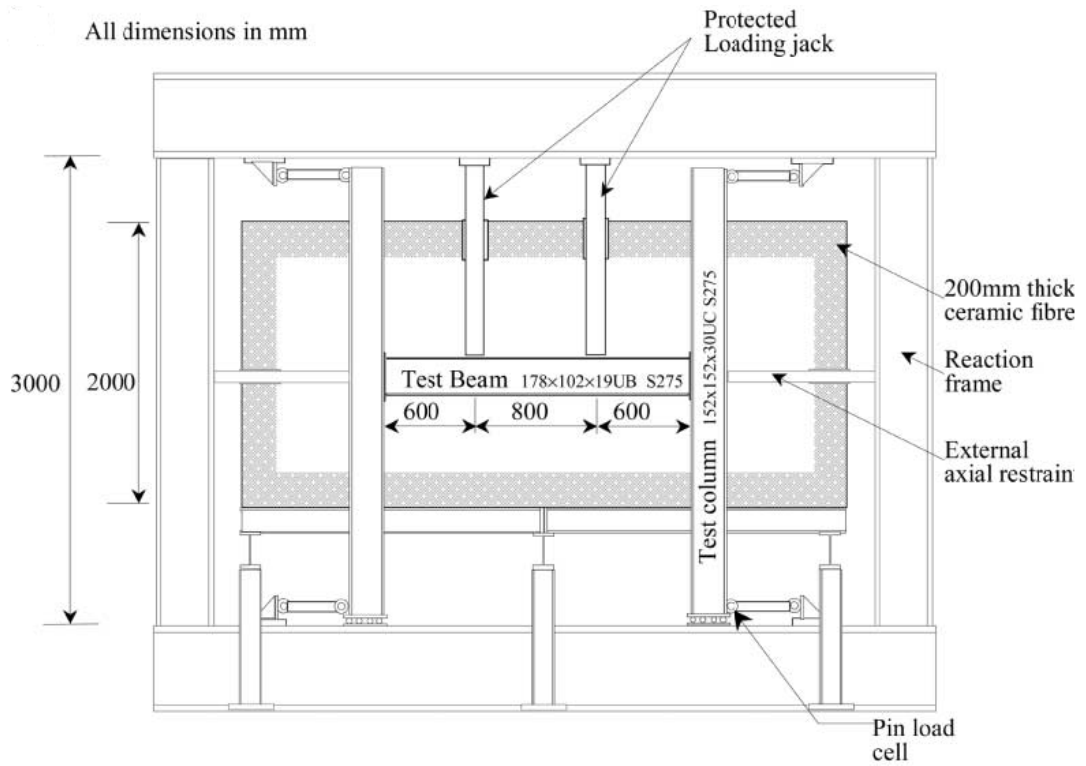


Figure 2.23  Elevation view of test setup for test program performed by Liu et al. (2002) [from Liu et al. (2002)]
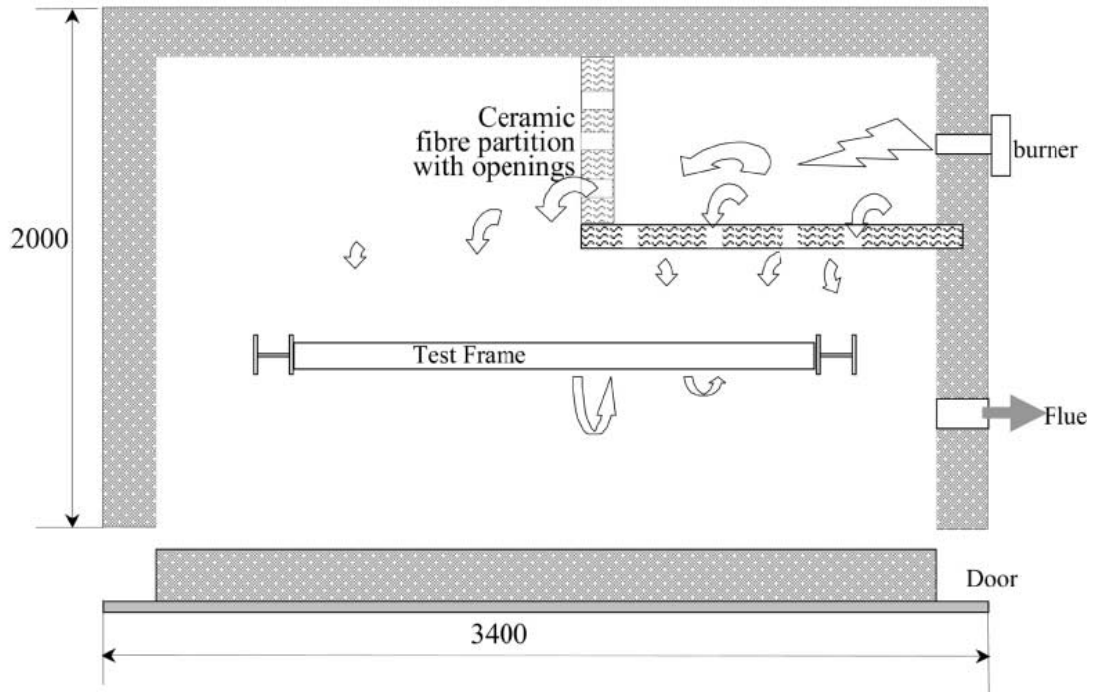
Figure 2.24  Plan view of furnace for test program performed by Liu et al. (2002) [from Liu et al. (2002)]
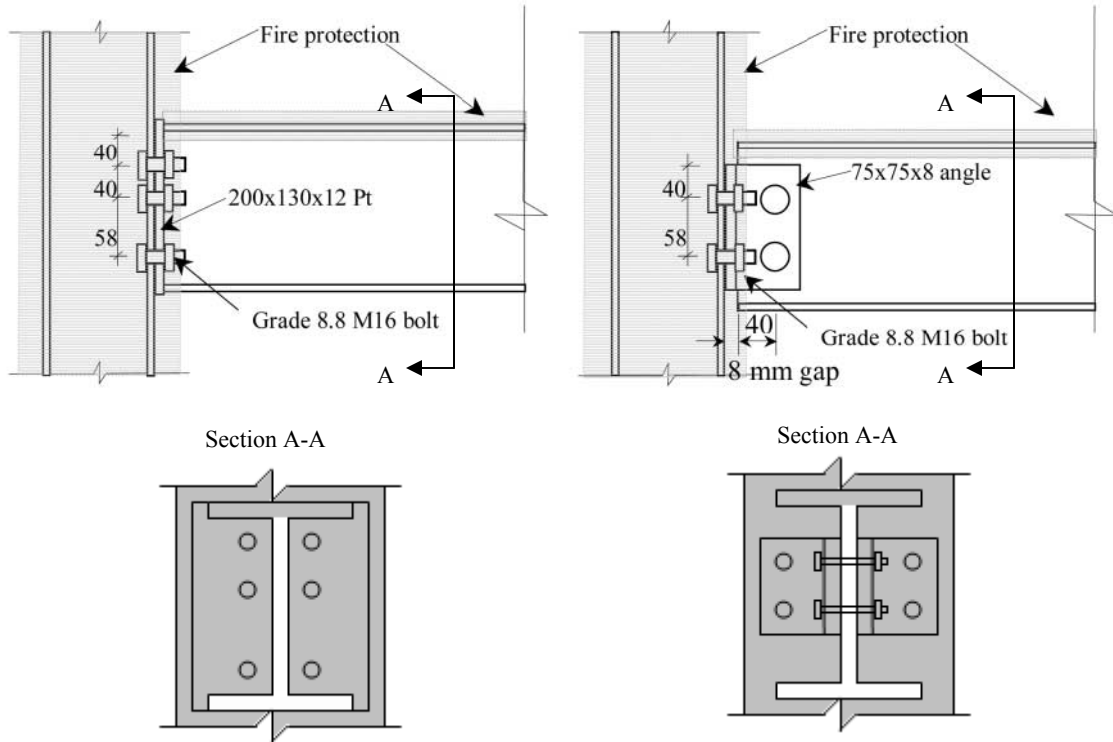
Figure 2.25 Flush end-plate (left) and web-cleated (right) connections used in tests by Liu et al. (2002) [from Liu et al. (2002)]
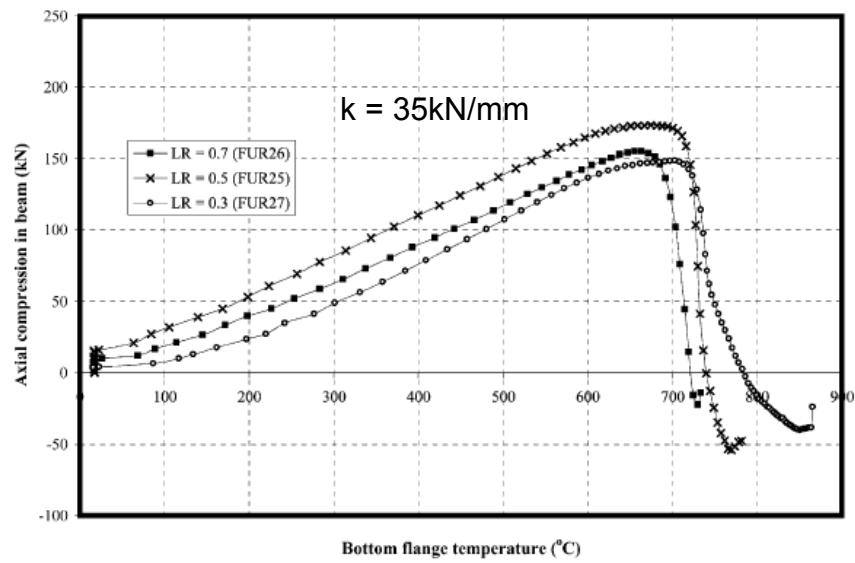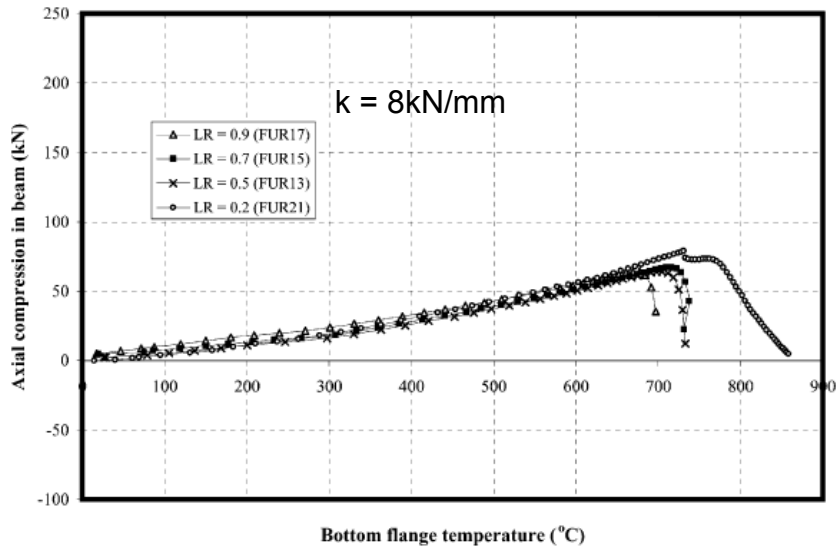
Figure 2.26  Measured axial compression force in beam from test results from Liu et al. (2002)
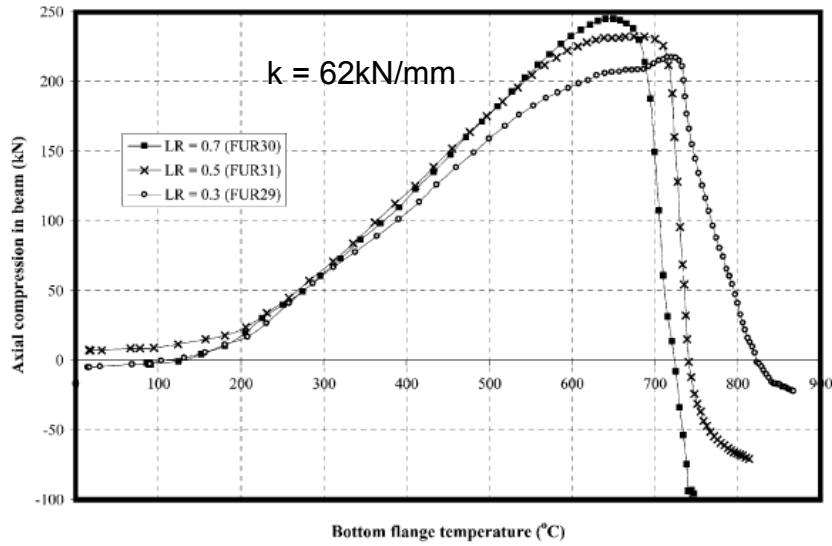
(c)
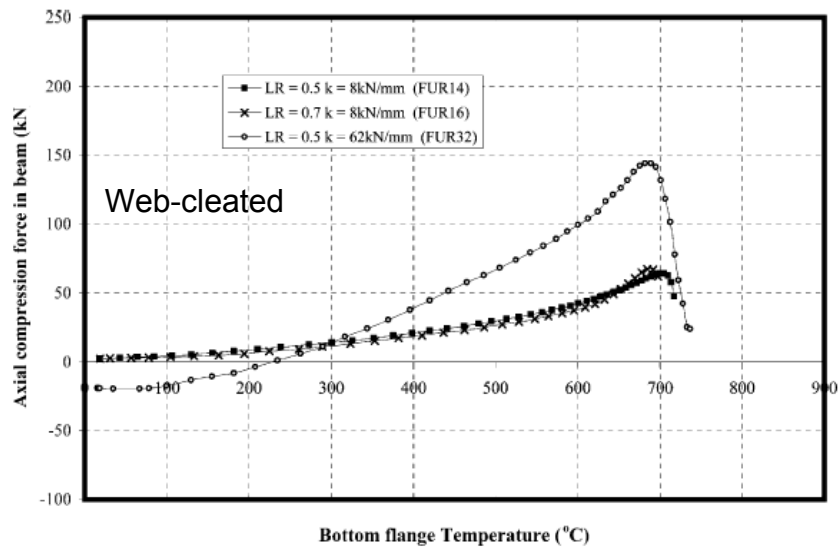


(d)

Figure 2.26  (Cont'd) Measured axial compression force in beam from test results from Liu et al. (2002) (a) k = 8 kN/mm (b) k = 35 kN/mm (c) k = 62 kN/mm (d) Web-cleated [from Liu et al. (2002)]

Figure 2.27  Setup used in test performed by Yu (2006) [from Yu (2006)]
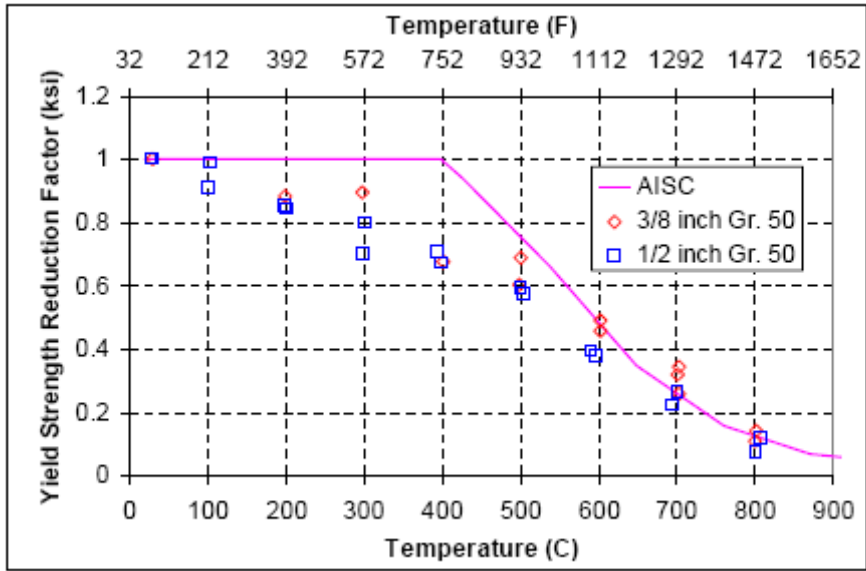
(a)
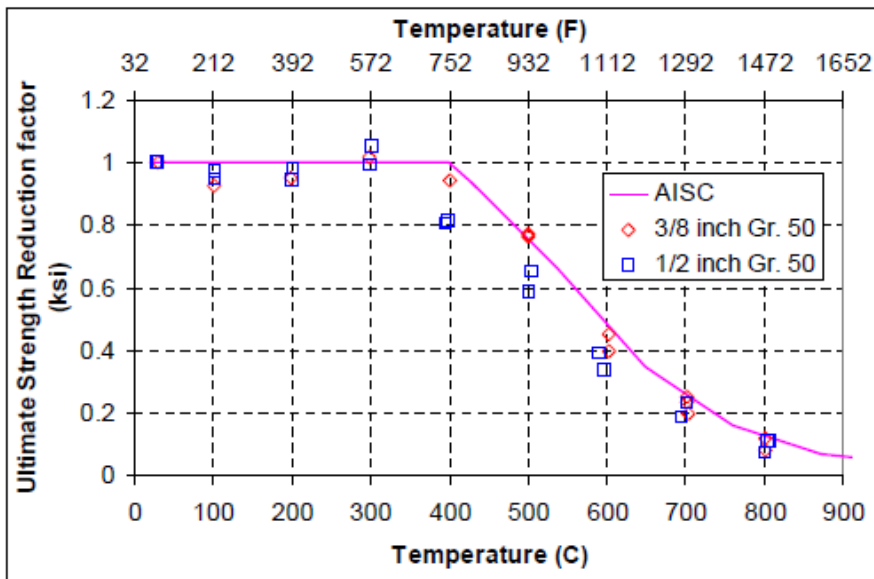


(b)

Figure 2.28 Comparison of results from tests performed by Yu (2006) to AISC (2001) for (a) yield strength (b) ultimate strength [from Yu (2006)]

52
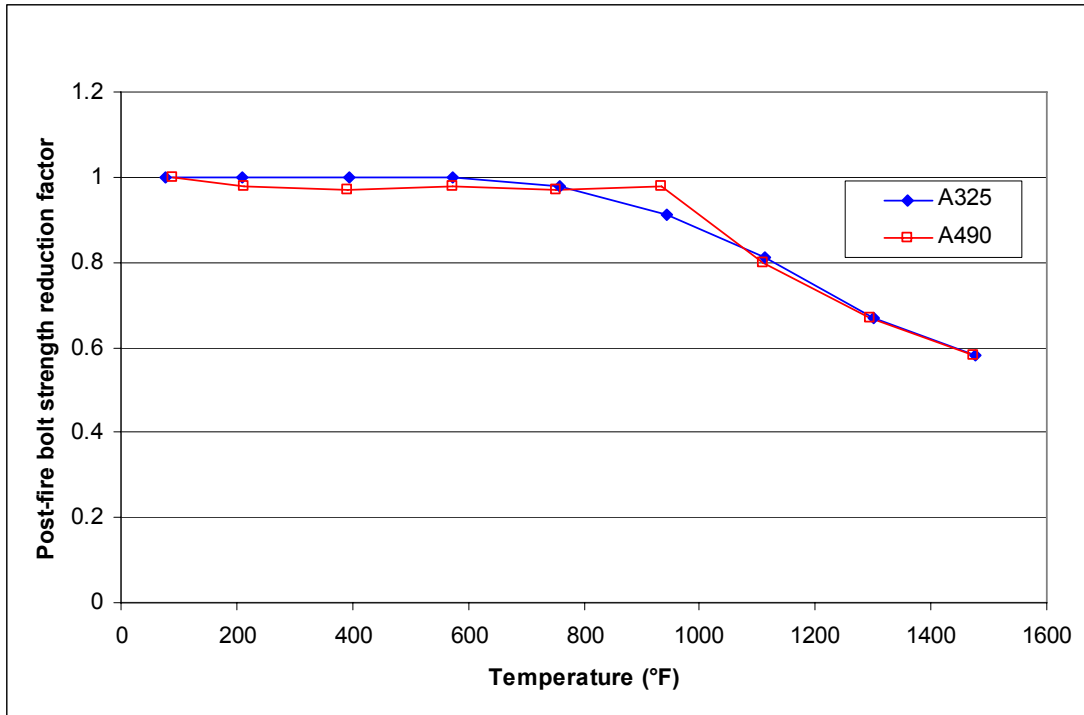
Figure 2.29  Reduction factors for post-fire bolt strength from tests performed by Yu (2006)
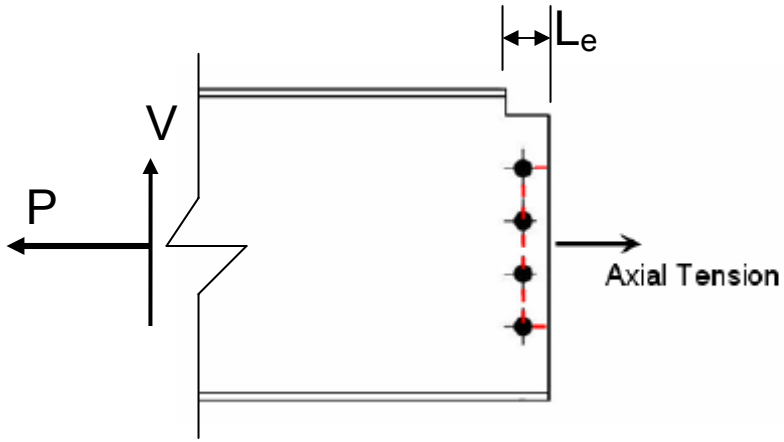
(a)
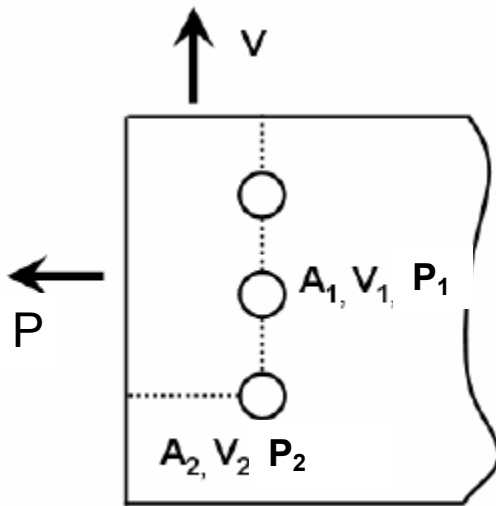


(b)

Figure 2.30  Block shear under (a) axial tension (Yu, 2006) (b) orthogonal forces (Yu, 2006) [from Yu (2006)]

**Shear Tab Connection**

**Thermocouples on bolts and welds**
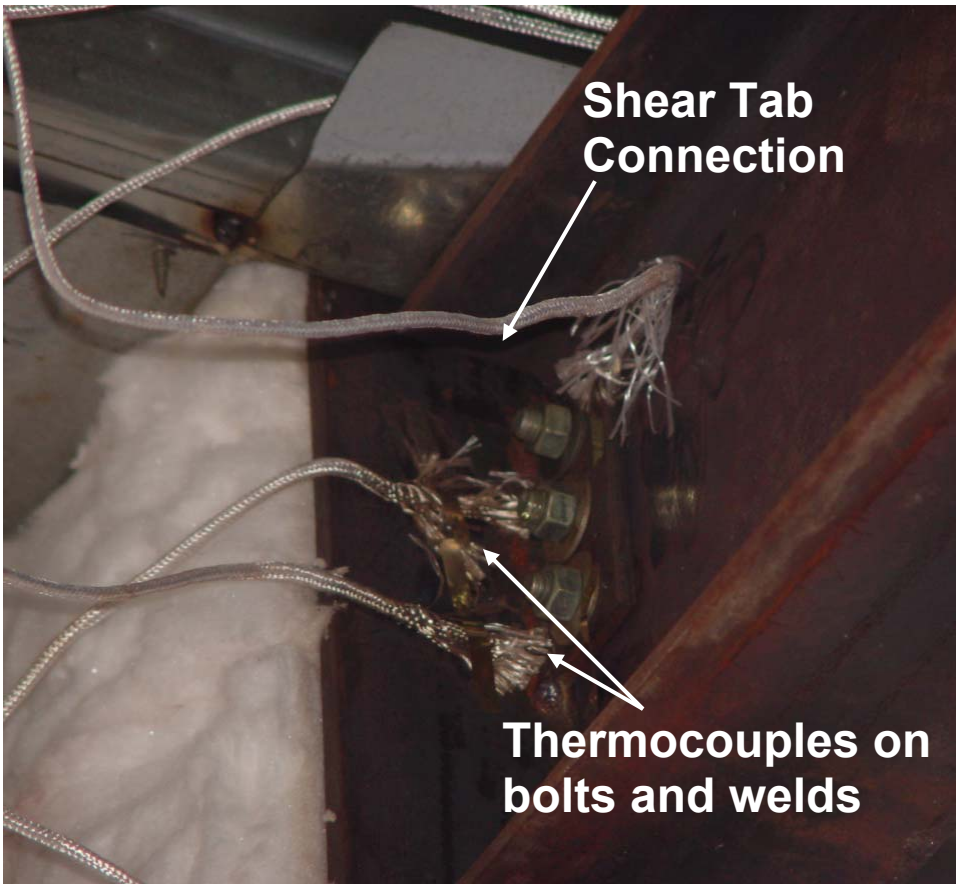
Figure 2.31  Photograph of unprotected shear tab connection (Catella, 2008)
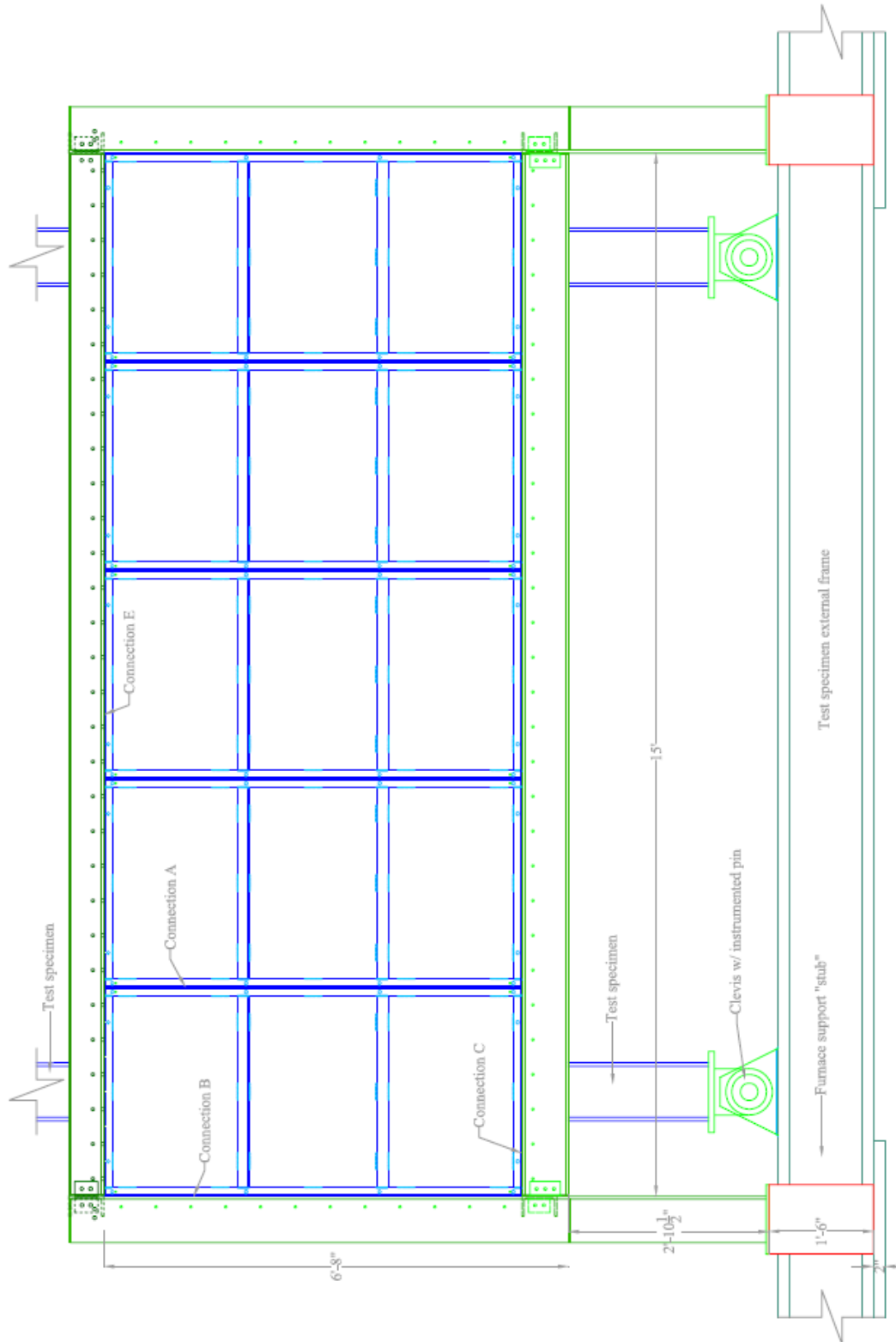
Figure 2.32  Front view of assembled furnace [from Catella (2008)]

56
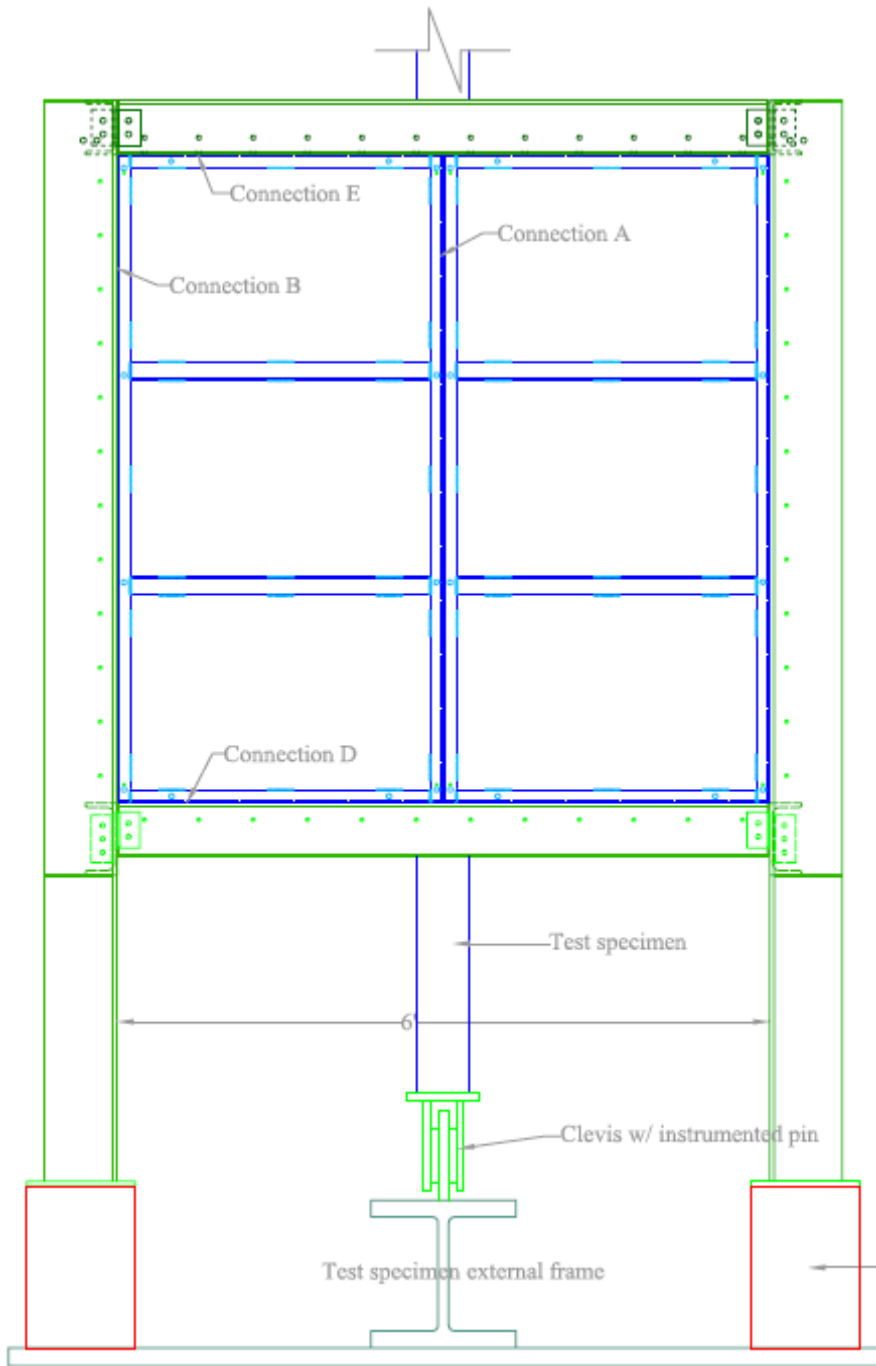
Figure 2.33  Side view of assembled furnace [from Catella (2008)]
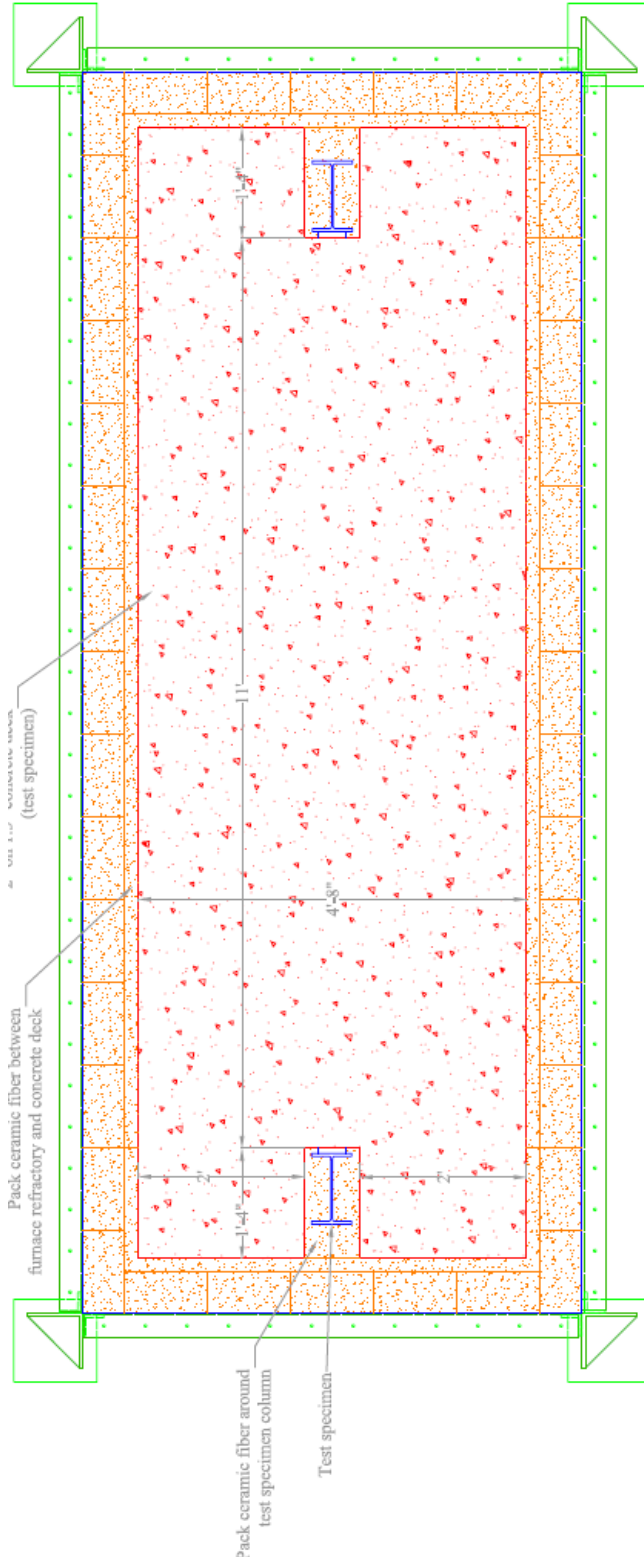
Figure 2.34  Top view of assembled furnace (Catella, 2008)
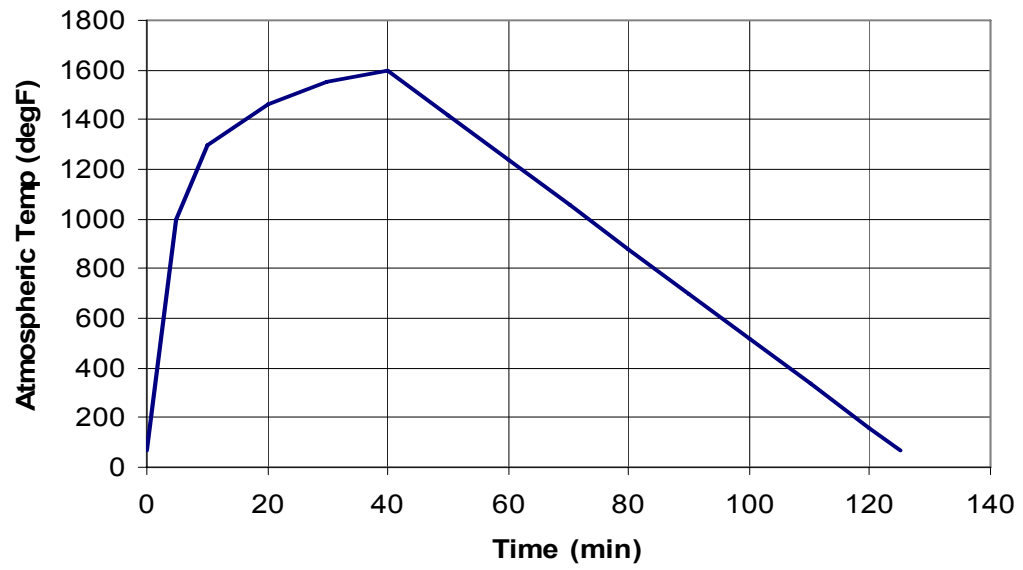
Figure 2.35  Time-temperature curve for the high temperature furnace assessment
test/structural fire test of steel shear tab connections [from Catella (2008)]
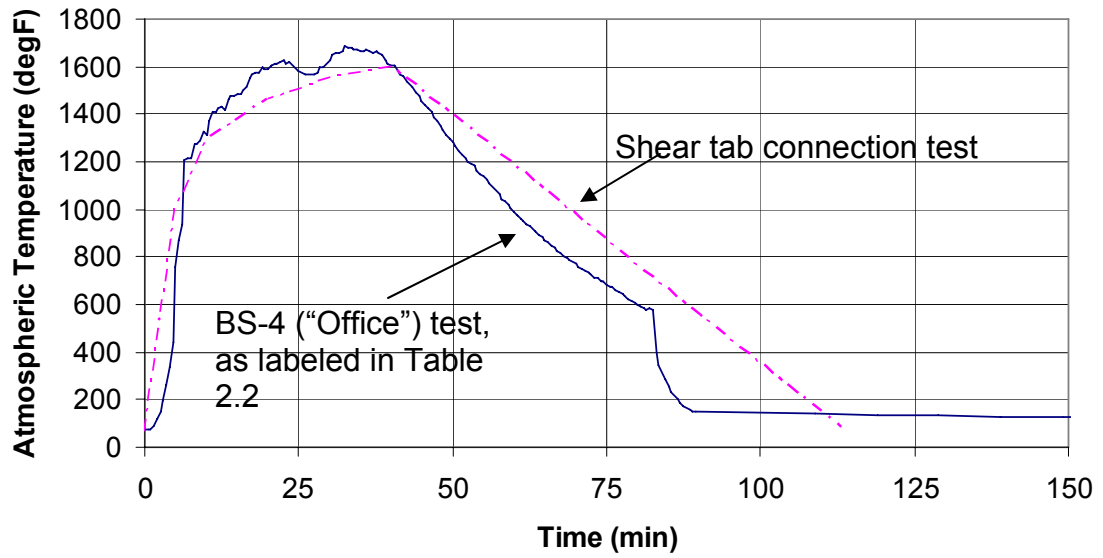
Figure 2.36 Comparison of between atmospheric temperatures recorded in the British Steel-4 test, as listed in Table 2.2, also referred to as the "Office" test performed at Cardington Labs and the proposed time-temperature curve for the structural fire test of a shear tab connection (Catella, 2008)
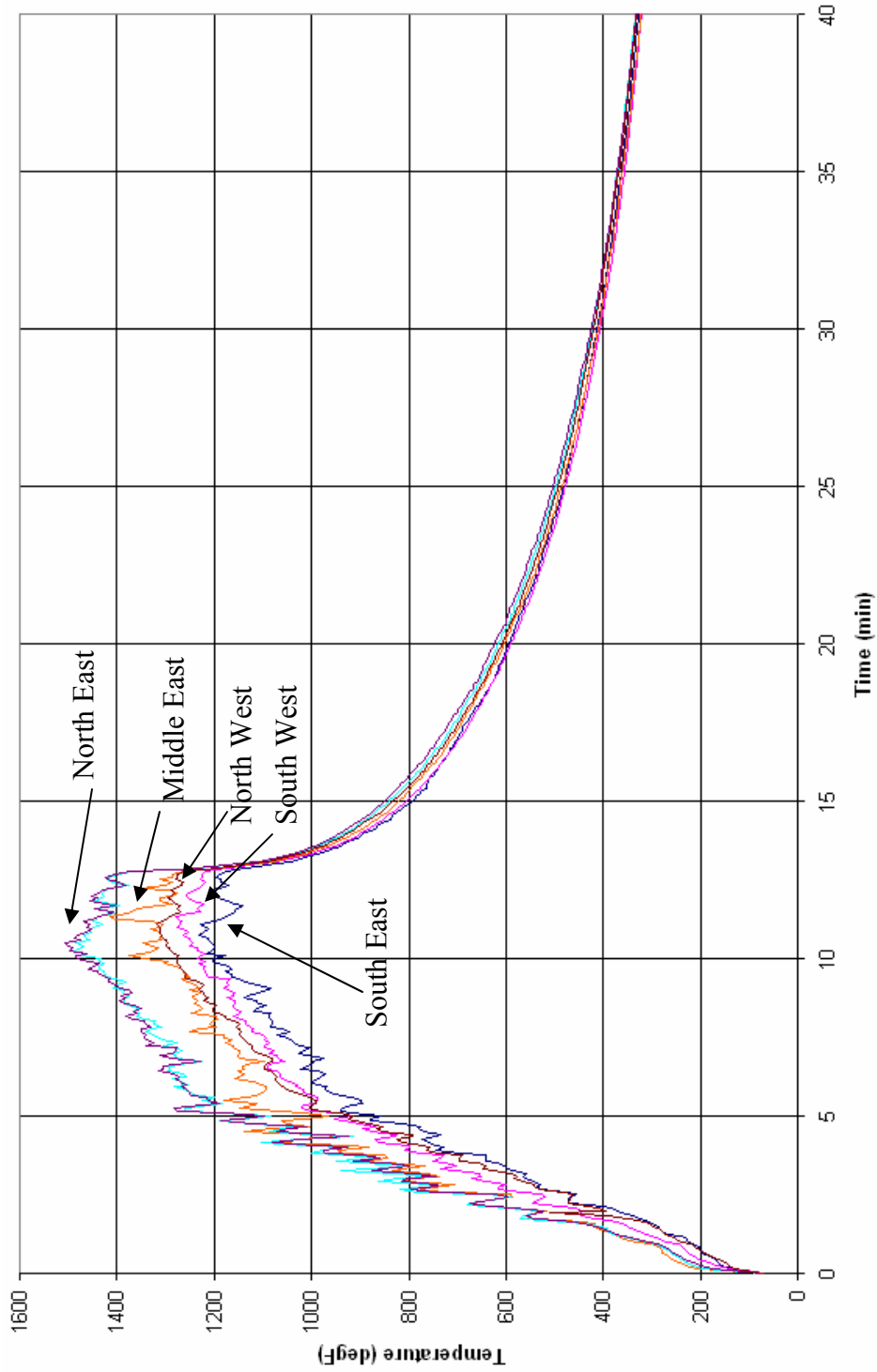
Figure 2.37  Atmospheric temperature distribution in the furnace for the high temperature shear tab connection test (Catella, 2008)

61
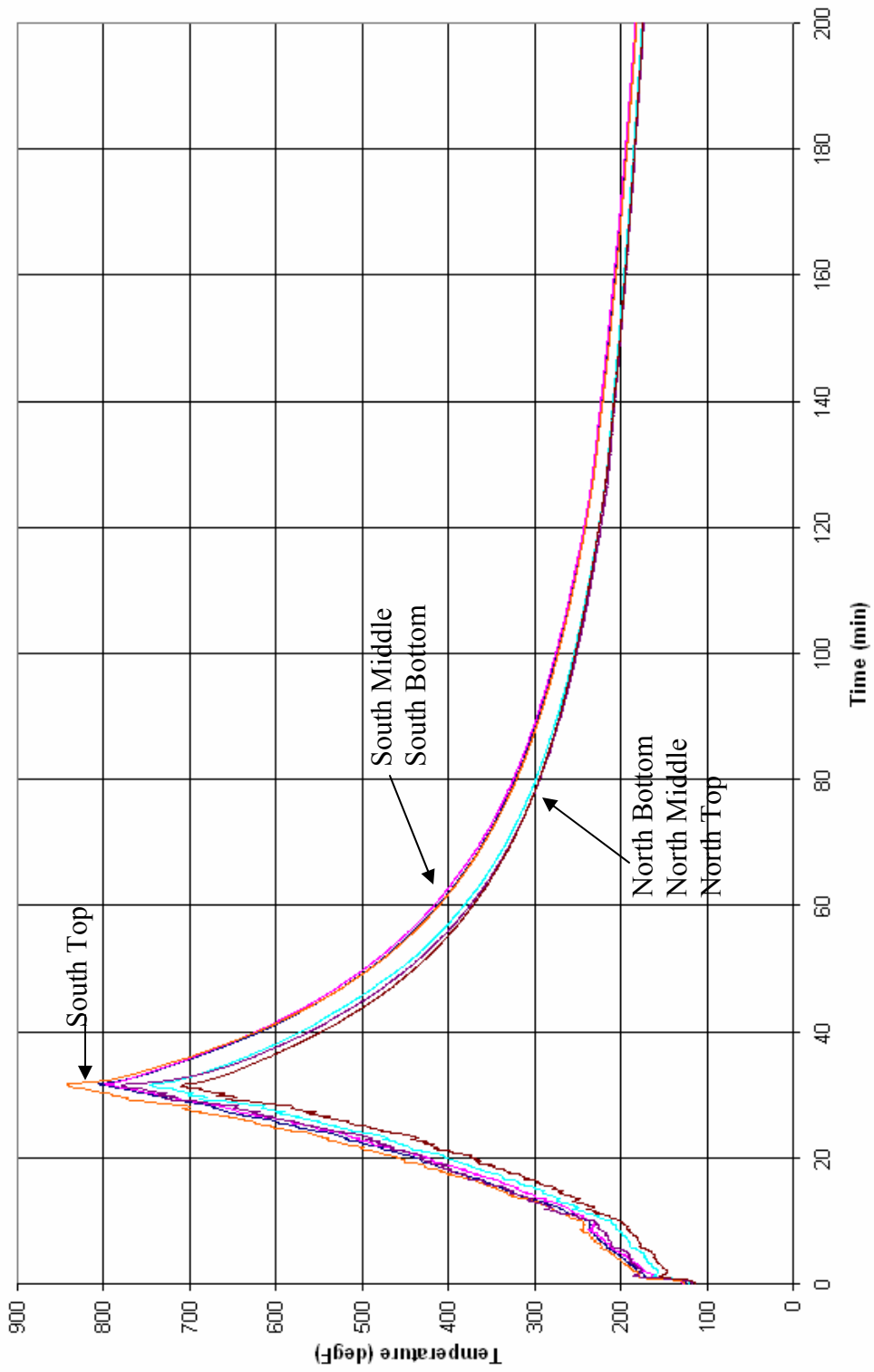
Figure 2.38  Temperatures of bolts used in each shear tab connection (Catella, 2008)
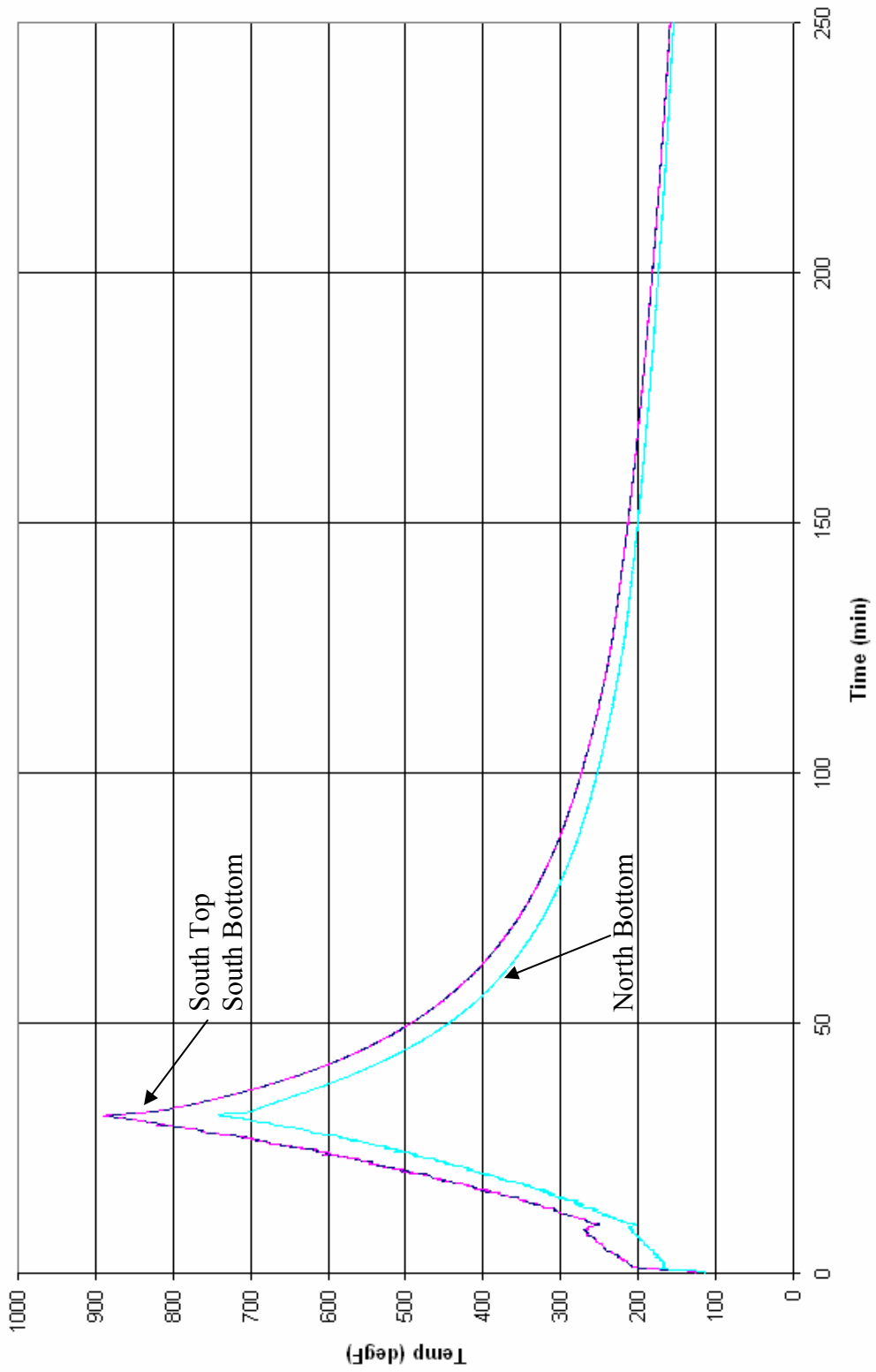
Figure 2.39  Temperatures of shear tab (base material) in each connection (Catella, 2008)
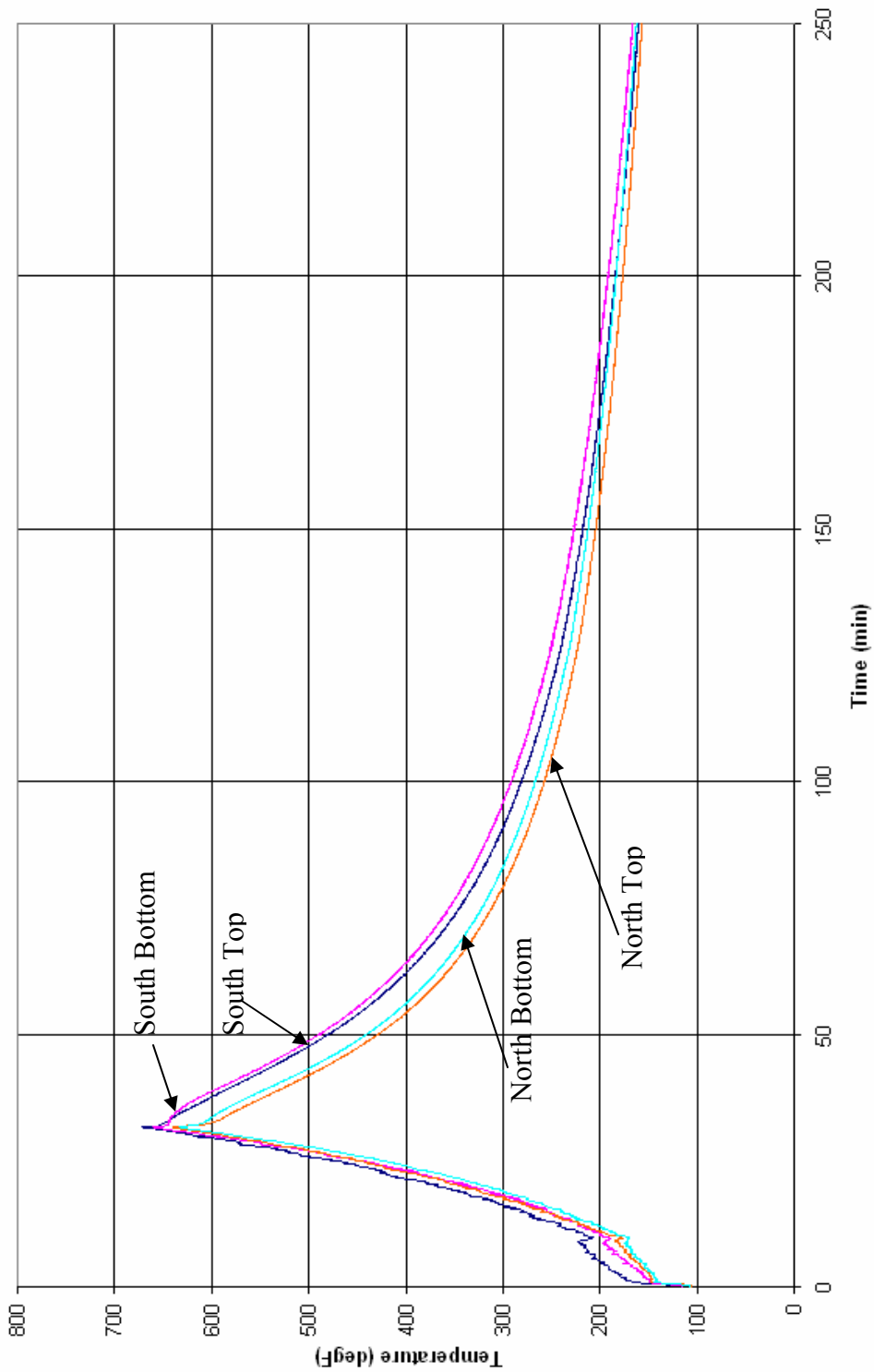
Figure 2.40  Temperatures of welds used in each shear tab connection (Catella, 2008)
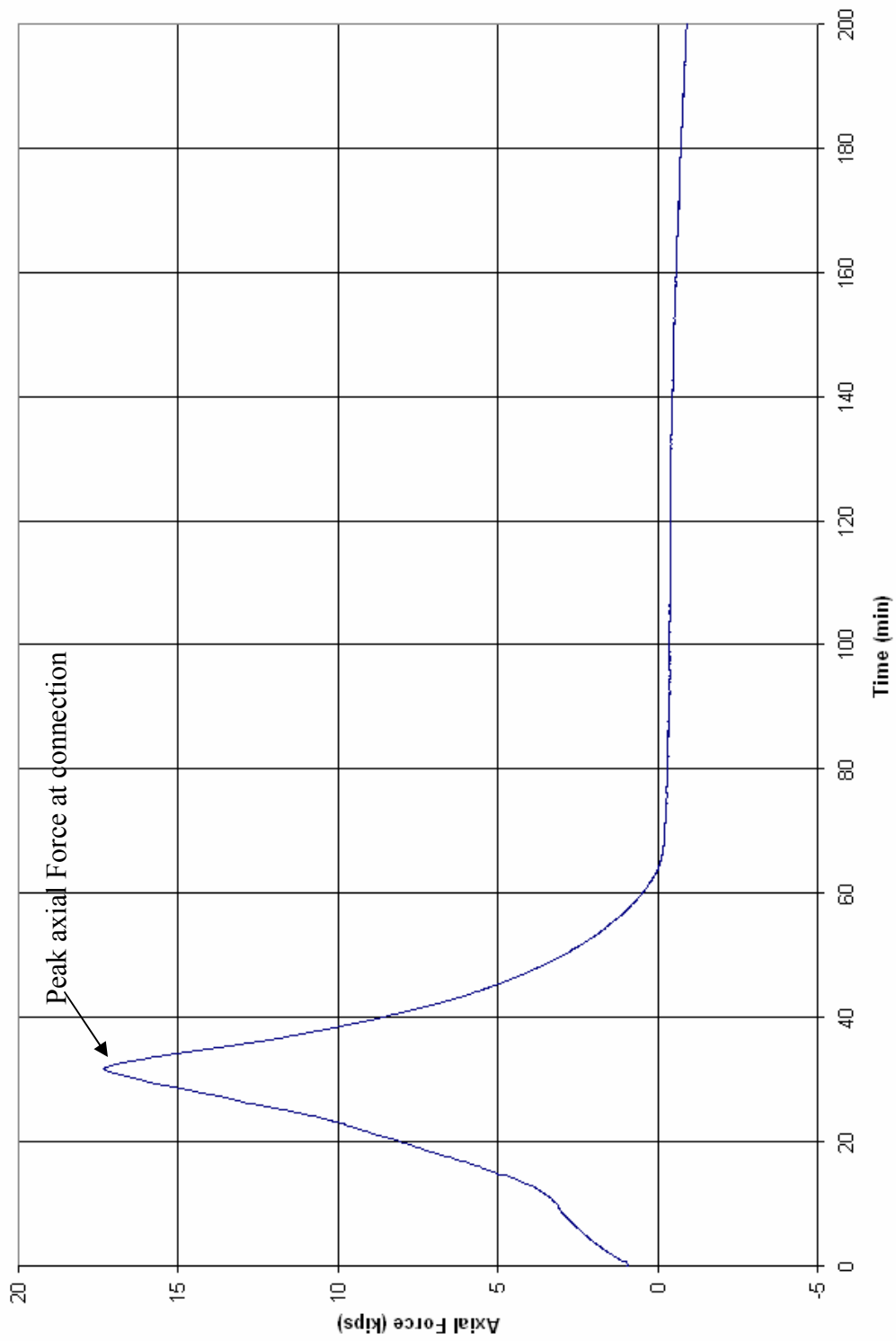
Figure 2.41  Axial force developed at the connections over the first 200 minutes of the structural fire test (Catella, 2008)
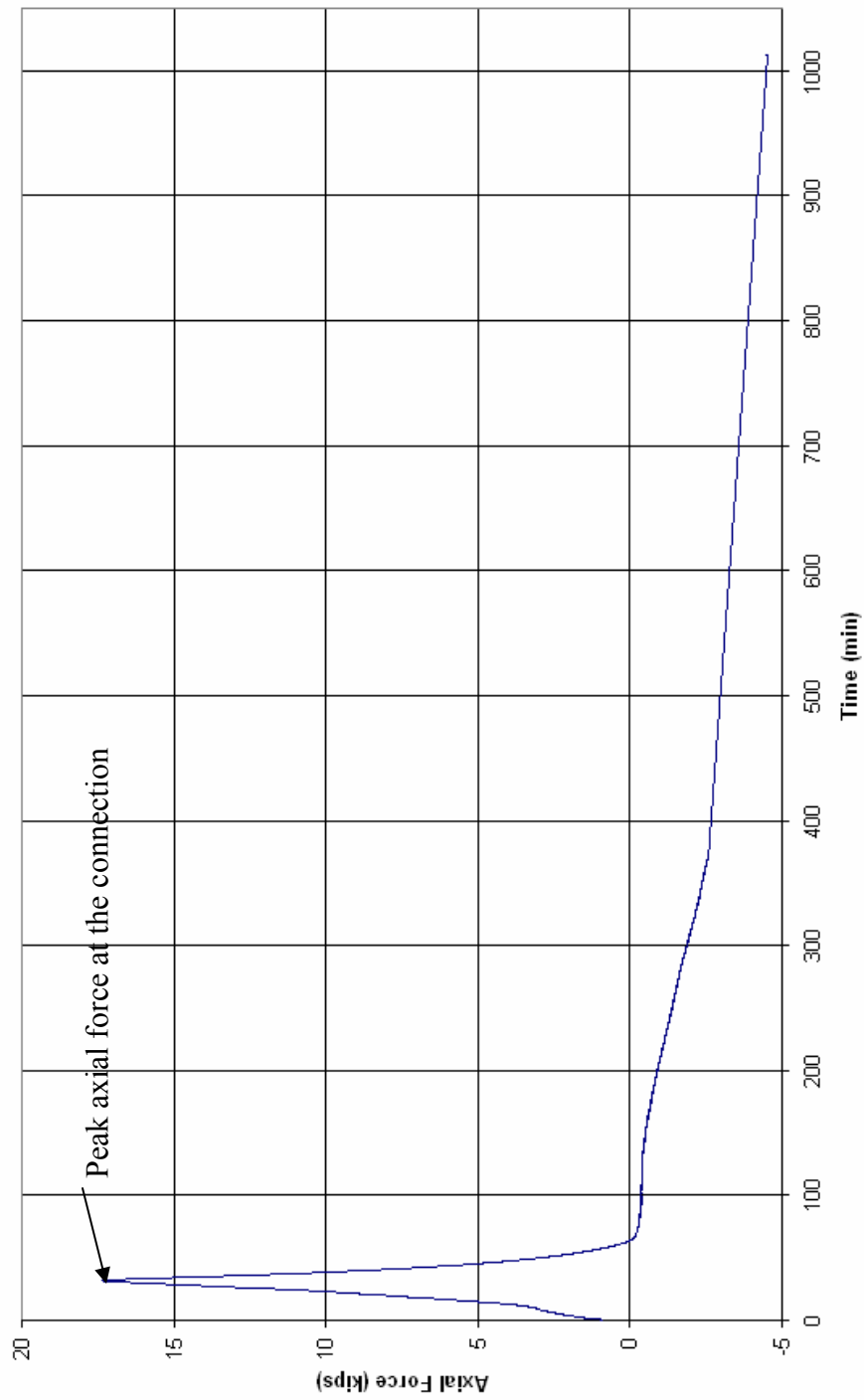
Figure 2.42  Axial force developed at the connections over the entirety of the test
(Catella, 2008)
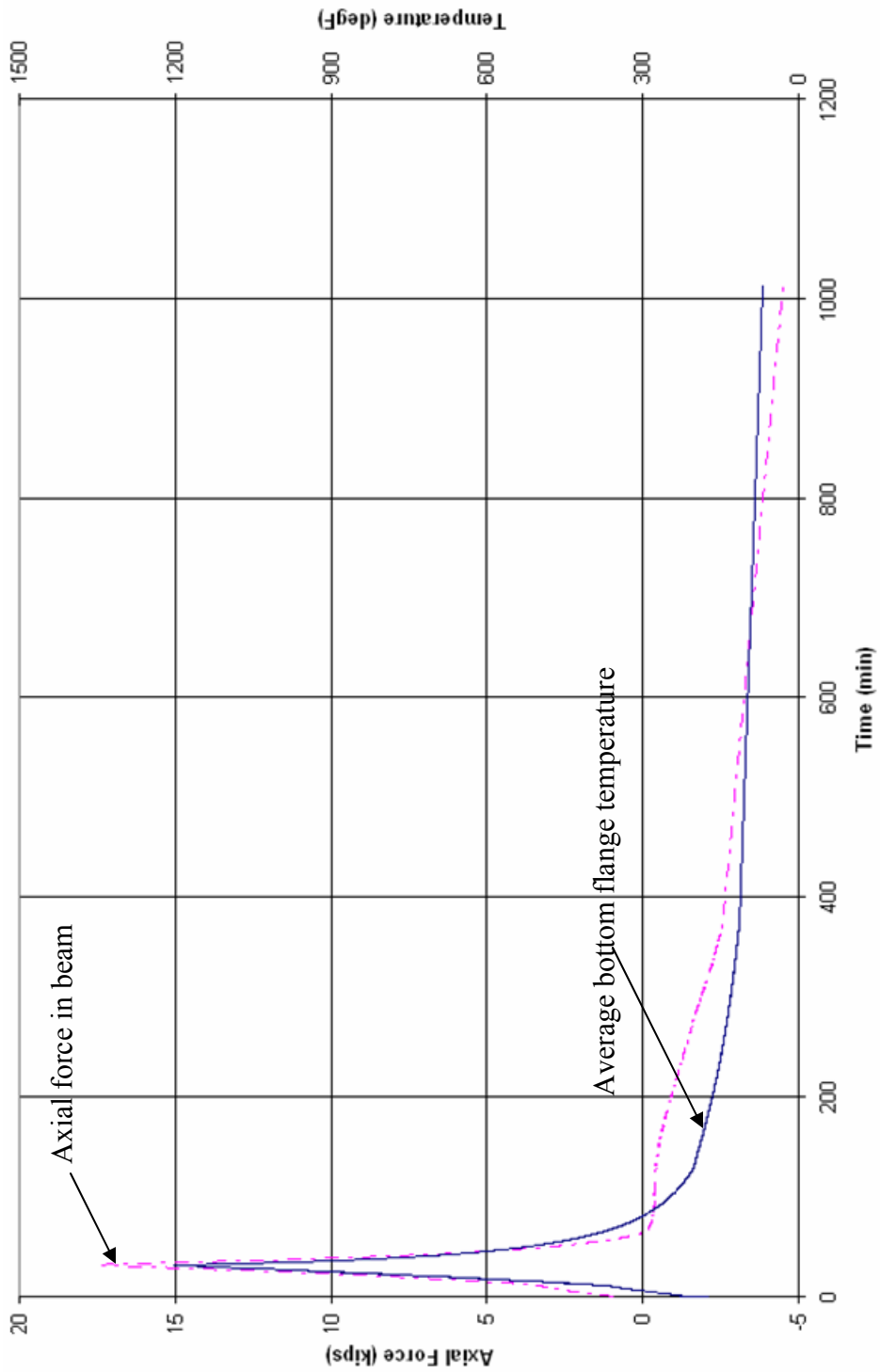
Figure 2.43  Axial force and average bottom flange temperature plotted over the entirety of the test (Catella, 2008)
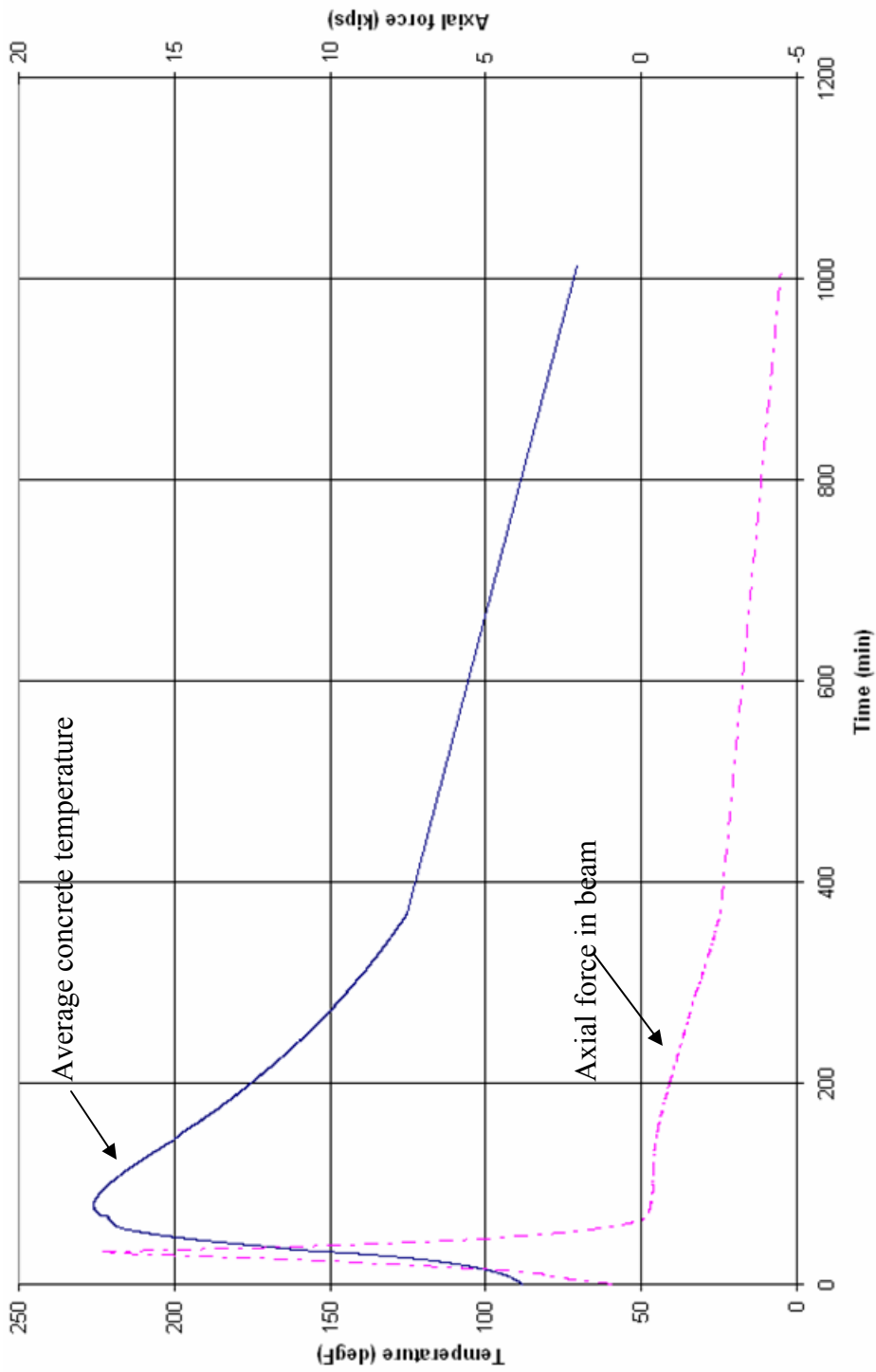
Figure 2.44  Axial force and average concrete deck temperature plotted over the entirety of the test (Catella, 2008)

68
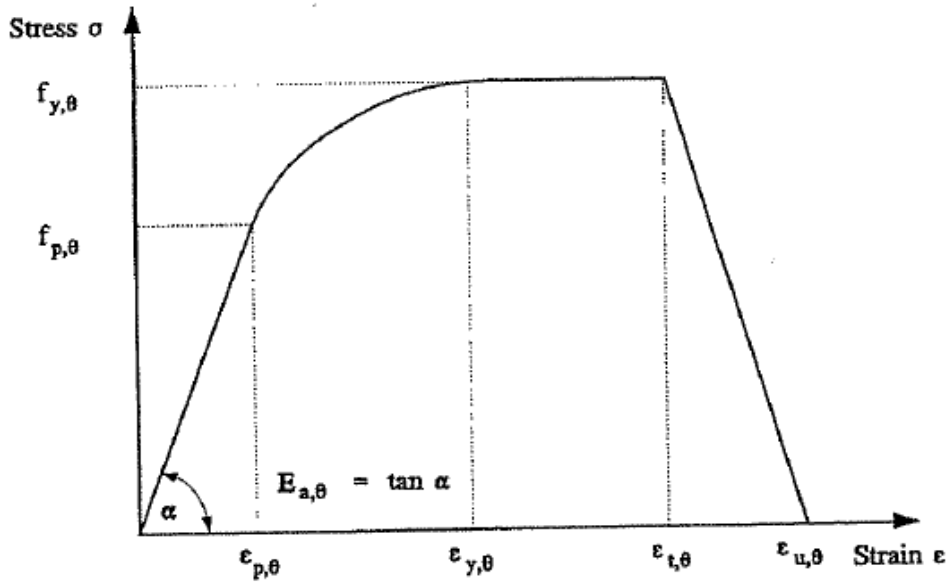
Figure 2.45 Stress-strain relationship for steel at elevated temperatures (EC3, 1995)
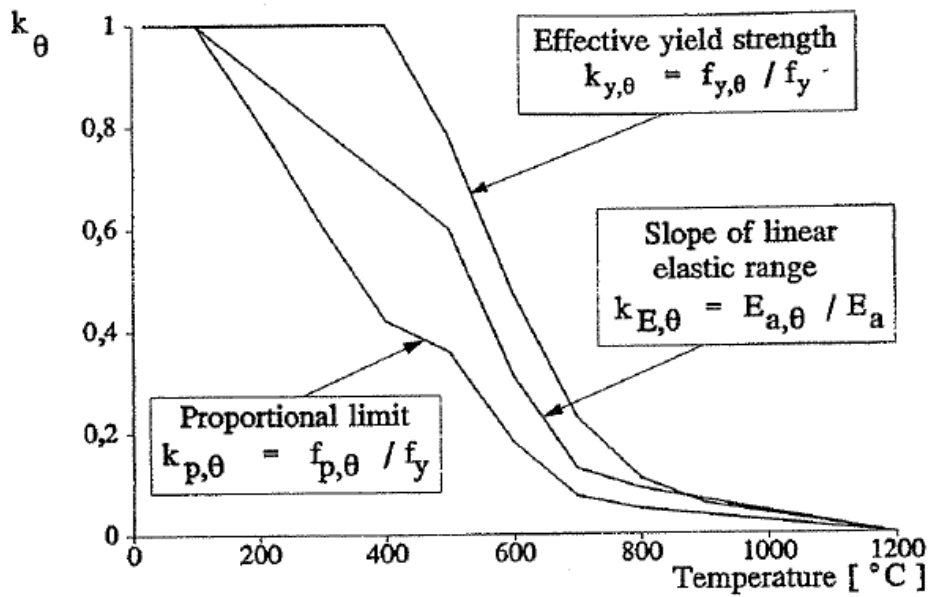


Figure 2.46 Reduction factors for the stress-strain relationship of steel at elevated temperatures (EC3, 1995)
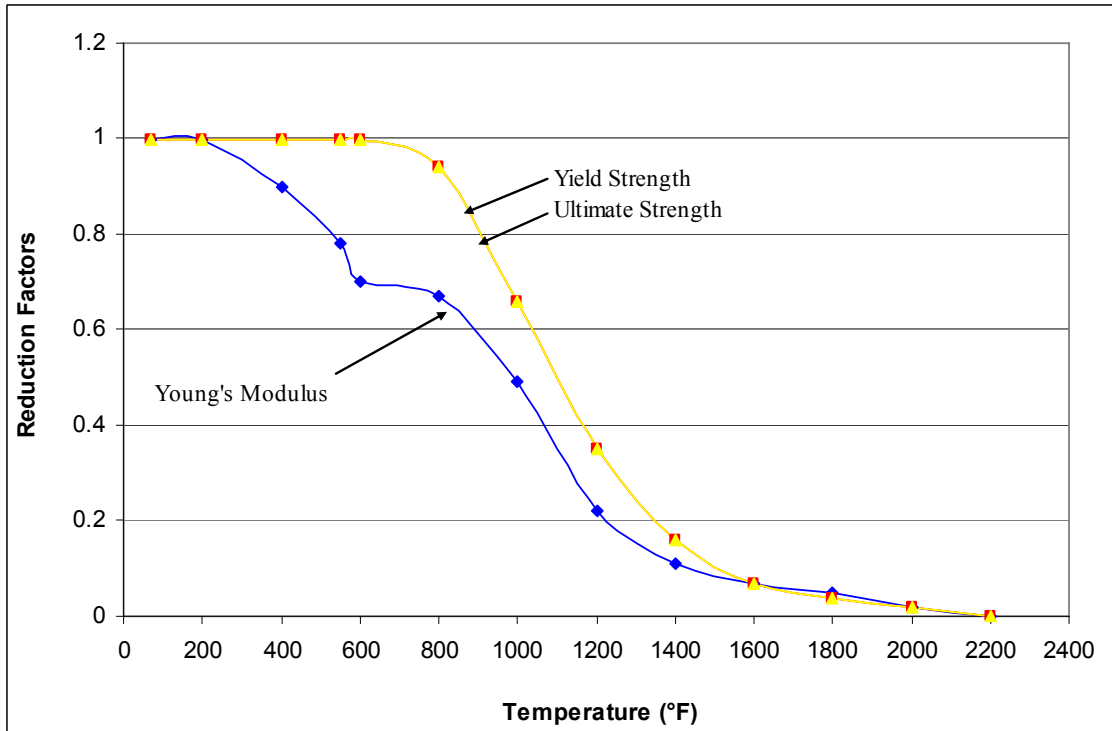
Figure 2.47  AISC reduction factors for Young's modulus, yield strength, and ultimate strength of steel at elevated temperatures (AISC, 2005)
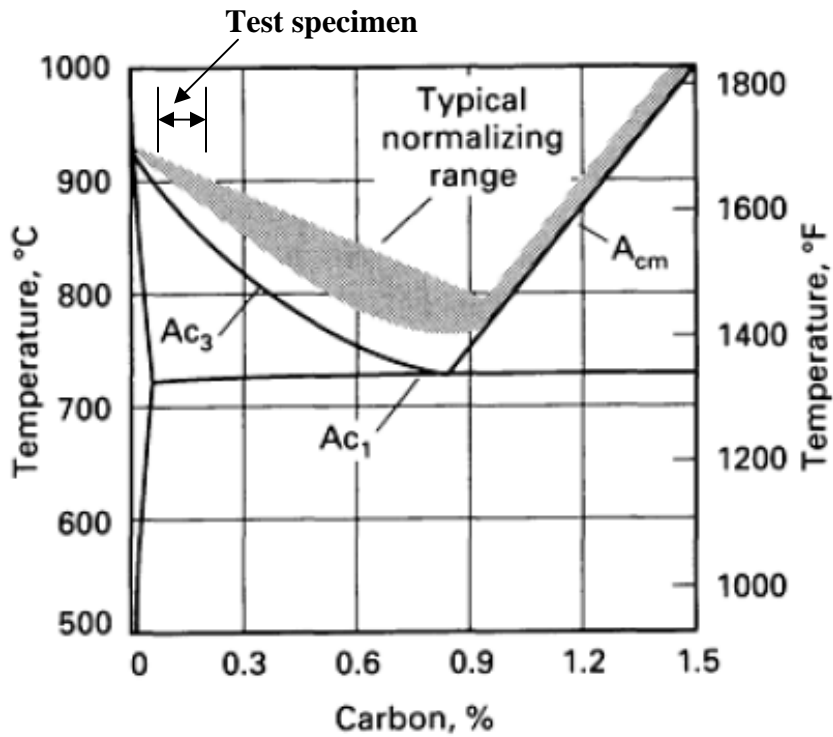
Figure 2.48  Partial iron-iron carbide phase diagram showing typical normalizing range for plain carbon steels (ASM, 2002)
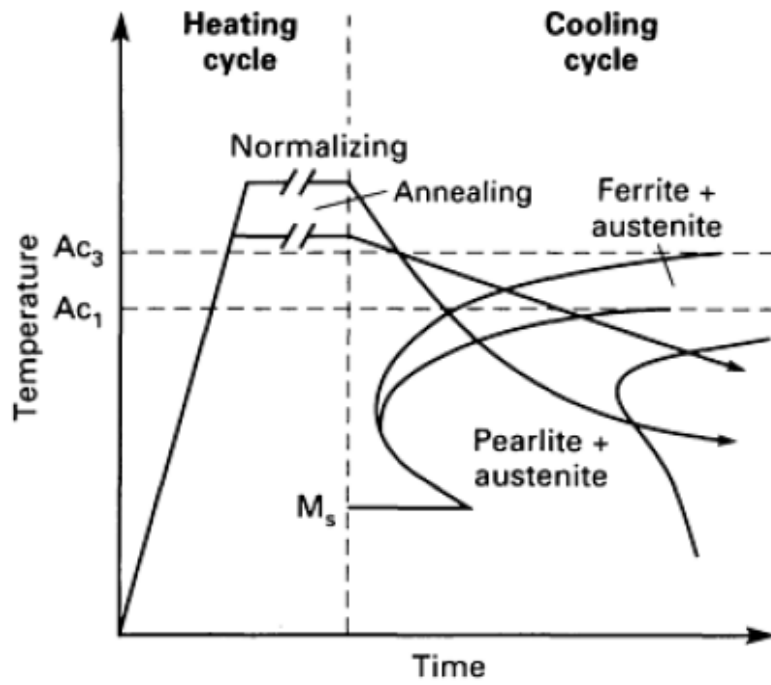
Figure 2.49 Comparison of time-temperature cycles for normalizing and full annealing (ASM, 2002)
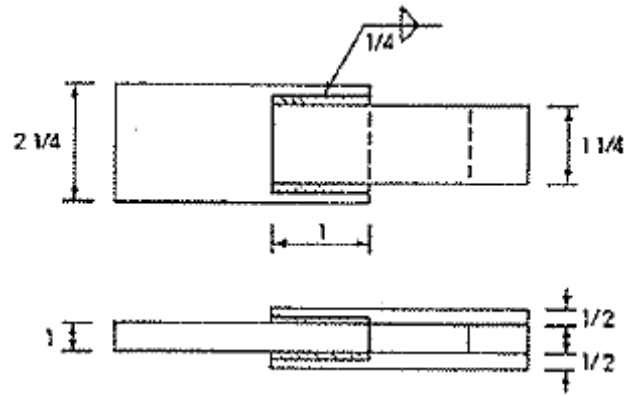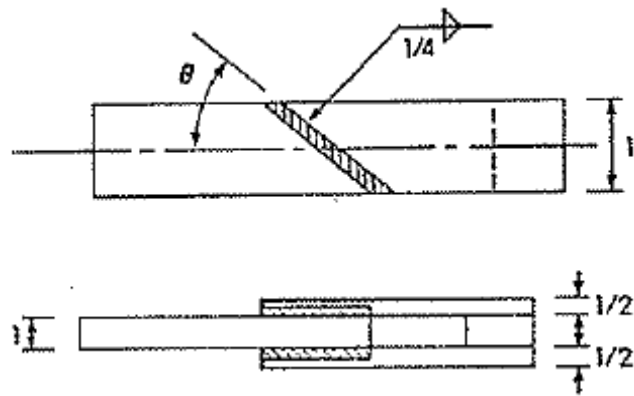
Figure 2.50  Diagram of the coupons tested (a) Longitudinal weld (b) Inclined weld angle
(Butler and Kulak, 1971)
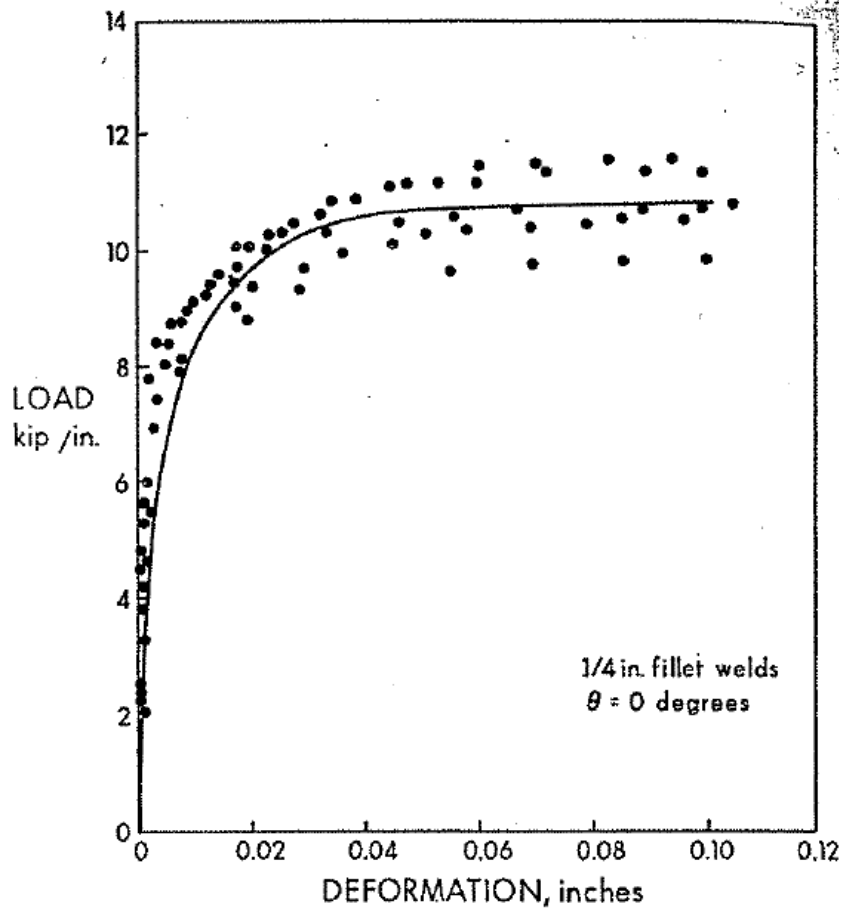
Figure 2.51  Load-deformation response of the longitudinal fillet weld (Butler and Kulak, 1971)
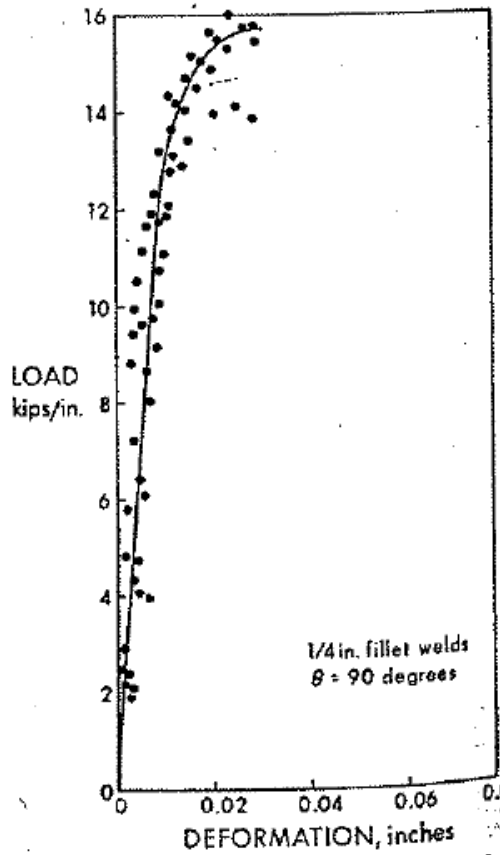
Figure 2.52  Load-deformation response of the transverse fillet weld (Butler and Kulak, 1971)

| θ, degrees | 0 | 30 | 60 | 90 |
|---|---|---|---|---|
| $R_{ult}$, kips/in | 10.9 | 14.6 | 15.4 | 15.7 |
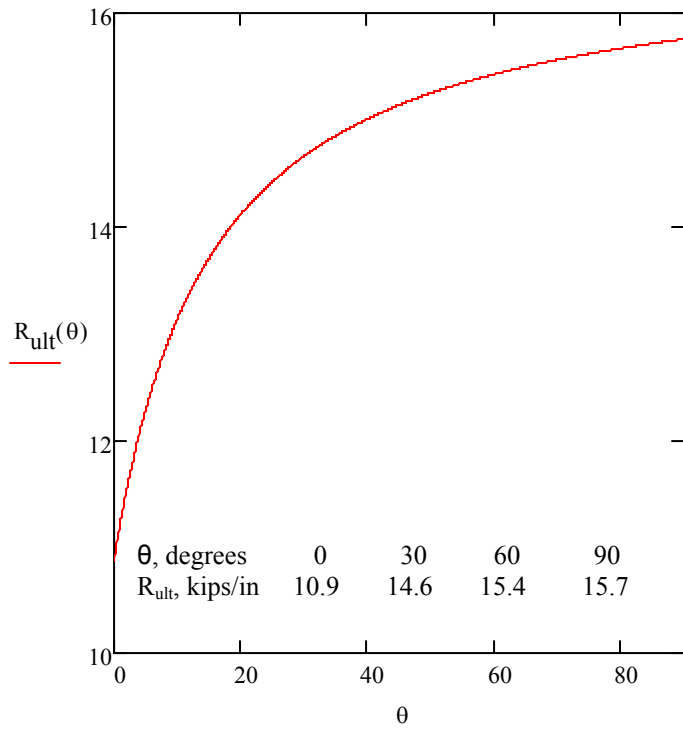
Figure 2.53  Ultimate load vs. weld angle (Butler and Kulak, 1971)



| θ, degrees | 0 | 30 | 60 | 90 |
|---|---|---|---|---|
| $\Delta_{max}$, in | 0.105 | 0.042 | 0.031 | 0.026 |
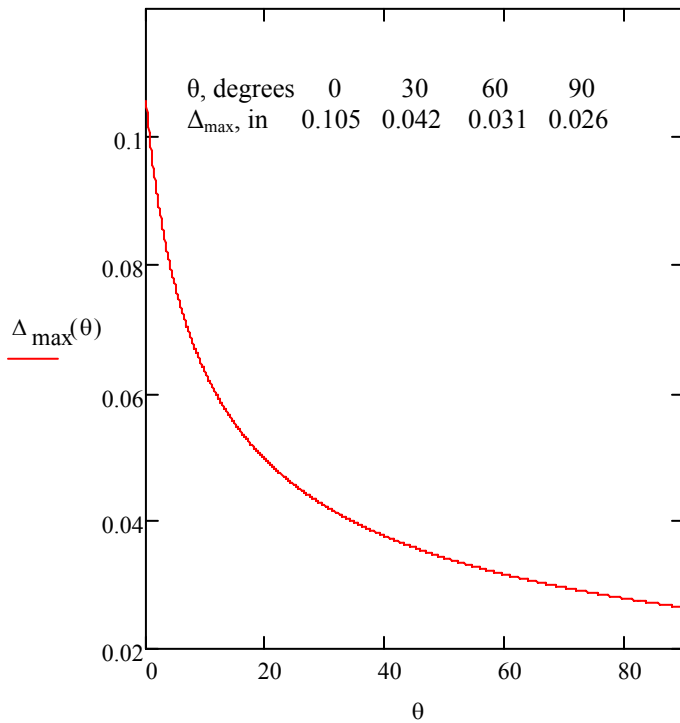
Figure 2.54  Maximum deformation vs. weld angle (Butler and Kulak, 1971)
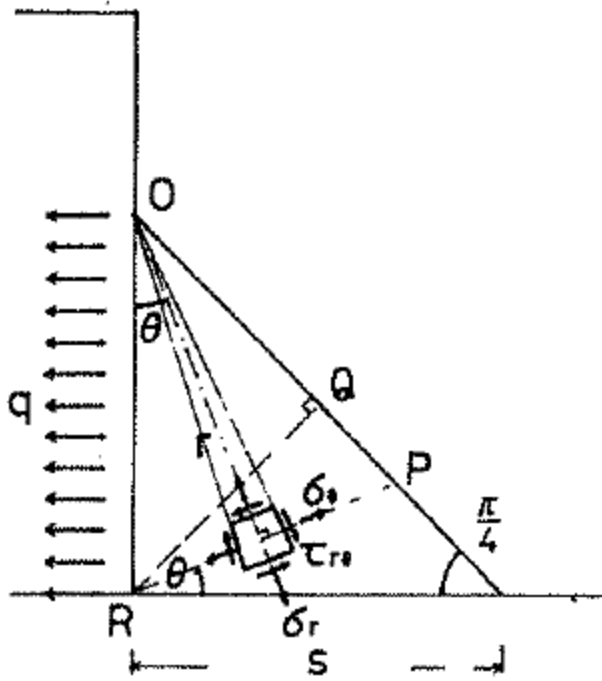
Figure 2.55  Transverse fillet weld for approximate approach from theory of elasticity (Kato and Morita, 1974)

**Chapter 3     Test Program**

**3.1     General**
This chapter presents the program utilized to conduct the tests for this research. A test matrix is first defined. The design of the test specimen is discussed. The test set-up is then outlined. The materials used for the tests are then presented. The test protocol and procedure are then described.

**3.2     Test Matrix**
All test specimens involved E71-T8 electrode, with the welding performed using the flux core arc welding (FCAW) procedure. Details about the weld metal are given in Section 3.6.2.

A test matrix was developed using a limited number of specimens to obtain the most meaningful results. Once the testing was complete, it was important to be able to develop relationships for weld strength over a wide range of elevated temperatures. It was also important to be able to fully understand the behavior of the weld at different stages in the cooling process. A test matrix was required for both the tests at elevated temperatures and for the post-fire tests that were performed. It is important to note that the tests done for both the elevated temperature and post-fire scenario tests were constant temperature tests, which means that the temperature was increased or decreased to the desired test temperature and held, and then load was applied until failure of the specimen occurred.

**3.2.1     Elevated Temperature Tests**
The test matrix for the elevated temperature tests is given in Table 3.1. The specimen was first tested at ambient temperature, 70°F, so that the results could be normalized to room temperature. The normalization of results will be discussed in further detail in Chapter 5. All subsequent specimens were heated until the desired temperature was achieved and the temperature was held for 40 minutes, as will be discussed in the test protocol in Section 3.8.

The elevated temperature tests consisted of 10 specimens. Temperature was the only parameter during these tests, and the temperature was systematically varied. The temperatures tested were 70°F, 350°F, 600°F, 700°F, 800°F, 900°F, 1000°F, 1200°F, 1400°F, and 1600°F.

**3.2.2     Post-Fire Scenario Tests**
The test matrix for the post-fire scenario tests is shown in Table 3.2. The post-fire scenario tests comprised of heating each specimen to 1600°F and allowing them to cool to different temperatures before being tested. The heat treatment option used was annealing, or furnace cooling, which was discussed in Chapter 2. The first specimen tested was allowed to cool to ambient temperature before tension load was applied. The other specimens in the test matrix were allowed to cool to 1200°F, 1000°F, 800°F, and 600°F before being tested.

### 3.3    Test Specimen Design

The test specimen was designed in accordance with AISC (2005). Since the weld was of particular interest, the specimen was designed so that the weld would be the limiting failure mode at room temperature. A diagram of the test specimen is shown in Figure 3.1 and a photograph of the test specimen is shown in Figure 3.2. The test specimen consisted of the pull plates, lap plates, transverse welds on the top lap plates, and longitudinal welds on the bottom lap plates. Upon loading the specimen in tension, the transverse welds were intended to fail.

To accomplish the objectives of the test program, the design strength, $\phi Rn$, of the welds for the test specimen should be lower than that of the base material to ensure that the welds fail. For this design, the resistance factor, $\phi = 1.0$ due to the fact that failure was to be predicted as accurately as possible. The nominal design strength, Rn for welds according to ASIC Eqn. (J2-3) is:

$$Rn = Fw \cdot Aw \qquad\qquad (3.1)$$

For tension applied normal to the weld axis according to AISC Table J2.5,

$$Fw = 0.60 \cdot F_{EXX} \qquad\qquad (3.2)$$

where:

$F_w$ = nominal strength of the weld metal per unit area (ksi)
$A_w$ = effective area of the weld (in$^2$)
$F_{EXX}$ = electrode classification number (ksi)

The nominal ultimate strength of the weld, $F_{EXX}$, was equal to 70 ksi for the electrode type used in this testing. The material properties of the weld will be discussed in further detail in Section 3.6.2.

Transverse welds were used in this design as opposed to longitudinal welds. As discussed in Chapter 2, transverse welds experience an increase in strength and a decrease in ductility. When designing this specimen, this increase in strength was considered. To account for the increase in strength, the strength of the weld was multiplied by 1.5 as is required for a transverse weld according to AISC (2005).

Free body diagrams were drawn to compute the yield and ultimate loads of both the pull and lap plates. The limiting case of these was the yield of the pull plate. Equation 3.3 and Equation 3.4 show the yield and ultimate load of the lap plates, respectively:

$$P_{y\_lap} = 2 \cdot A_{g\_lap} \cdot F_{y\_lap} \qquad\qquad (3.3)$$
$$P_{U\_lap} = 2 \cdot A_{g\_lap} \cdot F_{U\_lap} \qquad\qquad (3.4)$$

where:

$P_{y\_lap}$ = yield load of the lap plate (kips)

$A_{g\_lap}$ = gross area of one lap plate, $t_{lap}$ * $w_{lap}$ (in$^2$)
$F_{y\_lap}$ = measured yield strength of the lap plate material (ksi)
$P_{U\_lap}$ = ultimate load of the lap plate (kips)
$F_{U\_lap}$ = measured ultimate strength of the lap plate material (ksi)
$t_{lap}$ = measured thickness of lap plate (in)
$w_{lap}$ = measured width of the lap plate (in)

Similarly, the equations for the yield and ultimate load of the pull plate are, respectively:

$$P_{y\_pull} = A_{g\_pull} \cdot F_{y\_pull} \tag{3.5}$$

$$P_{U\_pull} = A_{g\_pull} \cdot F_{U\_pull} \tag{3.6}$$

where:

$P_{y\_pull}$ = yield load of the pull plate (kips)
$A_{g\_pull}$ = gross area of pull plate = $t_{pull}$ * $w_{pull}$ (in$^2$)
$P_{U\_pull}$ = ultimate load of the pull plate (kips)
$F_{U\_pull}$ = measured ultimate strength of the pull plate material (ksi)
$t_{pull}$ = measured thickness of pull plate (in)
$w_{pull}$ = measured width of the pull plate (in)

From these equations, it was found that the strength of the transverse weld at ambient temperature could not exceed 74 kips, which was the yield strength of the pull plate. To determine the strength of the transverse weld, a free body diagram was sketched from which the following equation was developed:

$$P_{weld} = 2 \cdot (0.6 \cdot F_{EXX} \cdot t_e \cdot L) \cdot F \tag{3.7}$$

where:

$P_{weld}$ = strength of transverse weld (kips)
$t_e$ = 0.707 * measured weld size, a (in)
L = measured weld length (in)
F = factor for transverse weld = 1.5 (Note: F = 1.0 for longitudinal weld)

The nominal weld strength is 70 ksi; for the design 80 ksi was used to account for the fact that there is generally about a 10% increase in weld strength. The strength of the transverse weld at ambient temperature was 39.8 kips, therefore, it was determined that the weld would control the maximum load at ambient temperature. The design of the test specimens was done such that the weld would fail before the pull plate yielded at ambient temperature in the hopes that at an elevated temperature the weld would fail. Although the reduction in material properties and strength of steel at elevated temperatures is known, as discussed in Chapter 2, there is no data on strength reduction of weld metal at elevated temperatures. It was a concern that the material properties of the weld metal would not deteriorate as quickly as the base metal at elevated temperatures, causing a different failure mode, such as yield of the pull plate. Hence a conservative design with a capacity of 39.8 kips at room temperature was used, which was 54% of the pull plate yield strength at yield strength.

80

The design of the plates was controlled by the interior diameter of the furnace, as shown in Figure 3.3. The furnace has an interior diameter of 3 inches, which limited the allowable width of the pull plates to 2.5 inches, further limiting the width of the lap plate to 1.5 inches. The furnace is 17 inches long and it was desired for the lap plate to fit entirely within the furnace. The lap plate was therefore designed to be 7 inches long.

The nominal dimensions of the plates are as follows: the pull plates are each 2.5" wide and ½" thick and the lap plate is 1.5" wide and ¾" thick. As shown in Figure 3.1 and Figure 3.2, there are two lap plates, one on either side of the pull plates. There is a 2" gap between the two pull plates. The size of the transverse weld is ¼". It was desired that the weld in the top plate fail in each test, so the configuration of the weld is different in the top and bottom pull plates. On the top plate, the transverse weld is 1.5" long and goes across the width of the lap plate on both sides of the pull plate. Both lap plates are welded to the bottom pull plates, both in the longitudinal and transverse directions, with a 2.5" set of longitudinal and 1.5" long transverse weld as shown in Figure 3.2(a). The welding procedure will be discussed in further detail in Section 3.6.2.

## 3.4    Test Set-up

The test set-up was the same for both the elevated temperature tests and the post-fire scenario tests. The instrumentation for the two types of tests was also the same due to the fact that the same furnace was used for heating the specimens and the same data was required from the two tests, namely the temperature output and the ultimate load achieved by the specimen.

The test set-up is shown labeled in Figure 3.4. Note that the test specimen is shown in the testing machine with the furnace, cooper cooling plates, and ceramic fire blanket in place as they were during a typical test or post-fire scenario test. The individual components of the test set-up will be discussed in this section.

The length of the test specimens was controlled by the test set-up. The specimens were required to be 68" long. The length had to accommodate three different dimensions. The first is the 8"-12" grip length for each pull plate in the 600 kip SATEC machine that the specimen was tested in, requiring that the specimen be about 20" additional in length. The second is that the furnace used was 17" long. The third was the cooling system, which will be discussed later in this chapter, which required 20" of length.

Due to the fact that the testing machine is run hydraulically, the oil in the grips can not exceed 150°F. The furnace temperature in all of the tests far exceeds this limit and heat conduction was of concern. It was unreasonable to make the pull plates excessively long to allow the heat to dissipate, which led to the need of a cooling system.

The specimen was cooled with two copper cooling plates; each consisted of soldered material, shown in Figure 3.5. A cooling plate was clamped to each pull plate at 4" above or below the furnace. The cooling plates cooled the steel specimen with the use of cold

tap water. Copper was chosen for the cooling plates due to the fact that copper is a good conductor of heat. The copper cooling plates were 6 inches long with a channel running through them to maximize the cold water contact with the test specimen. Rubber hoses were connected to the cooling plates, which can also be seen in Figure 3.5, which ran cold tap water from a sink through the plates throughout the duration of the tests to ensure that the grips remained within the allowable temperature range. The cold water that went through the channel in the cooling plates was then removed by a rubber hose and drained back into the sink.

Before any tests were conducted in the testing machine, it was important to ensure that the cooling system functioned as designed in order that the copper cooling plates removed an adequate amount of heat. The cooper cooling plates were soldered as opposed to welded, which also limited the temperature they were allowed to reach.

Prior to performing elevated temperature tests in the testing machine, the copper cooling plates were tested on a piece of steel bar stock that was heated in the furnace. A thermocouple was placed above and below the cooling plate to measure the temperature and to asses whether the temperature was reduced to less than 150°F. A thermocouple was also placed on the center of the steel bar inside the furnace to monitor the specimen temperature inside the furnace. The cooper cooling plate was clamped to the specimen about 4 inches above the furnace, as shown in Figure 3.6.

The data from this preliminary test is shown in Figure 3.7. It can be seen that the steel inside of the furnace reached 1600°F, which is the maximum temperature to be achieved during the elevated temperature tests, as presented in the test matrix in Section 3.2.

When the steel inside of the furnace was at its maximum temperature, the steel outside of the furnace and underneath the cooling plate was about 600°F. Note this is much greater than the allowable grip temperature of 150°F. The steel above the cooling plate, corresponding to where the steel plate would be gripped by the SATEC testing machine; however reached a maximum of about 83°F throughout the duration of the test, keeping the temperature well within the allowable range. Therefore, it was determined that the cooper cooling plate removed an adequate amount of heat and the grips in the testing machine would not exceed the allowable during the elevated temperature tests.

The cooling system helped to significantly reduce the conduction of heat in the steel bar. Heat radiation was also a concern at the top of the furnace. To prevent heat from radiating out of the top of the furnace, a ceramic fire blanket was placed over the opening of the furnace to keep the heat from escaping. This not only prevented heat from radiating out of the furnace but also maximized the temperature inside the furnace to allow the specimen to heat up in a shorter amount of time.

### 3.5    Instrumentation

The instrumentation was the same for both the elevated temperature tests and the post fire scenario tests. The data that was of interest was the temperature and the applied load. From this data, time-temperature curves were developed for each test and the ultimate failure load was determined. Load-displacement curves were developed and their shapes were studied to observe if the failure was more ductile or brittle for fire or post-fire tests.

### 3.5.1   Temperature Data

The temperature data was recorded through the use of five thermocouples. Table 3.3 summarizes the array of the thermocouples that were used in the tests. The thermocouple labels indicated their location on the specimen. A diagram of the locations of the thermocouples on the test specimen is shown in Figure 3.8. A photograph of a typical specimen with the thermocouples is shown in Figure 3.9. Three of the thermocouples were located inside the furnace; one on the top weld metal (TC_W), one in the center of the lap plate (TC_LP), and one on the top pull plate about two inches above the weld (TC_PP). Data from the thermocouples inside the furnace was used to monitor the temperature of the specimen. Two of the thermocouples were outside of the furnace on the top pull plate; one above the top cooling plate (TC_CT) and one below the bottom cooling plate (TC_CB). Data from the thermocouples outside the furnace was used to ensure that the cooling system was performing properly, keeping the maximum temperature achieved by the grips below 150°F throughout the duration of the test, whether heating or cooling the specimen.

The thermocouples were configured to a CR5000 data acquisition system. The CR5000 was located next to the testing machine and is shown in Figure 3.10. Type K thermocouples were used. For all thermocouples, high temperature thermocouple wire with braided ceramic insulation was used. This type of thermocouple wire can be used for temperatures up to 2400°F. The CR5000 data acquisition system was set to record the temperature data every five seconds. This caused some slight jumps in the time temperature curve which will be discussed in more detail in Chapter 4.

The furnace utilized for all tests was controlled through the use of a CN2110-R20 digital temperature controller. The controller is shown in Figure 3.11. This type of controller is compatible with type K thermocouples and has a 20 Amp built in relay. A thermocouple that is a part of the furnace was attached to the controller so that the temperature inside the furnace could be easily set to a desired temperature.

The furnace that was used for the testing consisted of three zones. The furnace can be wired in such a way that either one, two, or all three zones are used. The wiring was done so that all three zones in the furnace were utilized. This was done to ensure a uniform heat distribution in the furnace throughout the heating and cooling of the specimen.

### 3.5.2 Load Data

It was necessary to have the load-displacement curve from the tests so that the ultimate capacity of the weld could be determined. The ultimate capacity, R(T) at each temperature, T are normalized and used to develop a reduction factor, $\phi(T)$. The concept of a reduction factor was discussed in Chapter 2 from Eurocode and relates the ultimate capacity at an elevated temperature, T to the ultimate capacity at ambient temperature. The reduction factor, $\phi(T)$ is defined as follows:

$$\phi(T) = \frac{R(T)}{R(T = 72°F)} \qquad (3.8)$$

where:

$\phi(T)$ = reduction factor at elevated temperature, T
R(T) = ultimate capacity at elevated temperature, T (kips)
R(T = 72°F) = ultimate capacity at ambient temperature (kips)

 The load-displacement curve, which will be discussed in detail in Chapter 4 and Chapter 5, was recorded from two different data acquisition systems: the SATEC testing machine output and the CR5000. The CR5000 was shown in Figure 3.10 and the testing machine controls and data acquisition system are shown in Figure 3.12. As previously mentioned, the data from the CR5000 was slightly jumpy due to the recording rate. For this reason, the load-displacement curve and the ultimate load from the testing machine output were used for the development of the reduction factors. These curves will be shown and discussed further in Chapter 4.

### 3.6     Material Properties

The test specimens were made up of two materials, namely, base metal and weld metal. Information about the properties of these materials and the procedure used for fabrication will be discussed.

### 3.6.1   Base Metal

The steel base metal was A588 bar stock. A588 steel is dual certified with A572 (Grade 50) steel, which means that A588 steel must undergo the same tests to meet the strength requirements and has the same chemical properties as A572 (Grade 50) steel. A588 steel has a nominal yield strength of 50 ksi and a nominal tensile strength of 65 ksi.

To obtain actual properties of the base metal used in the test specimens, room temperature material tests were performed. These properties were necessary due to the fact that the predicted strength should be as accurate as possible, therefore measured values were to be used in calculations instead of nominal values. Two different types of bar stock were used in the test specimen, which were both made of A588 steel, but had different dimensions; the bars tested were ½" x 2 ½" (for the pull plates) and ¾" x 1 ½" (for the lap plates). Prior to testing the specimens, the actual dimensions were measured and recorded, and will be discussed later in this chapter. The material was tested in the SATEC testing machine in tension until failure.

In lue of having coupons made of each material, an 8" long gage length was created by slightly reducing the area in the middle of a length of bar stock. This was achieved by grinding down about an eighth of an inch of material from each side of the bar. A series of punch marks were made every two inches along the center of the bar. A photograph of the bar with the punch marks and reduced area gage length can be seen in Figure 3.13. A measurement was made from the center of the specimen to each end of the gage length using a caliper before the test and the actual dimensions were recorded. These two measurements were added together to obtain the actual gage length. The measurements that were made and summed can be seen in Figure 3.14. The actual dimensions of the bar and actual gage length prior to testing are shown in Table 3.4.

An extensometer was attached to the specimens during the tensile test. A photograph of the extensometer attached to the specimen in the testing machine can be seen in Figure 3.15. The extensometer has to be removed once 2% strain is reached to avoid damaging it, thus allowing the strain at yield to be measured. The load and head travel were also measured and recorded to enable the remaining load-displacement curves to be obtained. The stress strain curve for up to 2% strain is shown in Figure 3.16. The load-displacement curve of the entire test is shown in Figure 3.17.

The loading rate followed the standard ASTM E8 (ASTM, 2004) protocol. The SATEC testing machine was programmed to follow a soft start followed by three loading zones. The soft start was displacement controlled and moved 0.10 in/min until a load of 100 lb was reached. The first zone loaded at a rate of 10,000 psi/min until the stress exceeded 30 ksi. The second zone was again displacement controlled and loaded at 0.08 in/min until the strain exceeded 0.018. The third and final zone loaded at a rate of 0.8 in/min until failure.

After the specimens failed, the pieces were placed back together and the caliper was again used to measure the elongation. The strain at failure was determined using the original length and the elongated length. The strain at fracture, $\varepsilon_{max}$, for both materials was around 20%. Table 3.5 gives the lengths of the bars before and after failure and the corresponding strains. A photograph of the failed specimen can be seen in Figure 3.18.

These material tests provided the actual measured yield and ultimate strengths to be used in all design calculations for the elevated temperature tests. It was found that the yield and ultimate strengths for the pull plate (½" x 2 ½") were 53 ksi and 73 ksi, respectively. The yield and ultimate strengths for the lap plate (¾" x 1 ½") were 54 and 75 ksi, respectively. These properties and the percent increases from the nominal properties are shown in Table 3.6.

### 3.6.2   Weld Metal
The welding process that was used was flux core arc welding (FCAW) and the electrode type was E71-T8. This type of electrode has a nominal ultimate strength of $F_{EXX} = 70$ ksi.

The FCAW process is representative of welding that can be done in the field due to the fact that the electrode used does not have gas shielding.

Type E71-T8 electrode is commonly used for flux core arc welding, as performed for these tests specimens. According to AWS A5.29 (AWS 2005), an electrode of type E7XTX will have a nominal tensile strength of 70-90 ksi and nominal yield strength of 58 ksi. The actual tensile strength of the electrode will be discussed in Chapter 5. This type of electrode is a low-alloy electrode used for FCAW, as specified in AWS 5.3.4.2 (AWS 2002), which produces a weld metal with greater yield strength than produced in regular (non low-alloy) electrode.

Due to the fact that the welds were critical in these tests, it was imperative that the welding for each specimen was done carefully and uniformly. To ensure this, the same welder was used for all specimens. A constant amperage and voltage, both falling in the middle of the acceptable range for this electrode, were used for all specimens.

As noted previously, a transverse weld was placed across the width of the lap plate. Since the lap plates were each 1.5 inches in width, it was important that the entire weld was of good quality and that none of it was affected by the stop or start of the welding. To ensure that the entire length of the weld was good quality, runoff plates were utilized as shown in Figure 3.19. After the weld was complete the runoff plates were removed and the extra weld was grinded off the specimen.

### 3.7    Measured Dimensions

As discussed previously in this chapter, the measured dimensions of the lap plates, pull plates, and weld size were used in calculations for design and later in subsequent chapters for assessment of test results. These measurements include the width and thickness of the pull and lap plates, the length of both of the transverse welds on the top plate, and the size of the weld. These measurements are given in Table 3.7. The measurements shown in Table 3.7 of the lap and pull plates are defined as follows: w PP is the average width of both pull plates, t PP is the average thickness of both pull plates, w LP is the average width of both lap plates, and t LP is the average thickness of both lap plates. In Table 3.7, weld measurements are also shown. These measurements were made prior to testing and are defines as follows: L $weld_1$ is the length of the transverse weld on one of the lap plates, L $weld_2$ is the length of the transverse weld on the other lap plate, and a is average leg size of both transverse welds on the two lap plates.

Measurements of the weld were also made after the specimen was tested. After testing, the weld fractured; therefore the throat of the weld could easily be measured. These measurements will be used to normalize the test results by the area of the weld, which will be discussed in further detail in Chapter 5. A schematic of these measurements are labeled and shown in Figure 3.20. Note that the dimension labeled $a_1$ is the average leg size of the weld on the pull plate, $a_2$ is the average leg size of the weld on the lap plate, and te is the throat of the weld, measured along the failure plane. The angle of the

fracture surface of the fillet weld is denoted by θa and θb on the top and bottom of the top pull plate, respectively. The measured fracture angles will be discussed in Chapter 4. The process used to make these measurements, the formulas used to compute the area of the welds, and the magnitudes of these measurements and the areas will be tabulated and discussed further in Chapter 5.

## 3.8     Test Protocol and Procedure

A test protocol was necessary for both the elevated temperature tests and the post-fire scenario tests. The test protocol and procedure was developed prior to any testing and was followed for all tests. The procedures for both types of tests will be discussed in this section.

### 3.8.1   Elevated Temperature Test

The first step in the test protocol is to take all pertinent measurements, so that measured dimensions can be used as opposed to nominal dimensions, which was discussed previously.

The necessary thermocouples are then tac-welded onto the specimen. As noted previously, there are three thermocouples in the furnace: one on the weld metal; one on the center of the lap plate; and one on the top pull plate.

The specimen is then placed through the furnace and inserted into the bottom grip of the SATEC testing machine and clamped into place. The top grip of the testing machine is left unclamped during the heating of the specimen. This is due to the fact that thermal elongation takes place as the specimen is heated. When the bar is restrained, axial forces can develop. Since this was not desired, the specimen was not clamped into the top grips to allow for thermal elongation to take place.

The cooling system is then put into place. Prior to the first test, the rubber hoses were attached to the cooper cooling plates with a hose clamp and also attached to a sink with a drain. They remained like this for the duration of the testing. The cooper cooling plates with the rubber hoses are first clamped onto the specimen, using C clamps, about 4" above and below the furnace. The water is then turned on to ensure there are no leaks or kinks in the hose before the furnace is turned on. The ceramic fire blanket is then placed over the top opening of the furnace to prevent heat radiation.

The two thermocouples are then attached to the test specimen above and below the cooling plates to monitor the temperature of the steel that is just above or below the grips. This is to ensure that the steel of the test specimen near the grips does not exceed 150°F, which as mentioned in Section 3.4, is the maximum temperature the grips of the machine can achieve. These thermocouples do not need to be tac-welded and can be attached to the specimen using duct tape.

The data acquisition system is then turned on. The furnace is then plugged in and set to the desired set point temperature for the particular test. Note it is advisable to set the set point about 100-150°F above the desired temperature to speed up the heating process. The specimen is then heated to the desired temperature. The specimen reaches the desired temperature once the thermocouple reading from the weld metal reaches the desired temperature. This temperature is then held for 40 minutes to allow for any fluctuation in the weld temperature in order to average around the desired temperature. One the weld reached the desired temperature, the set point was slowly lowered to about 50°F above the desired temperature to average it.

Lower temperatures were observed to be much less stable. At temperatures above 1400°F, this was easily done by setting the set point to about 50°F above the desired temperature. The weld temperature would increase very steadily and maintain the desired temperature with only about plus or minus a 5°F variation. At lower temperatures, there was much more variation, sometimes as great as plus or minus 50°F. The set point had to constantly be adjusted to account for sharp increases or decreases. The weld did not steadily maintain the target temperature as much as it averaged around the target temperature for 40 minutes.

After the weld is at the desired temperature for 40 minutes, the top grips of the SATEC testing machine are clamped shut around the specimen and the load is readjusted so that the test begins with zero applied load. The specimen is then subjected to tension at a rate of 0.10 in/min. The load is applied until failure of the specimen occurs.

The specimen is then allowed to cool inside of the furnace by resetting the set point temperature to 70°F. After the furnace temperature is down to about 300°F, the ceramic fire blanket is removed from the top of the furnace to expedite cooling. This is not done earlier in the cooling process because keeping the grips within their allowable temperature range is important.

Once the specimen is cooled down to about 100°F, it can be removed. This is done by first turning off the water and removing the cooling plates. Since the specimen has fractured at the transverse welds, it is now in two pieces. The bottom cross head is lowered until the top piece of the specimen comes out of the furnace. The two pieces of the test specimen are then carefully removed and placed aside to cool completely.

Once the specimen is removed, the load and temperature data are collected from both the testing machine output and the data acquisition system, as discussed previously in Section 3.5. This data will later be plotted and analyzed. The furnace is then unplugged and the data acquisition system is shut off.

Upon complete cooling of the specimen the necessary post-test weld measurements are taken to determine the actual size of the transverse weld and the area of the failure surface of the transverse weld. The measurements consist of the lengths of the transverse

weld, the weld size on both plates, and the weld size along the failure plane of the welds. These measurements are used for normalization of results and are discussed in more detail in Chapter 5.

### 3.8.2  Post-Fire Scenario Test

A majority of the procedure for the heating of the specimen for the post-fire scenario tests is the same as for the elevated temperature tests. In the post-fire scenario tests, however, once the weld temperature is maintained for 40 minutes, the top grips are not clamped shut. The top grips remain unclamped until directly before application of load. Upon the weld temperature being maintained for 40 minutes, the set point temperature is reset to the desired test temperature. For example, for the specimen that is tested at ambient temperature, the controller set point is reset to 70°F. Like the elevated temperature tests, the ceramic fire blanket is removed once the furnace is down to about 300°F to expedite cooling.

Once the weld has reached the desired test temperature, the top grips are clamped shut. Tension load is then applied at the same rate as for the elevated temperature tests at 0.10 in/min until the specimen fails. The specimen then continues to cool until it reaches about 100°F and can be safely removed from the testing machine. The specimen is removed as it was for the elevated temperature tests. For the test that is cooled down to room temperature, the specimen can be immediately removed.

Once the specimen has been removed, the same procedure from the elevated temperature tests are be followed. More specifically, the load and temperature data is collected, the furnace and data acquisition system are turned off, and the necessary measurements of the weld are recorded upon complete cooling of the specimen.

### 3.9    Summary

This chapter presented the test program for both the elevated temperature tests and the post-fire scenario tests. A test matrix was defined. The test specimen design was then discussed. The details of the test set-up were presented, along with the instrumentation plan. The material properties, both the base metal and weld metal, used for the test specimen were then discussed. Data from the room temperature material tests of the steel bar stock was shown. The measured dimensions were then discussed. The test protocol and procedure were presented for both the elevated temperature tests and the post-fire scenario tests.

Table 3.1  Test matrix for elevated temperature tests

| Specimen | Test Temperature (°F) |
|----------|-----------------------|
| 1        | 70                    |
| 2        | 350                   |
| 3        | 600                   |
| 4        | 700                   |
| 5        | 800                   |
| 6        | 900                   |
| 7        | 1000                  |
| 8        | 1200                  |
| 9        | 1400                  |
| 10       | 1600                  |

Table 3.2  Test matrix for post-fire scenario

| Specimen | Maximum Temperature Achieved (°F) | Test Temperature (°F) |
|----------|-----------------------------------|-----------------------|
| P1       | 1600                              | 70                    |
| P2       | 1600                              | 600                   |
| P3       | 1600                              | 800                   |
| P4       | 1600                              | 1000                  |
| P5       | 1600                              | 1200                  |

Table 3.3  Thermocouples configured with the CR5000 data acquisition system used for the elevated temperature and post-fire scenario test.

| Channel | Sensor Type         | Label  | Description     |
|---------|---------------------|--------|-----------------|
| 1       | Type K Thermocouple | TC_W   | Weld            |
| 2       | Type K Thermocouple | TC_PP  | Top Pull Plate  |
| 3       | Type K Thermocouple | TC_LP  | Lap Plate       |
| 4       | Type K Thermocouple | TC_CT  | Above Top CP    |
| 5       | Type K Thermocouple | TC_CB  | Below Bottom CP |

Table 3.4  Measured dimensions of bar stock for material test

| Plate | Measured Dimensions (in) | | Reduced Area (in) | Gage Length (in) | |
|---|---|---|---|---|---|
| | Thickness | Width | Width | Theoretical | Actual |
| 1/2"x2.5" | 0.504 | 2.499 | 2.458 | 8.000 | 8.580 |
| 3/4"x1.5" | 0.751 | 1.496 | 1.468 | 8.000 | 8.580 |

Table 3.5  Strain of bar stock at failure

| Plate | x1 (in) | | x2 (in) | | Total (in) | | $\Delta L$ (in) | $\varepsilon_{max}$ |
|---|---|---|---|---|---|---|---|---|
| | Original | Elongated | Original | Elongated | Original | Elongated | | |
| 1/2"x2.5" | 4.293 | 5.391 | 4.287 | 4.622 | 8.580 | 10.375 | 1.795 | 0.209 |
| 3/4"x1.5" | 4.312 | 5.417 | 4.268 | 4.644 | 8.580 | 10.625 | 2.045 | 0.238 |

Table 3.6  Nominal and measured material properties for base metal

| Plate | Yield Strength (ksi) | | | Ultimate Strength (ksi) | | |
|---|---|---|---|---|---|---|
| | Nominal | Measured | % Increase | Nominal | Measured | % Increase |
| 1/2"x2.5" | 50 | 52.9 | 5.8 | 65 | 73.2 | 12.6 |
| 3/4"x1.5" | 50 | 54.1 | 8.2 | 65 | 74.6 | 14.8 |

Table 3.7  Measured dimensions of elevated temperature test specimens prior to testing

| Specimen | Temperature | Dimensions (in) | | | | | | | |
|---|---|---|---|---|---|---|---|---|---|
| | (°F) | w PP | t PP | w LP | t LP | L weld1 | L weld2 | Lw avg | a |
| 1 | 70 | 2.501 | 0.557 | 1.480 | 0.753 | 1.583 | 1.543 | 1.563 | 0.255 |
| 2 | 350 | 2.509 | 0.532 | 1.496 | 0.764 | 1.440 | 1.458 | 1.449 | 0.341 |
| 3 | 600 | 2.499 | 0.512 | 1.475 | 0.766 | 1.454 | 1.448 | 1.451 | 0.323 |
| 4 | 700 | 2.521 | 0.521 | 1.479 | 0.752 | 1.427 | 1.467 | 1.447 | 0.367 |
| 5 | 800 | 2.498 | 0.513 | 1.486 | 0.758 | 1.533 | 1.516 | 1.525 | 0.358 |
| 6 | 900 | 2.510 | 0.525 | 1.487 | 0.747 | 1.501 | 1.492 | 1.497 | 0.376 |
| 7 | 1000 | 2.516 | 0.532 | 1.486 | 0.753 | 1.511 | 1.460 | 1.486 | 0.338 |
| 8 | 1200 | 2.497 | 0.516 | 1.478 | 0.754 | 1.536 | 1.539 | 1.537 | 0.347 |
| 9 | 1400 | 2.498 | 0.529 | 1.498 | 0.751 | 1.502 | 1.499 | 1.501 | 0.348 |
| 10 | 1600 | 2.494 | 0.560 | 1.482 | 0.753 | 1.489 | 1.496 | 1.493 | 0.340 |
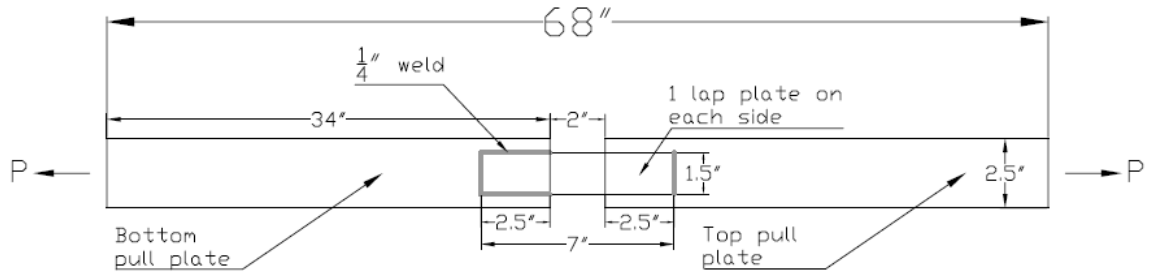
(a)
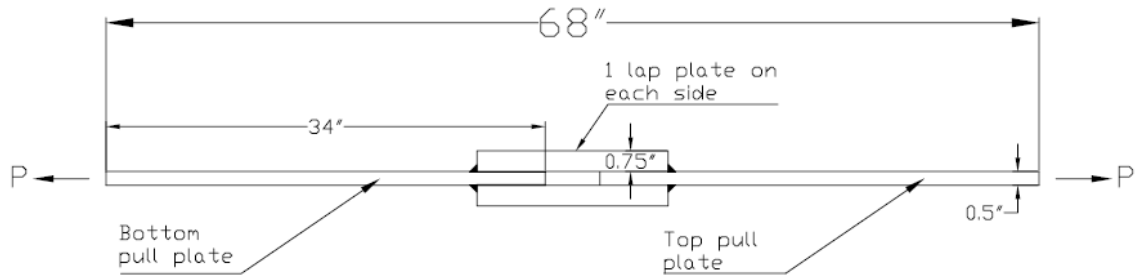


(b)

Note: Not drawn to scale

Figure 3.1  Front view of test specimen with dimensions (b) Side view of test specimen with dimensions
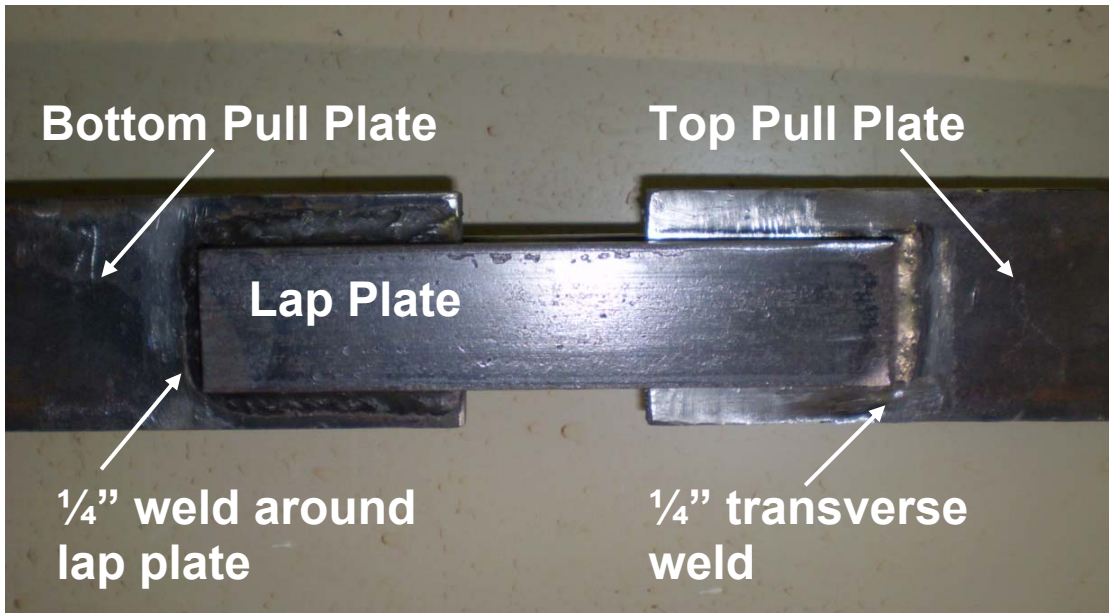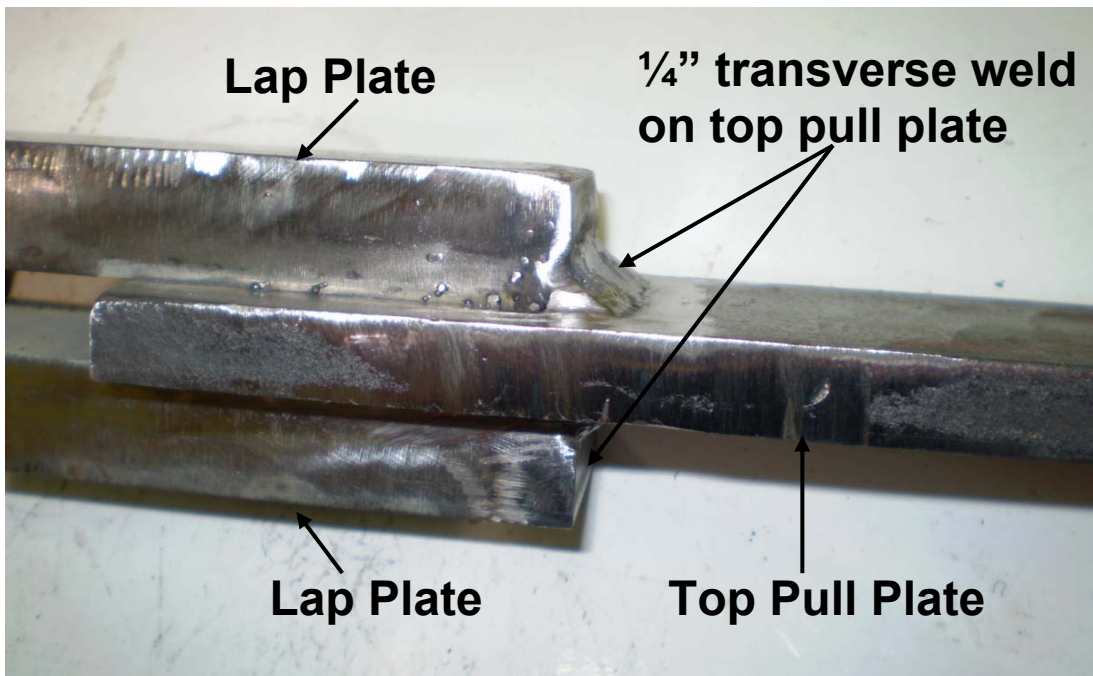
Figure 3.2 (a) Photograph of the front view of the test specimen (b) Photograph of the side view of the test specimen
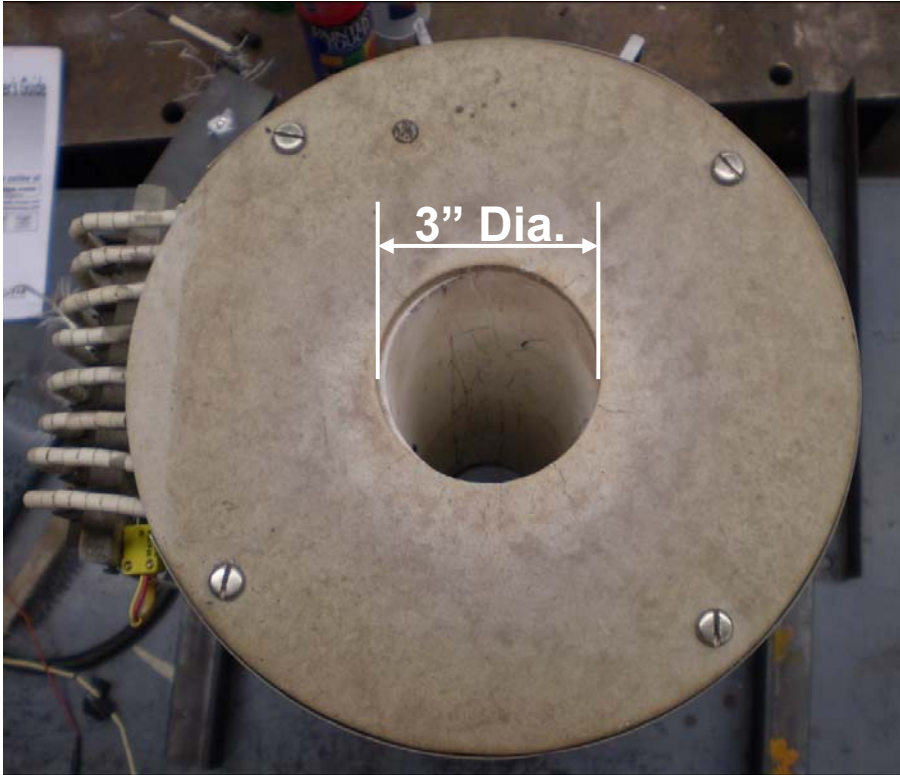
Figure 3.3  Photograph of the top of the furnace, showing the interior 3-inch diameter of the furnace
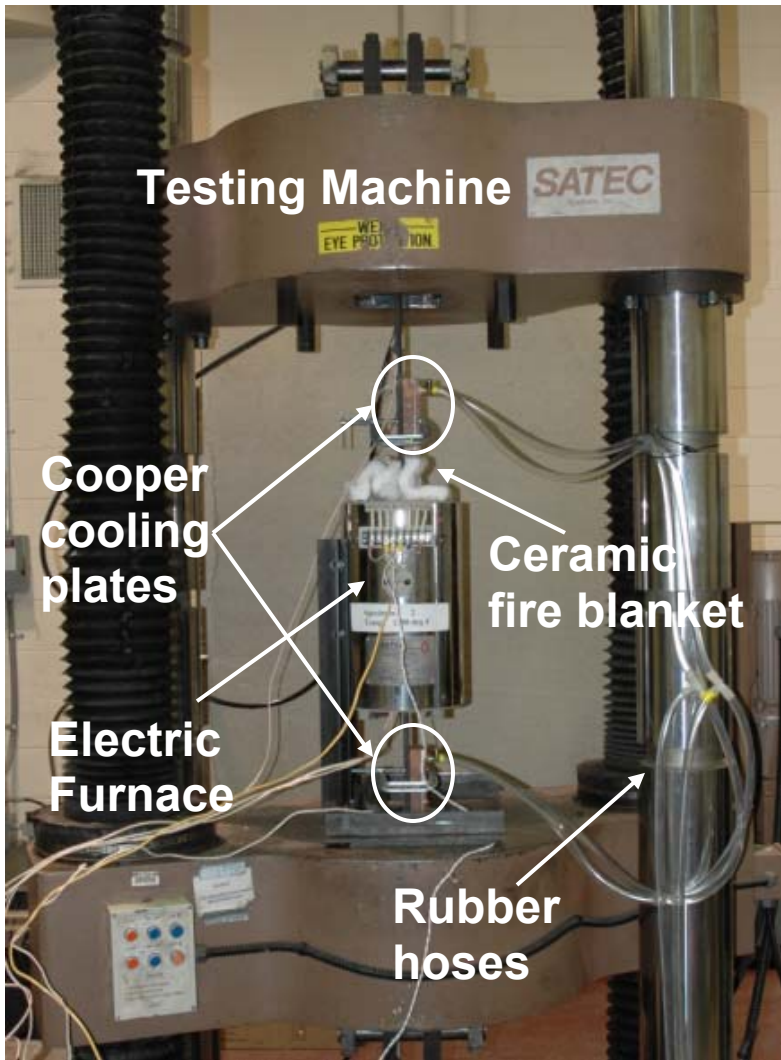
Figure 3.4  Photograph of labeled test set-up
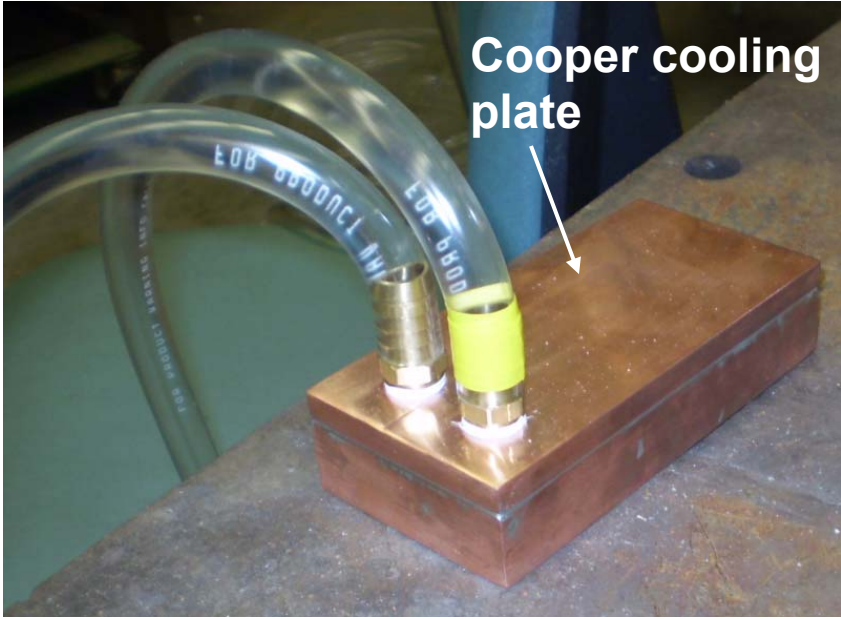
Figure 3.5  Photograph of cooper cooling plates used in test set-up
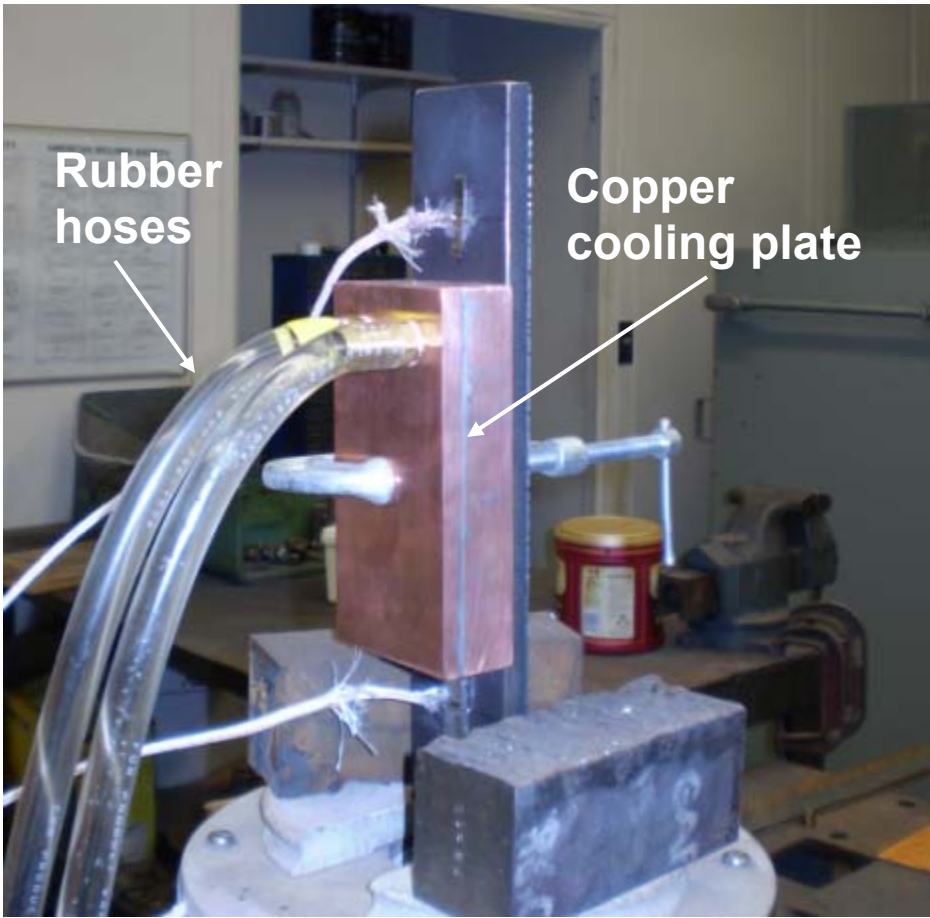
Figure 3.6  Photograph of thermocouples during the cooling system test
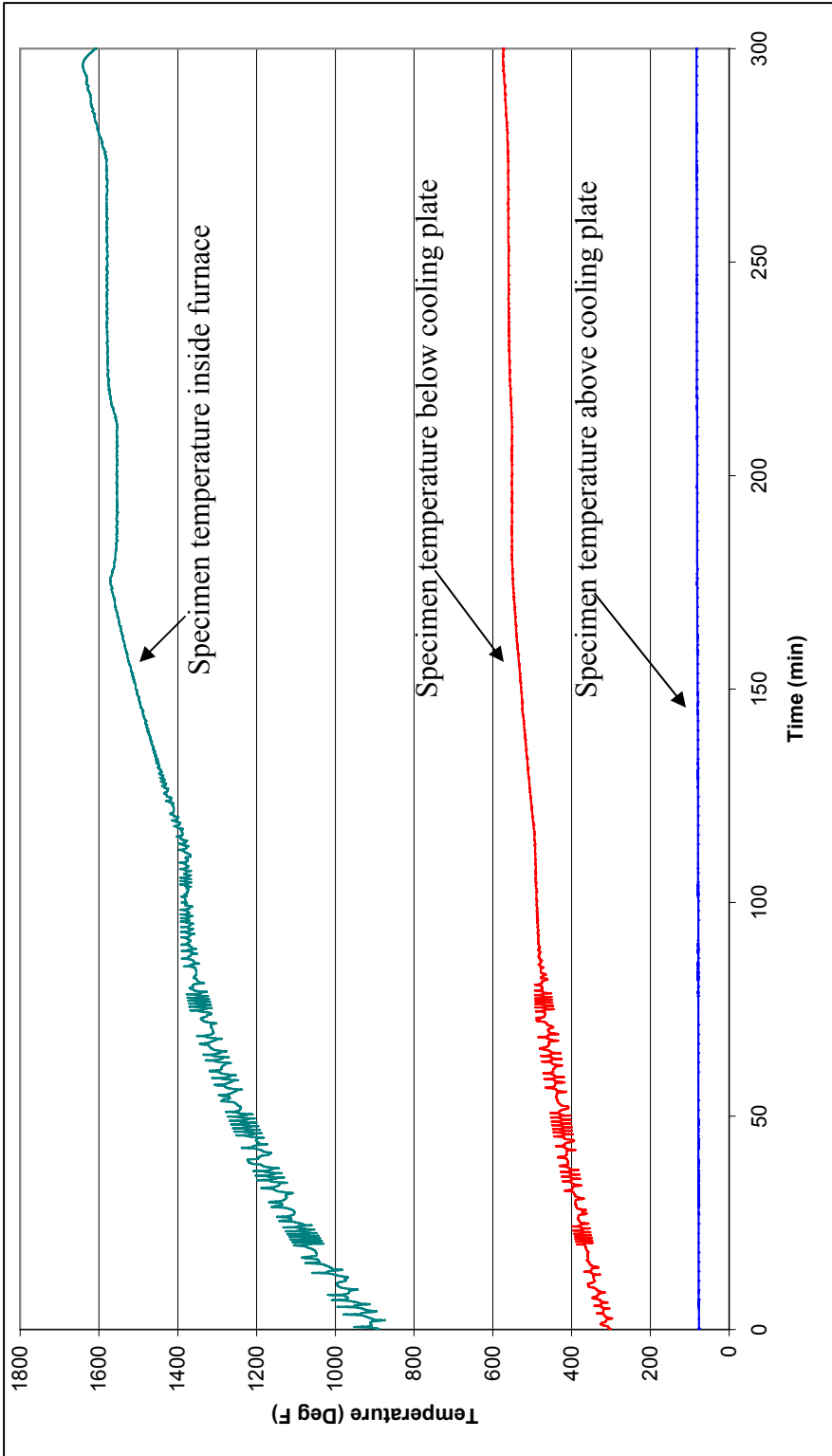
Figure 3.7  Time-temperature curve for pre-elevated temperature test
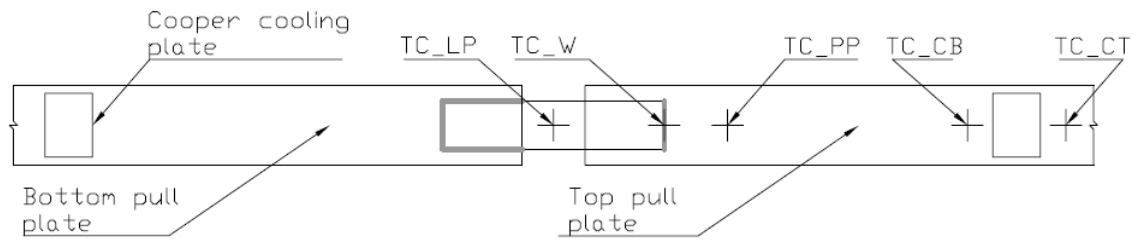
Figure 3.8  Diagram of thermocouples on test specimen
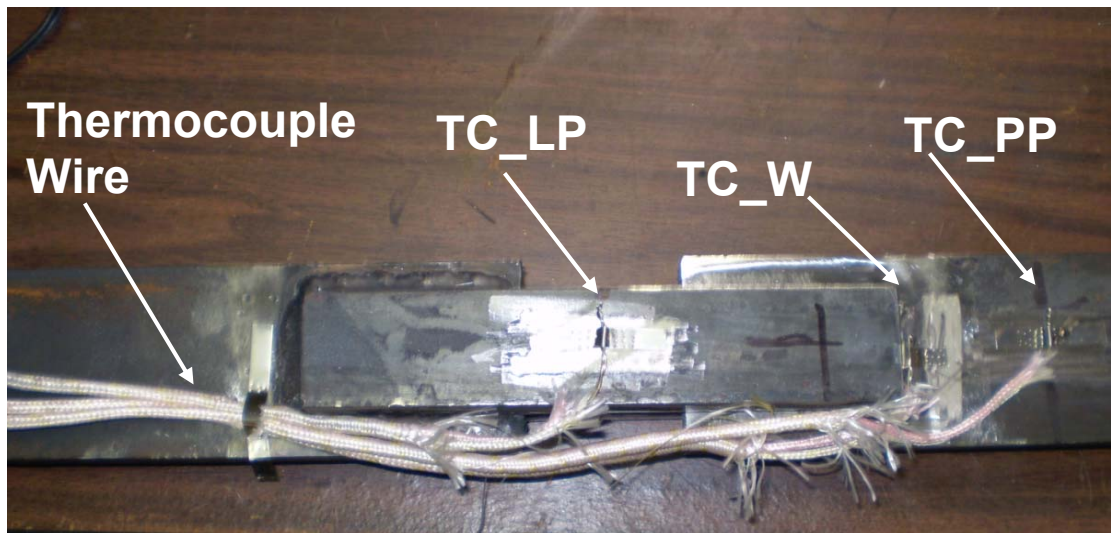


Figure 3.9  Photograph of the thermocouples on a typical test specimen portion inside furnace
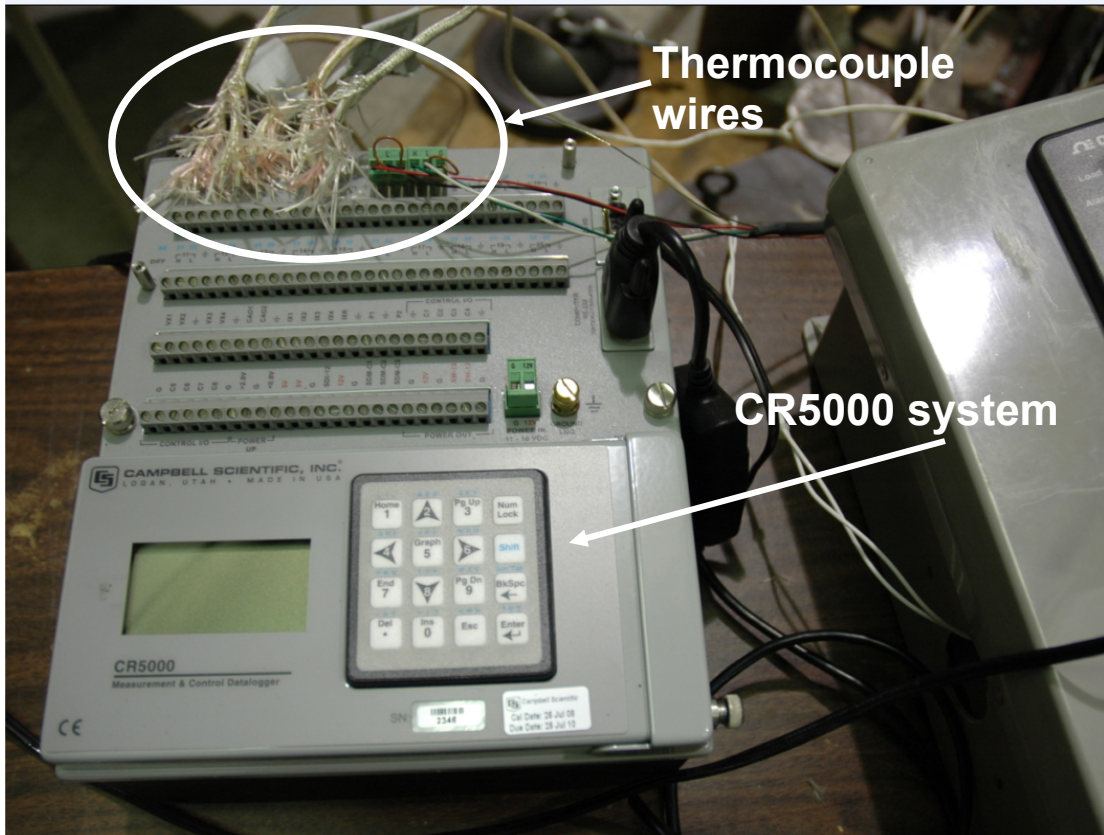
Figure 3.10  Photograph of CR5000 data acquisition system



Figure 3.11  Photograph of digital temperature controller

Figure 3.12  Photograph of the controls and data acquisition for the SATEC testing machine
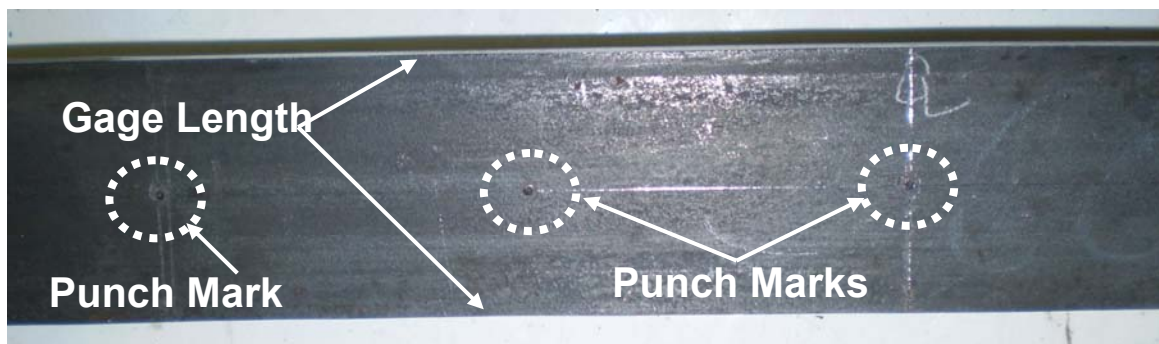


Figure 3.13  Photograph of the reduced area and punch marks (circled) prior to test
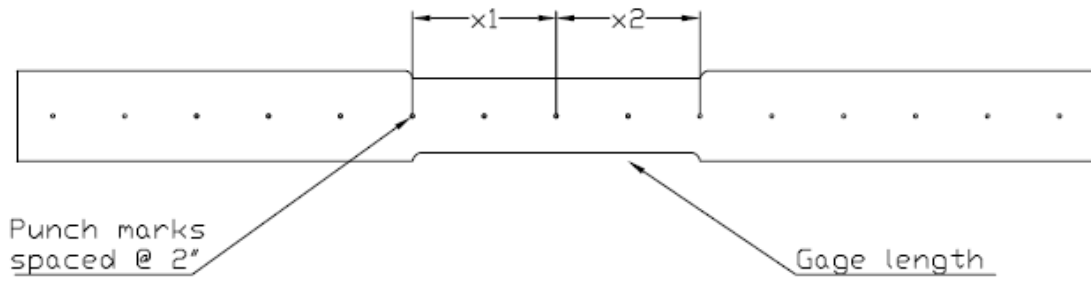
Figure 3.14  Measurements of actual gage length



Figure 3.15  Photograph of bar and extensometer in testing machine
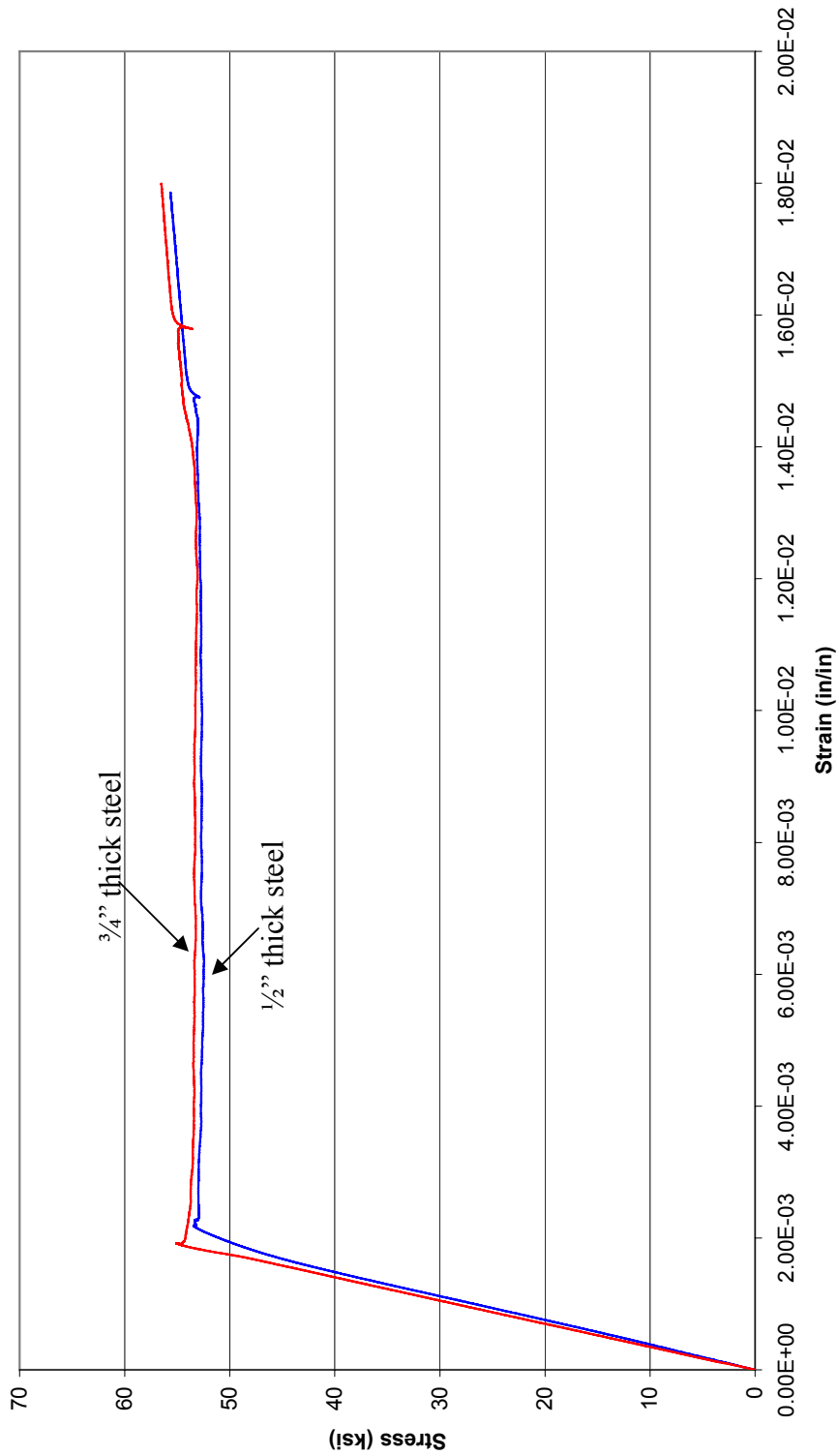
Figure 3.16  Stress-strain curve of ½" and ¾" thick steel from extensometer for up to 2% strain
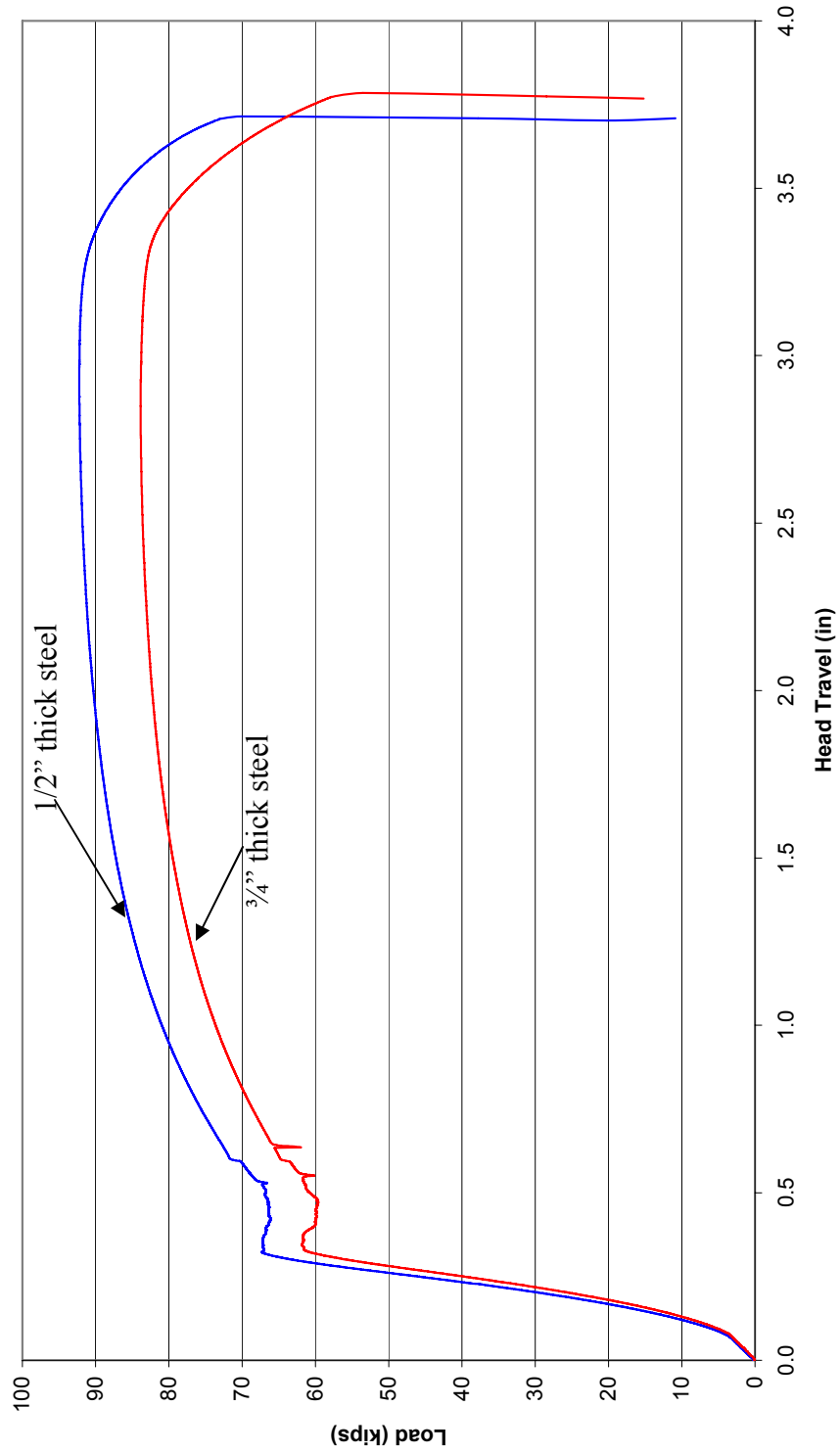
Figure 3.17  Load-displacement curve of ½" and ¾" thick steel
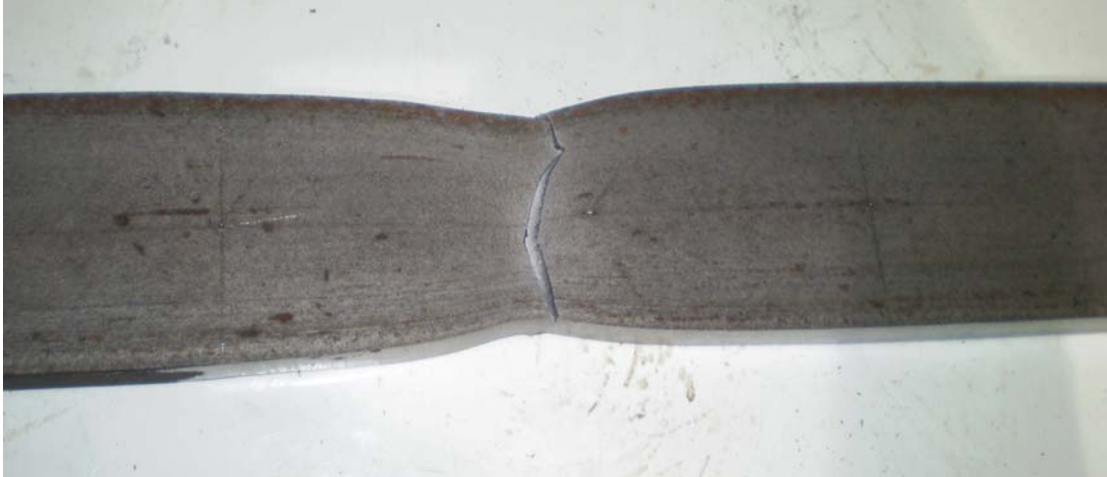
Figure 3.18  Photograph of the bar after failing in tension, showing necking and fracture
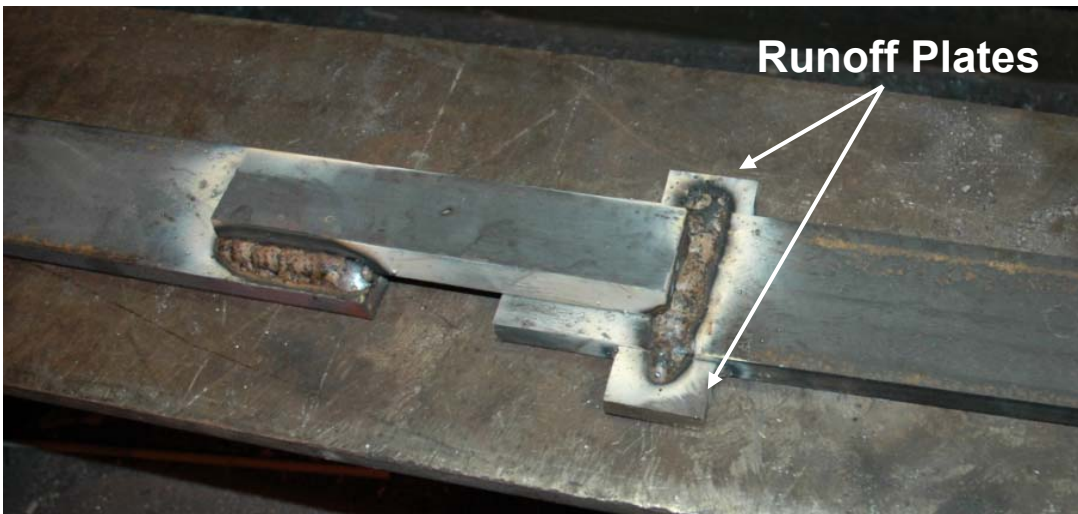


Figure 3.19  Photograph of the test specimen with the runoff plates used during the welding process

(a)



(b)
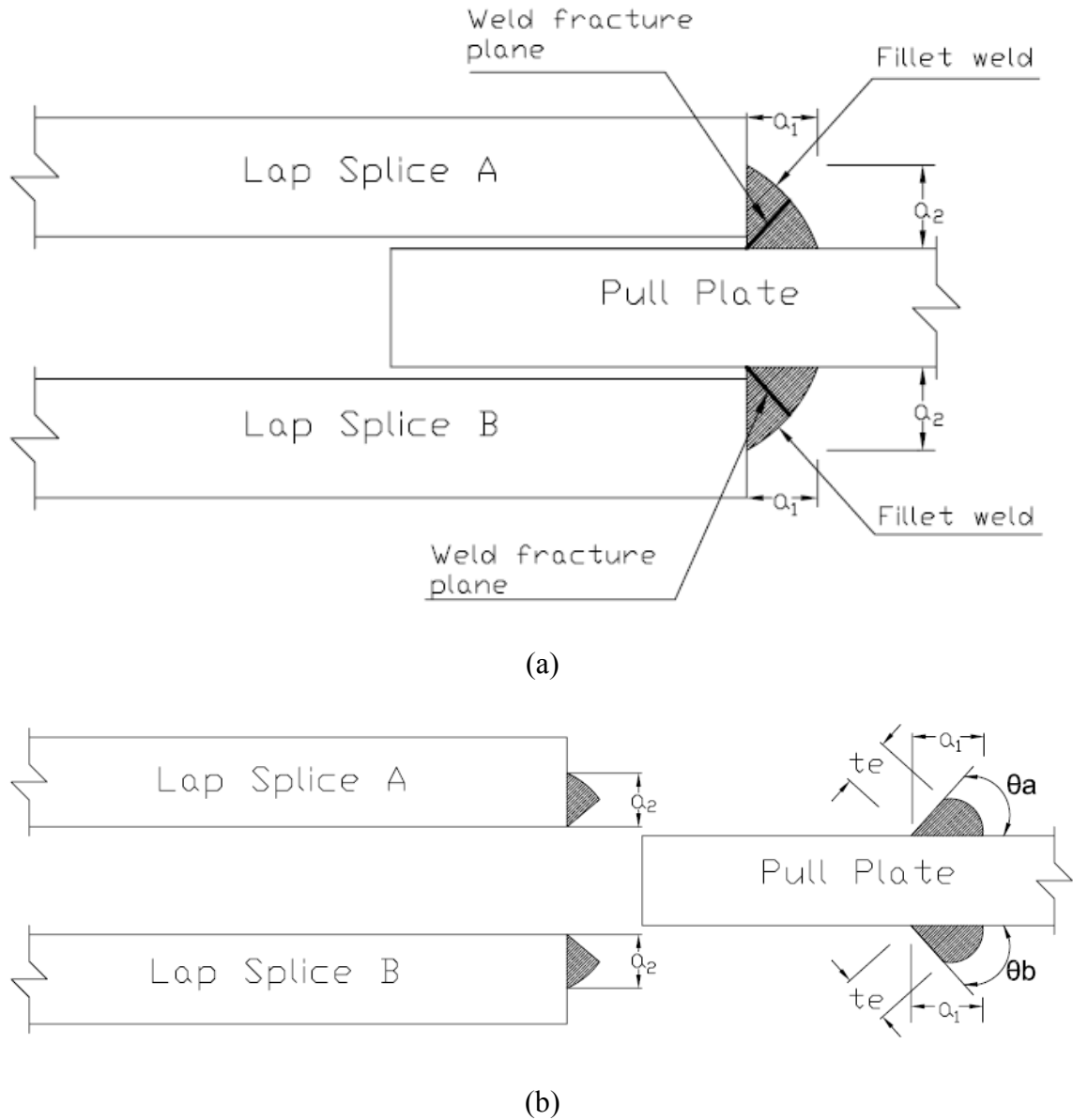
Figure 3.20  Schematic of the weld size measurements, a1, a2, and te and the weld fracture angles, θa and θb made after testing each specimen: (a) Test specimen before weld fracture (b) Test specimen after weld fracture

## Chapter 4       Test Observations

### 4.1      General

This chapter presents the test observations from both the elevated temperature and post-fire scenario tests. For each of the specimens tested, both temperature and load data will be presented. This will include both qualitative and quantitative results. The temperature data used to develop the time-temperature curves is from the CR5000 data acquisition system and the load data used to develop the specimen load-displacement curves is from the output of the SATEC testing machine.

### 4.2      Elevated Temperature Tests

As discussed in Section 3.2, ten elevated temperature tests were performed at selected temperatures. From these tests, it was desired that a well defined curve be determined for the reduction of weld strength at elevated temperatures. First general qualitative observations will be discussed. Then, the temperature and load data from each test will be discussed. Note that the tests will be discussed in the order of increasing temperature. The maximum load for each specimen the SATEC testing machine is given in Table 4.1. These ultimate loads will be normalized and used to develop a reduction factor for determining strength at elevated temperatures in Chapter 5.

### 4.2.1    Qualitative Observations

Prior to starting any tests, the weld on the specimens and plate material was examined and measured. The measurements of the pull and lap plates were fairly constant, as was expected since the material for all specimens was from the same bar stock. Recall the measurements are given in Chapter 3. It was apparent from visual observations and measurements that the size of the transverse fillet weld varied in most of the specimens. Specimens 1 and 2 had a ¼" leg size for the weld, which was specified in the design. The remainder of the specimens, however, had a larger weld size. The load data from each test was therefore normalized by the area of the weld to account for the variation in weld size and will be discussed in Chapter 5.

Recall from Chapter 3 that the test temperature was averaged for forty minutes. Table 4.1 shows the actual average temperature during this 40 minute period for each specimen. Observe that the furnace temperature was accurate in that the specified test temperature was always within 2% of the actual averaged temperature.

Observations made from loading the specimens at elevated temperatures generally matched what were expected. As the temperature increased, the failure load of the specimen generally decreased. As mentioned previously in this section, there was a variation in weld size between the specimens. For this reason, if two specimens were tested at close temperatures, within 100°F of each other, the load achieved at the lower temperature could actually be slightly higher if the specimen had a slightly larger weld. As noted previously, this was remedied by normalizing the results by the measured area of the weld.

An extensometer could not be used to measure the displacement during the elevated temperature tests; therefore the head travel from the SATEC testing machine output was used. For this reason, seating is observed in the load-displacement responses. The stiffening behavior after the specimen becomes seated will be discussed for each specimen.

### 4.2.2    Specimen 1: 70°F

The test of Specimen 1 was conducted at ambient temperature, therefore only the load-displacement data will be discussed. The load-displacement response for Specimen 1 is shown in Figure 4.1. Specimen 1 reached a load of 42 kips and displaced 0.29", when fracture simultaneously occurred in both transverse fillet welds. From the load-displacement curve, it is observed that the failure was quite abrupt in that the load dropped off quickly after the welds fractured.

As load was initially applied Specimen 1 became seated, where upon the load displacement relationship shows a stiffening behavior. The stiffening after seating was 277.8 kip/in. This stiffness matched well that of the elastic stiffness of the nominal ¾ inch thick specimen for the material test. This indicates an accurate result is achieved for specimen stiffness based on the post-seating elastic stiffness of the specimen.

A photograph of Specimen 1 after the welds fractured is shown in Figure 4.2, where the failed transverse welds on the lap plate and top pull plate can be seen. Figure 4.3 is a photograph of the side view of the weld on the top pull plate of Specimen 1. Also shown in Figure 4.3 are the angles of the fracture surface of the transverse fillet welds on the lap plates, θa and θb (θa and θb were defined previously in Figure 3.20 (b)). The average fracture surface is 42.5°, which is within 6% of the assumed AISC fracture surface of 45°.

### 4.2.3    Specimen 2: 350°F

The time-temperature data for Specimen 2 is shown in Figure 4.4. The furnace took about 20 minutes to reach the temperature of 350°F. Due to the rapid temperature increase, the temperature data is noisy and fluctuates significantly during heating and also during the 40 minute interval when the temperature was held at the test temperature. The actual temperature, averaged over forty minutes was 356.6°F, as mentioned in Table 4.1. As shown in Figure 4.4, the temperature above and below the cooling plates was under 90°F, which is well below the allowable temperature of 150°F.

The load-displacement response for Specimen 2 is shown in Figure 4.5. As load was initially applied Specimen 2 became seated, where upon the load displacement relationship shows a stiffening behavior. After seating, a stiffening of 237.8 kip/in was observed, which is 14% less than Specimen 1. Specimen 2 reached a load of 43 kips and displacement of 0.28 inches when a transverse weld fractured. The load of 43 kips is slightly above that of Specimen 1 due to the larger weld sizes in Specimen 2. The weld

on one side of the lap plate failed at the ultimate load and the weld on the other side failed just after at about 42 kips.

A photograph of Specimen 2 after the welds fractured is shown in Figure 4.6, where the failed transverse welds on the lap plate and top pull plate can be seen. Figure 4.7 is a photograph of the side view of the weld on the top pull plate of Specimen 2. Due to the fact that Specimen 2 was tested at a temperature of 350°F, it looks similar to Specimen 1 after it was tested, where the fracture plane of the weld is not jagged. Also shown in Figure 4.7 are the angles of the fracture surface of the transverse fillet welds on the lap plates, θa and θb. The average fracture surface is 80°, which is a 47% variation from the angle of the fracture surface of Specimen 1. The fracture angle on the top lap plate, θa is completely flat, with a fracture angle of 90°.

### 4.2.4   Specimen 3: 600°F
The time-temperature data for Specimen 3 is shown in Figure 4.8. The furnace took a little under an hour to reach 600°F. Similar to Specimen 2, the temperature data fluctuates during heating and also during the 40 minute interval when the temperature was held at the test temperature.

The load-displacement response for Specimen 3 is shown in Figure 4.9. As load was initially applied Specimen 3 became seated, where upon the load displacement relationship shows a stiffening behavior. After seating, a stiffening of 243.5 kip/in was observed, which is 12% less than Specimen 1. At a load of 41 kips and a displacement of 0.28 inches the transverse welds fractured. Although Specimen 3 was tested at a greater temperature, the decrease in load capacity is quite small. As discussed previously this is due to the fact that the ultimate load has not yet been normalized by the size of the weld. Similar to Specimen 1 and Specimen 2, the failure is abrupt, with the load dropping off quickly after weld fracture.

A photograph of Specimen 3 after the welds fractured is shown in Figure 4.10, where the failed transverse welds on the lap plate and top pull plate can be seen. Figure 4.11 is a photograph of the side view of the weld on the top pull plate of Specimen 3. Also shown in Figure 4.11 are the angles of the fracture surface of the transverse fillet welds on the lap plates, θa and θb. The average fracture surface is 50°, which is a 15% variation from the angle of the fracture surface of Specimen 1.

### 4.2.5   Specimen 4: 700°F
The time-temperature data for Specimen 4 is shown in Figure 4.12. The furnace took an about an hour to reach the temperature of 700°F. Similar to Specimen 2, the temperature data fluctuates during heating and also during the 40 minute interval when the temperature was held at the test temperature.

The load-displacement response for Specimen 4 is shown in Figure 4.13. As load was initially applied Specimen 4 became seated, where upon the load displacement

relationship shows a stiffening behavior. After seating, a stiffening of 228.4 kip/in was observed, which is 18% less than Specimen 1. The transverse fillet weld fractured at a load of 34 kips and a displacement of 0.26 inches. Similar to the other specimens, the failure is abrupt, with the load dropping off quickly after weld fracture.

A photograph of Specimen 4 after the welds fractured is shown in Figure 4.14, where the failed transverse welds on the lap plate and top pull plate can be seen. Figure 4.15 is a photograph of the side view of the weld on the top pull plate of Specimen 4. The failure plane of Specimen 4 appears to be a little jagged. Also shown in Figure 4.15 are the angles of the fracture surface of the transverse fillet welds on the lap plates, $\theta a$ and $\theta b$. The average fracture surface is 50.5°, which is a 16% variation from the angle of the fracture surface of Specimen 1.

### 4.2.6    Specimen 5: 800°F
The time-temperature data for Specimen 5 is shown in Figure 4.16. The furnace took an about an hour to reach 800°F. Similar to Specimen 2, the temperature data fluctuates during heating and also during the 40 minute interval when the temperature was held at the test temperature.

The load-displacement response for Specimen 5 is shown in Figure 4.17. As load was initially applied Specimen 5 became seated, where upon the load displacement relationship shows a stiffening behavior. After seating, a stiffening of 235.9 kip/in was observed, which is 15% less than Specimen 1. The transverse fillet welds fractured at a load of 40 kips and a displacement of 0.28 inches. Similar to the other specimens, the failure is abrupt, with the load dropping off quickly after weld fracture. Note that there is an increase in the maximum load compared to Specimen 4. Upon normalizing the results by the measured area of the weld, there will not be an increase in capacity. This will be shown in Chapter 5.

A photograph of Specimen 5 after the welds fractured is shown in Figure 4.18, where the failed transverse welds on the lap plate and top pull plate can be seen. Figure 4.19 is a photograph of the side view of the transverse fillet weld on the top pull plate of Specimen 5. Also shown in Figure 4.19 are the angles of the fracture surface of the transverse fillet welds on the lap plates, $\theta a$ and $\theta b$. The average fracture surface is 46.5°, which is a 9% variation from the angle of the fracture surface of Specimen 1.

### 4.2.7    Specimen 6: 900°F
The time-temperature data for Specimen 6 is shown in Figure 4.20. The furnace took an about an hour and a half to achieve the temperature of 900°F. Similar to Specimen 2, the temperature data fluctuates during heating and also during the 40 minute interval when the temperature was held at the test temperature. Unlike the previous specimens tested, there is no temperature data plotted for the lap plate. This was due to the fact that the thermocouples on the lap plate malfunctioned during testing.

110

The load-displacement response for Specimen 6 is shown in Figure 4.21. As load was initially applied Specimen 6 became seated, where upon the load displacement relationship shows a stiffening behavior. After seating, a stiffening of 208.1 kip/in was observed, which is 25% less than Specimen 1. One of the transverse fillet welds fractured at a load of 37 kips. Specimen 6 had a more ductile failure than the specimens tested at the lower temperatures, as observed from the load-displacement response. After the first weld fracture at the load of 37 kips, the load then dropped off and the specimen reloaded to 18 kips, where the other transverse fillet weld fractured. The transverse fillet welds fractured at displacements of 0.29 and 0.33 inches. The displacement of 0.33 inches is more than that of the other specimens tested at lower temperatures. Specimen 6 was also different in that all other specimens that were tested at lower temperatures experienced weld fracture at the same time.

A photograph of Specimen 6 after the welds fractured is shown in Figure 4.22, where the failed transverse welds on the lap plate and top pull plate can be seen. Figure 4.23 is a photograph of the side view of the weld on the top pull plate of Specimen 6. The fracture plane of Specimen 6 is jagged, and varies over the length of the weld, which causes the angle of the fracture plane to vary over the length of the weld as well. Also shown in Figure 4.23 are the angles of the fracture surface of the transverse fillet welds on the lap plates, $\theta a$ and $\theta b$. The average fracture surface is 35.5°, which is a 20% variation from the angle of the fracture surface of Specimen 1. Note that Specimen 6 has an average weld fracture angle that is less than Specimen 1, unlike all other specimens tested at lower temperatures.

### 4.2.8   Specimen 7: 1000°F
The time-temperature data for Specimen 7 is shown in Figure 4.24. The furnace took an about an hour and a half to achieve the temperature of 1000°F. Similar to Specimen 2, the temperature data fluctuates during heating and also during the 40 minute interval when the temperature was held at the test temperature.

The load-displacement response for Specimen 7 is shown in Figure 4.25. As load was initially applied Specimen 7 became seated, where upon the load displacement relationship shows a stiffening behavior. After seating, a stiffening of 197.6 kip/in was observed, which is 29% less than Specimen 1. Both transverse fillet welds fractured at a load of 26 kips and displacement of 0.22 inches. Unlike the abrupt failure observed in Specimens 1, 2, 3, 4, and 5, the failure of Specimen 7 was slightly more ductile. From the observations made about Specimen 6 and Specimen 7, it is concluded that as the temperature increases, the weld fracture becomes more gradual. Specimen 7 has experienced the most significant reduction in capacity compared to the specimens tested at lower temperatures. At all lower temperatures, the load was reduced by about 20%, whereas at 1000°F, there is a reduction of about 38% in Specimen 7.

A photograph of Specimen 7 after the welds fractured is shown in Figure 4.26, where the failed transverse welds on the lap plate and top pull plate can be seen. Figure 4.27 is a

photograph of the side view of the weld on the top pull plate of Specimen 7. The fracture plane of Specimen 7 is significantly more jagged than Specimen 6, and it appears that as the test temperature increases the fracture angle of the weld deviates from that at ambient temperature. Also shown in Figure 4.27 are the angles of the fracture surface of the transverse fillet welds on the lap plates, θa and θb. The average fracture surface is 51.5°, which is a 17% variation from the angle of the fracture surface of Specimen 1.

### 4.2.9    Specimen 8: 1200°F

The time-temperature data for Specimen 8 is shown in Figure 4.28. The furnace took just under two hours achieve the temperature of 1200°F. Similar to Specimen 2, the temperature data fluctuates during heating and also during the 40 minute interval when the temperature was held at the test temperature.

The load-displacement response for Specimen 8 is shown in Figure 4.29. As load was initially applied Specimen 8 became seated, where upon the load displacement relationship shows a stiffening behavior. After seating, a stiffening of 148.5 kip/in was observed, which is 46% less than Specimen 1. At the load of 16 kips one of the transverse fillet welds fractured. Like Specimen 6, the transverse welds on each side fractured at different times. The other transverse weld fractured at the load of 7 kips. Specimen 8 developed displacement of 0.17 and 0.20 inches when the transverse fillet welds fractured.

A photograph of Specimen 8 after the welds fractured is shown in Figure 4.30, where the failed transverse welds on the lap plate and top pull plate can be seen. Figure 4.31 is a photograph of the side view of the weld on the top pull plate of Specimen 8. The fracture plane of Specimen 8 is similar to that of Specimen 7. The lap plates and pull plate of Specimen 8 are darker in color than they were for specimens tested at the lower temperatures. Also shown in Figure 4.31 are the angles of the fracture surface of the transverse fillet welds on the lap plates, θa and θb. The average fracture surface is 30°, which is a 42% variation from the angle of the fracture surface of Specimen 1. Similar to Specimen 6, the average weld fracture angle is less than that of Specimen 1.

### 4.2.10  Specimen 9: 1400°F

The time-temperature data for Specimen 9 is shown in Figure 4.32. The furnace took about 4 hours achieve the temperature of 1400°F, which is significantly longer than the other specimens tested at the lower temperatures. Similar to Specimen 2, the temperature data fluctuates during heating and also during the 40 minute interval when the temperature was held at the test temperature. Specimen 9 does not have temperature data for the lap plate or top pull plate, since during the test the thermocouples on the lap plate and pull plate malfunctioned.

In Specimen 9, the temperature of the pull plate above the top cooling plate increased to about 100°F. To prevent any further increase, extra ceramic fire blanket was placed inside of the opening on the top of the furnace to reduce radiation, maintaining the

temperature of the specimen above the cooling plate to about 90°F. The temperature of the specimen below the cooling plate that was below the furnace did not exceed 75°F throughout the testing.

The load-displacement response for Specimen 9 is shown in Figure 4.33. As load was initially applied Specimen 8 became seated, where upon the load displacement relationship shows a stiffening behavior. After seating, a stiffening of 99.8 kip/in was observed, which is 64% less than Specimen 1. At the load of 9 kips both transverse fillet welds fractured. The shape of the load-displacement curve for Specimen 9 has a longer plateau near the maximum load than the other specimens tested at lower temperatures. This indicates that the failure becomes much more ductile as temperature increases. Specimen 9 has only about 20% of the capacity at ambient temperature, showing that a significant reduction in strength occurs at 1400°F. Specimen 9 had 0.17 inches of displacement at weld fracture.

A photograph of Specimen 9 after the welds fractured is shown in Figure 4.34, where the failed transverse weld on the lap plate and top pull plate can be seen. Figure 4.35 is a photograph of the side view of the weld on the top pull plate of Specimen 9. Also shown in Figure 4.35 are the angles of the fracture surface of the transverse fillet welds on the lap plates, θa and θb. The average fracture surface is 32.5°, which is a 31% variation from the angle of the fracture surface of Specimen 1. The fracture plane of Specimen 9 is similar to that of Specimen 8, varying by only 8%. The texture of the lap plates and pull plate was more rough and the weld had a slightly darker appearance than that of the specimens tested at lower temperatures.

### 4.2.11  Specimen 10: 1600°F
The time-temperature data for Specimen 10 is shown in Figure 4.36.For Specimen 10, the furnace took about 4 hours to achieve the temperature of 1600°F. Similar to Specimen 2, the temperature data fluctuates during heating and also during the 40 minute interval when the temperature was held at the test temperature.

Similar to Specimen 9, Specimen 10 does not have temperature data for the lap plate or top pull plate. This is due to the same problems that were experienced with Specimen 9. Similar to Specimen 10, extra ceramic fire blanket had to be placed inside the top opening of the furnace to prevent excess radiation.

The load-displacement response for Specimen 10 is shown in Figure 4.37. As load was initially applied Specimen 8 became seated, where upon the load displacement relationship shows a stiffening behavior. After seating, a stiffening of 72.4 kip/in was observed, which is 74% less than Specimen 1. The maximum load was 7 kips and is only slightly less that found in Specimen 9. At peak load, Specimen 10 has a displacement of 0.19 inches. Similar to Specimen 9, the shape of the load-displacement curve shows a longer plateau near the maximum load than the other specimens tested at the lower temperatures, indicating that the failure becomes much more ductile as the temperature

113

increases. Specimen 10 has only about 20% of the capacity at ambient temperature, showing that a significant reduction occurs at 1600°F.

When Specimen 10 fractured, the weld did not completely break apart as it did in the other tests, resulting in Specimen 10 being in one piece when it was removed. Upon removal of Specimen 10, the weld fracture was observed and is shown in Figure 4.38.

## 4.3 Post-Fire Scenario Tests

As discussed in Section 3.2, five post-fire scenario tests were performed at selected temperatures. From these tests, it was desired that a well defined relationship be determined for the reduction of weld strength and stiffness during post-fire conditions. The ultimate load achieved, the stiffness, and the failure plane of the weld will be presented. First general qualitative observations will be discussed. Then, the temperature and load data from each test will be discussed. The maximum load data from the SATEC testing machine, the stiffness, and the average transverse weld fracture angle for each specimen is summarized in Table 4.2. The ultimate loads will be normalized and used to develop a reduction factor in Chapter 5.

### 4.3.1 Qualitative Observations

As previously discussed, in the post-fire scenario tests, the specimens were heated to 1600°F and then cooled to the selected test temperatures. The post-fire scenario tests were similar to the elevated temperature tests in that prior to testing the weld was observed and measured and found to be larger than ¼", as specified in the design. Therefore, it was determined that the results of the post-fire scenario tests would have to be normalized by the area of the weld, which will be discussed in further detail in Chapter 5. Also similar to the elevated temperature tests, the cooling system and thermocouples were put into place and observed prior to testing.

Recall from Chapter 3 that the test temperature was averaged for forty minutes. Table 4.2 shows the actual average temperature during this 40 minute period for each specimen. Observe that for Specimen P2 and P4 there was a little less than 5% variation between the target temperature and the actual average temperature. This will be discussed in more detail in the following sections. The actual averaged temperature for Specimens P1, P3, and P5 had less than 2% variation.

Upon removal of the test specimens, the first difference observed from the elevated temperature tests was that the surface of the base metal and weld metal flaked off easily when touched. After the elevated temperature tests, the specimens were not observed to have this characteristic. The specimens had also changed in both color and texture; the specimen appeared to be lighter and had a rougher texture than the specimens that were tested in the elevated temperature tests. Photographs of each specimen after testing will be shown and discussed in this section.

Similar to the elevated temperature tests, the inclination of the weld fractured plane from visual observations did not appear to be at 45° as assumed in AISC. Photographs of the failure plane of each specimen will be shown in the following sections. As discussed in Chapter 3, after testing the weld leg size and weld throat are measured.

### 4.3.2 Specimen P1: 70°F

The digital time-temperature data for Specimen P1 was not recorded due to the CR5000 data acquisition system malfunctioning. However, during the duration of the test, the thermocouples were functioning and the data was scanned to ensure that Specimen P1 was heated to 1600°F and cooled down to ambient temperature prior to testing. It was observed that the furnace took about 4 hours to reach 1600°F and about another 4 hours to cool down to ambient temperature.

The load-displacement relationship for Specimen P1 is shown in Figure 4.39 where it is compared with that of Specimen 1. Specimen P1 failed at 42 kips, which is the same ultimate load as Specimen 1 tested at ambient temperature. The load-displacement relationship has a stiffness after seating of 209.3 kips/in, which is 25% less than that of Specimen 1. The load-displacement relationship is more ductile. After the ultimate load was reached, the transverse fillet weld on one side fractured in Specimen P1; therefore the load dropped off and reloaded to about 20 kips when the weld on the other side fractured. Specimen P1 had 0.30 and 0.34 inches of displacement. At ultimate load, the displacement was 0.30 inches which is about 3% increase from Specimen 1.

A photograph of Specimen P1 after the welds fractured is shown in Figure 4.40, where the failed transverse weld on the lap plate and top pull plate can be seen. Figure 4.41 is a photograph of the side view of the weld on the top pull plate of Specimen P1. The fracture plane of Specimen P1 is uniform, similar to Specimen 1. The average fracture plane of Specimen P1 is 46°, which is an 8% increase from Specimen 1. The lap plates and pull plate are much lighter in color and have a rougher texture. The steel and weld flaked off easily when touched.

### 4.3.3 Specimen P2: 600°F

The time-temperature data for Specimen P2 is shown in Figure 4.42. The furnace took about 3 hours to reach the temperature of 1600°F and about another 3 hours to cool down to 600°F. There was 4.75% variation between the target temperature and the actual averaged temperature that Specimen P2 was tested at. The actual averaged temperature for Specimen P2 was 571.5°F. There is no temperature data beyond 350 minutes due to the fact that the thermocouples malfunctioned.

The load-displacement relationship for Specimen P2 is shown in Figure 4.43 where it is compared to the response of Specimen 3. Specimen P2 has the transverse fillet welds fracture at 38.5 kips, which is slightly less than the failure load of Specimen P1. Specimen 3, which was tested at 600°F during the elevated temperature tests, failed at 41 kips. Therefore, there is good agreement between Specimen 3 and Specimen P2. The

load-displacement relationship for Specimen P2 has a stiffness after seating of 204.5 kips/in which is 16% less than that of Specimen 3. The peak load occurred at a displacement of 0.28 inches in Specimen P2.

A photograph of Specimen P2 after the welds fractured is shown in Figure 4.44, where the failed transverse weld on the lap plate and top pull plate can be seen. Figure 4.45 is a photograph of the side view of the weld on the top pull plate of Specimen P2. The average fracture plane of Specimen P2 is 66.5°, which has a 36% increase from Specimen 1, indicating that the weld fracture angle is flatter for Specimen P2 than it was at ambient temperature. The weld fracture plane of Specimen P2 has a 25% increase from Specimen 3, indicating that the fracture surface is flatter at the same test temperature upon fracture during cooling. The color and texture of the lap and pull plates of Specimen P2 are very similar to that of Specimen P1.

### 4.3.4   Specimen P3: 800°F
The time-temperature data for Specimen P3 is shown in Figure 4.46. The furnace took about 4 hours to reach the temperature of 1600°F and a little over an hour to cool down to 800°F.

The load-displacement relationship for Specimen P3 is shown in Figure 4.47 where it is compared to Specimen 5. Specimen P3 achieved a maximum load of 43 kips, which is slightly greater than that of Specimen P2. Although a decrease in load capacity would be expected with increasing temperature, the results will be normalized by the area of the weld in Chapter 5. Recall that Specimen 5, which was tested at 800°F during the elevated temperature tests, failed at 40 kips. Therefore, Specimen P3 had a slightly larger capacity. The load-displacement relationship for Specimen P3 has a stiffness after seating of 201.0 kips/in, which is 15% less than that of Specimen 5, and reached a greater displacement of 0.35 at peak load.

A photograph of Specimen P3 after it fractured is shown in Figure 4.48, where the weld on the lap plate and top pull plate can be seen. Figure 4.49 is a photograph of the side view of the weld on the top pull plate of Specimen P3. When the weld fractured, it was at an average angle of 55.5°, which has a 23% increase from Specimen 1 and a 16% increase from Specimen 5. Similar to Specimen P2, the average weld fracture angle is flatter than that at ambient temperature and at the corresponding elevated temperature test. The fracture plane of the weld of Specimen P3 is more jagged than Specimen P1 and P2 and there is significantly more weld on the lap plates then on the top pull plate after the welds fractured.

### 4.3.5   Specimen P4: 1000°F
The time-temperature data for Specimen P4 is shown in Figure 4.50. The furnace took about 3 hours to reach the temperature of 1600°F and about an hour to cool down to 1000°F. There was 4.32% variation between the target temperature and the actual

averaged temperature that Specimen P4 was tested at. The actual averaged temperature for Specimen P4 was 956.8°F.

The load-displacement relationship for Specimen P4 is shown in Figure 4.51 where it is compared to that of Specimen 7. Specimen P4 achieved a maximum load of 30 kips. Recall that Specimen 7, which was tested at 1000°F during the elevated temperature tests, failed at 26 kips. Therefore, Specimen P4 had a greater capacity. The load-displacement relationship for Specimen P4 has a stiffness after seating of 177.9 kips/in, which is 10% less than that of Specimen 7, and reached a greater displacement of 0.32 at peak load.

A photograph of Specimen P4 after it fractured is shown in Figure 4.52, where the weld on the lap plate and top pull plate can be seen. Figure 4.53 is a photograph of the side view of the weld on the top pull plate of Specimen P4. When the weld fractured, it was at an average angle of 54.0°, which has a 21% increase from Specimen 1 and a 5% increase from Specimen 7. Similar to Specimen P2, the average weld fracture angle is flatter than that at ambient temperature and at the corresponding elevated temperature test. The fracture plane of Specimen P4 is more jagged than at lower test temperatures. Also, the lap plates, pull plate, and the weld are lighter in color and the texture is mill scale.

### 4.3.6   Specimen P5: 1200°F
The time-temperature data for Specimen P5 is shown in Figure 4.54. The furnace took about 3 and a half hours to reach the temperature of 1600°F and a little less than an hour to cool down to 1200°F.

The load-displacement relationship of Specimen P5 is shown in Figure 4.55 where it is compared to that of Specimen 8. Specimen P5 achieved a maximum load of 18 kips. Recall that Specimen 8, which was tested at 1200°F during the elevated temperature tests, achieved a maximum load of 16 kips. Therefore, the two specimens had very similar capacities. The load-displacement relationship for Specimen P5 has a stiffness after seating of 134.3 kips/in, which is 10% less than that of Specimen 8, and reached a greater displacement of 0.24 at peak load.

A photograph of Specimen P5 after the welds fractured is shown in Figure 4.56, where the failed transverse weld on the lap plate and top pull plate can be seen. Figure 4.57 is a photograph of the side view of the weld on the top pull plate of Specimen P5. When the weld fractured, it was at an average angle of 34.5°, which has a 19% decrease from Specimen 1 and a 13% increase from Specimen 8. After Specimen P5 fractured, the weld, lap plates, and pull plate are similar to Specimen P4 in that the lap plates, pull plate, and weld metal are lighter in color and had mill scale that would easily chip off when touched.

### 4.4   Summary
This chapter presented the qualitative and quantitative observations for both the elevated temperature tests and post-fire scenario tests. This includes the temperature and load data

for each specimen. Time-temperature curves and load-displacement relationships were presented and discussed for both the elevated temperature and post-fire scenario tests. It was concluded that during the elevated temperature tests, when the specimen was heated above 800°F the failure of the weld became more ductile. It was also concluded that during the post-fire scenario tests at temperatures at 800°F and above, the weld metal tends to soften, resulting in a more ductile weld fracture.

Table 4.1  Results for elevated temperature tests

| Specimen | Target Temperature (°F) | Actual Average Temperature (°F) | Pult (kip) | k (kip/in) | θ | | |
|---|---|---|---|---|---|---|---|
| | | | | | θa (deg) | θb (deg) | θavg (deg) |
| 1 | 70 | - | 41.76 | 277.8 | 51 | 34 | 42.5 |
| 2 | 350 | 356.6 | 15.87 | 237.8 | 90 | 70 | 80.0 |
| 3 | 600 | 608.8 | 41.07 | 243.5 | 32 | 68 | 50.0 |
| 4 | 700 | 710.8 | 40.13 | 228.4 | 51 | 50 | 50.5 |
| 5 | 800 | 804.3 | 25.73 | 235.9 | 44 | 49 | 46.5 |
| 6 | 900 | 865.6 | 36.86 | 208.1 | 34 | 37 | 35.5 |
| 7 | 1000 | 1007.3 | 43.29 | 197.6 | 45 | 58 | 51.5 |
| 8 | 1200 | 1224.3 | 37.43 | 148.8 | 22 | 38 | 30.0 |
| 5 | 1400 | 1390.5 | 7.29 | 99.8 | 34 | 31 | 32.5 |
| 10 | 1600 | 1600.4 | 8.62 | 72.4 | - | - | - |

Table 4.2  Results for post-fire scenario tests

| Specimen | Target Temperature (°F) | Actual Average Temperature (°F) | Pult (kip) | k (kip/in) | θ | | |
|---|---|---|---|---|---|---|---|
| | | | | | θa (deg) | θb (deg) | θavg (deg) |
| P1 | 70 | - | 41.76 | 209.3 | 45 | 47 | 46.0 |
| P2 | 600 | 571.5 | 38.50 | 204.5 | 73 | 60 | 66.5 |
| P3 | 800 | 785.7 | 42.80 | 201.0 | 53 | 58 | 55.5 |
| P4 | 1000 | 956.8 | 31.60 | 177.9 | 48 | 60 | 54.0 |
| P5 | 1200 | 1212.1 | 17.80 | 134.3 | 32 | 37 | 34.5 |

Figure 4.1  Load-displacement response for Specimen 1

Figure 4.2  Photograph of Specimen 1 after fracture, where the weld on the lap plate and top base plate is visible



Figure 4.3  Photograph of a side view Specimen 1, where the profile of the fractured weld on the top pull plate is visible

Figure 4.4  Time-temperature curve for Specimen 2

Figure 4.5  Load-displacement response for Specimen 2

123

Figure 4.6  Photograph of Specimen 2 after fracture, where the weld on the lap plate and top base plate is visible



Figure 4.7  Photograph of a side view Specimen 2, where the profile of the fractured weld on the top pull plate is visible

Figure 4.8  Time-temperature curve for Specimen 3
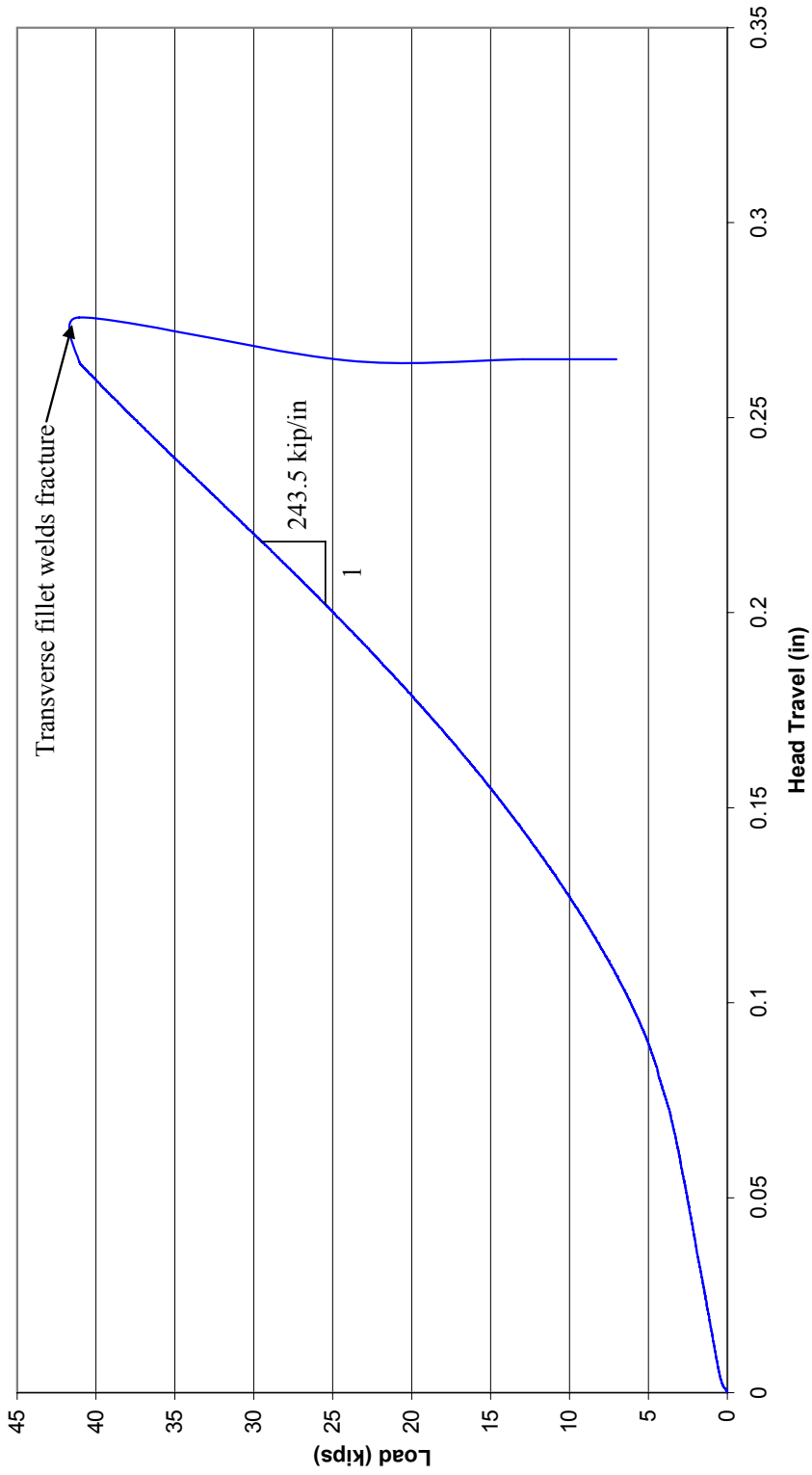
Figure 4.9  Load-displacement response for Specimen 3

126

Figure 4.10  Photograph of Specimen 3 after fracture, where the weld on the lap plate and top base plate is visible



Figure 4.11  Photograph of a side view Specimen 3, where the profile of the fractured weld on the top pull plate is visible

Figure 4.12  Time-temperature curve for Specimen 4
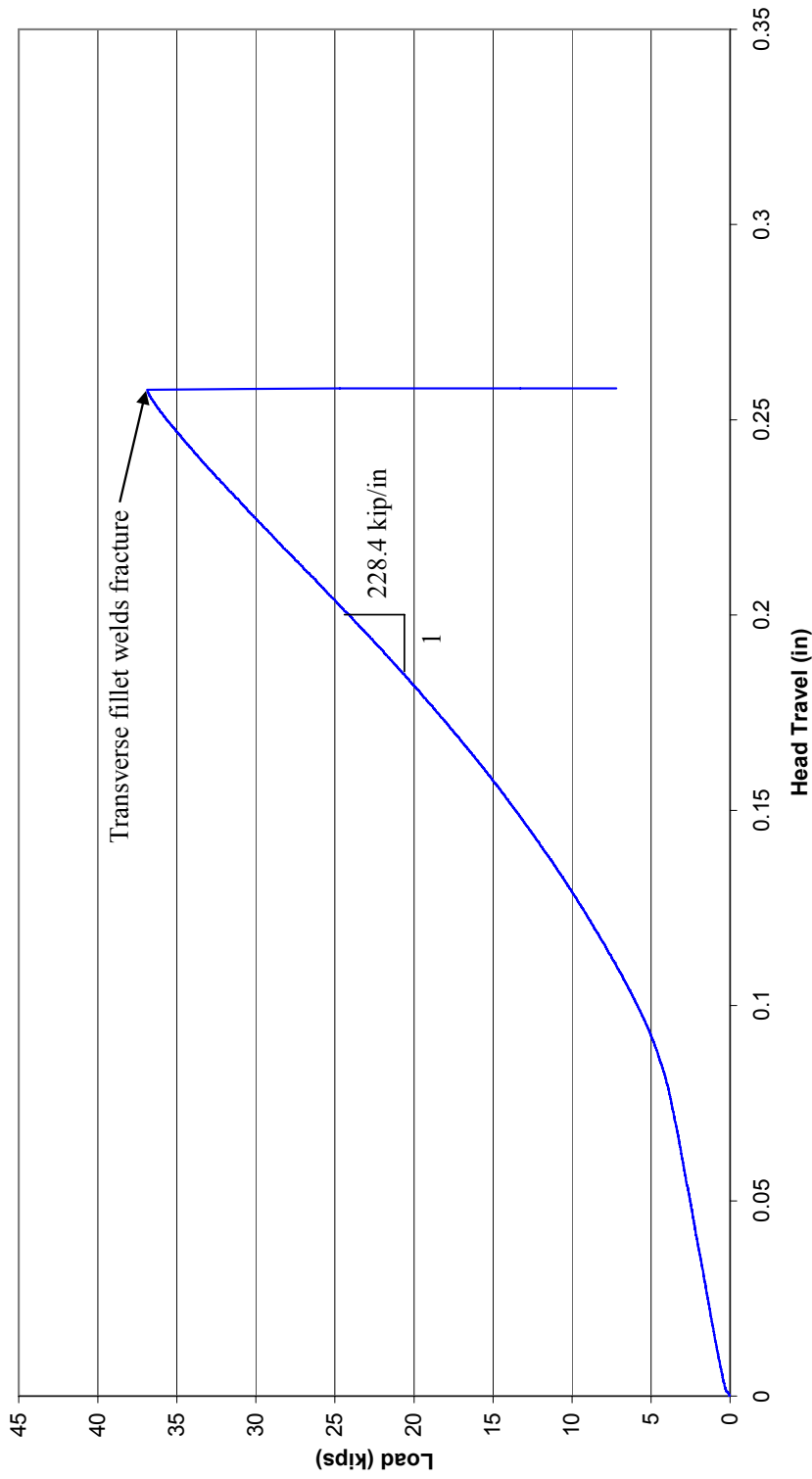
Figure 4.13  Load-displacement response for Specimen 4

Figure 4.14  Photograph of Specimen 4 after fracture, where the weld on the lap plate and top base plate is visible



Figure 4.15  Photograph of a side view Specimen 4, where the profile of the fractured weld on the top pull plate is visible

Figure 4.16  Time-temperature curve for Specimen 5

131
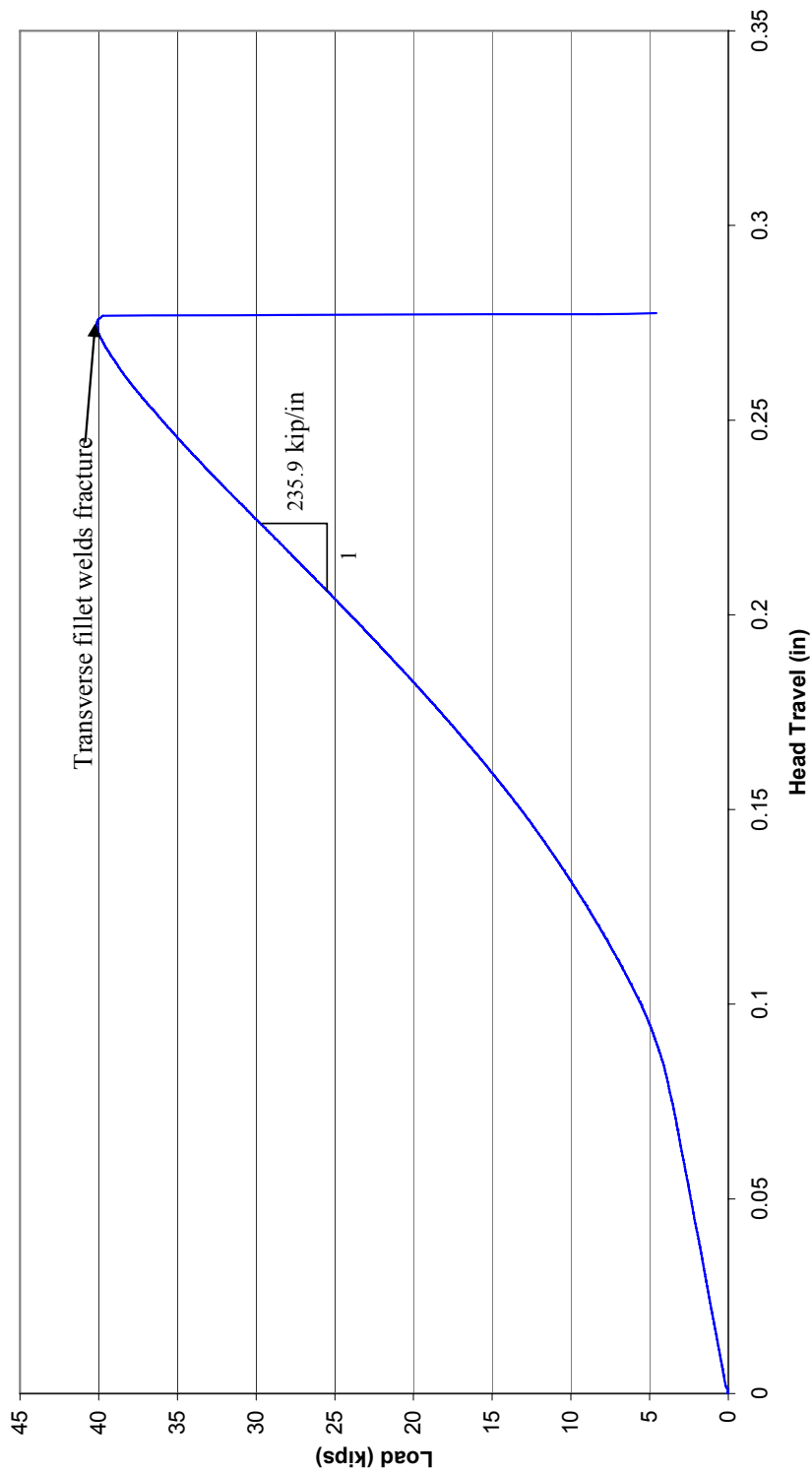
Figure 4.17  Load-displacement response for Specimen 5

Figure 4.18 Photograph of Specimen 5 after fracture, where the weld on the lap plate and top base plate is visible



Figure 4.19 Photograph of a side view Specimen 5, where the profile of the fractured weld on the top pull plate is visible
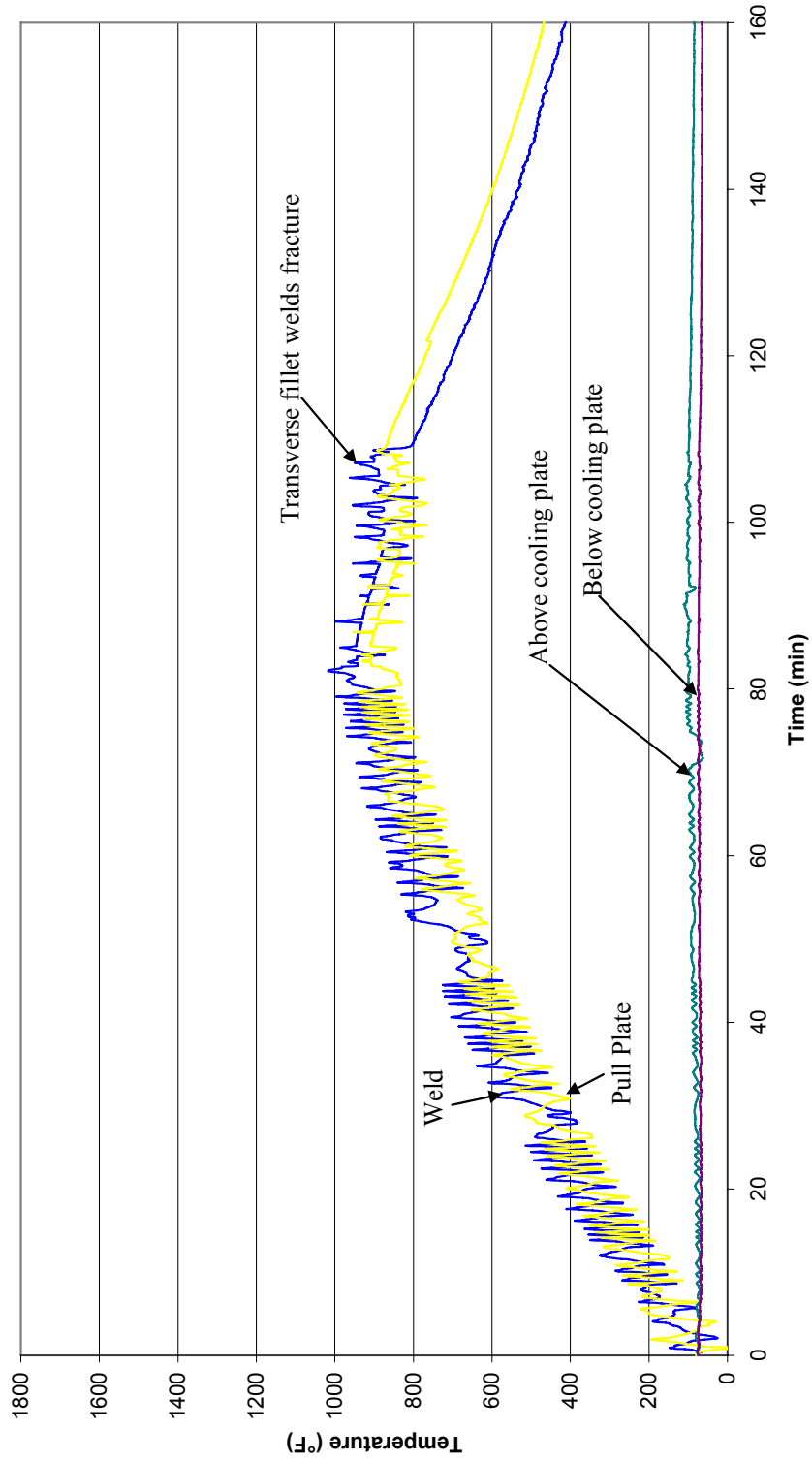
Figure 4.20  Time-temperature curve for Specimen 6

134
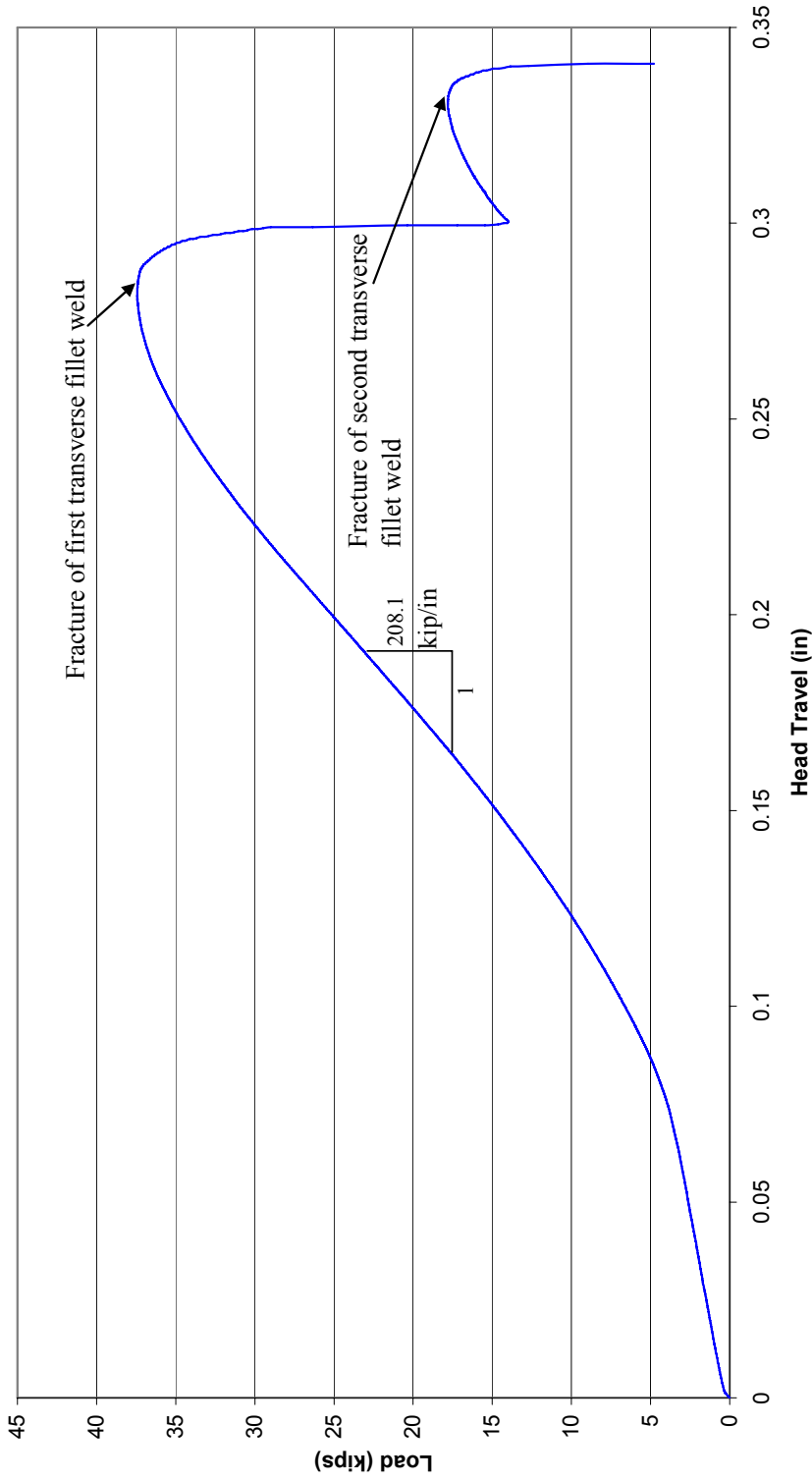
Figure 4.21  Load-displacement response for Specimen 6

Figure 4.22  Photograph of Specimen 6 after fracture, where the weld on the lap plate and top base plate is visible
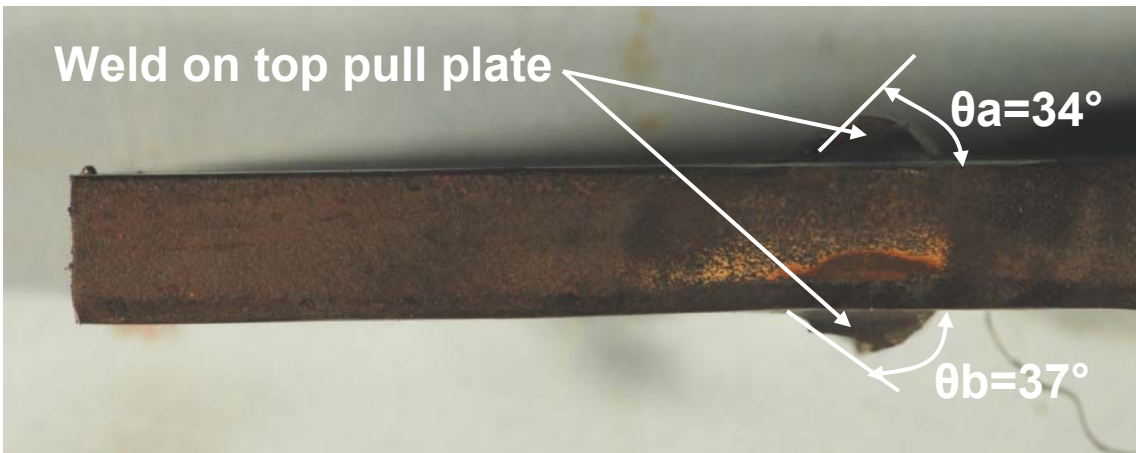


Figure 4.23  Photograph of a side view Specimen 6, where the profile of the fractured weld on the top pull plate is visible
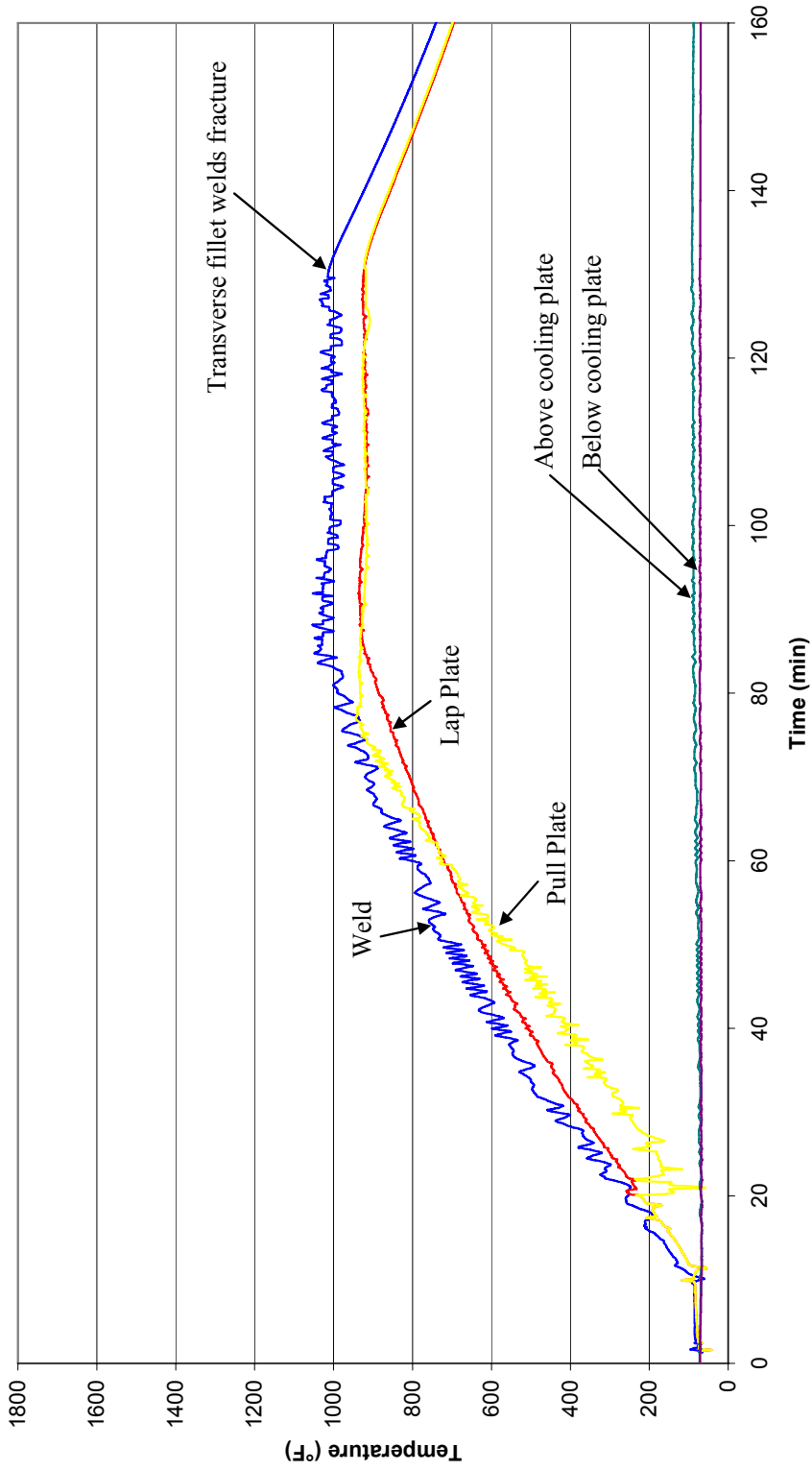
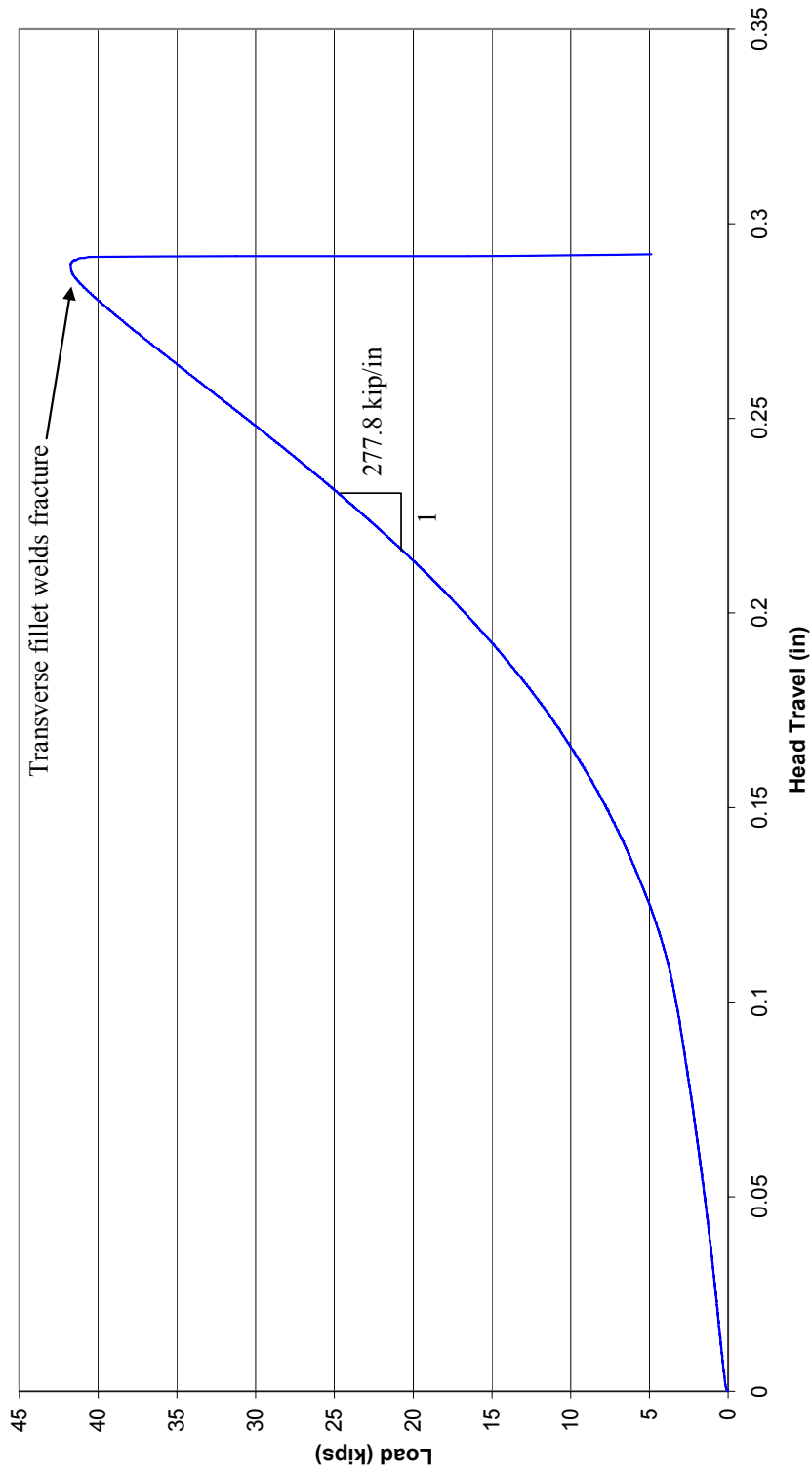Figure 4.24  Time-temperature curve for Specimen 7

137
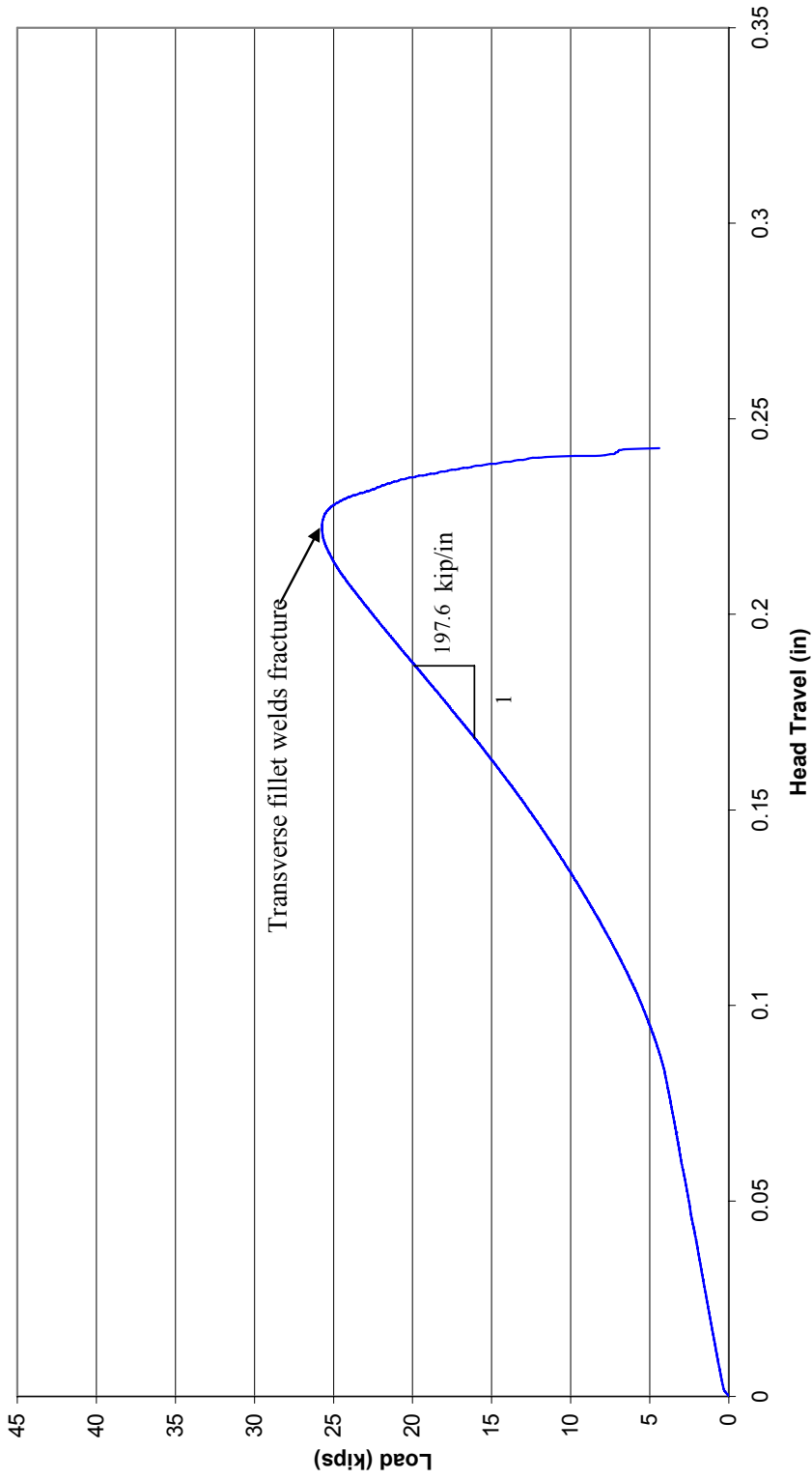
Figure 4.25  Load-displacement response for Specimen 7

Figure 4.26  Photograph of Specimen 7 after fracture, where the weld on the lap plate and top base plate is visible
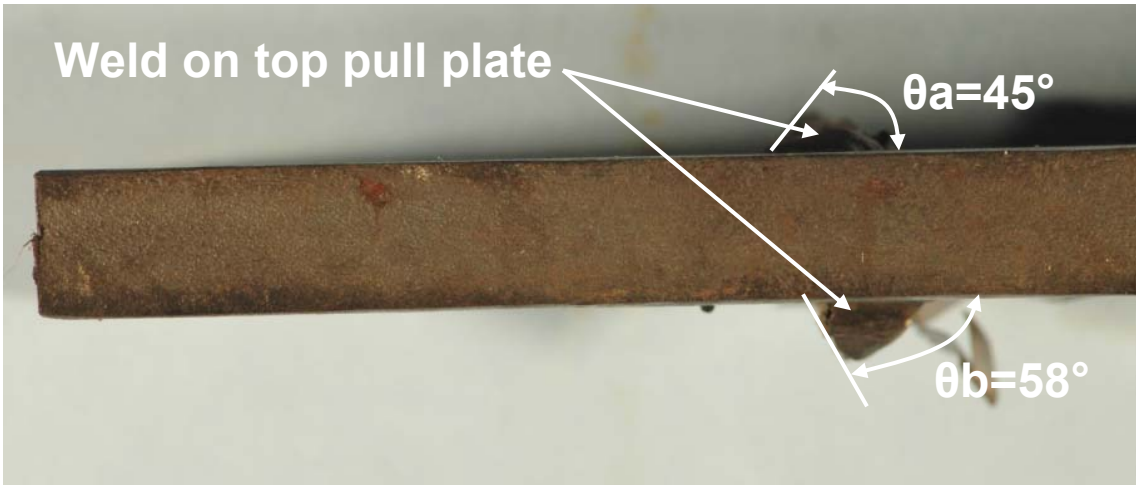


Figure 4.27  Photograph of a side view Specimen 7, where the profile of the fractured weld on the top pull plate is visible
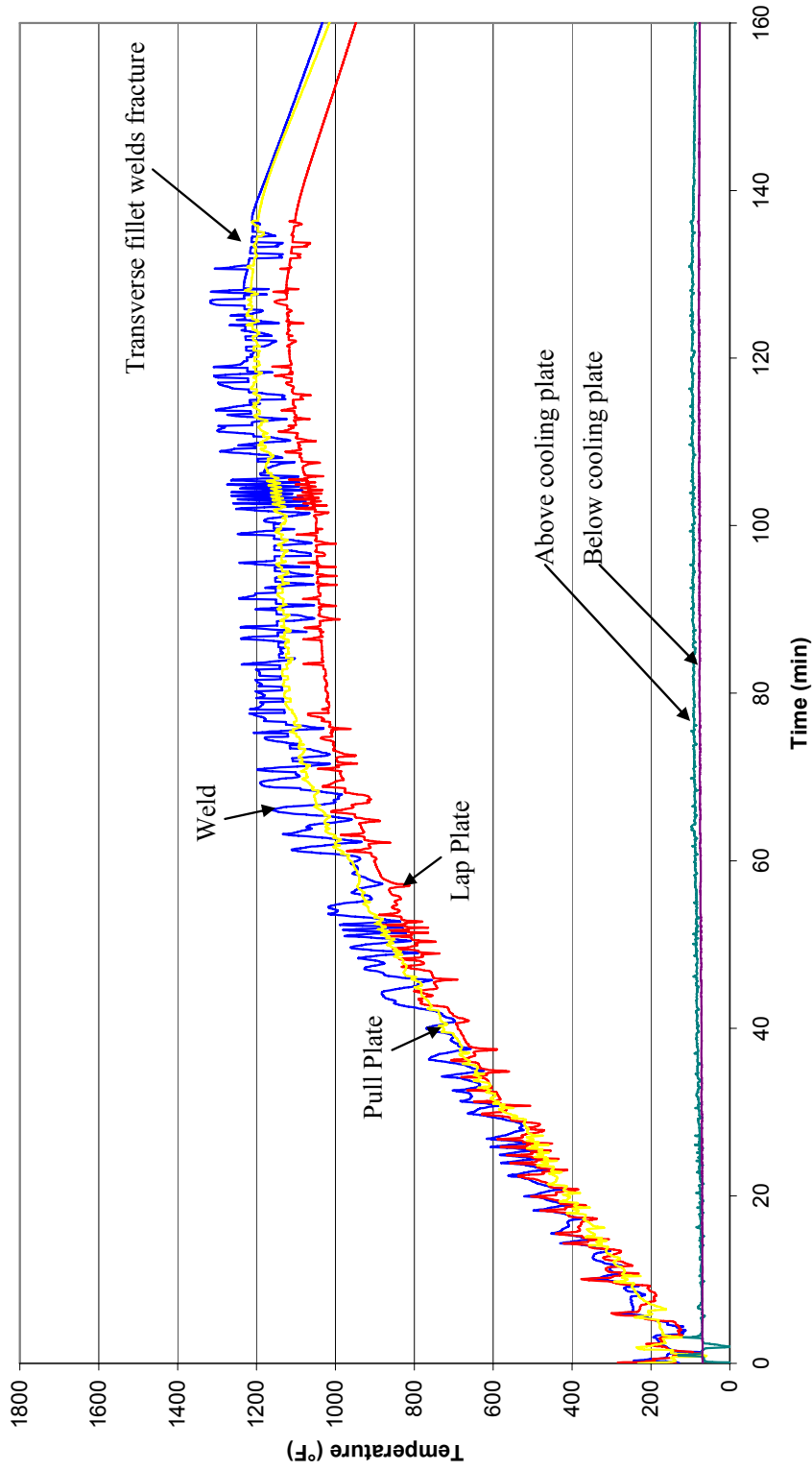
Figure 4.28   Time-temperature curve for Specimen 8
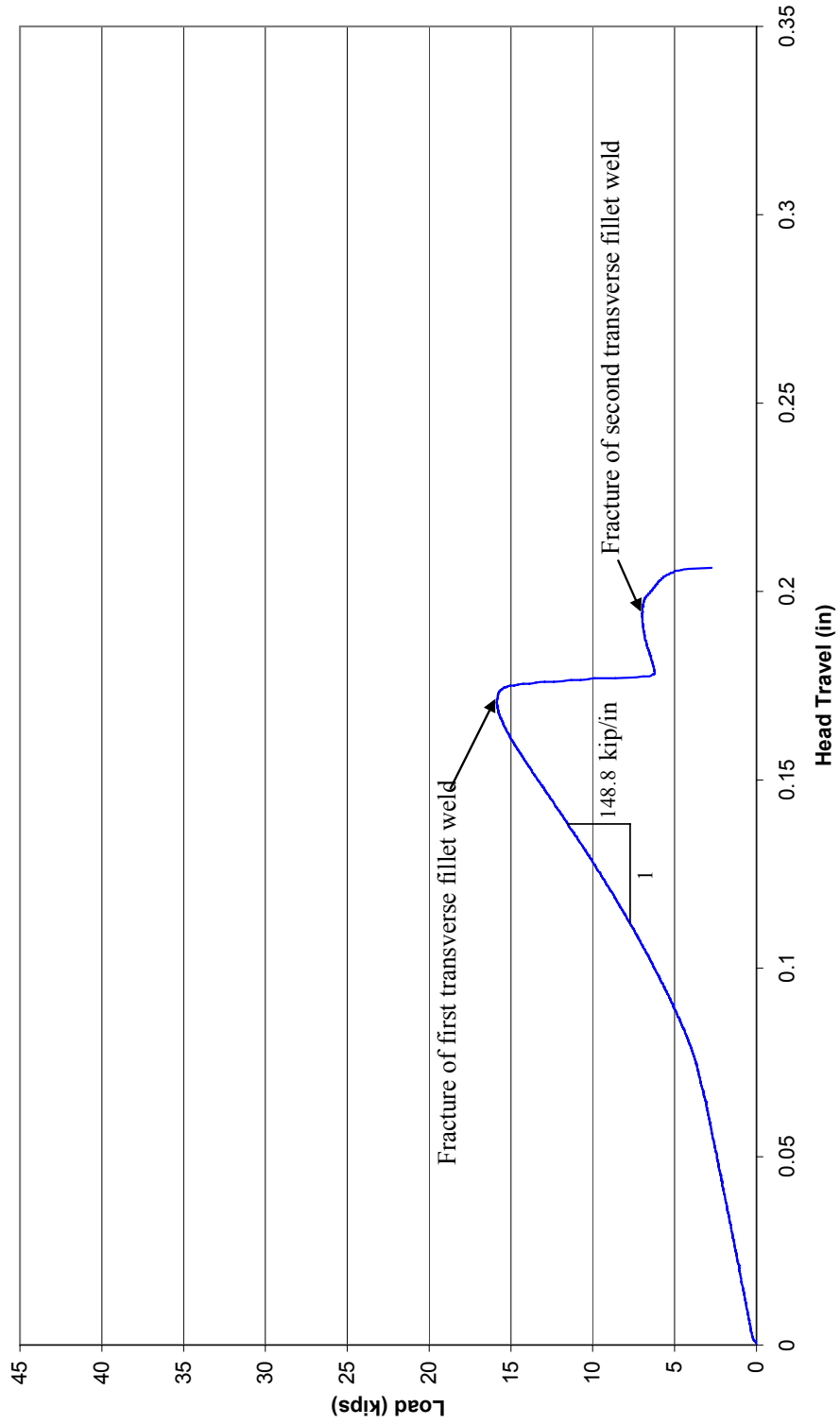
Figure 4.29  Load-displacement response for Specimen 8

Figure 4.30  Photograph of Specimen 8 after fracture, where the weld on the lap plate and top base plate is visible
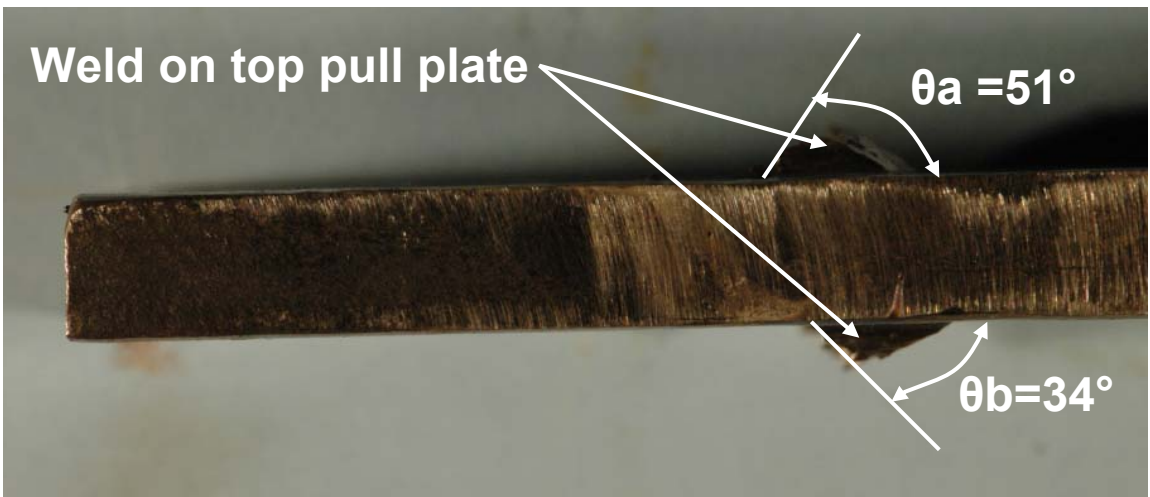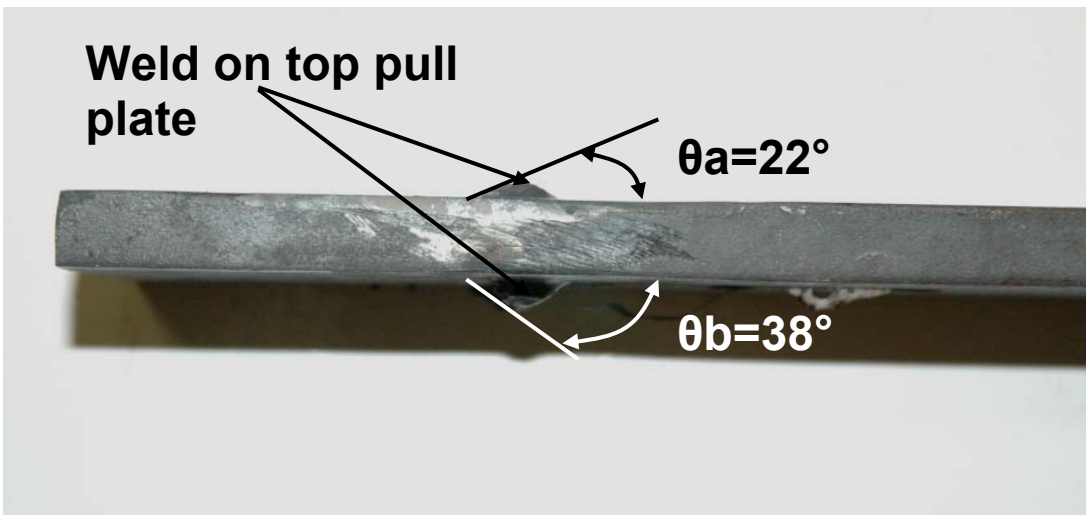


Figure 4.31  Photograph of a side view Specimen 8, where the profile of the fractured weld on the top pull plate is visible
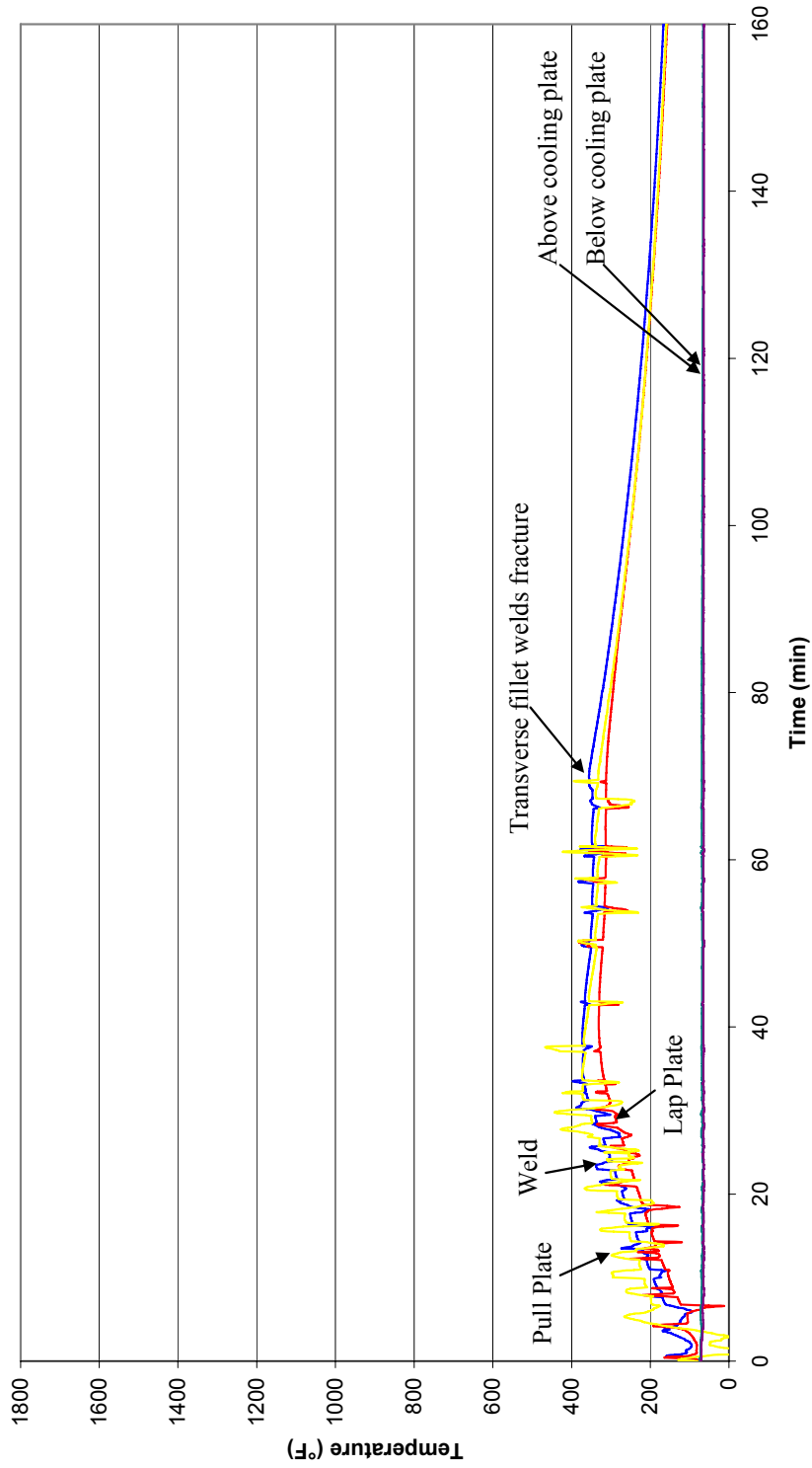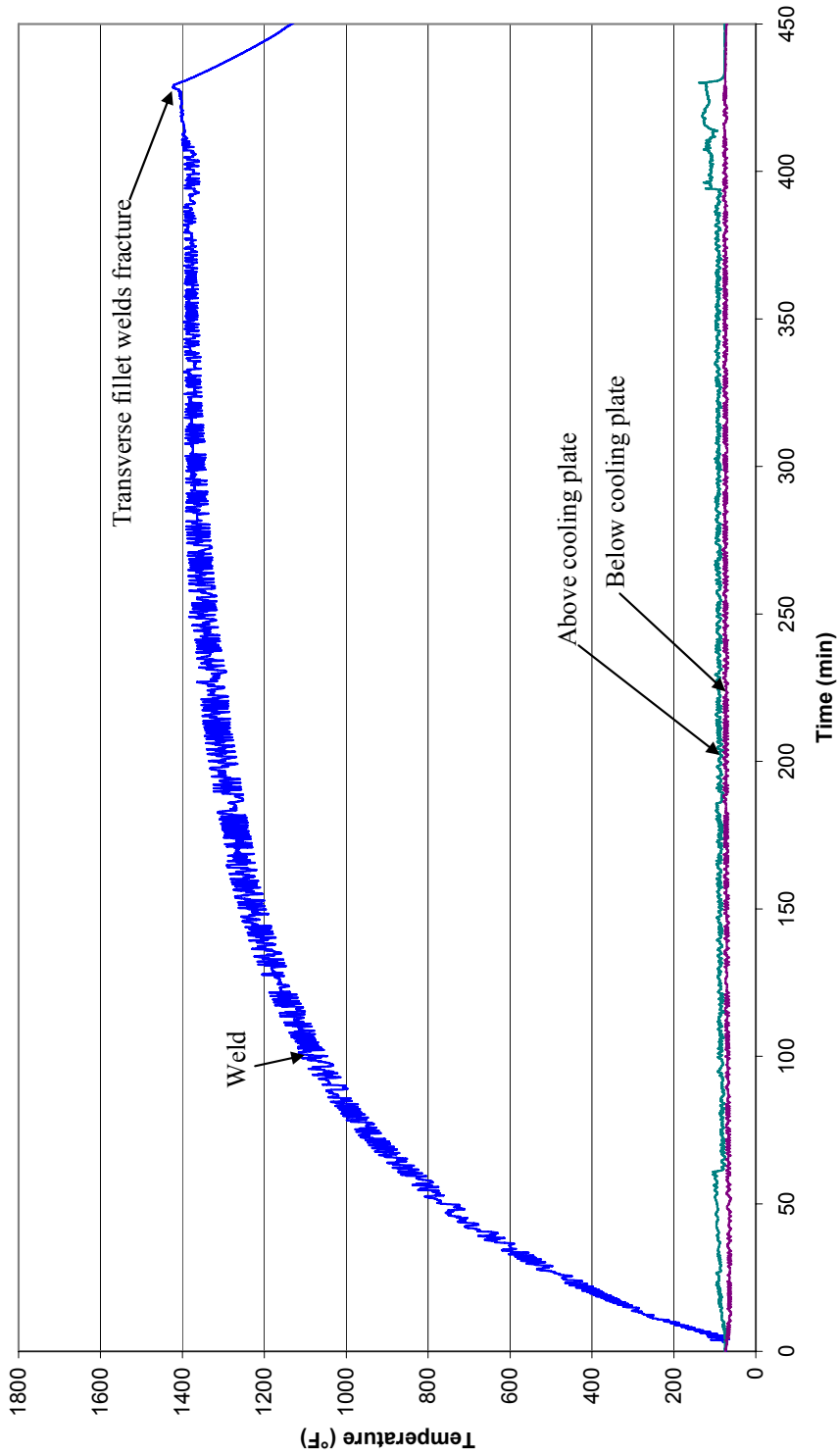
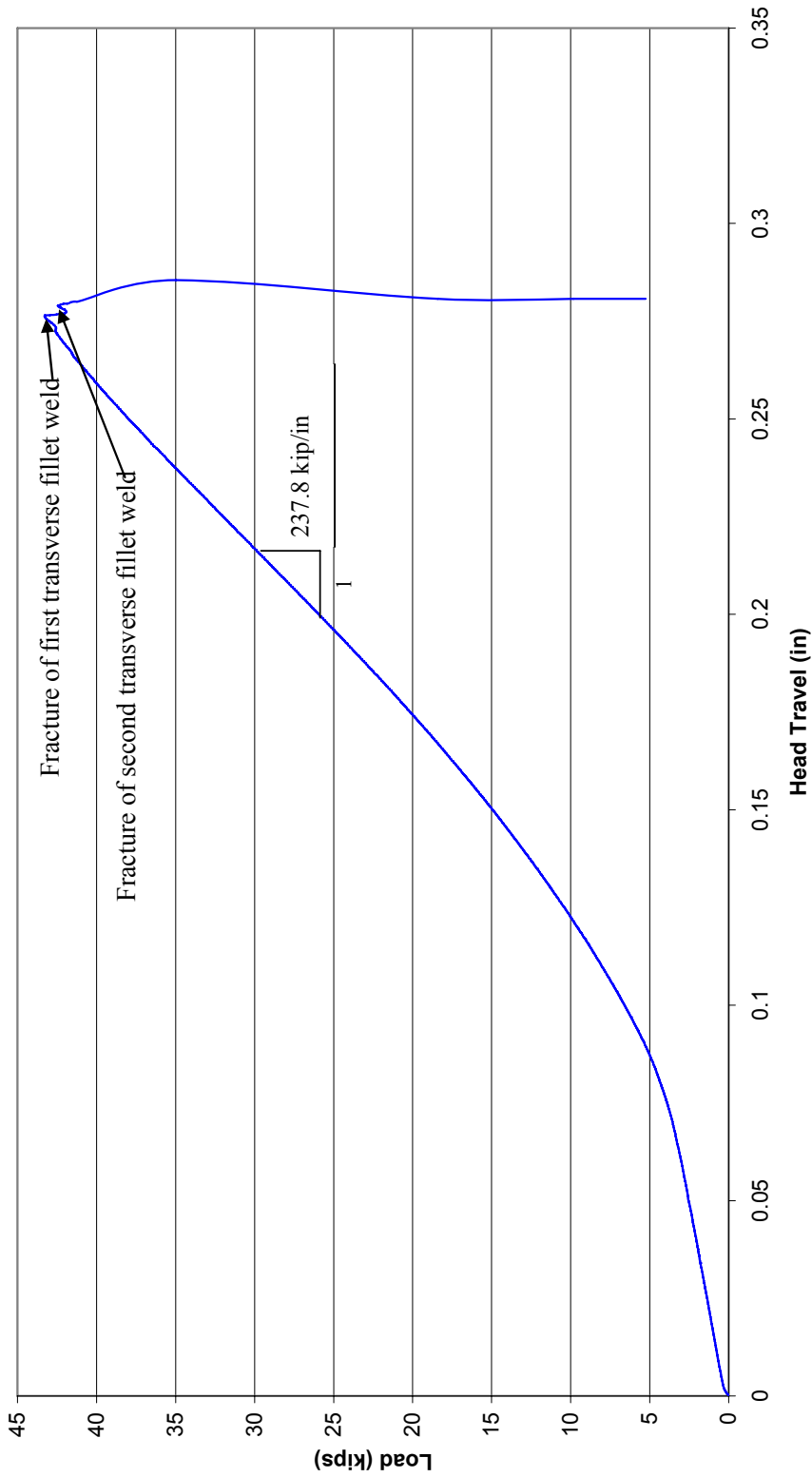Figure 4.32  Time-temperature curve for Specimen 9
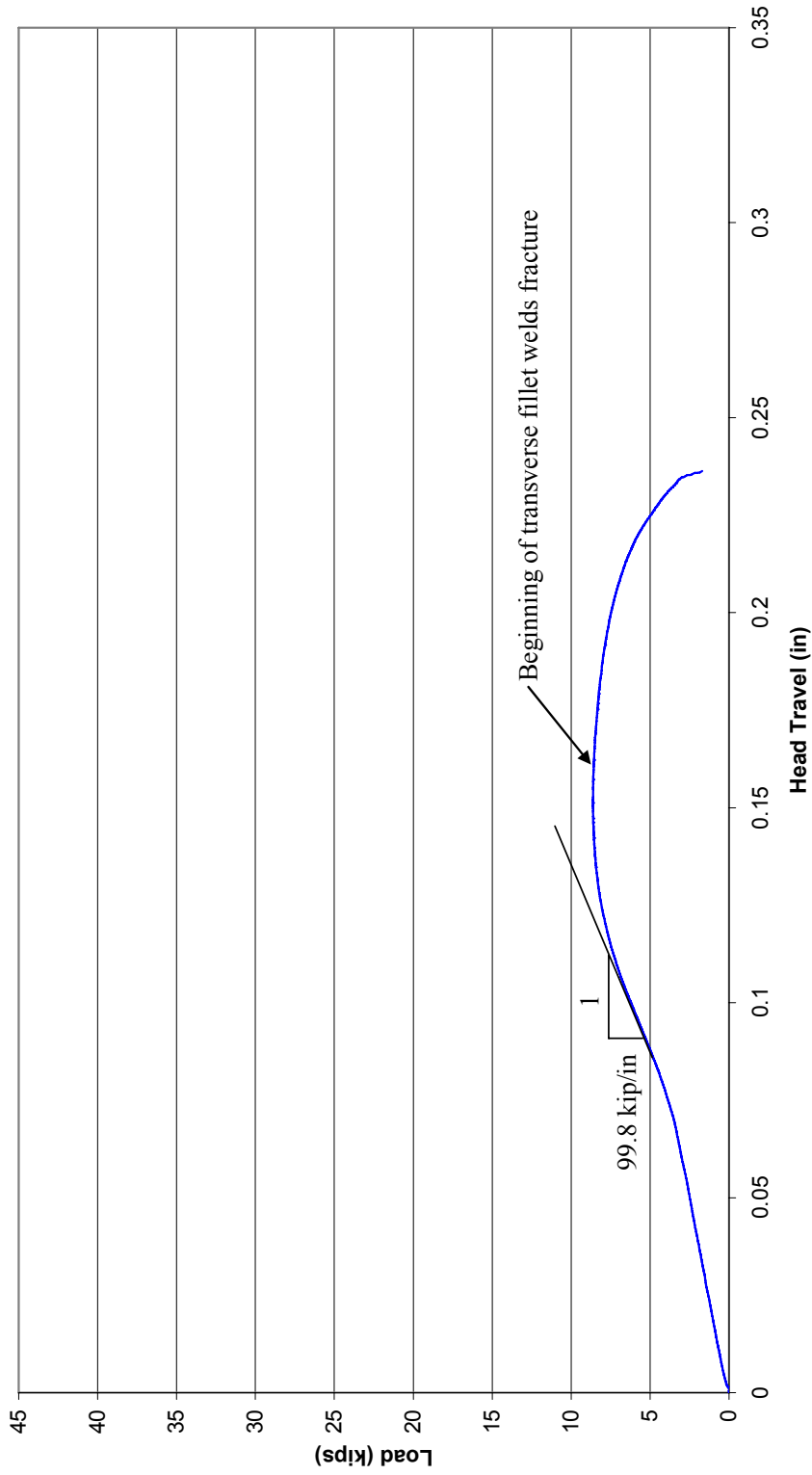
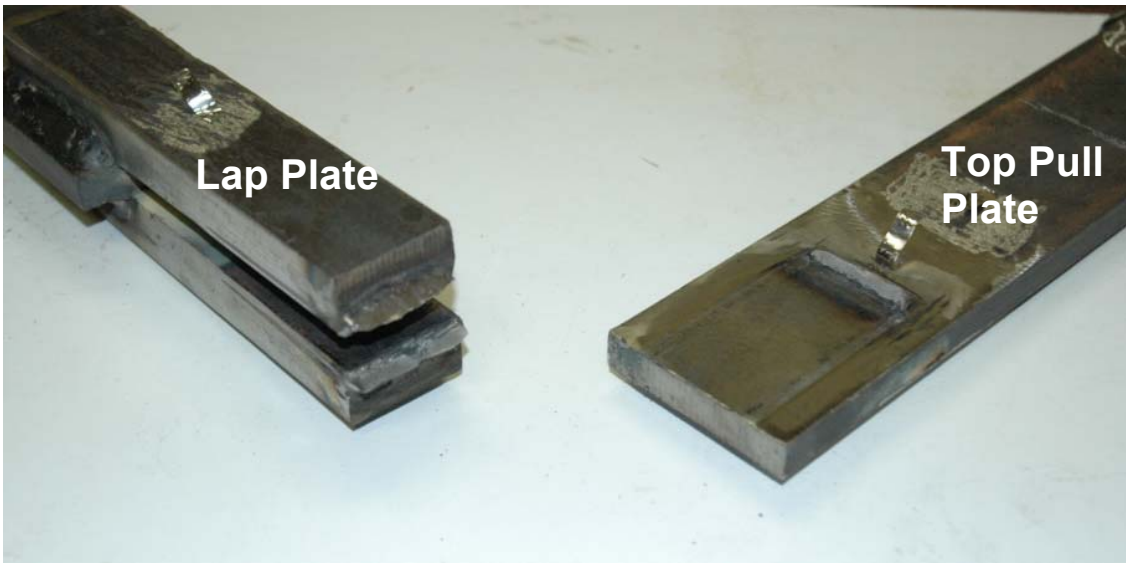Figure 4.33  Load-displacement response for Specimen 9
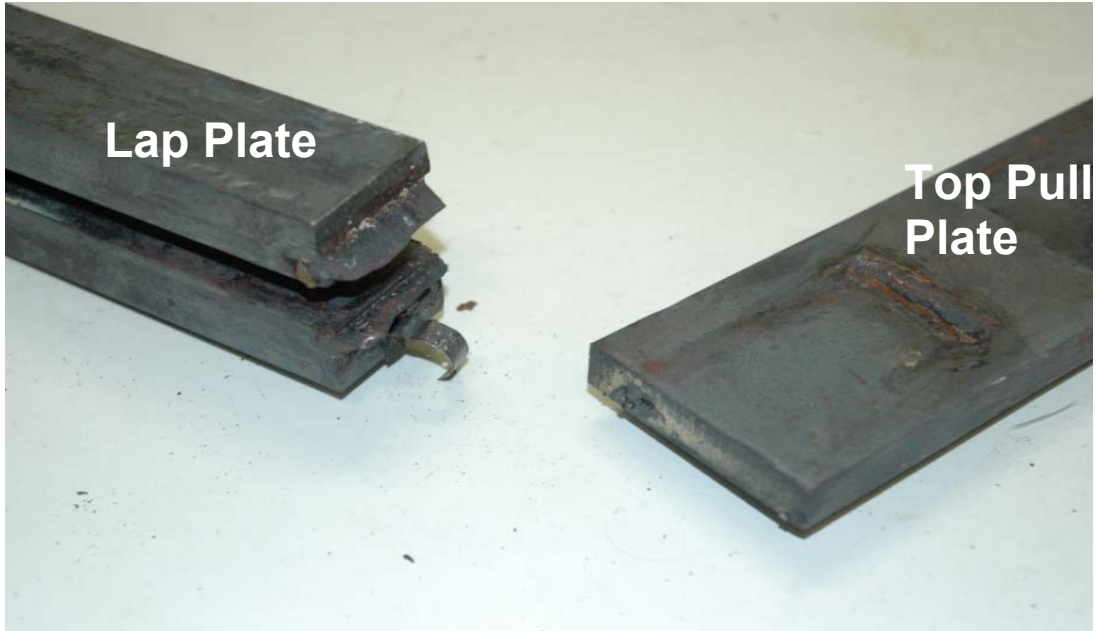
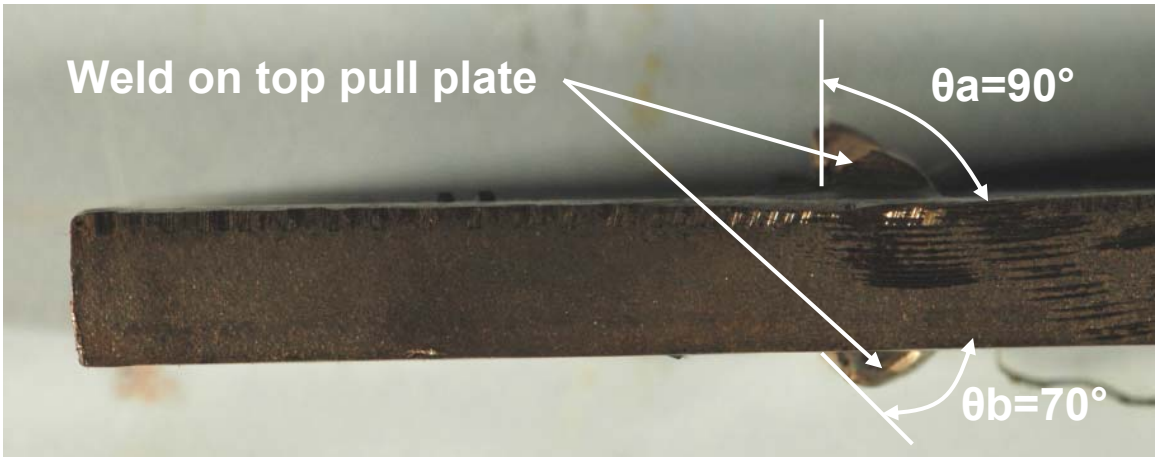Figure 4.34  Photograph of Specimen 9 after fracture, where the weld on the lap plate and top base plate is visible
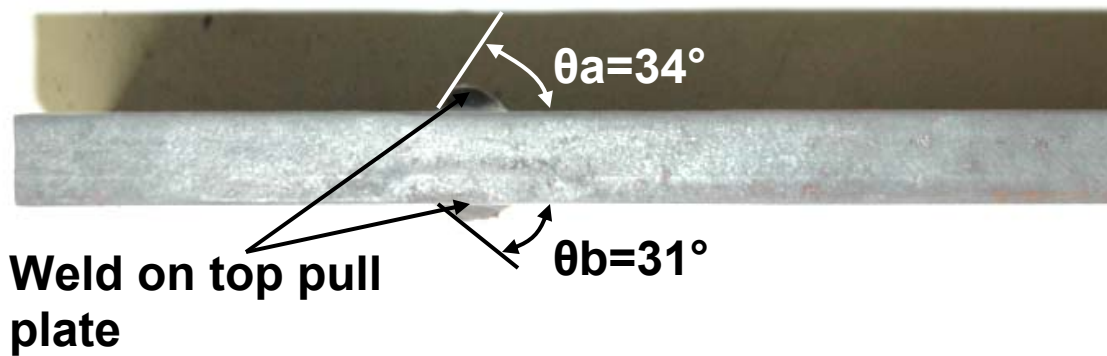


Figure 4.35  Photograph of a side view Specimen 9, where the profile of the fractured weld on the top pull plate is visible
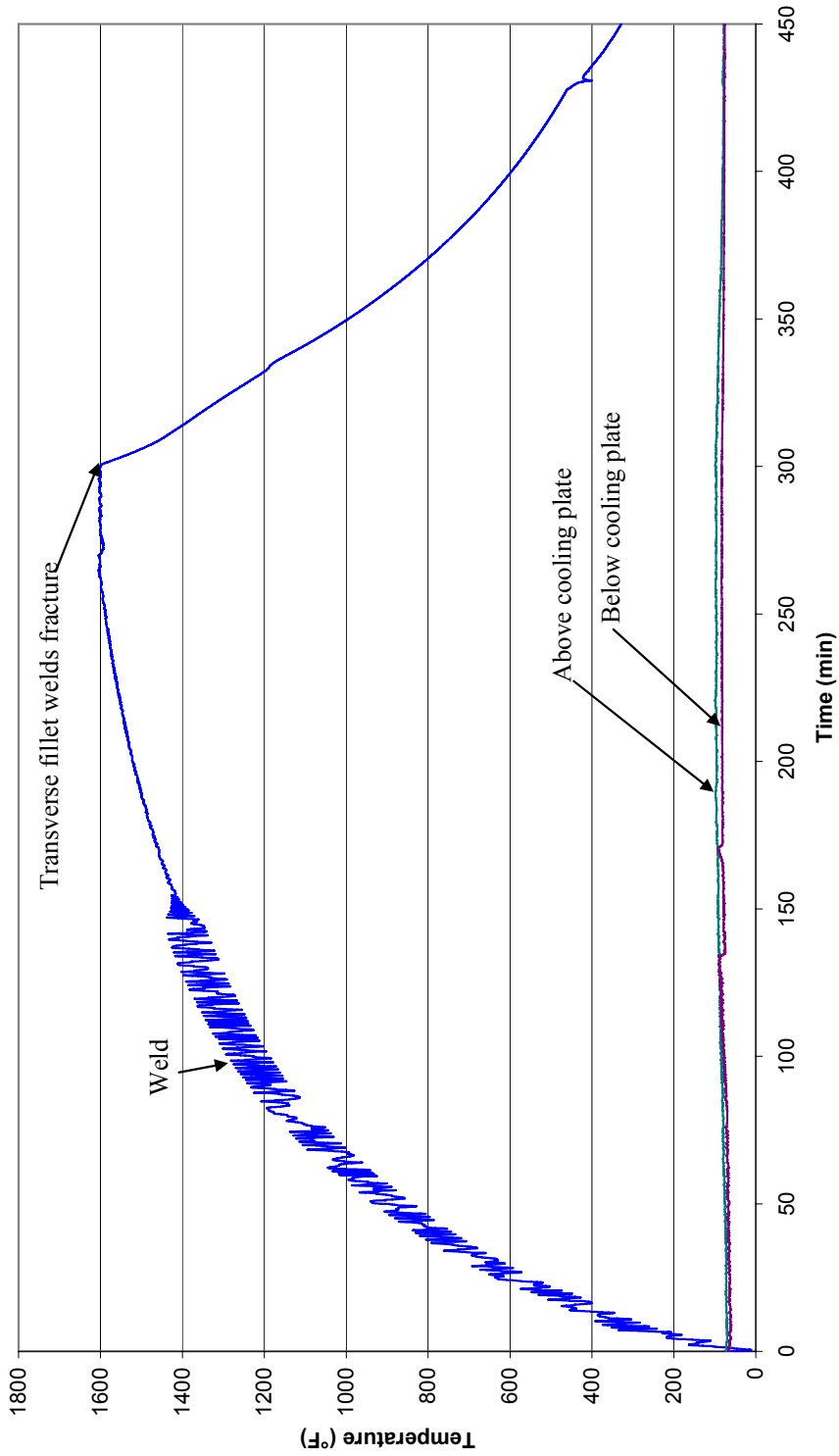
Figure 4.36  Time-temperature curve for Specimen 10

146
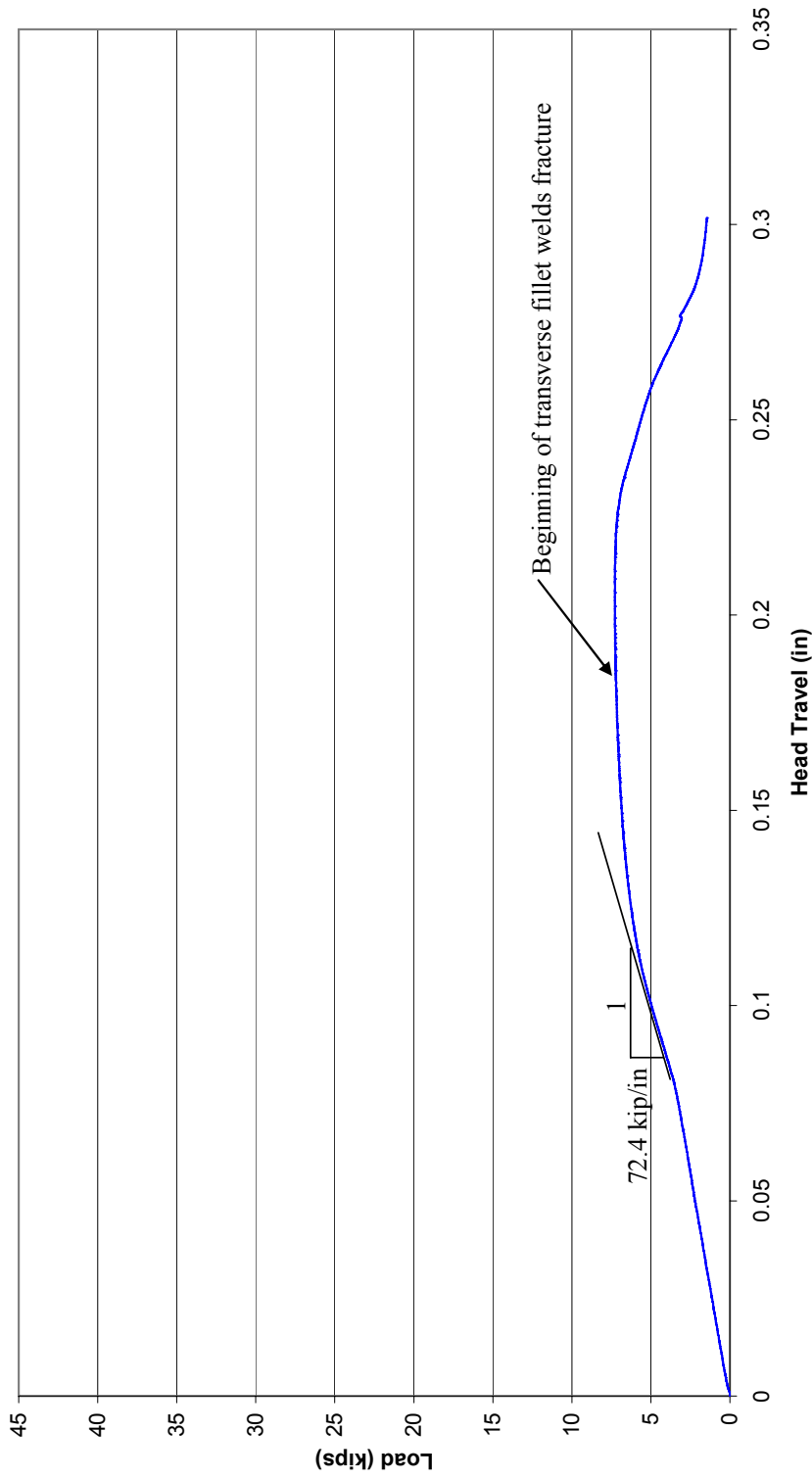
Figure 4.37  Load-displacement response for Specimen 10
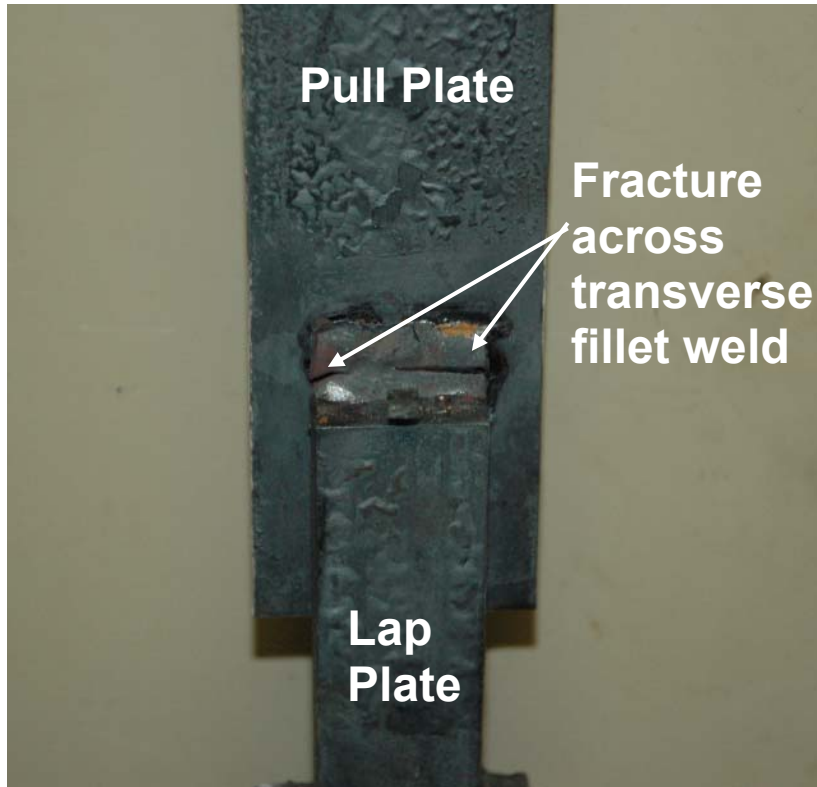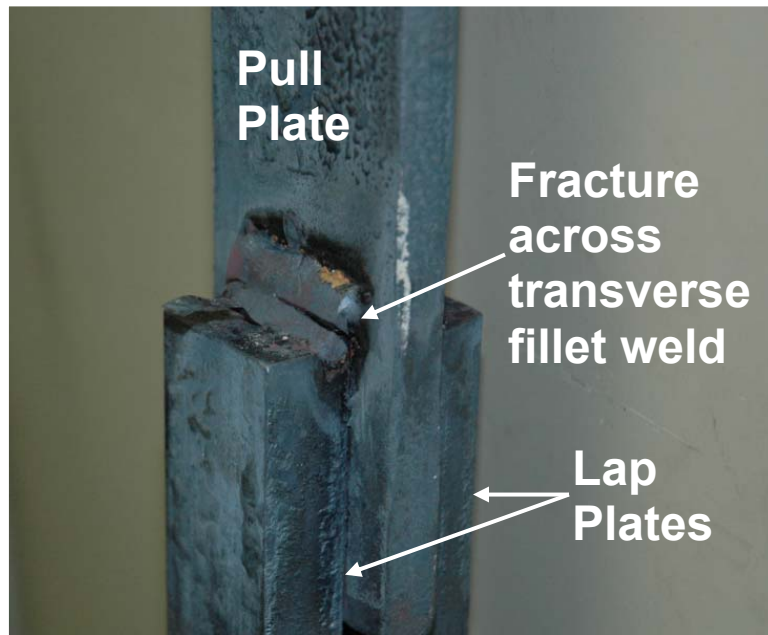
Figure 4.38  Photograph of Specimen 10 after testing with fracture across the transverse weld: (a) top view (b) side view
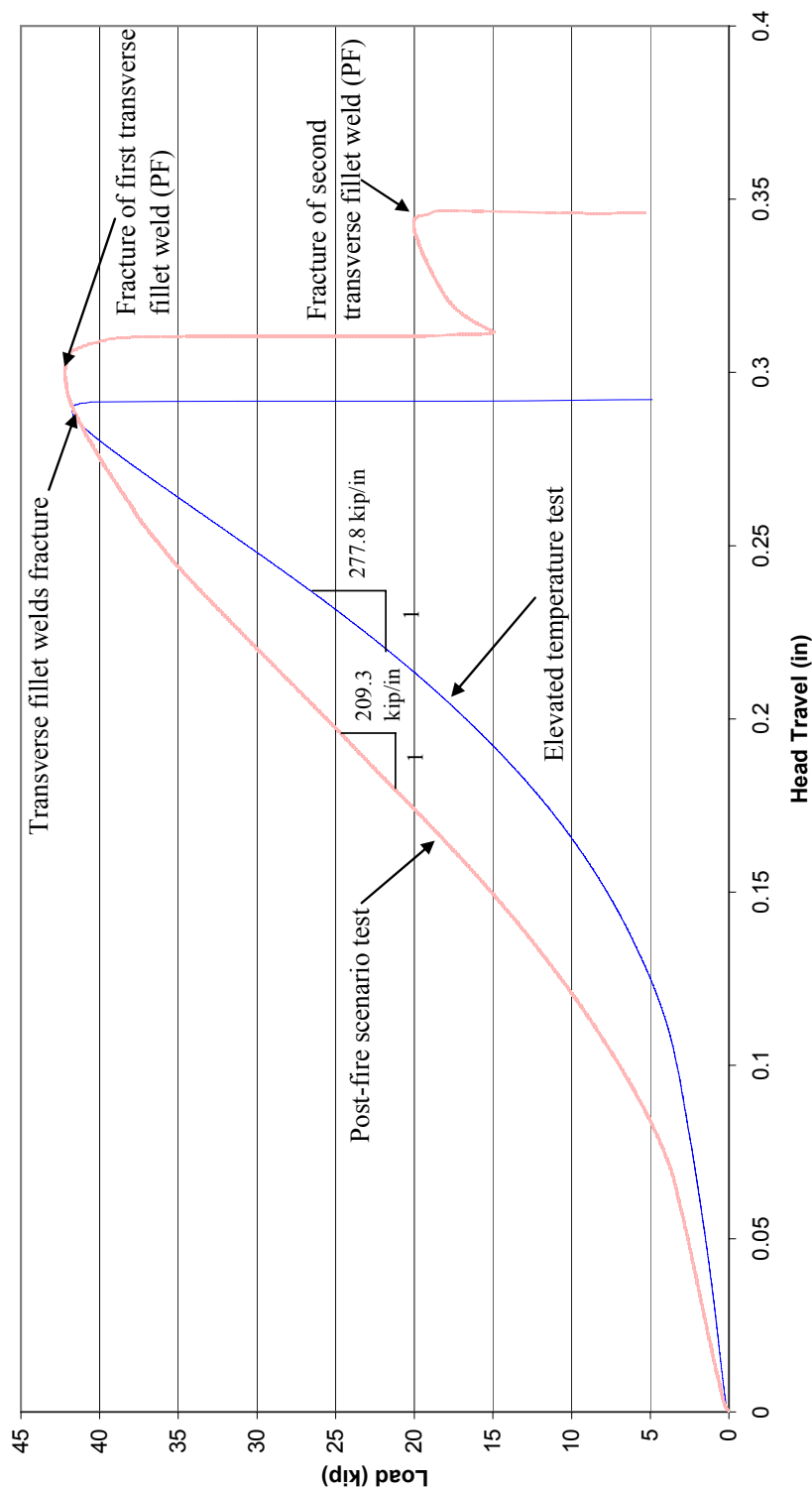
Figure 4.39  Comparison of load-displacement responses for Specimen P1 with corresponding elevated temperature test, Specimen 1

149
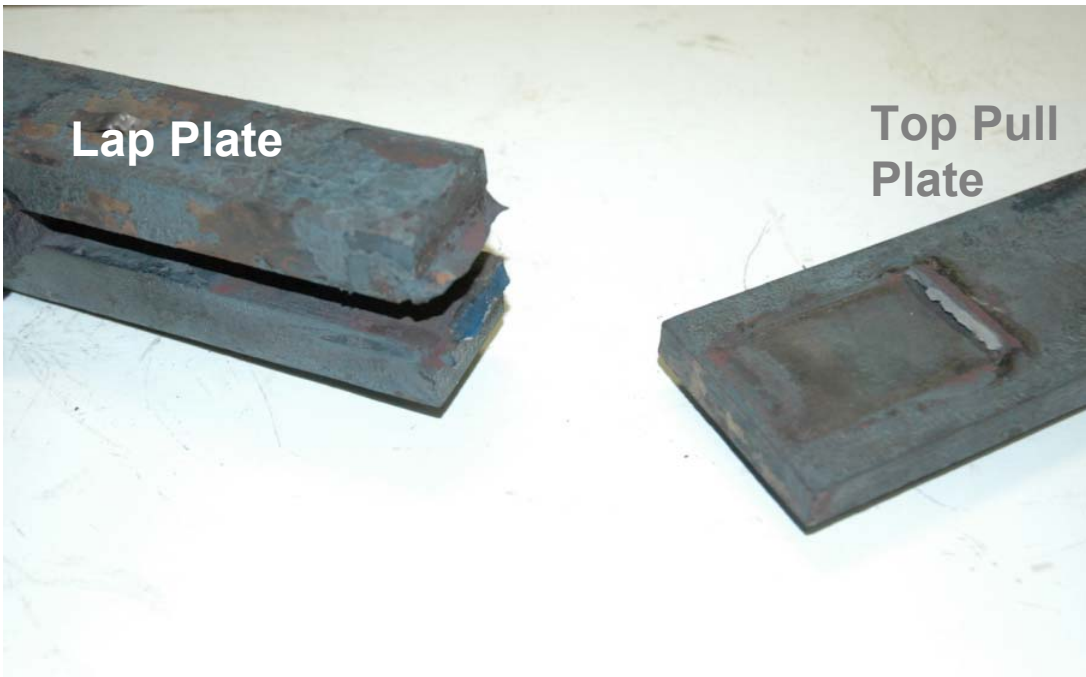
Figure 4.40  Photograph of Specimen P1 after fracture, where the weld on the lap plate and top base plate is visible
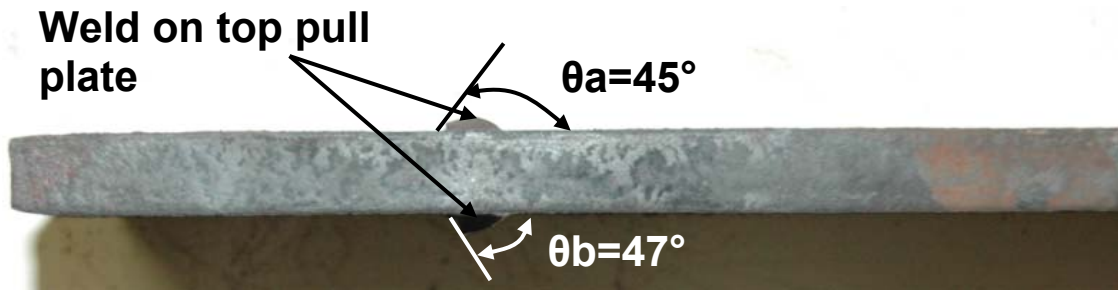


Figure 4.41  Photograph of a side view Specimen P1, where the profile of the fractured weld on the top pull plate is visible
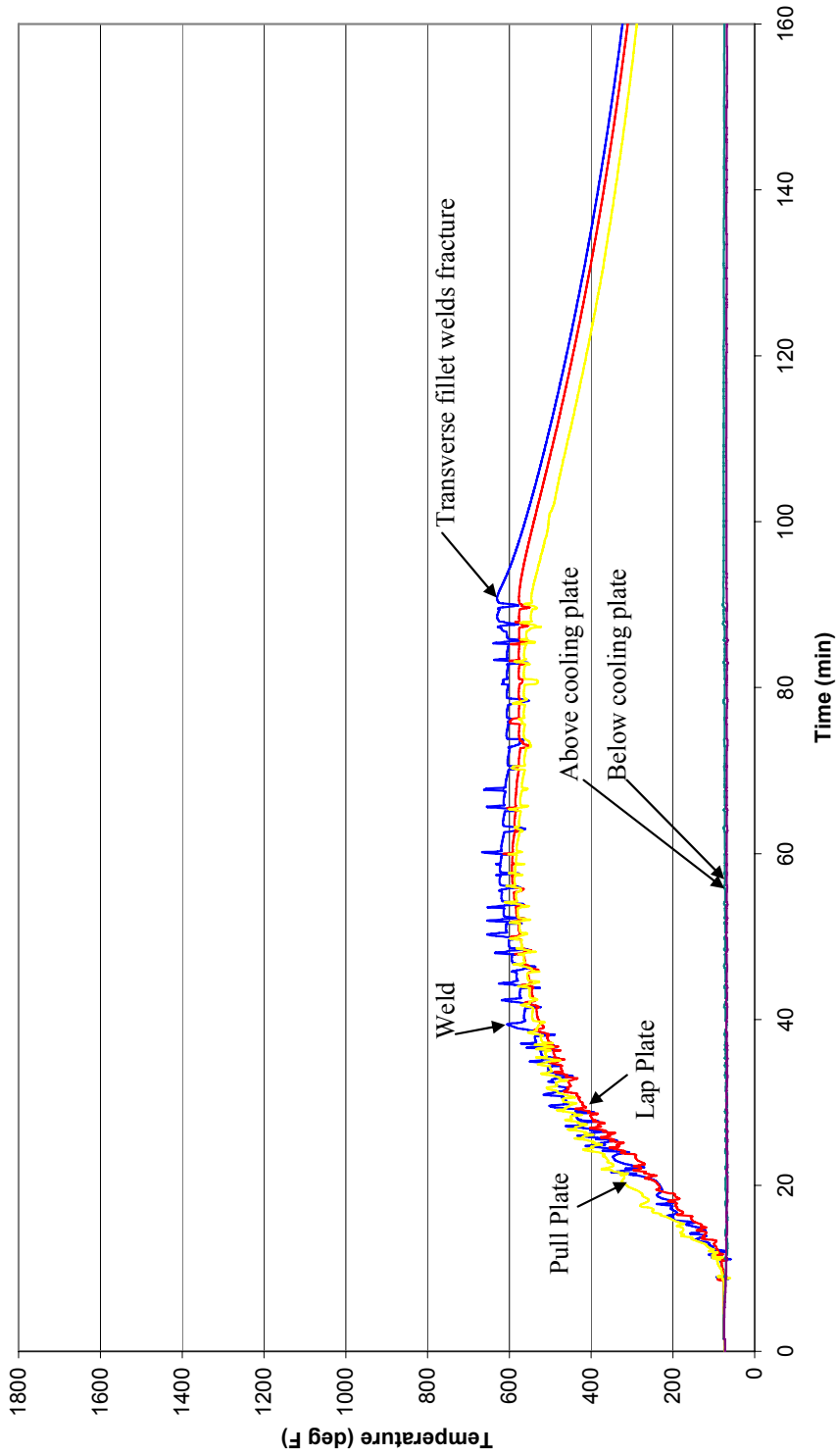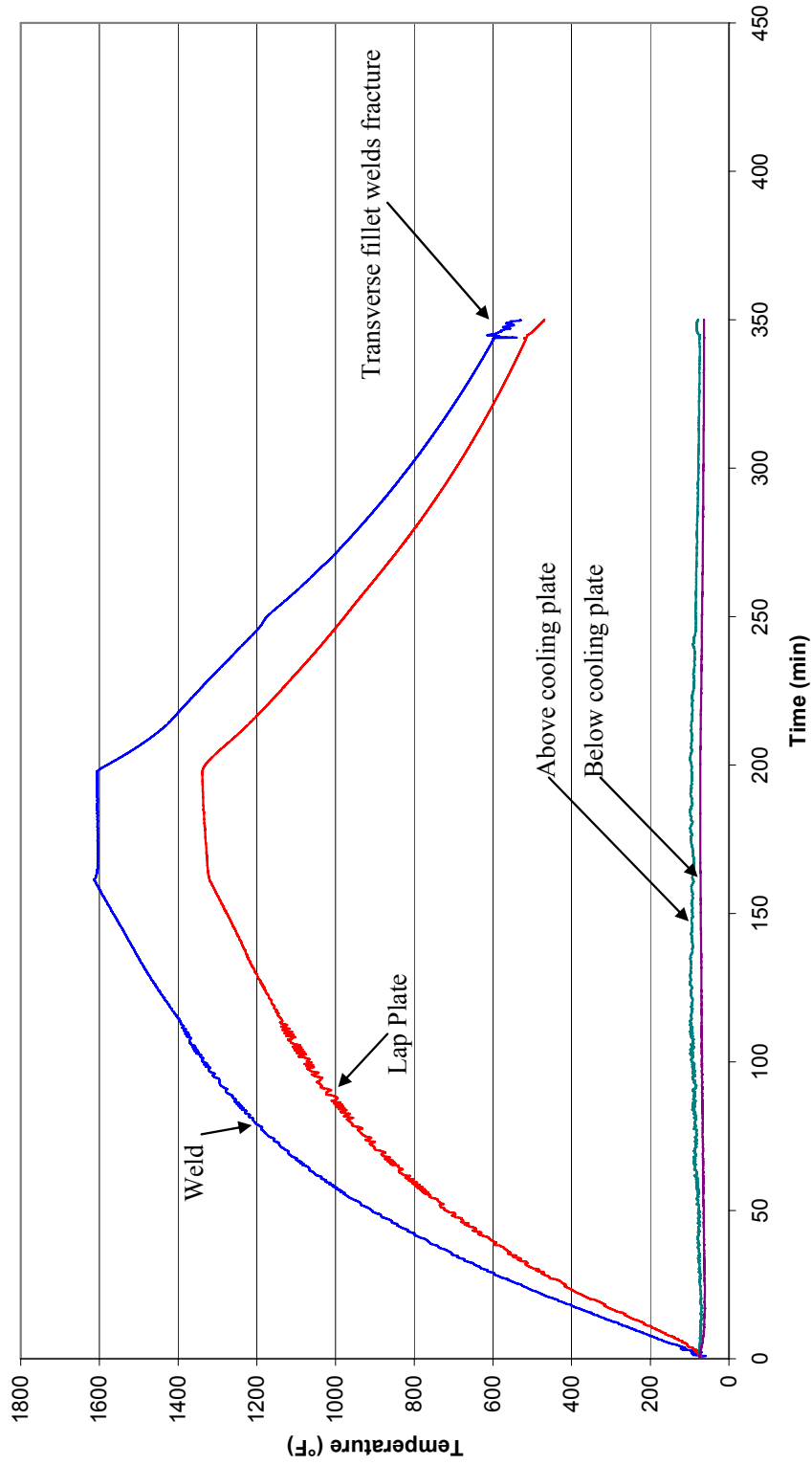
Figure 4.42  Time-temperature curve for Specimen P2

151
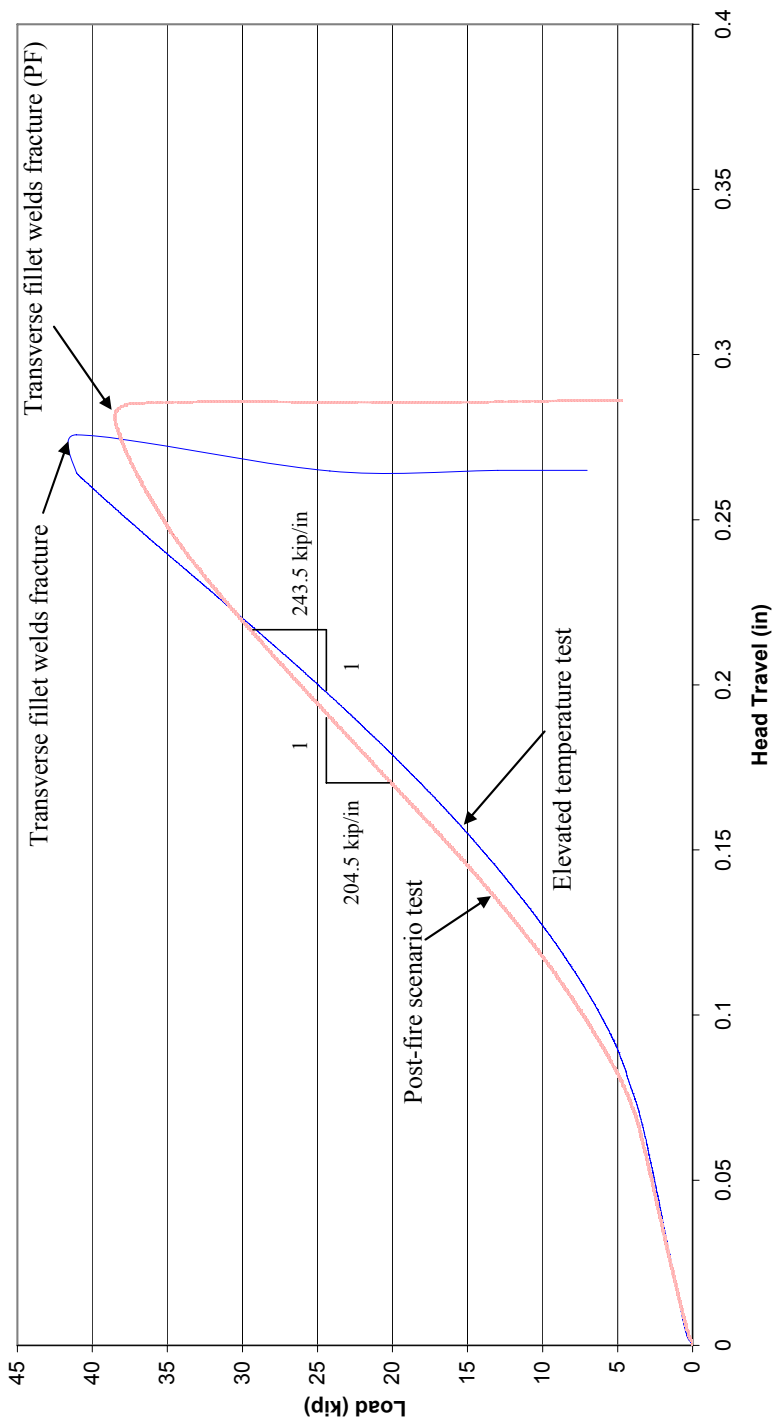
Figure 4.43  Comparison of load-displacement responses for Specimen P2 with corresponding elevated temperature test, Specimen 3
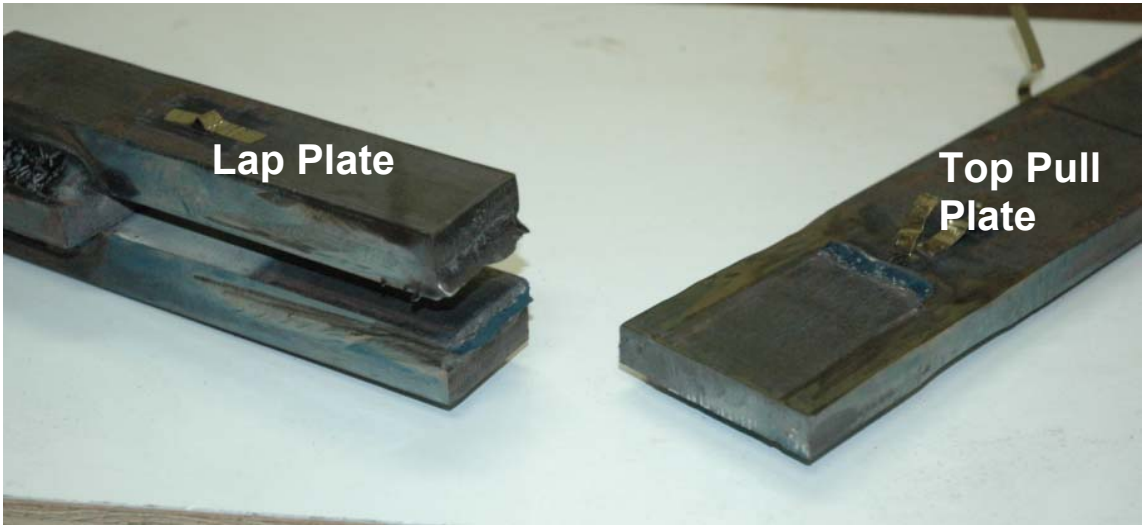
Figure 4.44  Photograph of Specimen P2 after fracture, where the weld on the lap plate and top base plate is visible
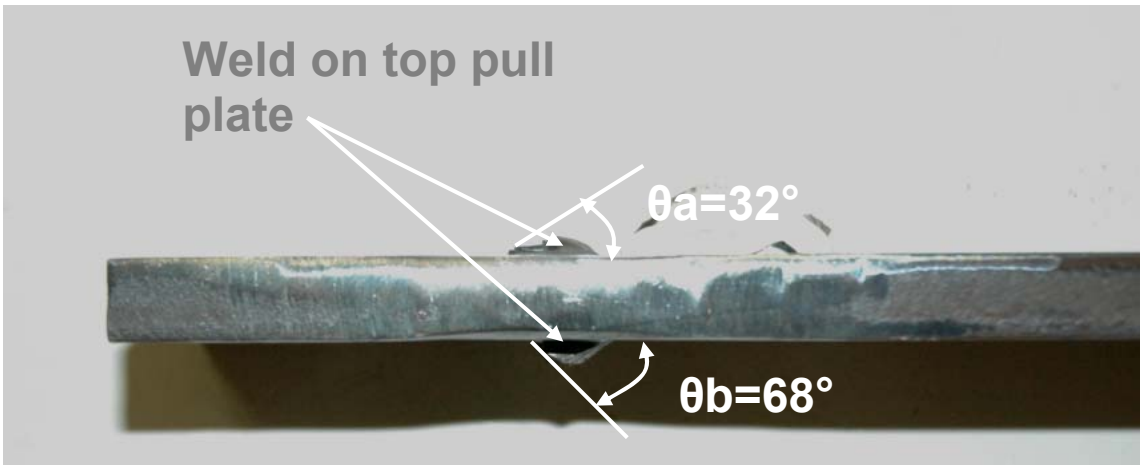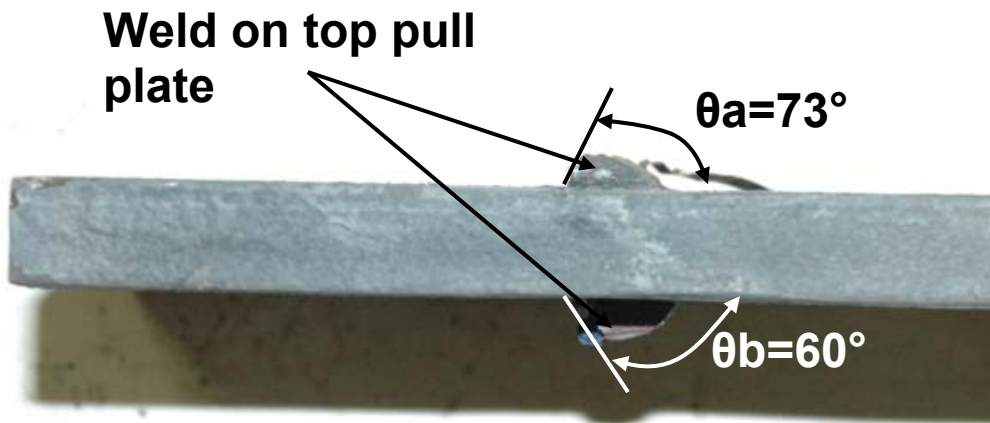


Figure 4.45  Photograph of a side view Specimen P2, where the profile of the fractured weld on the top pull plate is visible
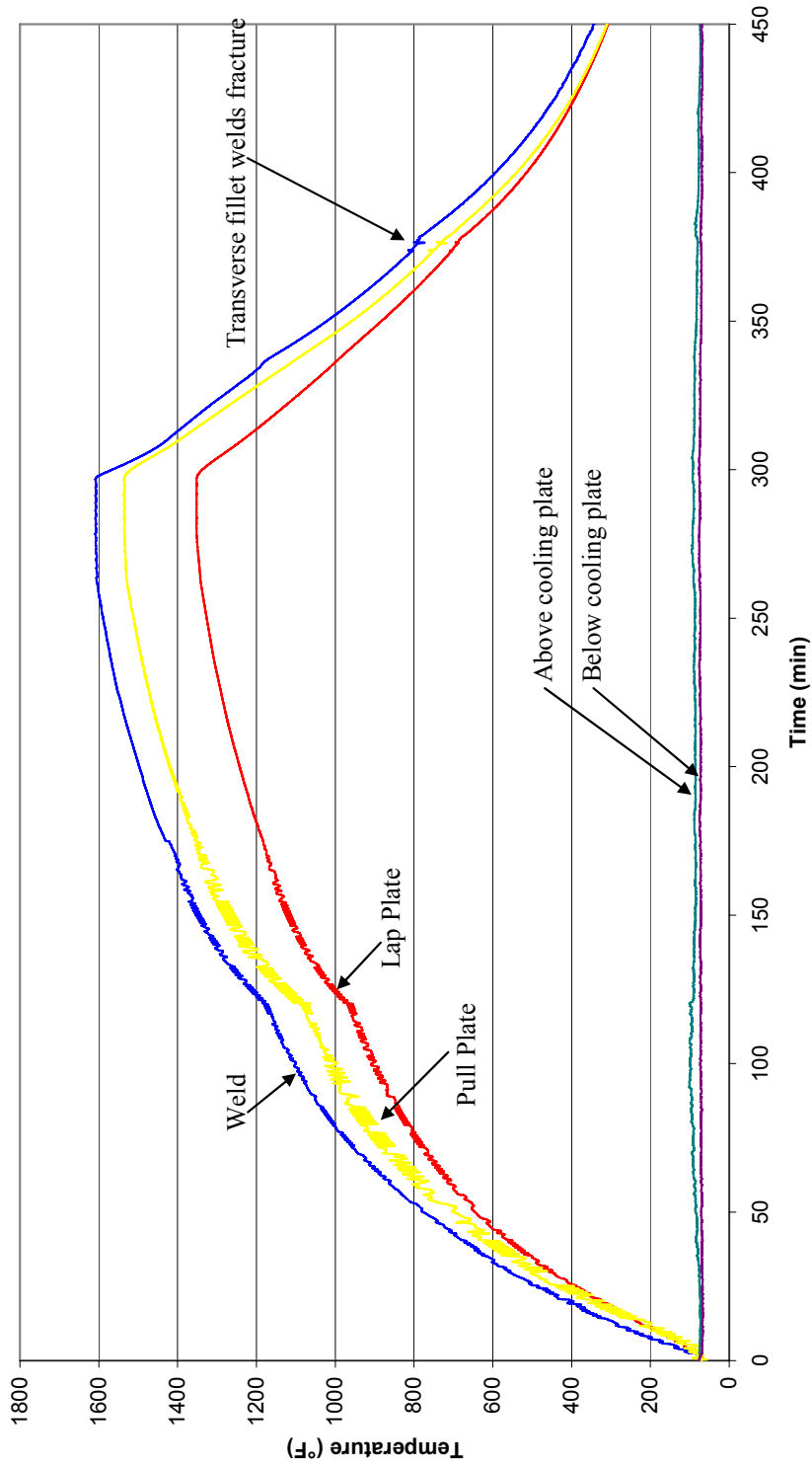
Figure 4.46  Time-temperature curve for Specimen P3

154
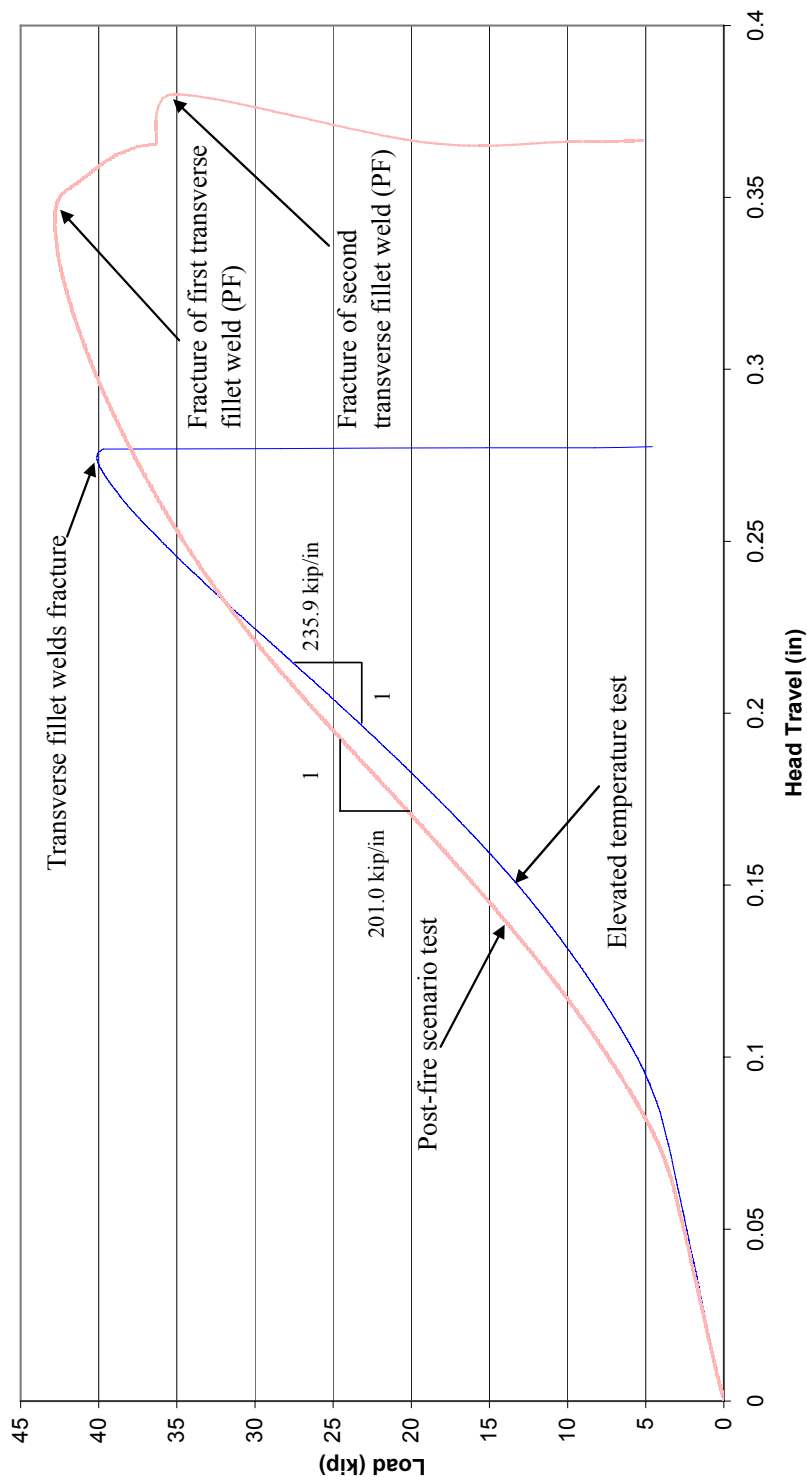
Figure 4.47  Comparison of load-displacement curves for Specimen P3 with corresponding elevated temperature test, Specimen 5

Figure 4.48  Photograph of Specimen P3 after fracture, where the weld on the lap plate and top base plate is visible
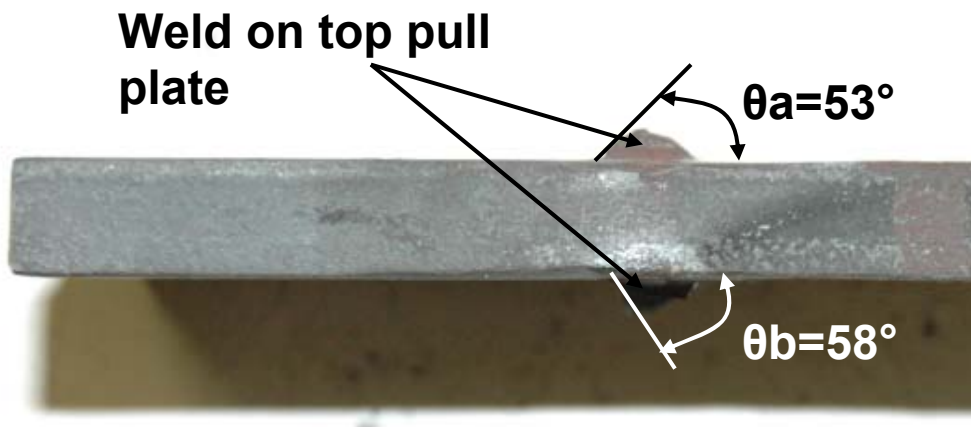


Figure 4.49  Photograph of a side view Specimen P3, where the profile of the fractured weld on the top pull plate is visible
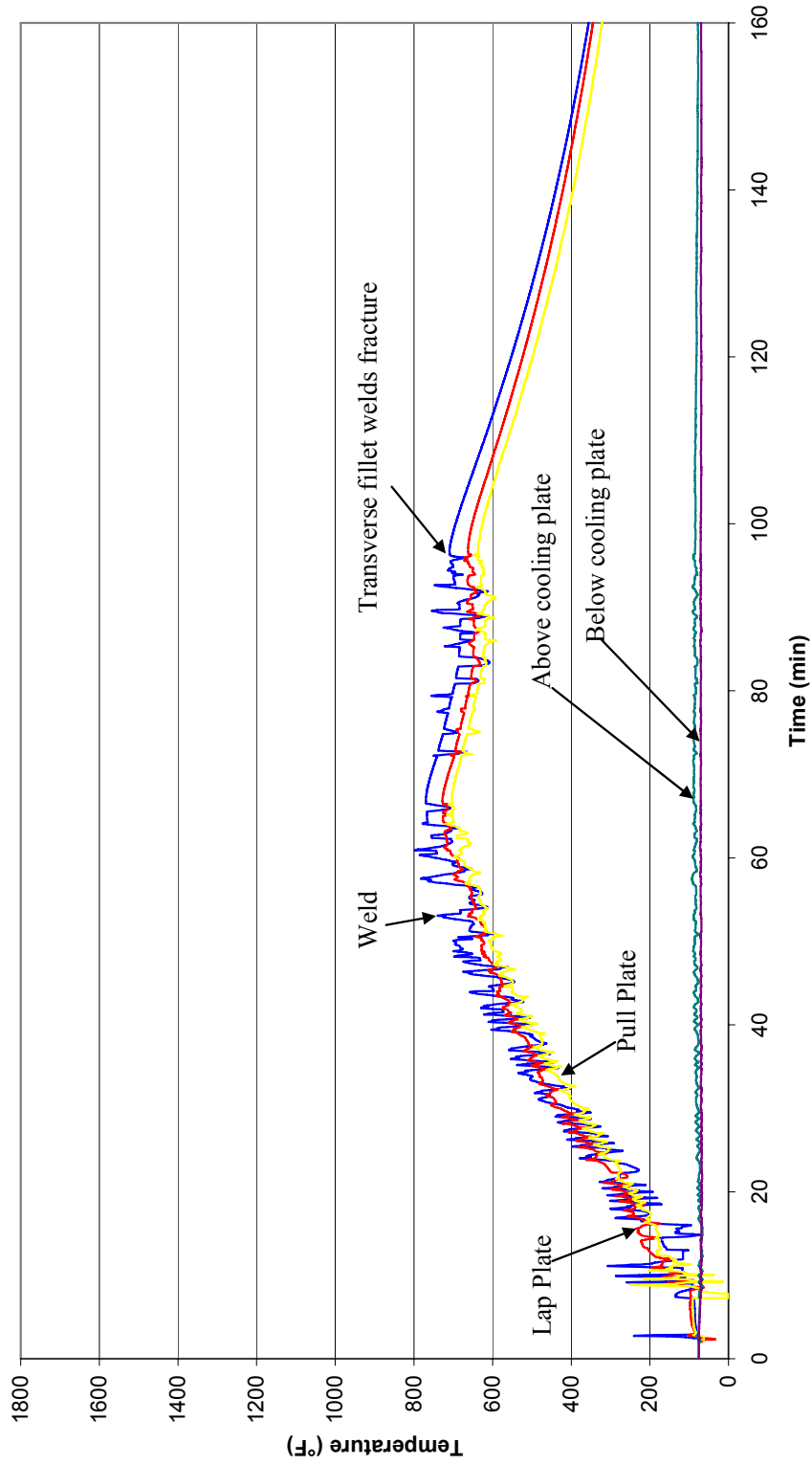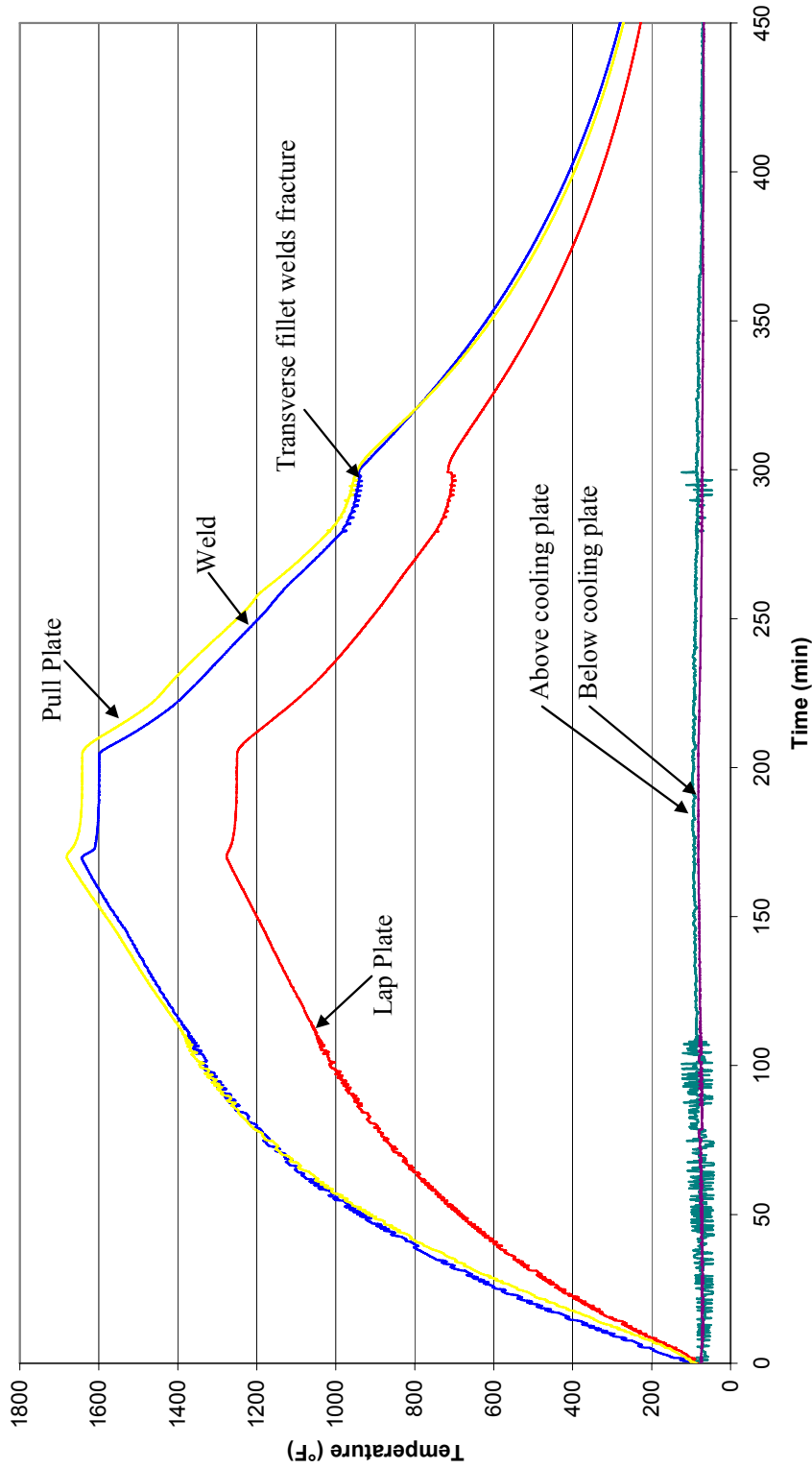
Figure 4.50  Time-temperature curve for Specimen P4
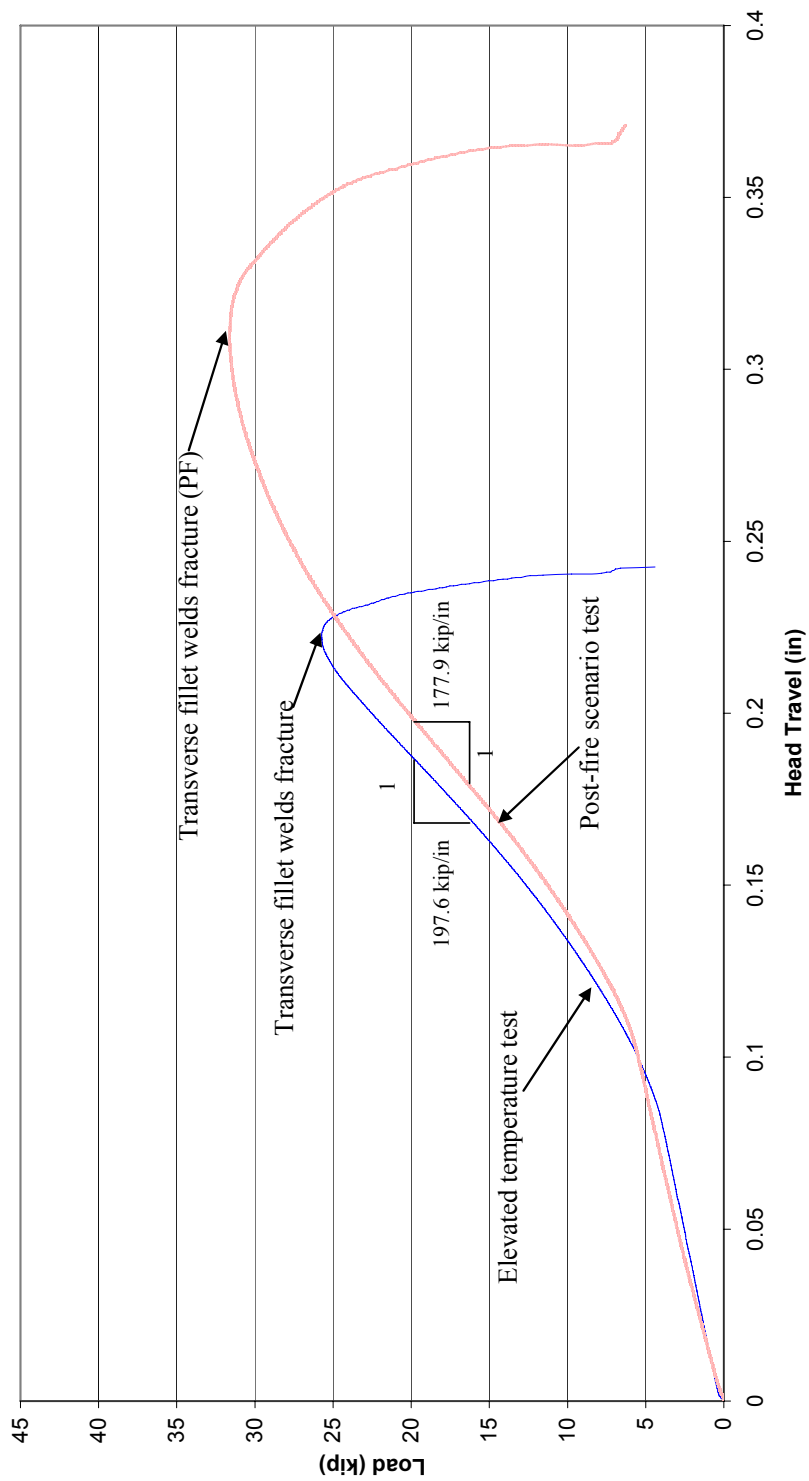
Figure 4.51  Comparison of load-displacement responses for Specimen P4 with corresponding elevated temperature test, Specimen 7

Figure 4.52  Photograph of Specimen P4 after fracture, where the weld on the lap plate and top base plate is visible
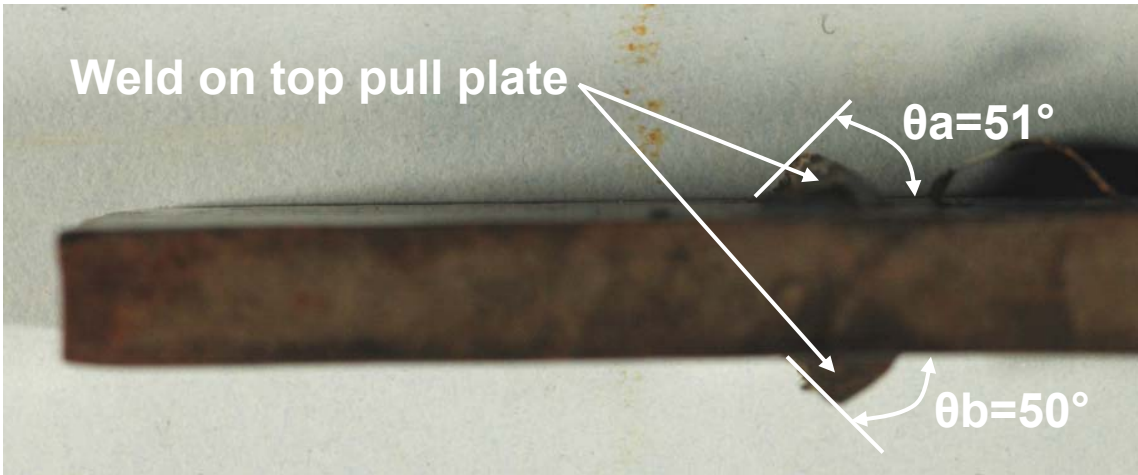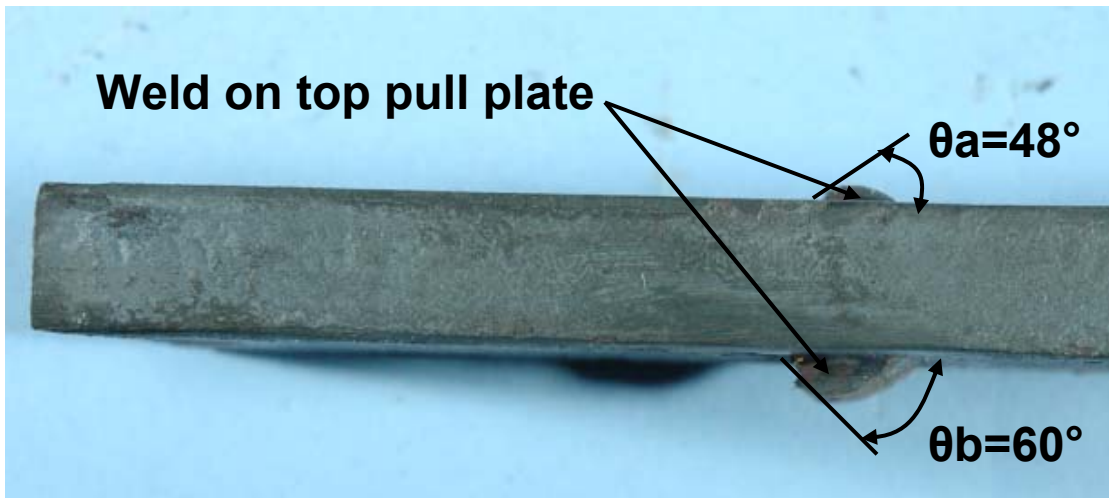


Figure 4.53  Photograph of a side view Specimen P4, where the profile of the fractured weld on the top pull plate is visible
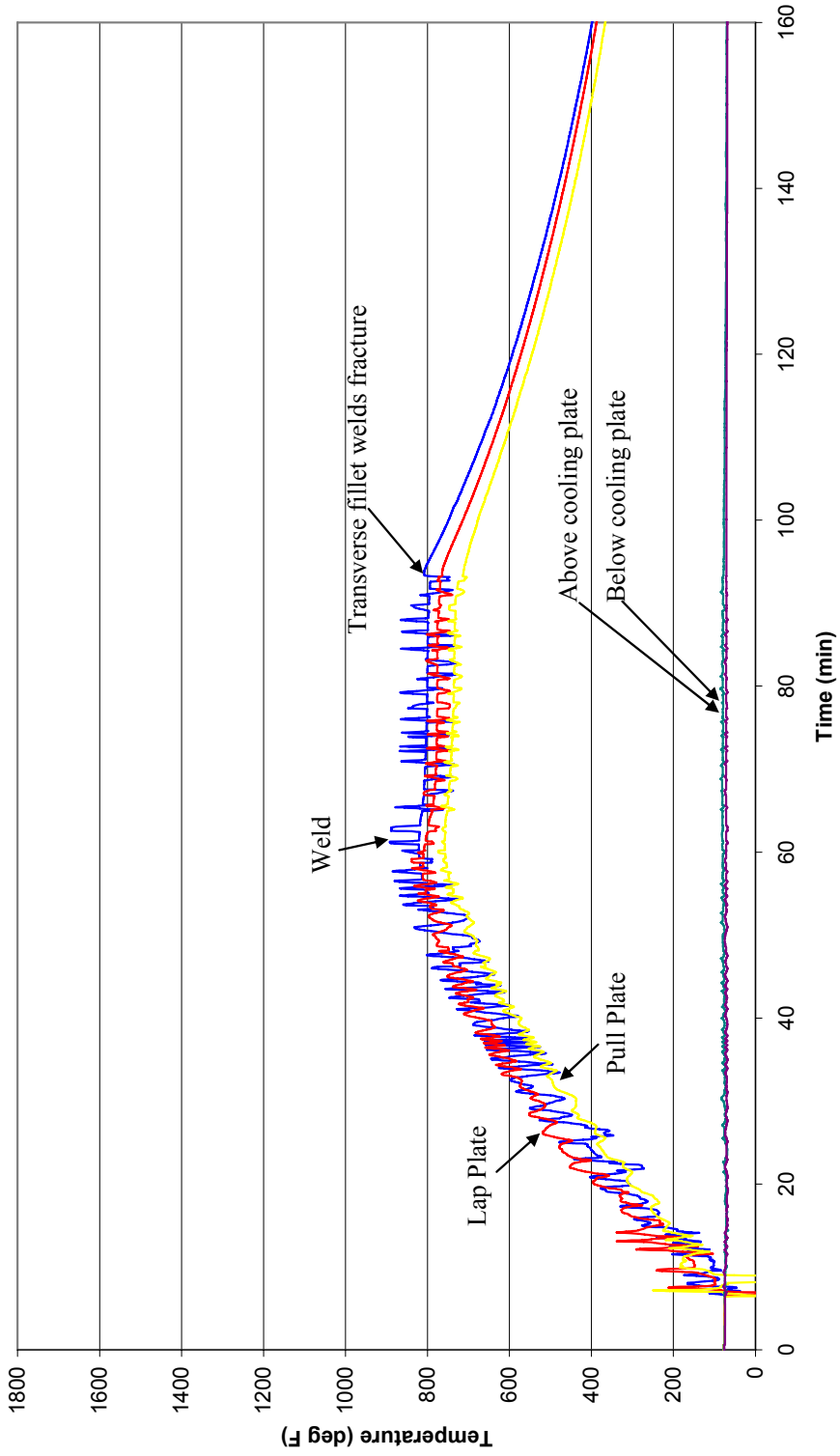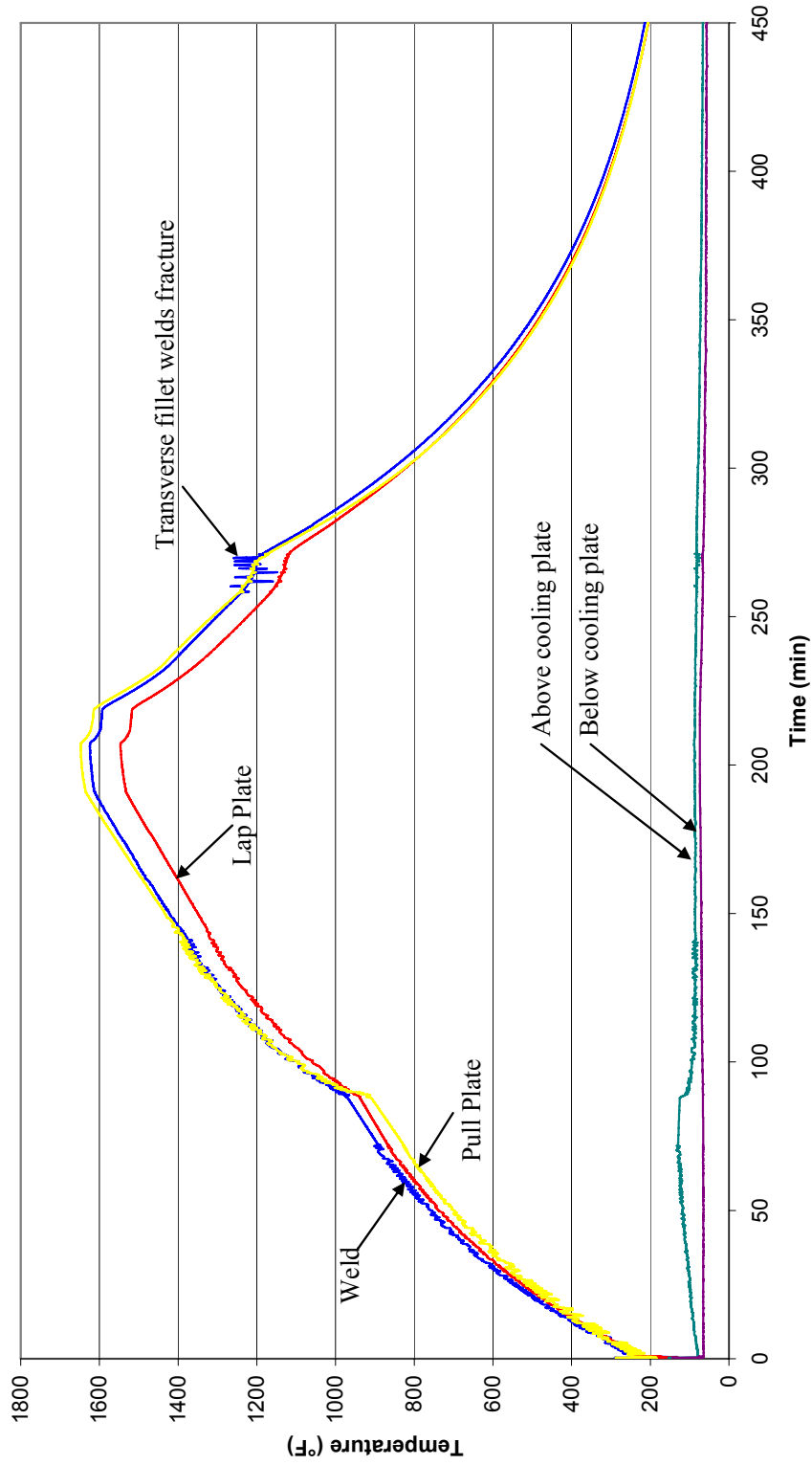
Figure 4.54  Time-temperature curve for Specimen P5

160
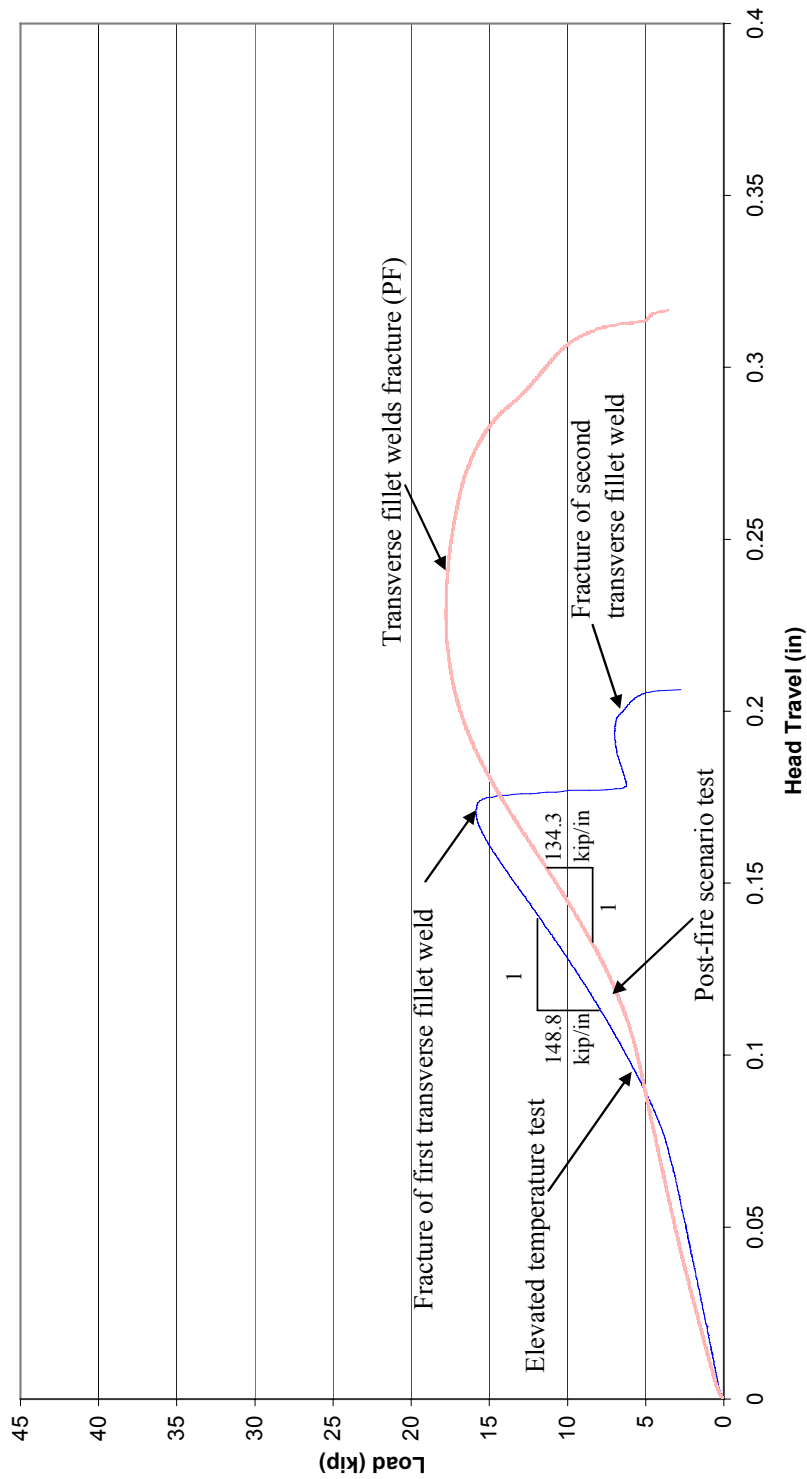
Figure 4.55  Comparison of load-displacement responses for Specimen P5 with corresponding elevated temperature test, Specimen 8
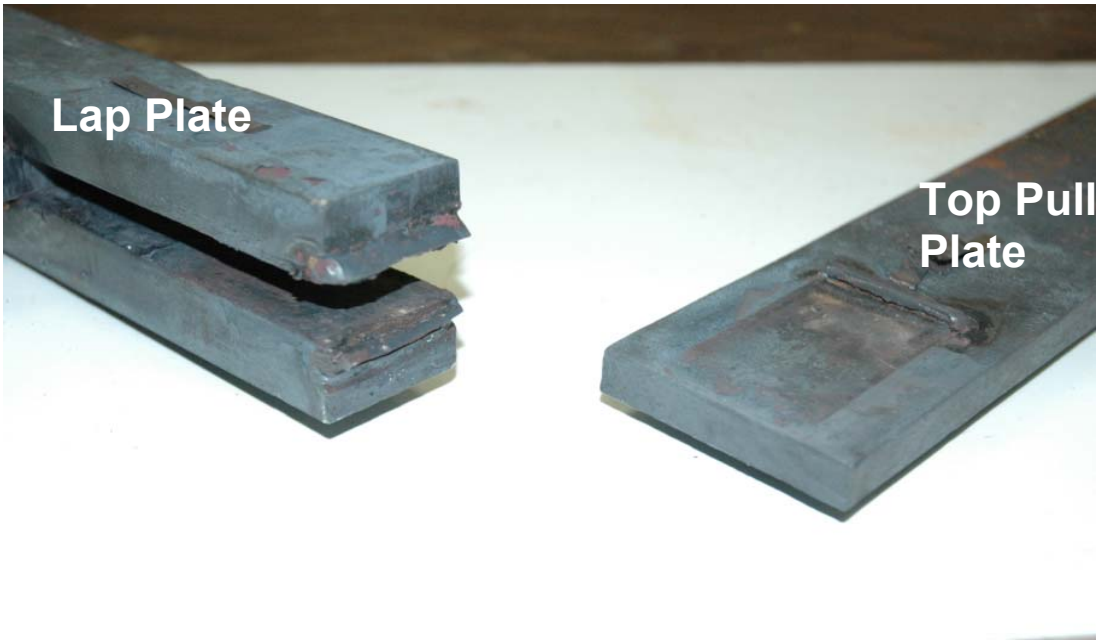
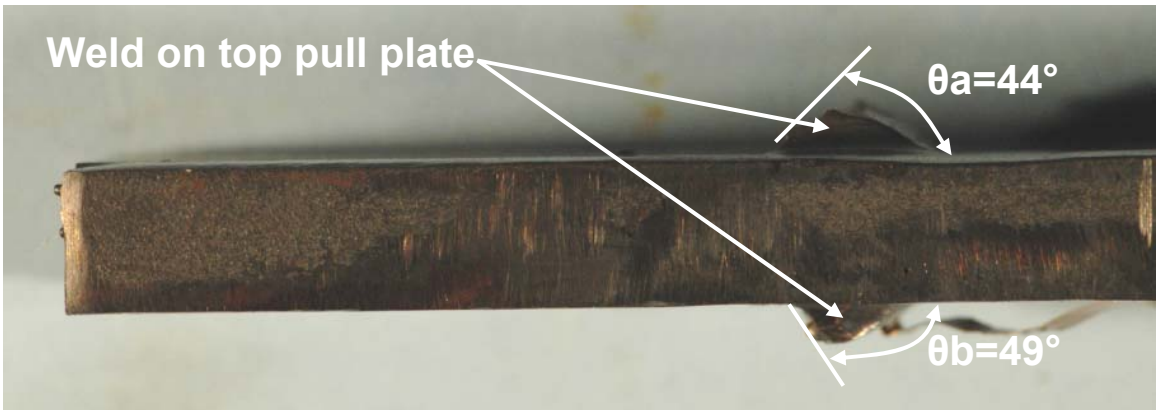Figure 4.56  Photograph of Specimen P5 after fracture, where the weld on the lap plate and top base plate is visible
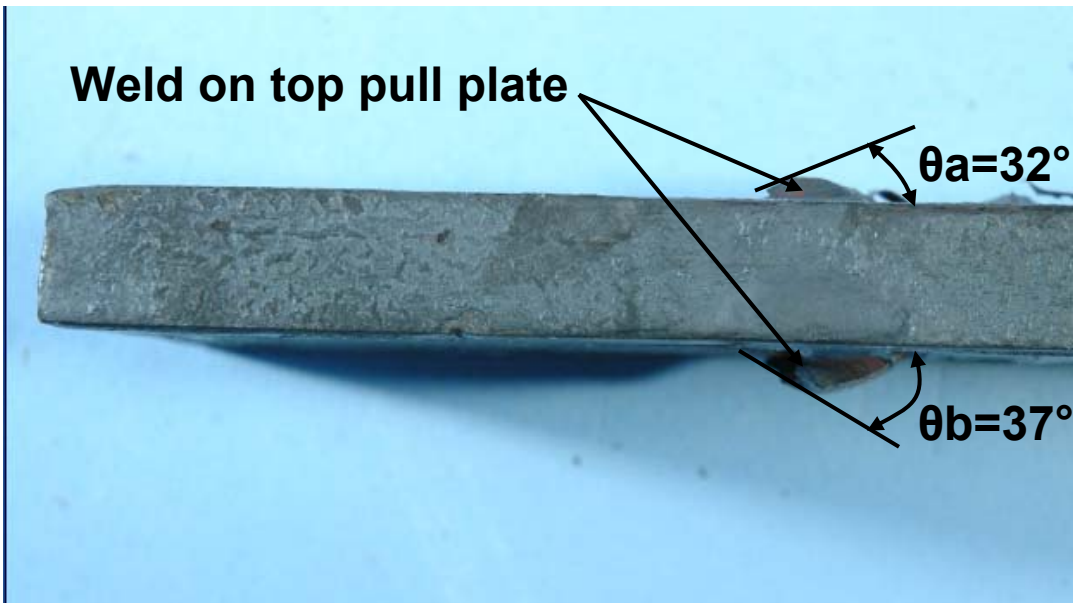


Figure 4.57  Photograph of a side view Specimen P5, where the profile of the fractured weld on the top pull plate is visible

## Chapter 5      Evaluation of Test Results

### 5.1    General

In this chapter the test results from both the elevated temperature tests and post-fire scenario tests are evaluated. This includes discussion of the normalization of the results considering the measured area of the transverse fillet weld and the strength reduction factor that is developed for design at elevated temperatures. The stiffness of the weld and the measured angle of weld fracture are discussed. These results are compared to current design recommendations from AISC (2005) and Eurocode (1995). The strength of the transverse weld is also compared to results from previous research that was discussed in Chapter 2.

### 5.2    Elevated Temperature Tests

To assess the effect of temperature on strength, stiffness, and angle of weld fracture the results from each test were compared. The comparison for strength is made on the basis of ultimate tensile stress of the weld. This required normalizing the load capacity of each specimen by the area of the fractured transverse fillet weld. Both measured weld fracture area and area based on an assumed 45° angle of fracture were used.

### 5.2.1   Measured Dimensions and Material Properties

As discussed previously in Chapter 3, once the specimen was removed from the SATEC testing machine and cooled down, the areas of the transverse fillet welds that failed are measured. This is done in two different ways, one using the assumed 45° failure plane, as assumed in AISC (2005) and one that measures the exposed fracture surface.

A photograph of a typical weld after being tested is shown in Figure 5.1. To obtain the area of the weld using the assumed 45° fracture angle, measurements of the weld leg were taken along the length of the weld. Five leg measurements were made along the 1.5 inch long length of the weld using a digital caliper. A photograph of the caliper is shown in Figure 5.2. Multiple measurements were made and averaged. In some cases, there was a large variation in different parts of the same weld.

The size of the weld leg from the five measurements for the leg of the weld on the pull plate and the five measurements on the lap plate was then recorded. This was done for both of the fillet welds on the specimen, which are denoted as weld A and weld B. The measurements are given in Table 5.1 for the transverse welds. The averaged weld leg sizes are denoted by $a_1$ and $a_2$ which corresponds to the average weld leg size on the pull plate and on the lap plate, respectively. There is a different $a_1$ and $a_2$ for weld A and weld B. The measured weld leg sizes, $a_1$ and $a_2$ are shown in Figure 3.20(b). The lengths of the welds across the pull plate were also measured. Each length was measured on the lap plate and the pull plate and were averaged for each weld, so that there were two lengths, denoted by $L_A$ and $L_B$ for welds A and B, respectively.

The area of the weld was then computed for weld A and weld B and summed to obtain the area of both transverse welds on the specimen, denoted by $A_{w,c}$. This computation is done using the assumed 45° fracture angle, as specified in AISC (2005), where for weld A:

$$A_A = 0.707 \cdot \left( \frac{a_1 + a_2}{2} \right) \cdot L_A \qquad (5.1)$$

where:

$A_A$ = area of weld A (in$^2$)
$a_1$ = averaged measured weld dimension on the pull plate for weld A (in)
$a_2$ = averaged measured weld dimension on the lap plate for weld A (in)
$L_A$ = averaged measured length of weld A (in)

Similarly, the area of weld B is computed using the following equation:

$$A_B = 0.707 \cdot \left( \frac{a_1 + a_2}{2} \right) \cdot L_B \qquad (5.2)$$

where:

$A_B$ = area of weld B (in$^2$)
$a_1$ = averaged measured weld dimension on the pull plate for weld B (in)
$a_2$ = averaged measured weld dimension on the lap plate for weld B (in)
$L_B$ = averaged measured length of weld B (in)

The total area of the weld for the specimen is then computed by summing $A_A$ and $A_B$,

$$A_{w,c} = A_A + A_B \qquad (5.3)$$

where:

$A_{w,c}$ = Computed area of the weld using the assumed 45° fracture plane (in$^2$)

The computed areas $A_{w,c}$ of the weld for Specimens 1-10 using the assumed 45° fracture plane are shown in Table 5.1.

Due to the fact that the 45° fracture plane is an assumption, the area of the weld fracture surface was also determined using measurements that took the actual failure angle into account. Although the fracture plane of a weld is taken to be 45° in practice, the elevated temperature may have had an effect on the failure of the weld.

Similar to what was done previously; five measurements of the width of the fracture surface were taken along the length of the weld to account for the jagged fracture surface across the weld, leading to different values along the length. Each measurement was done by lining an index card along the throat and making a pencil mark at the edge of the fracture of the weld. The distance from the bottom of the index card to the pencil mark was then measured with the digital caliper and recorded. The measured distance across the throat of the weld is denoted by $t_e$. The measurements were denoted by $te_A$ and $te_B$ and for weld A and weld B, respectively, as shown in Figure 3.20(b).The equation used to compute the average measured area of the fracture surface of the weld, denoted by $A_{w,m}$ is then:

164

$$A_{w,m} = \left(\frac{te_A + te_B}{2}\right) \cdot (L_A + L_B) \tag{5.4}$$

where:

$A_{w,m}$ = average measured area of the fracture surface of the weld (in$^2$)
$te_A$ = averaged measured weld throat on the pull plate for weld A (in)
$te_B$ = averaged measured weld throat on the pull plate for weld B (in)
$L_A$ = averaged measured length of weld A (in), from Table 5.1
$L_B$ = averaged measured length of weld B (in), from Table 5.1

The measured areas of the transverse weld fracture surface for Specimens 1-10 are given in Table 5.2.

The tensile strength of the weld, $\sigma_{u,exp}$, was computed from the fracture load at the different temperatures that were tested. Recall from Section 3.3, that the ultimate load of the weld was determined as follows:

$$P_{weld} = 2 \cdot (0.6 \cdot F_{EXX} \cdot t_e \cdot L) \cdot F \tag{3.7}$$

Therefore, to determine the tensile strength of the weld, $\sigma_{u,exp}$, at the temperature of interest, this equation was rewritten as:

$$\sigma_{u,exp} = \frac{P_{ult}}{0.6 \cdot A_w \cdot F} \tag{5.5}$$

Where $P_{ult}$ is the specimen ultimate load reported in Table 4.1, F = 1.5, and $A_w$ is either the calculated ($A_{w,c}$) or measured ($A_{w,m}$) area of the transverse fillet weld fracture surface.

The tensile weld strengths are computed and shown in Table 5.3 and Table 5.4 using the computed throats ($\sigma_{u,exp\_c}$) and measured throats ($\sigma_{u,exp\_m}$), respectively. The tensile strength of the weld is plotted against temperature and is shown in Figure 5.3 for the computed and measured throats of the weld. Note that tensile strength of weld metal degrades at elevated temperatures, developing a significant strength reduction at temperatures above 800°F.

### 5.2.2  Reduction Factor for Strength

A strength reduction factor was developed for the weld metal at elevated temperatures. The strength reduction factor is the ratio of the tensile strength at a specified elevated temperature to the tensile strength at ambient temperature, T = 72°F. The strength reduction factor is denoted by $\phi_c$ and $\phi_m$, based on the computed and measured area of the transverse fillet welds, respectively, where:

$$\phi_c(T) = \frac{\sigma_{u,exp\_c}(T)}{\sigma_{u,exp\_c}(T = 72°F)} \tag{5.6}$$

and

$$\phi_m(T) = \frac{\sigma_{u,exp\_m}(T)}{\sigma_{u,exp\_m}(T = 72°F)} \tag{5.7}$$

165

In Equations 5.6 and 5.7,

$\phi_c(T)$ = reduction factor for load capacity at temperature T considering the computed area of the weld

$\phi_m(T)$ = reduction factor for load capacity at temperature T considering the measured area of the weld

$\sigma_{u,exp\_c}(T)$ = weld tensile strength at temperature T based on computed throat area, see Table 5.3

$\sigma_{u,exp\_c}(T = 72°F)$ = weld tensile strength at ambient temperature based on computed throat area, see Table 5.3

$\sigma_{u,exp\_m}(T)$ = weld tensile strength at temperature T based on measured throat area, see Table 5.4

$\sigma_{u,exp\_m}(T = 72°F)$ = weld tensile strength at ambient temperature based on measured throat area, see Table 5.4

The strength reduction factors, $\phi_c(T)$ and $\phi_m(T)$ are given in Table 5.5 and Table 5.6, respectively. The results are plotted and compared to each other in Figure 5.4. From Figure 5.4, it appears that for the elevated temperature tests that there is good agreement with the two results due to the fact that the two curves follow the same trend for both the computed and measured area of the weld. Note that much like the strength of steel at elevated temperatures, the weld strength is observed to significantly reduce at 800°F.

## 5.2.3   Reduction Factor for Stiffness

The stiffness k of the specimens was obtained from the slope of the load-displacement response after seating occurred, as discussed and presented in Chapter 4. The stiffness of the specimens tested at elevated temperature are given in Table 4.1 and shown plotted in Figure 5.5. It is observed from Figure 5.5 that the stiffness decreases with increasing temperature. A reduction factor for the stiffness of the specimen, denoted by $\phi_k$, is determined using the following equation:

$$\phi_k(T) = \frac{k(T)}{k(T = 72°F)}$$

(5.8)

where:

$\phi_k(T)$ = reduction factor for stiffness of specimen at temperature T
$k(T)$ = stiffness of the specimen at temperature T (kip/in)
$k(T=72°F)$ = stiffness of the specimen at ambient temperature (kip/in)

The stiffness is a function of the cross-sectional area, length, and Young's Modulus of a specimen. Since the head travel from which the stiffness is based had parts of the specimen inside and outside the furnace, and their deformations were not individually measured, the reduction in Young's Modulus, E cannot be computed from the stiffness, k. However, the results in Figure 5.5 do imply that there is a reduction in Young's Modulus with increase in temperature since the properties and length of each specimen outside the furnace were the same. The reduction factors for the stiffness of the specimen

166

are tabulated in Table 5.7 and plotted in Figure 5.6. The stiffness begins to decrease with an increase in temperature in almost a linear manner.

## 5.2.4   Measured Weld Fracture Angle

In Chapter 4, the angles of fracture of the transverse welds were measured and are given in Table 4.1 for the specimens tested at elevated temperature. Recall that the angles θa and θb for each weld were measured and defined in Figure 3.20(b). The fracture angles, θa, θb, and the average of θa and θb (θavg), for each specimen are plotted and shown in Figure 5.7. The data from Specimen 2, tested at 350°F were discarded, since the failure was not through the weld, rather it occurred at the fusion plane between the weld and the base metal of the lap plate.

At ambient temperature, the average fracture angle θavg of the weld is 42.5°, which is only a 6% variation from 45°. The results for θavg appear to remain in the range of 30° to 50°; with lower values occurring at temperatures of 1200°F and 1400°F. Therefore, it appears that as the temperature increases above 1200°F, the fracture angle of the weld deviates from 45°.

## 5.3   Post-Fire Scenario Tests

In this section, the results from the post-fire scenario tests will be evaluated. This will include the actual dimensions and strength of the weld metal. The reduction of the strength and the stiffness will be discussed. The strength of the weld metal during cooling will help to shed some light on a connection's ability to resist axial forces that develop after a structure has been exposed to elevated temperatures. The weld strength was also of particular interest due to the fact that by cooling the specimen prior to testing, it in effect underwent a heat treatment process, which could change the material properties of the weld. The measured weld fracture angles will also be presented.

## 5.3.1   Measured Dimensions and Material Properties

Similar to the elevated temperature tests, the welds on specimens tested during the post-fire scenario tests varied in size. For this reason, the weld dimensions and area had to be accurately computed to determine the weld stress at fracture. The weld area was computed using the same procedures used for the elevated temperature tests. The computed area of the weld ($A_{w,c}$) and the measured area of the weld ($A_{w,m}$) are given in Table 5.8 and Table 5.9, respectively.

The tensile strength of the weld for each temperature tested during the post-fire scenario tests was computed using Equation 5.5 and is shown in Table 5.10 and Table 5.11, for $\sigma_{u,exp\_c}$ and $\sigma_{u,exp\_m}$, respectively. The tensile strength in the post-fire scenario tests are shown plotted against temperature in Figure 5.8 and Figure 5.9, considering the computed and measured areas of the weld, respectively. The results are shown compared to tensile strength of the weld for the elevated temperature tests. Although fewer temperatures were tested, it can be observed that the degradation of tensile strength of

weld metal in the post-fire scenario tests follows the same trend as for the elevated temperature tests, having the most significant reduction in strength at 800°F.

When observing the tensile weld strength in Figure 5.9 considering the measured weld area, it can be observed that there is a strength increase when the specimen cools down to the ambient temperature. This is result is expected since the post-fire scenario tests resembled the annealing heat treatment process, which causes some strength increase, as discussed in Section 2.5.

### 5.3.2    Reduction Factor for Strength
The reduction factor for strength for the weld during post-fire conditions was developed similarly to the reduction factor for weld strength at elevated temperatures. Equation 5.6 and Equation 5.7 were used to compute the reduction factors during post-fire conditions, denoted by $\phi_c$ and $\phi_m$, for the computed and measured area of the weld, respectively. The results are given in Tables 5.12 and 5.13, respectively, and plotted in Figures 5.10 and 5.11.

Based on the measured weld area, it can be observed that when a specimen is heated to 1600°F and cooled to a specified elevated temperature prior to testing, the weld failed at a slightly higher load then when the specimen was simply heated to the corresponding elevated temperature and tested. This is due to the fact that once the specimen heats to a temperature high enough for austenite to form and is then cooled in the furnace, the heat treatment process, annealing, which takes place causes an increase in strength upon cooling.

### 5.3.3    Reduction Factor for Stiffness
The stiffness k of each specimen was obtained from the slope of the load-displacement response after seating occurred, as discussed in Chapter 4. The results are given in Table 4.2 and shown plotted in Figure 5.12 for the specimens tested during post-fire conditions. In Figure 5.12 the results are corresponded to that for the elevated temperature tests. It is observed that the stiffness decreased with increasing temperature; however the trend is more gradual than that of the specimens tested at elevated temperatures. The reduction factor for the stiffness of the specimens, $\phi_k$, is determined using Equation 5.8. The values for $\phi_k$ are tabulated in Table 5.14 and are shown plotted as a function of temperature in Figure 5.13. The results from the post-fire scenario tests show that the stiffness begins to reduce at around 800°F.

### 5.3.4    Measured Weld Fracture Angle
In Chapter 4, the angles of fracture θ of the transverse welds were measured and are given in Table 4.2 for the specimens tested during post-fire conditions. The fracture angles, θa, θb, and the average of θa and θb (θavg), for each specimen are plotted in Figure 5.14. A comparison to the average fracture angles for the post-fire scenario and elevated temperature tests is given in Figure 5.15.

Upon being cooled to ambient temperature, the average fracture angle of the weld is 46°, which is only a 2% variation from 45°. When the specimens are tested at higher temperatures, the weld fracture angle increases in the post-fire scenario tests from that found at ambient temperature. At 600°F, there is a 36% increase from that measured at ambient temperature. After 800°F, the weld fracture angle gradually decreases to 34.5° at 1200°F, where it is below that found at ambient temperature.

## 5.4 Comparison to Current Design Criteria

The results for the reduction factor for strength from the elevated temperature tests are compared to the strength reduction found in the AISC Specification and Eurocode. The comparison to AISC will be for the elevated temperature tests.

### 5.4.1 Comparison to AISC Specification

As discussed in Chapter 2, Appendix 4 in the AISC Specification (AISC 2005) presents reduction factors for Young's Modulus, the yield strength, and the tensile strength of steel at elevated temperatures. The strength reduction factors from the AISC Specification along with the elevated temperature test results are tabulated in Table 5.15. To compare the behavior of weld metal to base metal (i.e., steel) at elevated temperature, the reduction factors for the tensile strength of the weld determined from the elevated temperature tests are plotted and compared with the reduction factor of the tensile strength of steel per AISC (2005) in Figure 5.16. Included in Figure 5.16 is the strength reduction factors per Eurocode (1995), which is discussed later.

Figure 5.16 shows that up until 800°F that there is variation between the reduction factors for steel and weld metal. The tensile strength of the steel per AISC (2005) does not experience any reduction until 800°F, whereas the tensile strength of steel is reduced by 6%. The tensile strength of the weld experiences a 13% reduction at 600°F. The tensile strength of the weld then plateaus at this value until 800°F. After the temperature reaches 800°F, the tensile strength of both steel and weld metal show a significant decrease in the strength. At 1600°F, the tensile strength of the steel and weld has experienced a reduction in strength of 93% and 84%, respectively.

### 5.4.2 Comparison to Eurocode

As discussed in Chapter 2, Eurocode (1995) presents reduction factors for the material properties of steel at elevated temperatures. The strength reduction factors from Eurocode along with the elevated temperature test results are tabulated in Table 5.16. A comparison of the strength reduction factor for the weld metal with that for steel per Eurocode is included in Figure 5.16.

Up until about 800°F, there is variation between the reduction factors for steel and weld metal. The tensile strength of the steel does not experience any reduction until after the temperature is above 800°F. However, as discussed previously, the tensile strength of the weld experiences a 13% reduction at 600°F. The tensile strength of the weld then plateaus at this value until 800°F, where beyond 800°F tensile strength of the weld begins

to reduce significantly. The two curves are in good agreement beyond 800°F. At 900°F, the tensile strength of steel is reduced by 22% and the tensile strength of the weld is reduced by 23%. After this point, the tensile strength of both the steel and the weld experience significant reduction in strength. At 1600°F, the tensile strength of the steel and weld has experienced a reduction of 94% and 84%, respectively.

Overall, the strength reduction factor for the weld metal is similar to that for steel per the AISC Specification (AISC 2005) and Eurocode (1995) except between 400°F and 800°F and above 1400°F. In the former temperature range the weld metal strength reduction factor is less, whereas above 1400°F, it is greater.

## 5.5    Comparison to Past Research
In Chapter 2 past research on steel connections, namely bolted connections, was discussed. The behavior of bolted connections during fire and post-fire conditions will now be summarized so that a comparison of the behavior of welded connections during fire and post-fire conditions can be made. In Section 2.3.3, the Cardington tests were presented. In the Cardington tests it was found that at elevated and post-elevated temperatures that bolt shear failure took place in the connections as a result of the bolts losing strength due to the elevated temperature. In Section 2.3.5, the behavior of bolted connections in fire and post-fire conditions was summarized and it was found by Yu (2006) that similar to the results from the Cardington tests, bolts lose shear strength in post-fire conditions.

Note that shear strength was only lost if the bolts were heated to a temperature that was higher than their tempering temperature, which is achieved in a fire. Therefore, it can be concluded that in fire and post-fire conditions, bolted connections lose structural integrity. This loss of strength due to the exposure to elevated temperatures, in conjunction with the axial forces that develop during the cooling phase of a fire can result in bolt failure after a fire.

The reduction factors from Yu's research for the shear strength of bolts at elevated temperatures are shown in Table 2.3. Shown in Figure 5.17 is a comparison of the strength reduction factor for the elevated temperature tests by Yu for bolts and the weld metal test results.  It is observed that at elevated temperatures the bolts had a reduction in strength at temperatures above 600°F. At temperatures between 400°F and 700°F, the weld has a greater strength reduction than both the A325 and A490 bolts. At temperatures above 700°F, both the A325 and A490 bolts experience a greater strength reduction than the weld metal. The strength reduction of the A325 bolts is greater than that of the A490 bolts. The reduction factor for the A325 bolts at 1000°F is about 40% greater than that of the weld metal.

The reduction factors from Yu's research for bolts in post-fire are shown in Table 2.4. Shown in Figure 5.18 is a comparison of the strength reduction factor for the post-fire tests by Yu for bolts and the weld metal test results. The post-fire tests performed by Yu

170

consisted of heating the bolts to specified elevated temperatures and cooling the bolts to ambient temperature prior to testing the bolts in single shear. It is observed in post-fire conditions that there was not a significant reduction in strength until about 900°F. At temperatures below 750°F the bolts retained at least 98% of their original capacity. At 1112°F the bolts dropped to about 80% of their original capacity. A significant drop in capacity, such as about 60% did not occur until about 1300°F. After 1400°F was reached, the bolts still retained above 50% of their original capacity.

The reduction factors of the strength of weld metal in post-fire conditions are shown to be less than those of the bolts for each corresponding temperature, as shown in Figure 5.18. An exception exists at the ambient temperature, i.e., at 72°F, where the reduction factor for the weld metal is lower than that for the bolts. The strength increase in the weld at ambient temperature is likely associated with the affects of annealing that took place. More tests would need to be done to establish at which temperature the effect of annealing would increase the post-fire weld strength relative to the ambient temperature strength before a fire.

 The reduction factor is shown to be reduced more in value for the weld metal as the temperature increases. Up until 800°F, the weld maintained about 90% of its original capacity. Although at this point there is not a great loss of capacity, the capacity is slightly greater than that which is found in bolts at this temperature, when the strength reduction factor is about 0.95 for bolts. At 1000°F, the weld retained 83% of the original capacity. However, at 1200°F, the weld was reduced to about 44% of its original capacity, whereas the bolts do not drop below 50% of their capacity at 1400°F. The weld will continue to lose strength at higher temperatures. Therefore it can be concluded that upon cooling after a fire, when large axial forces develop, welds may become more critical than bolts, due to the greater amount of strength reduction that occurs in the welds.

## 5.6    Summary

In this chapter, the development of reduction factors was described. The tensile strength of the weld was measured and found to behave similarly to steel in that it had a significant reduction of strength above 800°F. The results from the elevated temperature tests and post-fire scenario tests were compared and it was found that their strength reduction followed the same trend, however slightly greater values for the post-fire scenario tests exist.

The results for the strength reduction were compared to current design criteria from AISC (2005) and Eurocode (1995). When comparing the reduction of tensile strength of the weld metal to steel based on the AISC Specification (2005) and Eurocode (1995) it was observed that up until a temperature of 800°F that the weld metal experiences a reduction that is 13% greater than steel, however after exceeding a temperature of 800°F, there is good agreement between the two. Above 1400°F the weld metal is stronger than steel per the AISC Specification (2005) and Eurocode (1995). When comparing to past research, it

was found that the loss of strength found in the welds was generally larger than that relative to bolts, particularly at temperatures at 1200°F.

Data for the stiffness reduction was presented. Similar to the strength, the stiffness reduces as temperature increases. This reduction follows a similar trend as that proposed in the AISC Specification (2005) and Eurocode (1995) for the degradation of Young's Modulus. The angle of fracture was also presented. It was found that there was no specified trend for the angle of fracture with increasing temperature.

Table 5.1  Computed weld dimensions and area for the elevated temperature test using the assumed 45° failure plane

| Specimen | Measured Weld Dimension and Computed Area | | | | | | | | |
| --- | --- | --- | --- | --- | --- | --- | --- | --- | --- |
| | Weld A | | | | Weld B | | | | Area |
| | $a_1$ | $a_2$ | $L_A$ | $A_A$ | $a_1$ | $a_2$ | $L_B$ | $A_B$ | $A_{w,c}$ |
| | in | in | in | $in^2$ | in | in | in | $in^2$ | $in^2$ |
| 1 | 0.359 | 0.309 | 1.523 | 0.360 | 0.342 | 0.285 | 1.496 | 0.332 | 0.692 |
| 2 | 0.335 | 0.319 | 1.478 | 0.342 | 0.387 | 0.345 | 1.487 | 0.385 | 0.726 |
| 3 | 0.380 | 0.328 | 1.512 | 0.378 | 0.378 | 0.334 | 1.503 | 0.378 | 0.757 |
| 4 | 0.334 | 0.306 | 1.435 | 0.324 | 0.329 | 0.318 | 1.479 | 0.338 | 0.662 |
| 5 | 0.370 | 0.316 | 1.469 | 0.356 | 0.356 | 0.337 | 1.506 | 0.369 | 0.725 |
| 6 | 0.365 | 0.358 | 1.485 | 0.379 | 0.405 | 0.354 | 1.467 | 0.394 | 0.773 |
| 7 | 0.307 | 0.358 | 1.486 | 0.349 | 0.317 | 0.379 | 1.489 | 0.366 | 0.716 |
| 8 | 0.409 | 0.350 | 1.497 | 0.402 | 0.372 | 0.385 | 1.544 | 0.413 | 0.814 |
| 9 | 0.366 | 0.359 | 1.538 | 0.394 | 0.364 | 0.398 | 1.560 | 0.421 | 0.814 |
| 10 | 0.367 | 0.332 | 1.435 | 0.355 | 0.351 | 0.347 | 1.479 | 0.365 | 0.720 |


Table 5.2  Measured weld dimensions and area for the elevated temperature tests using measured throat

| Specimen | Measured Weld Dimension and Fracture Surface | | |
| --- | --- | --- | --- |
| | Weld A | Weld B | Area |
| | $te_A$ | $te_B$ | $A_{w,m}$ |
| | in | in | $in^2$ |
| 1 | 0.269 | 0.250 | 0.783 |
| 2 | 0.260 | 0.293 | 0.819 |
| 3 | 0.285 | 0.305 | 0.889 |
| 4 | 0.249 | 0.285 | 0.778 |
| 5 | 0.288 | 0.281 | 0.847 |
| 6 | 0.312 | 0.303 | 0.907 |
| 7 | 0.251 | 0.291 | 0.805 |
| 8 | 0.274 | 0.272 | 0.831 |
| 9 | 0.262 | 0.296 | 0.864 |
| 10 | 0.281 | 0.292 | 0.835 |

Table 5.3  Tensile strength of the weld from the elevated temperature tests using computed throat

| Specimen | Temperature | $P_{ult}$ (kip) | $te_{avg} =$ $0.707a_{avg}$ (in) | $L_{avg}$ (in) | $A_{w,c}$ (in$^2$) | $\sigma_{u,exp\_c}$ (ksi) |
|---|---|---|---|---|---|---|
| 1 | 70 | 41.76 | 0.229 | 1.509 | 0.692 | 80.0 |
| 2 | 350 | 43.29 | 0.245 | 1.482 | 0.726 | 78.9 |
| 3 | 600 | 41.07 | 0.251 | 1.507 | 0.757 | 71.9 |
| 4 | 700 | 36.86 | 0.227 | 1.457 | 0.662 | 73.7 |
| 5 | 800 | 40.13 | 0.244 | 1.488 | 0.725 | 73.2 |
| 6 | 900 | 37.43 | 0.262 | 1.476 | 0.773 | 64.1 |
| 7 | 1000 | 25.73 | 0.241 | 1.487 | 0.716 | 47.6 |
| 8 | 1200 | 15.87 | 0.268 | 1.520 | 0.814 | 25.8 |
| 9 | 1400 | 8.62 | 0.263 | 1.549 | 0.814 | 14.0 |
| 10 | 1600 | 7.29 | 0.247 | 1.457 | 0.720 | 13.4 |

Table 5.4  Tensile strength of the weld from the elevated temperature tests using measured throat

| Specimen | Temperature | $P_{ult}$ (kip) | $te_{avg}$ (in) | $L_{avg}$ (in) | $A_{w,m}$ (in$^2$) | $\sigma_{u,exp\_m}$ (ksi) |
|---|---|---|---|---|---|---|
| 1 | 70 | 41.76 | 0.259 | 1.509 | 0.783 | 70.6 |
| 2 | 350 | 43.29 | 0.276 | 1.482 | 0.819 | 70.0 |
| 3 | 600 | 41.07 | 0.295 | 1.507 | 0.889 | 61.2 |
| 4 | 700 | 36.86 | 0.267 | 1.457 | 0.778 | 62.8 |
| 5 | 800 | 40.13 | 0.285 | 1.488 | 0.847 | 62.7 |
| 6 | 900 | 37.43 | 0.307 | 1.476 | 0.907 | 54.6 |
| 7 | 1000 | 25.73 | 0.271 | 1.487 | 0.805 | 42.3 |
| 8 | 1200 | 15.87 | 0.273 | 1.520 | 0.831 | 25.3 |
| 9 | 1400 | 8.62 | 0.279 | 1.549 | 0.864 | 13.3 |
| 10 | 1600 | 7.29 | 0.286 | 1.457 | 0.835 | 11.5 |

Table 5.5  Reduction factor for strength at elevated temperatures using the computed area of the weld

| Specimen | Temperature | $P_{ult}$ (kip) | $\phi_c = \sigma_{u,exp\_c}(T)/\sigma_{u,exp\_c}(T=72°F)$ |
|---|---|---|---|
| 1 | 70 | 41.76 | 1.000 |
| 2 | 350 | 43.29 | 0.987 |
| 3 | 600 | 41.07 | 0.899 |
| 4 | 700 | 36.86 | 0.921 |
| 5 | 800 | 40.13 | 0.916 |
| 6 | 900 | 37.43 | 0.801 |
| 7 | 1000 | 25.73 | 0.595 |
| 8 | 1200 | 15.87 | 0.323 |
| 9 | 1400 | 8.62 | 0.175 |
| 10 | 1600 | 7.29 | 0.168 |

Table 5.6  Reduction factor for strength at elevated temperatures using the measured area of the weld

| Specimen | Temperature | Pult (kip) | $\phi_m = \sigma_{u,exp\_m}(T)/\sigma_{u,exp\_m}(T=72°F)$ |
|---|---|---|---|
| 1 | 70 | 41.76 | 1.000 |
| 2 | 350 | 43.29 | 0.991 |
| 3 | 600 | 41.07 | 0.866 |
| 4 | 700 | 36.86 | 0.888 |
| 5 | 800 | 40.13 | 0.888 |
| 6 | 900 | 37.43 | 0.773 |
| 7 | 1000 | 25.73 | 0.599 |
| 8 | 1200 | 15.87 | 0.358 |
| 9 | 1400 | 8.62 | 0.187 |
| 10 | 1600 | 7.29 | 0.163 |

Table 5.7  Reduction factors for stiffness of test specimens at elevated temperatures

| Specimen | Target Temperature | k | $\phi_k$ |
|---|---|---|---|
| | (°F) | (kip/in) | |
| 1 | 70 | 277.8 | 1.000 |
| 2 | 350 | 237.8 | 0.856 |
| 3 | 600 | 243.5 | 0.877 |
| 4 | 700 | 228.4 | 0.822 |
| 5 | 800 | 235.9 | 0.849 |
| 6 | 900 | 208.1 | 0.749 |
| 7 | 1000 | 197.6 | 0.711 |
| 8 | 1200 | 148.8 | 0.536 |
| 5 | 1400 | 99.8 | 0.359 |
| 10 | 1600 | 72.4 | 0.261 |

Table 5.8  Computed weld dimensions and area for the post-fire scenario tests using the assumed 45° failure plane

| Specimen | Measured Weld Dimension and Computed Area | | | | | | | | |
| | Weld A | | | | Weld B | | | | Area |
| | $a_1$ | $a_2$ | $L_A$ | $A_A$ | $a_1$ | $a_2$ | $L_B$ | $A_B$ | $A_{w,c}$ |
| | in | in | in | in$^2$ | in | in | in | in$^2$ | in$^2$ |
| P1 | 0.379 | 0.333 | 1.491 | 0.375 | 0.344 | 0.290 | 1.477 | 0.331 | 0.706 |
| P2 | 0.368 | 0.319 | 1.451 | 0.352 | 0.384 | 0.286 | 1.497 | 0.354 | 0.707 |
| P3 | 0.330 | 0.336 | 1.514 | 0.356 | 0.372 | 0.402 | 1.545 | 0.423 | 0.779 |
| P4 | 0.386 | 0.312 | 1.504 | 0.371 | 0.329 | 0.348 | 1.490 | 0.357 | 0.728 |
| P5 | 0.365 | 0.284 | 1.503 | 0.345 | 0.400 | 0.404 | 1.518 | 0.431 | 0.776 |

Table 5.9  Measured weld dimensions and area for the post-fire scenario tests using measured throat

| Specimen | Measured Weld Dimension and Fracture Surface | | |
| | Weld A | Weld B | Area |
| | $te_A$ | $te_B$ | $A_{w,m}$ |
| | in | in | in$^2$ |
| P1 | 0.242 | 0.257 | 0.741 |
| P2 | 0.280 | 0.264 | 0.801 |
| P3 | 0.318 | 0.253 | 0.874 |
| P4 | 0.270 | 0.207 | 0.714 |
| P5 | 0.218 | 0.290 | 0.766 |

Table 5.10  Tensile strength of weld from the post-fire scenario tests using computed throat

| Specimen | Temperature | Pult (kip) | teavg = 0.707aavg (in) | Lavg (in) | $A_{w,c}$ (in$^2$) | $\sigma_{u,exp\_c}$ (ksi) |
|----------|-------------|------------|------------------------|-----------|--------------------|---------------------------|
| P1 | 70 | 42.20 | 0.238 | 1.484 | 0.706 | 79.1 |
| P2 | 600 | 38.51 | 0.240 | 1.474 | 0.707 | 72.2 |
| P3 | 800 | 42.82 | 0.255 | 1.529 | 0.779 | 72.8 |
| P4 | 1000 | 31.63 | 0.243 | 1.497 | 0.728 | 57.6 |
| P5 | 1200 | 17.77 | 0.257 | 1.510 | 0.776 | 30.3 |

Table 5.11  Tensile strength of weld from the post-fire scenario tests using measured throat

| Specimen | Temperature | Pult (kip) | teavg (in) | Lavg (in) | $A_{w,m}$ (in$^2$) | $\sigma_{u,exp\_m}$ (ksi) |
|----------|-------------|------------|------------|-----------|--------------------|---------------------------|
| P1 | 70 | 42.20 | 0.240 | 1.484 | 0.741 | 78.7 |
| P2 | 600 | 38.51 | 0.272 | 1.474 | 0.801 | 63.7 |
| P3 | 800 | 42.82 | 0.286 | 1.529 | 0.874 | 64.9 |
| P4 | 1000 | 31.63 | 0.238 | 1.497 | 0.714 | 58.7 |
| P5 | 1200 | 17.77 | 0.254 | 1.510 | 0.766 | 30.7 |

Table 5.12  Reduction factor for strength, post-fire scenario tests using the computed area of the weld

| Specimen | Temperature | $P_{ult}$ (kip) | $\phi_c = \sigma_{u,exp\_c}(T)/\sigma_{u,exp\_c}(T=72°F)$ |
|---|---|---|---|
| P1 | 70 | 42.20 | 0.9896 |
| P2 | 600 | 17.77 | 0.8885 |
| P3 | 800 | 31.63 | 0.9099 |
| P4 | 1000 | 42.82 | 0.7196 |
| P5 | 1200 | 38.51 | 0.3792 |

Table 5.13  Reduction factor for strength, post-fire scenario tests using the measured area of the weld

| Specimen | Temperature | $P_{ult}$ (kip) | $\phi_m = \sigma_{u,exp\_m}(T)/\sigma_{u,exp\_m}(T=72°F)$ |
|---|---|---|---|
| P1 | 70 | 42.20 | 1.114 |
| P2 | 600 | 17.77 | 0.901 |
| P3 | 800 | 31.63 | 0.919 |
| P4 | 1000 | 42.82 | 0.831 |
| P5 | 1200 | 38.51 | 0.435 |

Table 5.14  Reduction factors for the stiffness for post-fire scenario tests

| Specimen | Target Temperature | k | $\phi_k$ |
|---|---|---|---|
| | (°F) | (kip/in) | |
| P1 | 70 | 209.3 | 1.000 |
| P2 | 600 | 204.5 | 0.977 |
| P3 | 800 | 201.0 | 0.960 |
| P4 | 1000 | 177.9 | 0.850 |
| P5 | 1200 | 134.3 | 0.642 |

Table 5.15  Tabulation of reduction factors for strength of steel from AISC (2005) and specimen weld metal at elevated temperatures

| Tensile Strength of Steel | | Tensile Strength of Weld Metal | |
|---|---|---|---|
| Steel Temperature (°F) | $k_u = F_{um}/F_u$ | Weld Temperature (°F) | $\phi_m = F_u(T)/F_u$ |
| 68 | 1.00 | 70 | 1.000 |
| 200 | 1.00 | 350 | 0.991 |
| 400 | 1.00 | 600 | 0.866 |
| 550 | 1.00 | 700 | 0.889 |
| 600 | 1.00 | 800 | 0.888 |
| 800 | 0.94 | 900 | 0.774 |
| 1000 | 0.66 | 1000 | 0.599 |
| 1200 | 0.35 | 1200 | 0.358 |
| 1400 | 0.16 | 1400 | 0.187 |
| 1600 | 0.07 | 1600 | 0.164 |
| 1800 | 0.04 | | |
| 2000 | 0.02 | | |
| 2200 | 0.00 | | |

Table 5.16  Tabulation of reduction factors for strength of steel from Eurocode (1995) and specimen weld metal at elevated temperatures

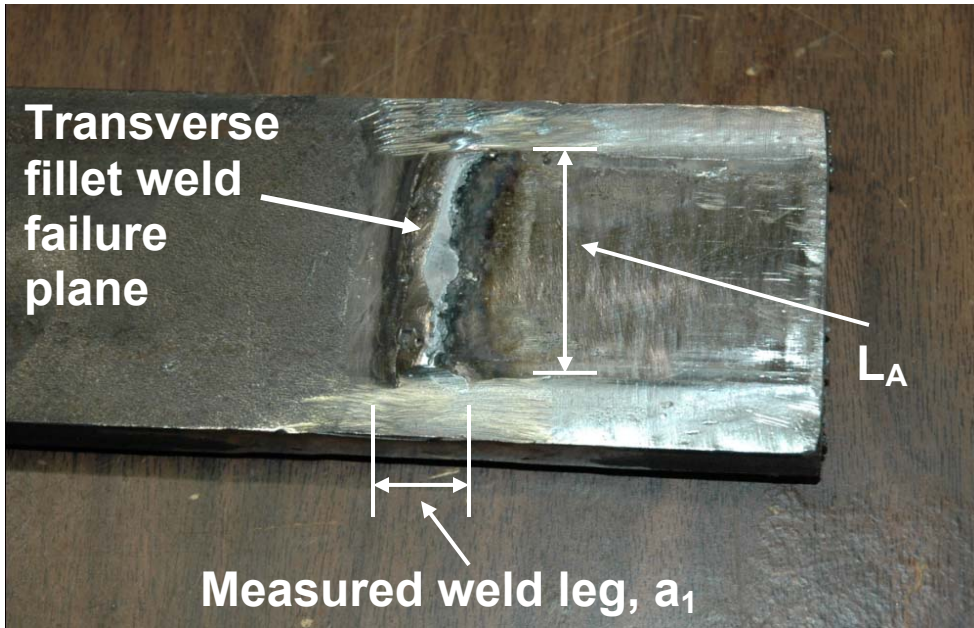| Tensile Strength of Steel | | Tensile Strength of Weld Metal | |
|---|---|---|---|
| Steel Temperature (°F) | $k_{y,\theta} = f_{y,\theta}/f_y$ | Weld Temperature (°F) | $\phi_m = F_u(T)/F_u$ |
| 68 | 1.000 | 70 | 1.000 |
| 212 | 1.000 | 350 | 0.991 |
| 392 | 1.000 | 600 | 0.866 |
| 572 | 1.000 | 700 | 0.889 |
| 752 | 1.000 | 800 | 0.888 |
| 932 | 0.780 | 900 | 0.774 |
| 1112 | 0.470 | 1000 | 0.599 |
| 1292 | 0.230 | 1200 | 0.358 |
| 1472 | 0.110 | 1400 | 0.187 |
| 1652 | 0.060 | 1600 | 0.164 |
| 1832 | 0.040 | | |
| 2012 | 0.020 | | |
| 2192 | 0.000 | | |

Figure 5.1  Photograph of typical fractured transverse fillet weld showing failure plane



Figure 5.2  Photograph of the digital caliper
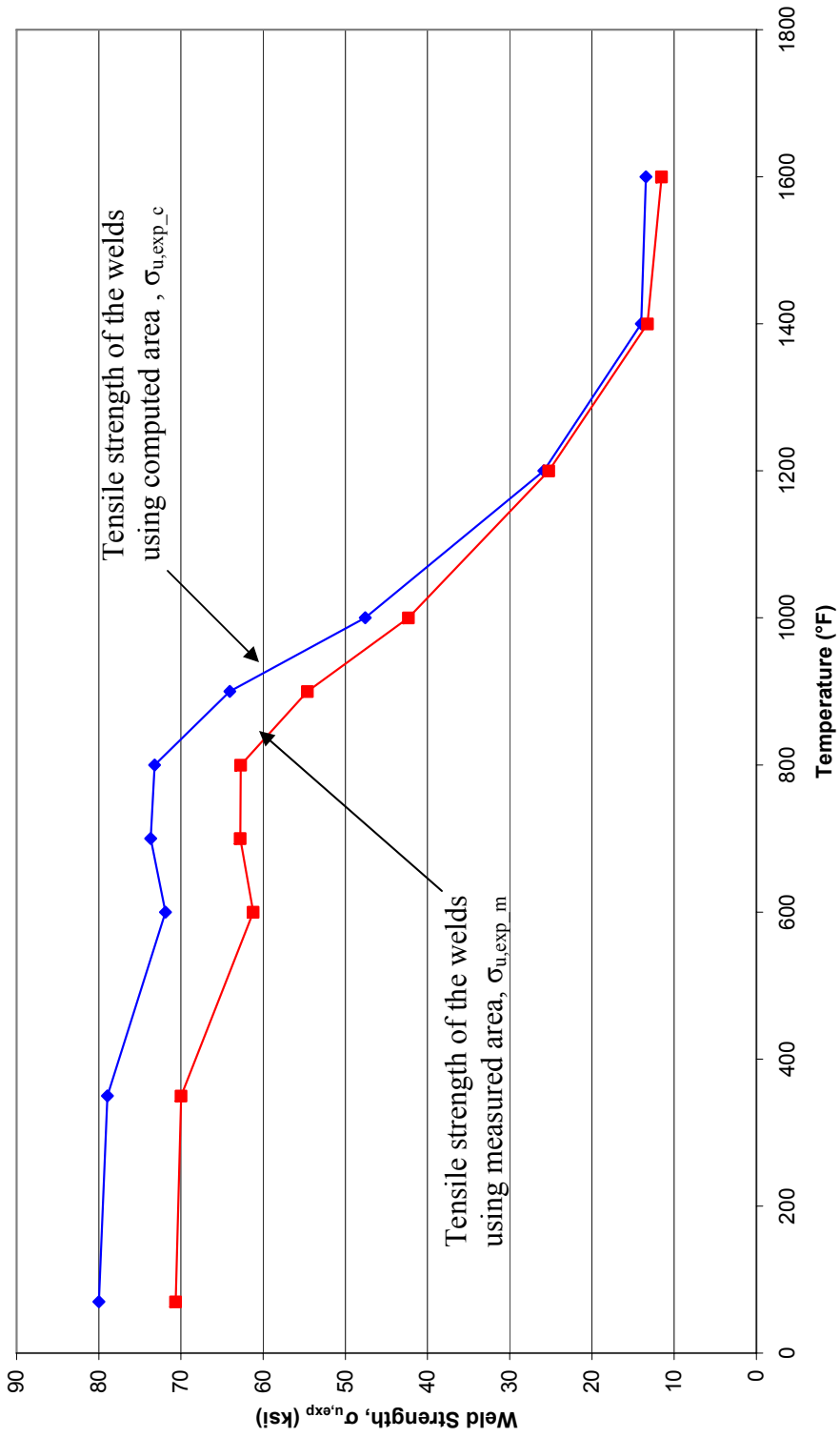
Figure 5.3  Tensile strength of weld metal as a function of temperature, elevated temperature tests

182
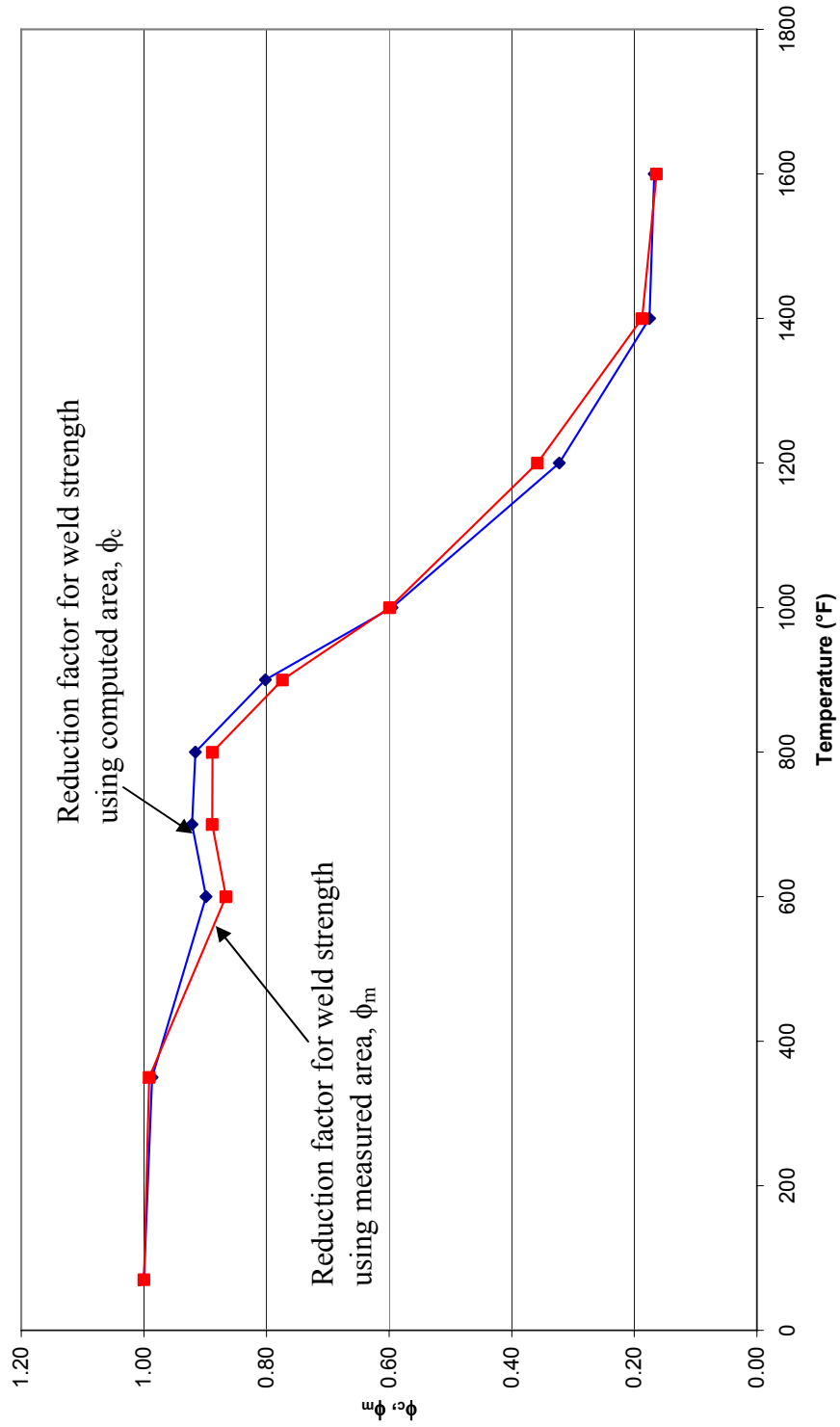
Figure 5.4  Reduction factor of weld strength at elevated temperatures
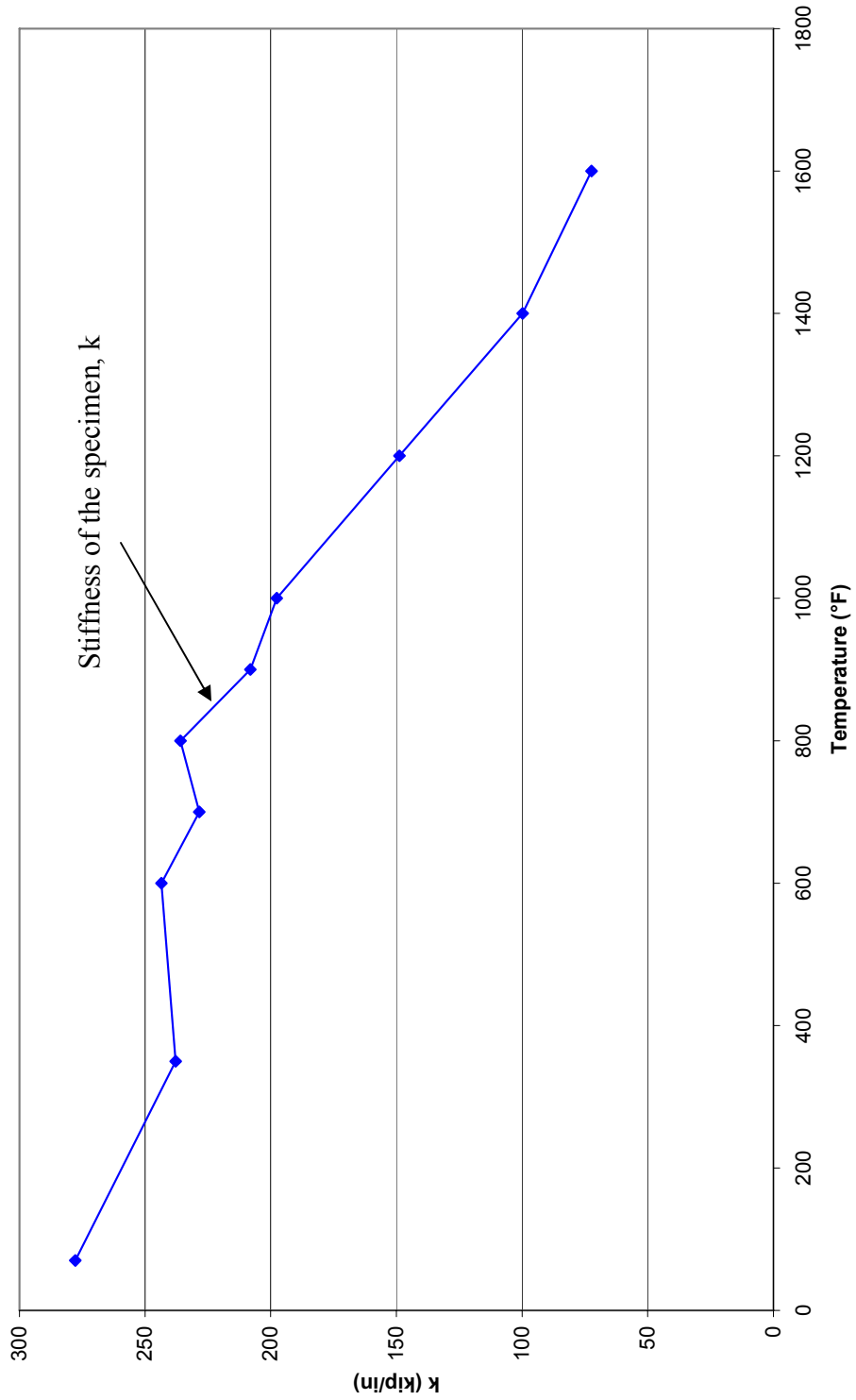
Figure 5.5  Stiffness of the specimen as a function of temperature, elevated temperature tests
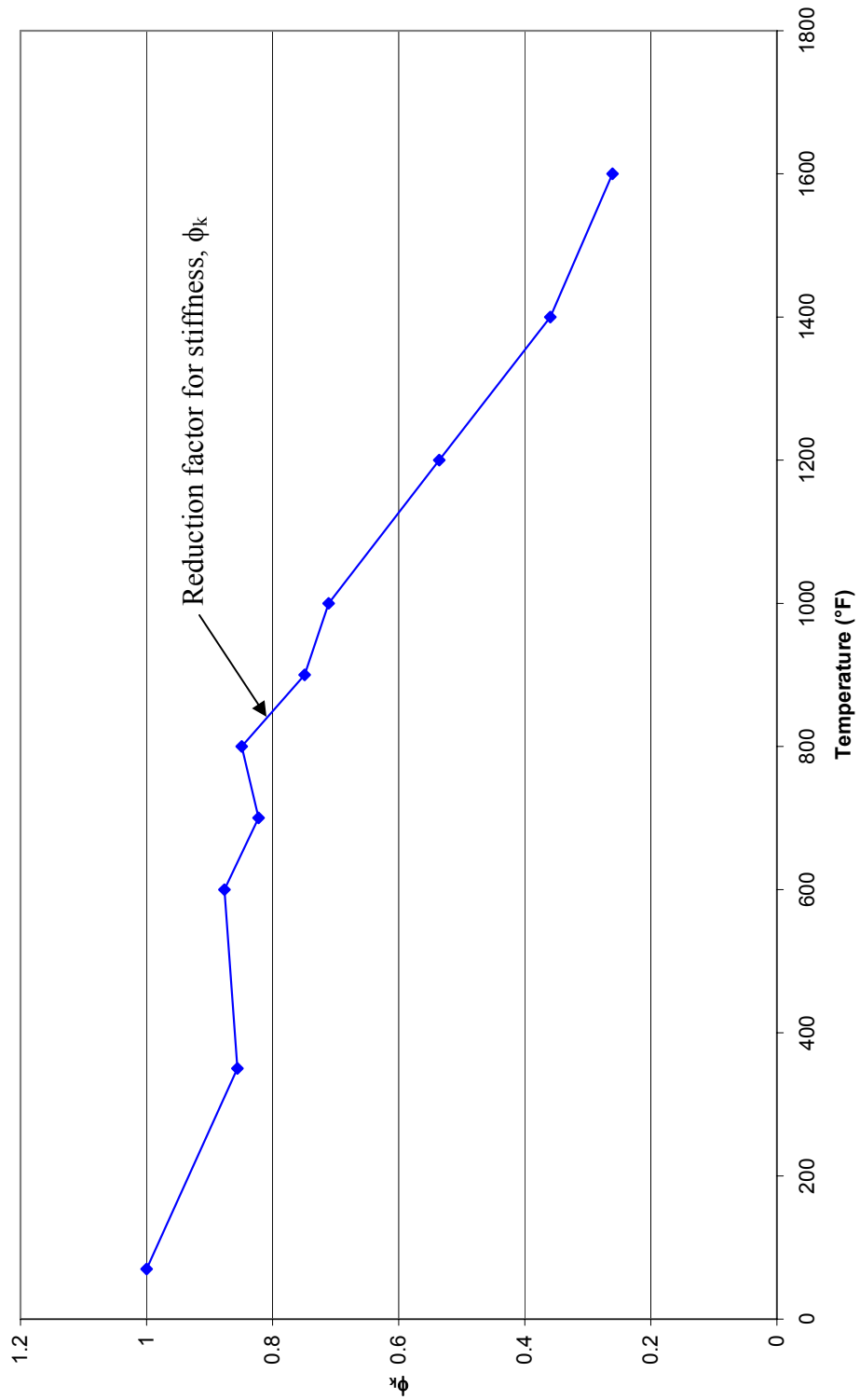
Figure 5.6  Reduction factor for the stiffness of the specimen at elevated temperatures
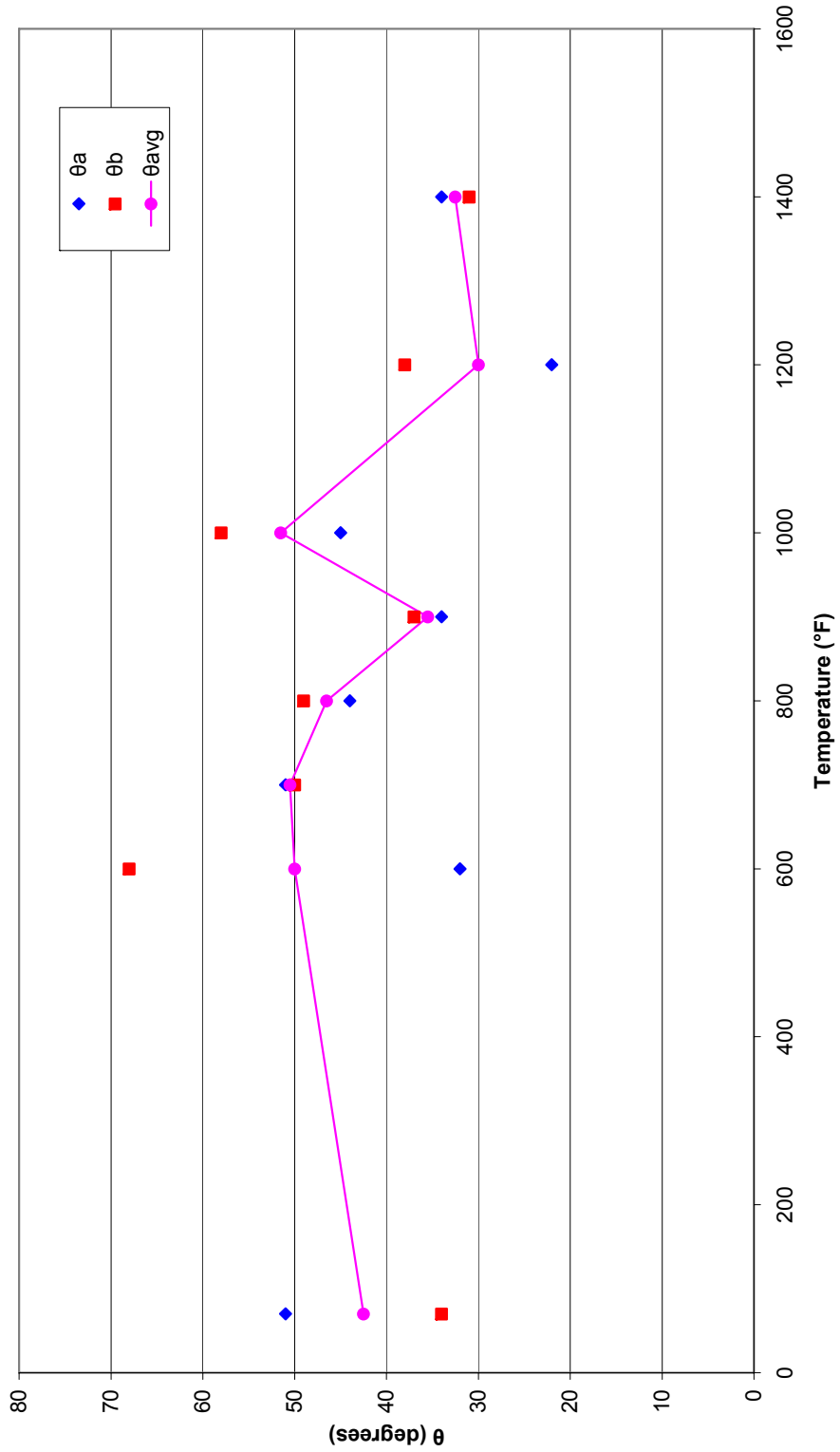
Figure 5.7  Measured fracture angle of the weld, elevated temperature tests
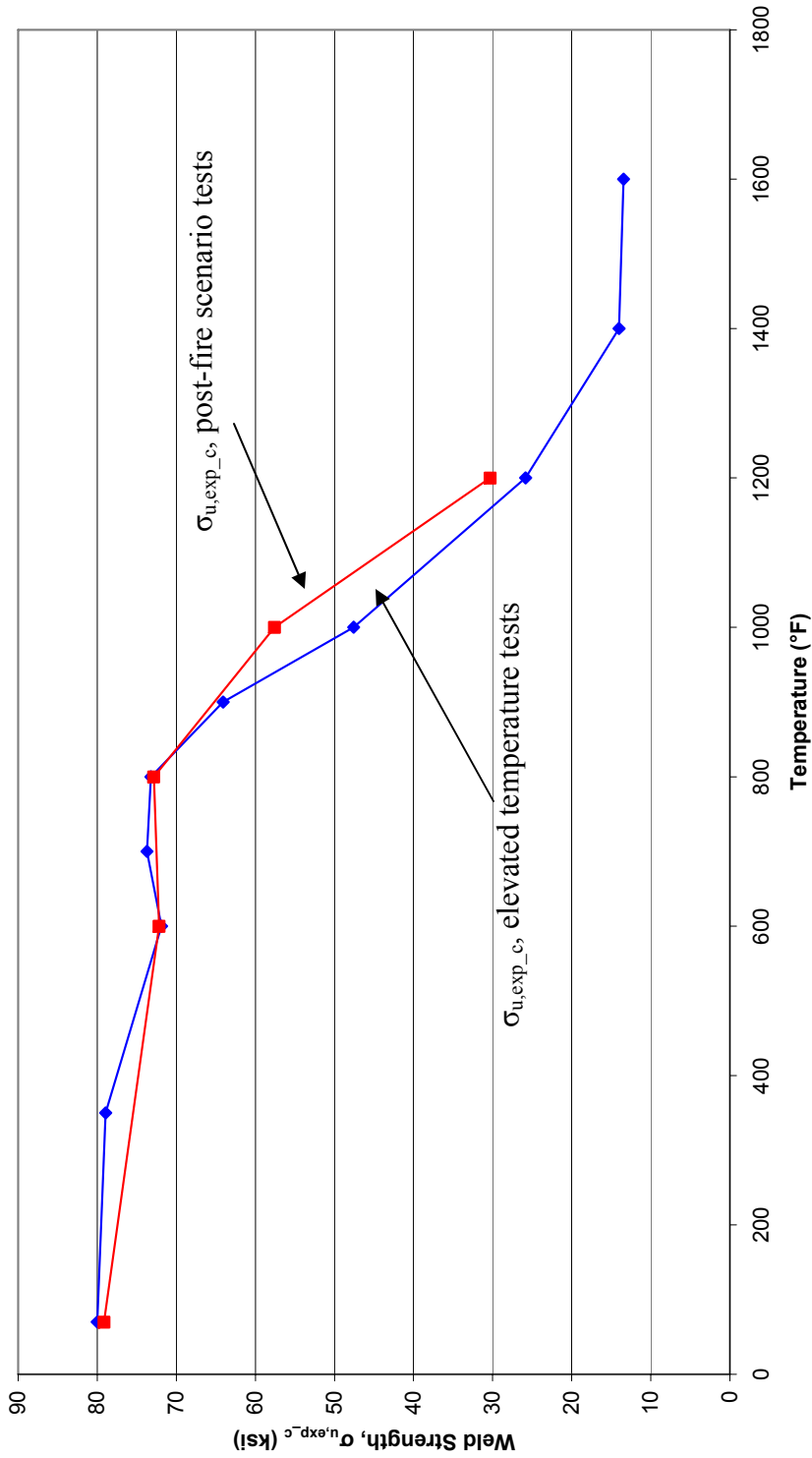
Figure 5.8  Comparison of tensile strength of weld metal for the elevated temperature and post-fire scenario tests with increasing temperature, assuming 45° failure plane

187
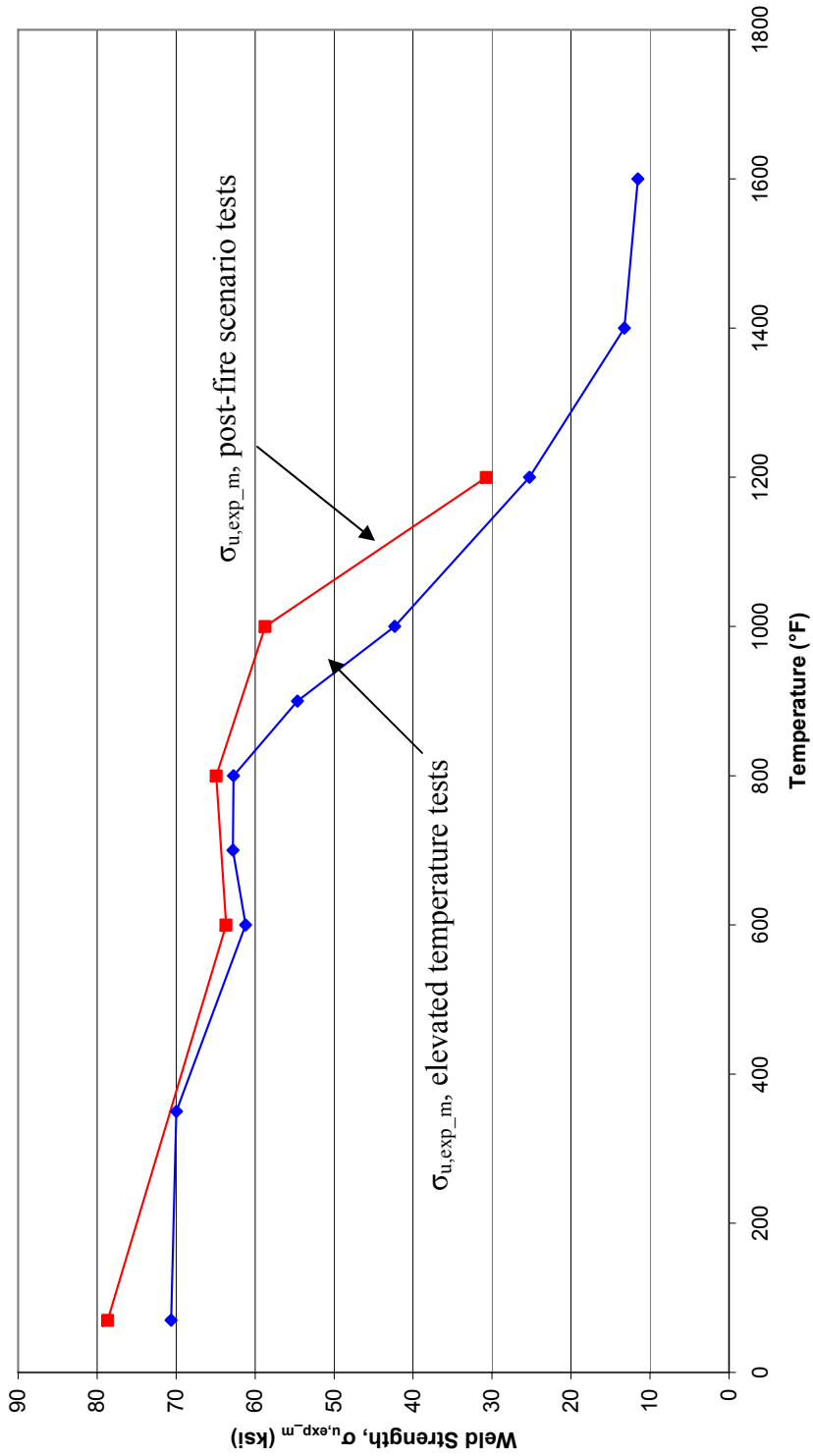
Figure 5.9  Comparison of tensile strength of weld metal for the elevated temperature and post-fire scenario tests with increasing temperature, using measured weld area

188
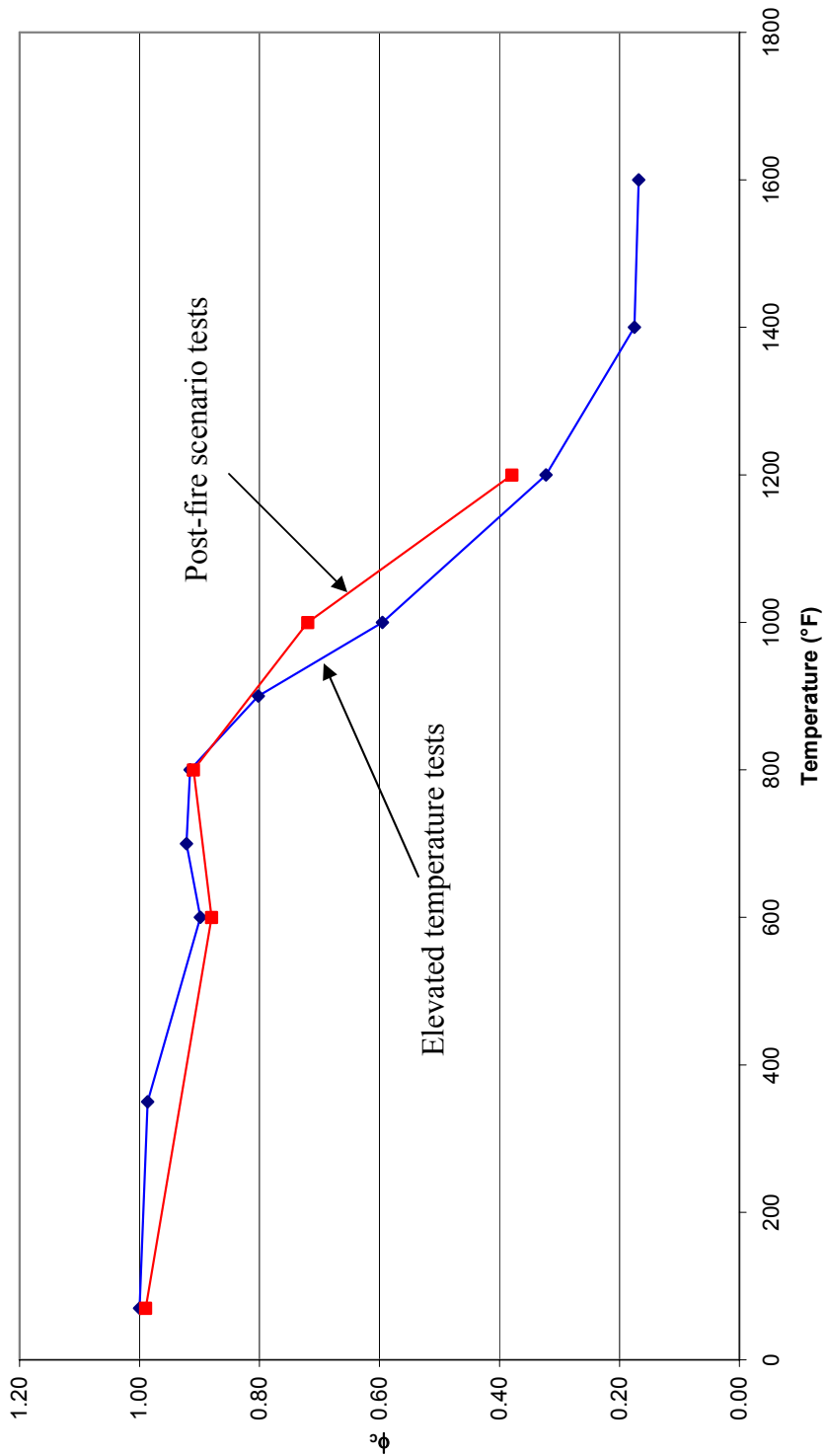
Figure 5.10 Comparison of reduction factor of strength of elevated temperature and post-fire scenario tests using assumed 45° failure plane

189
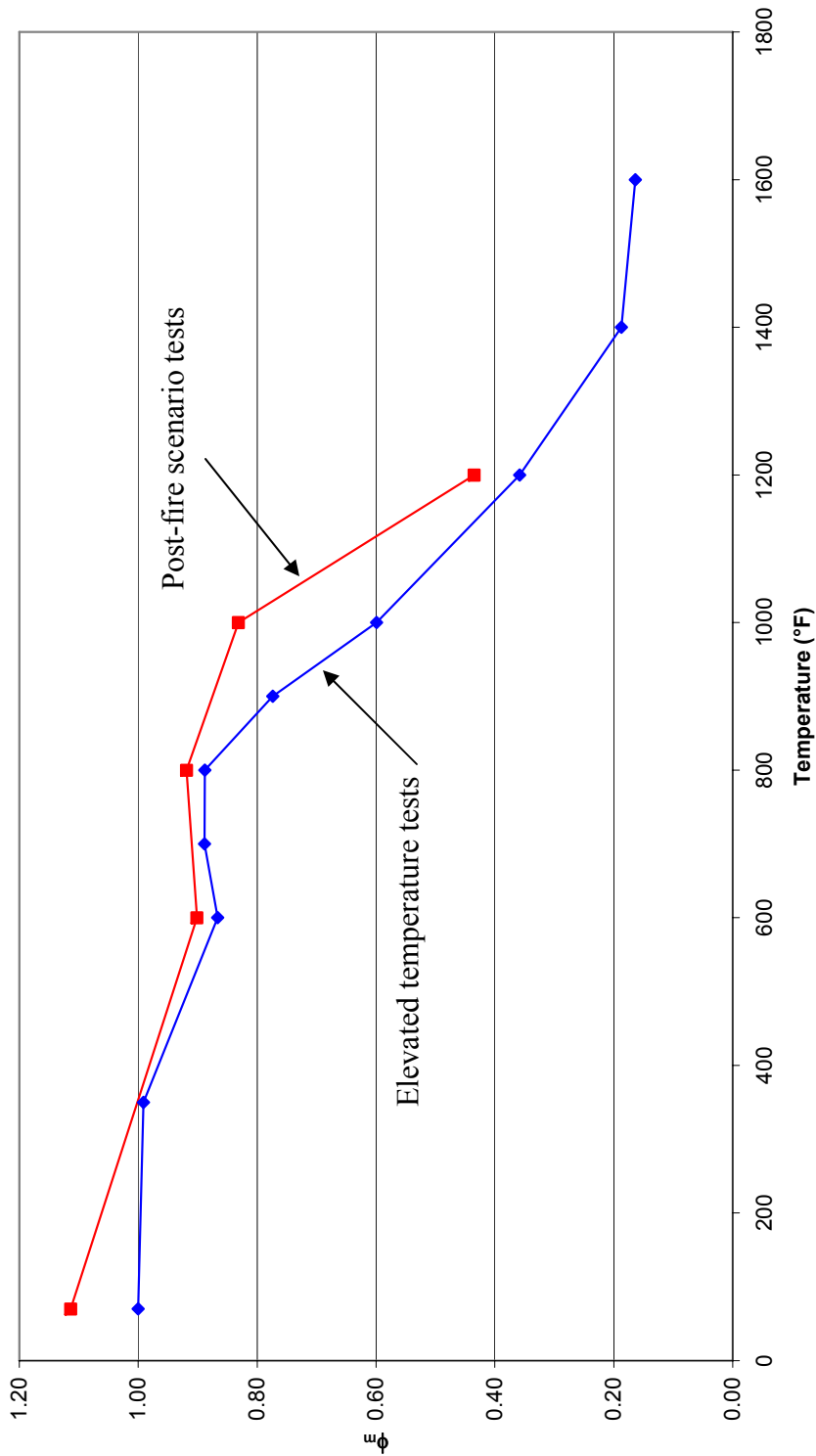
Figure 5.11  Comparison of reduction factor of strength of elevated temperature and post-fire scenario tests using the measured area of weld
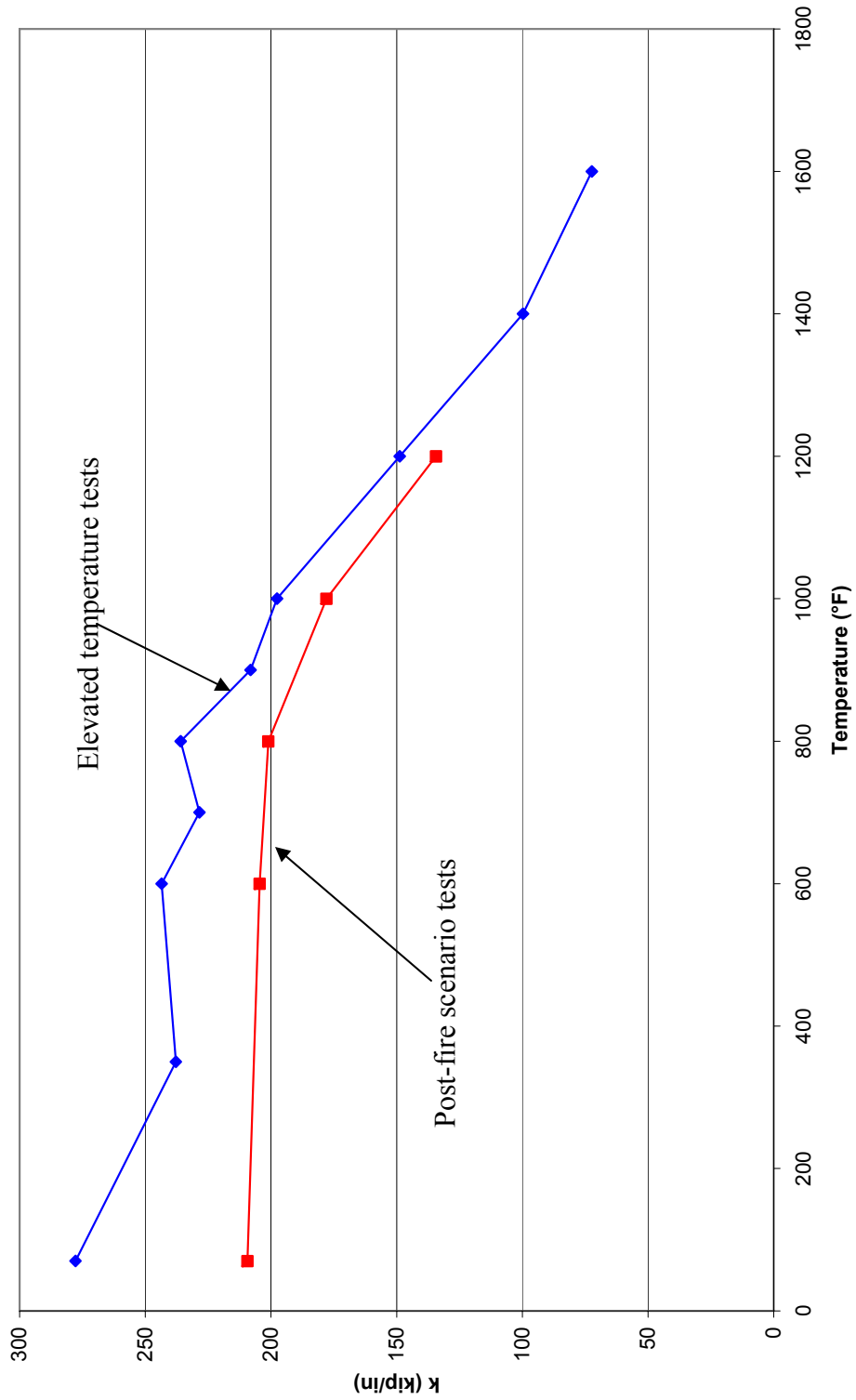
Figure 5.12  Comparison of the stiffness of the specimen of elevated temperature tests and post-fire scenario tests

191
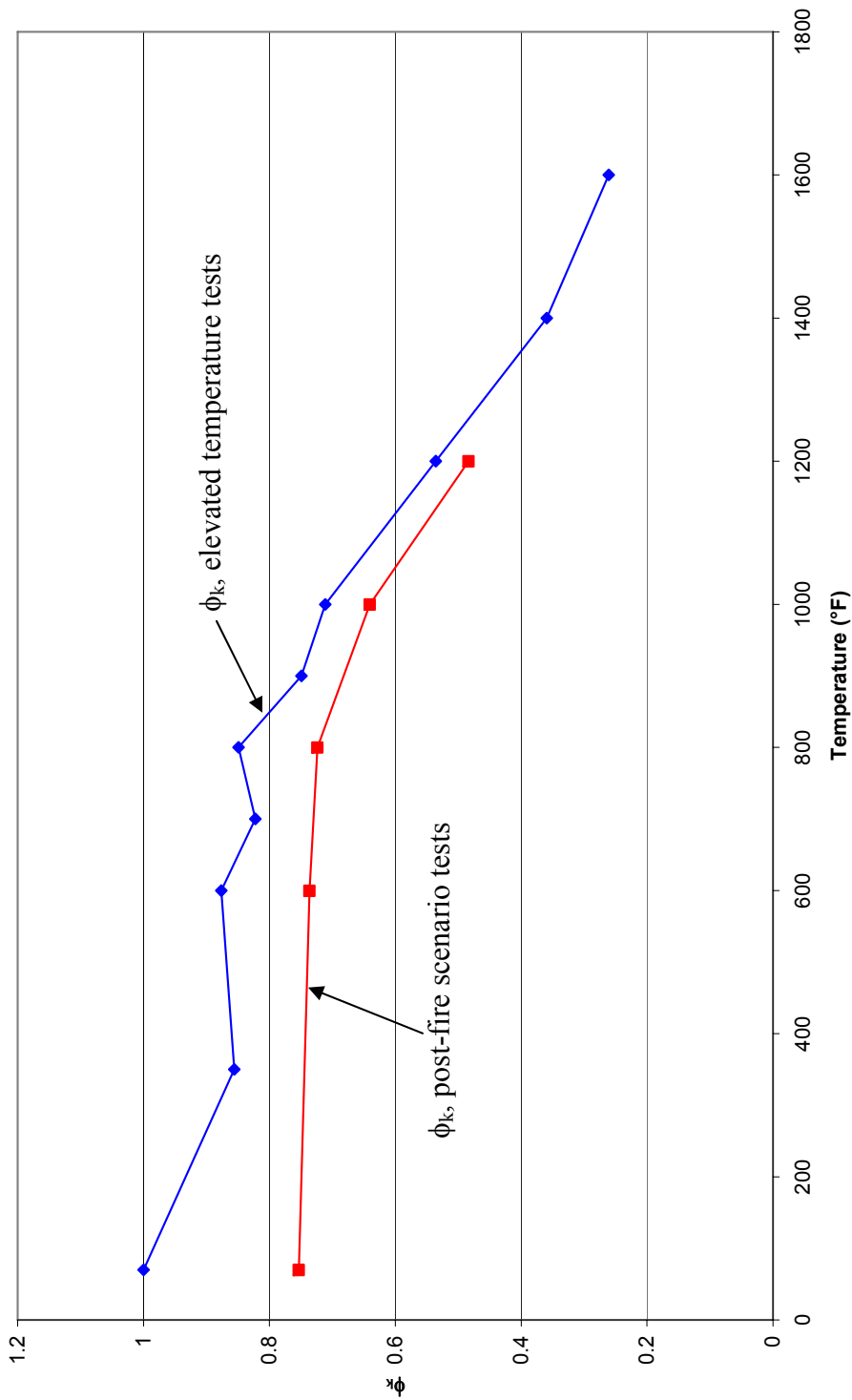
Figure 5.13  Comparison of the reduction factor for the stiffness of the specimen of elevated temperature and post-fire scenario tests

192
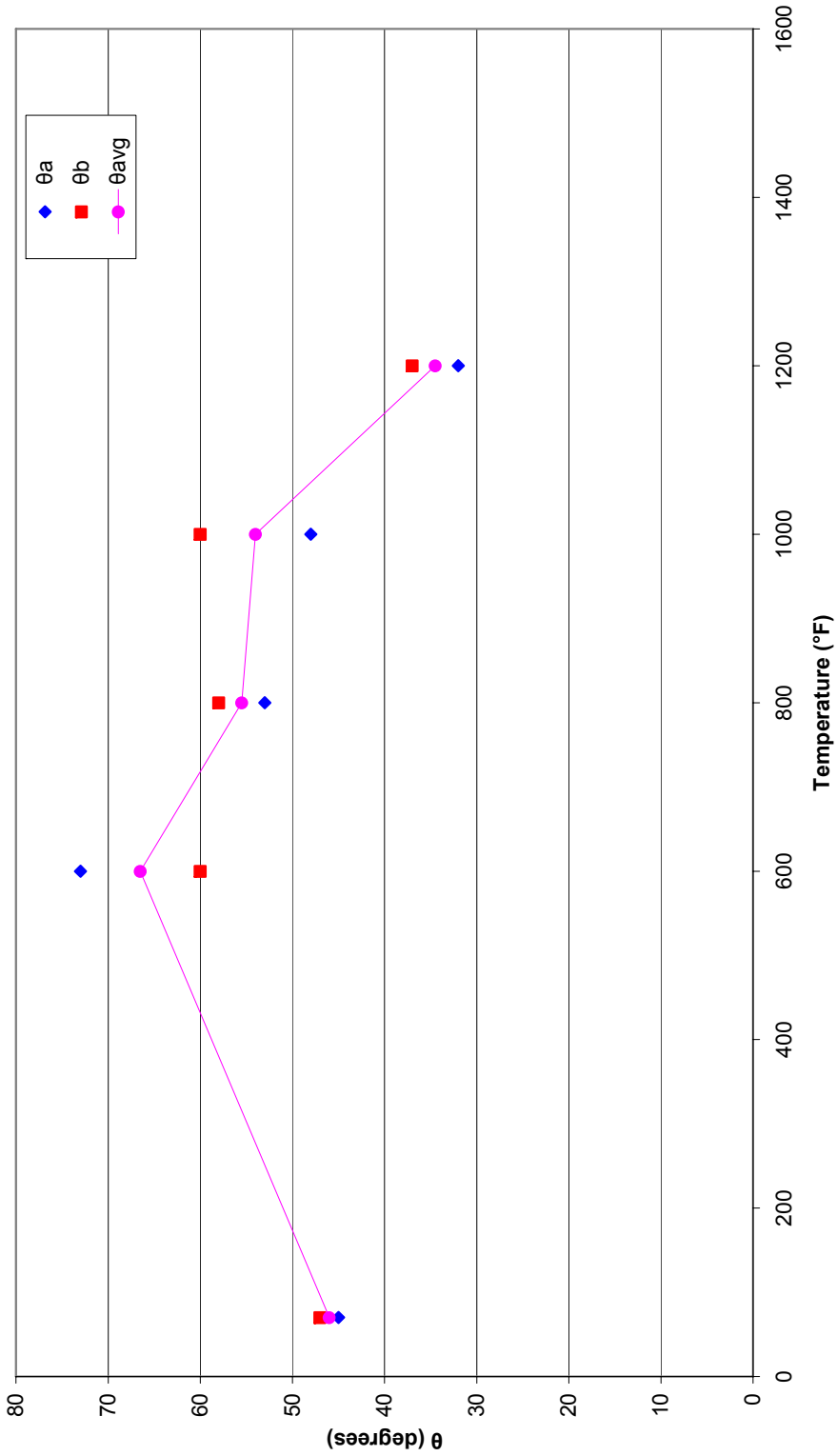
Figure 5.14  Measured fracture angle of the transverse fillet weld, post-fire scenario tests

193
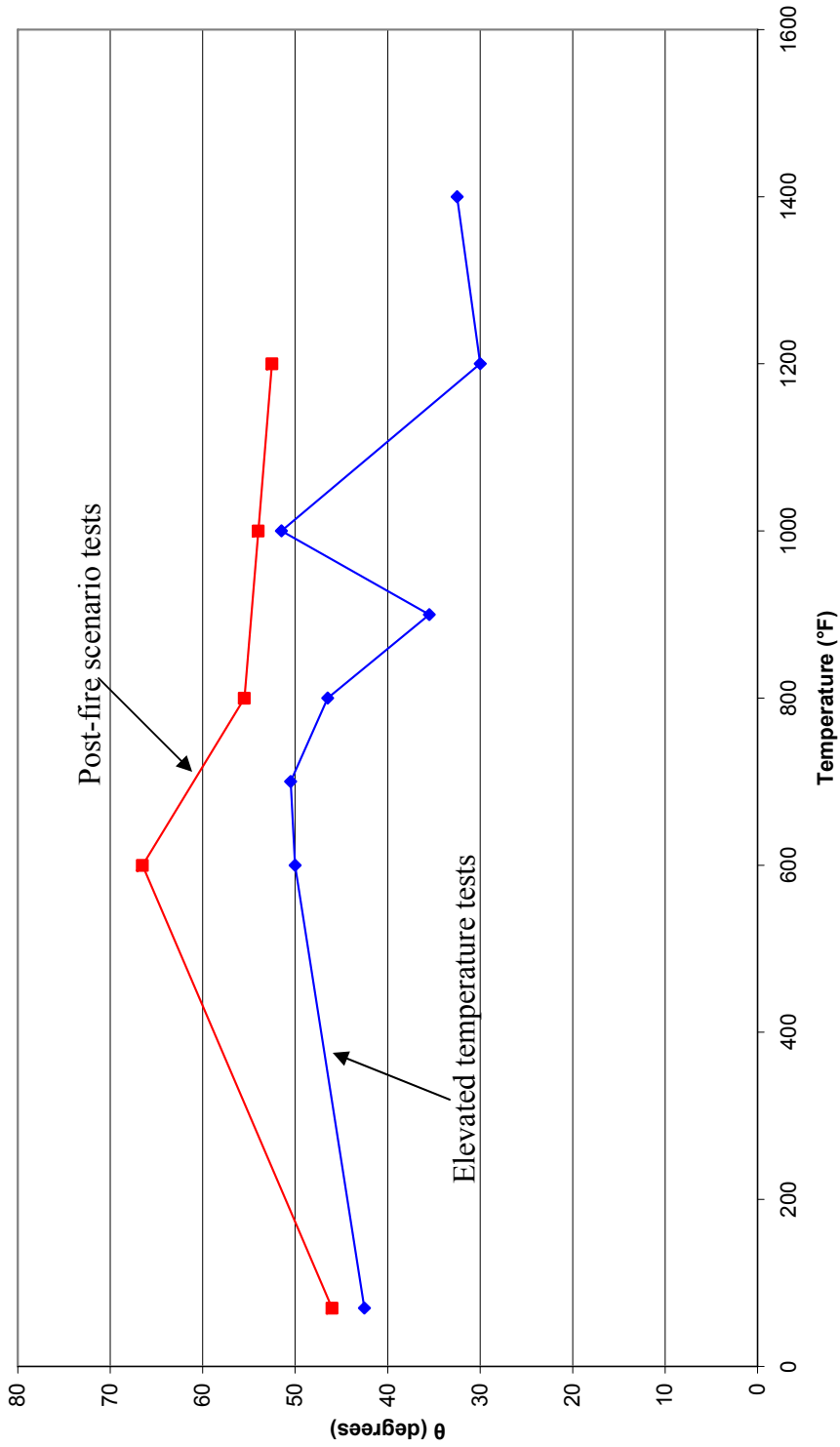
Figure 5.15  Comparison of average measured fracture angle of transverse fillet weld for the elevated temperature tests and post-fire scenario tests

194
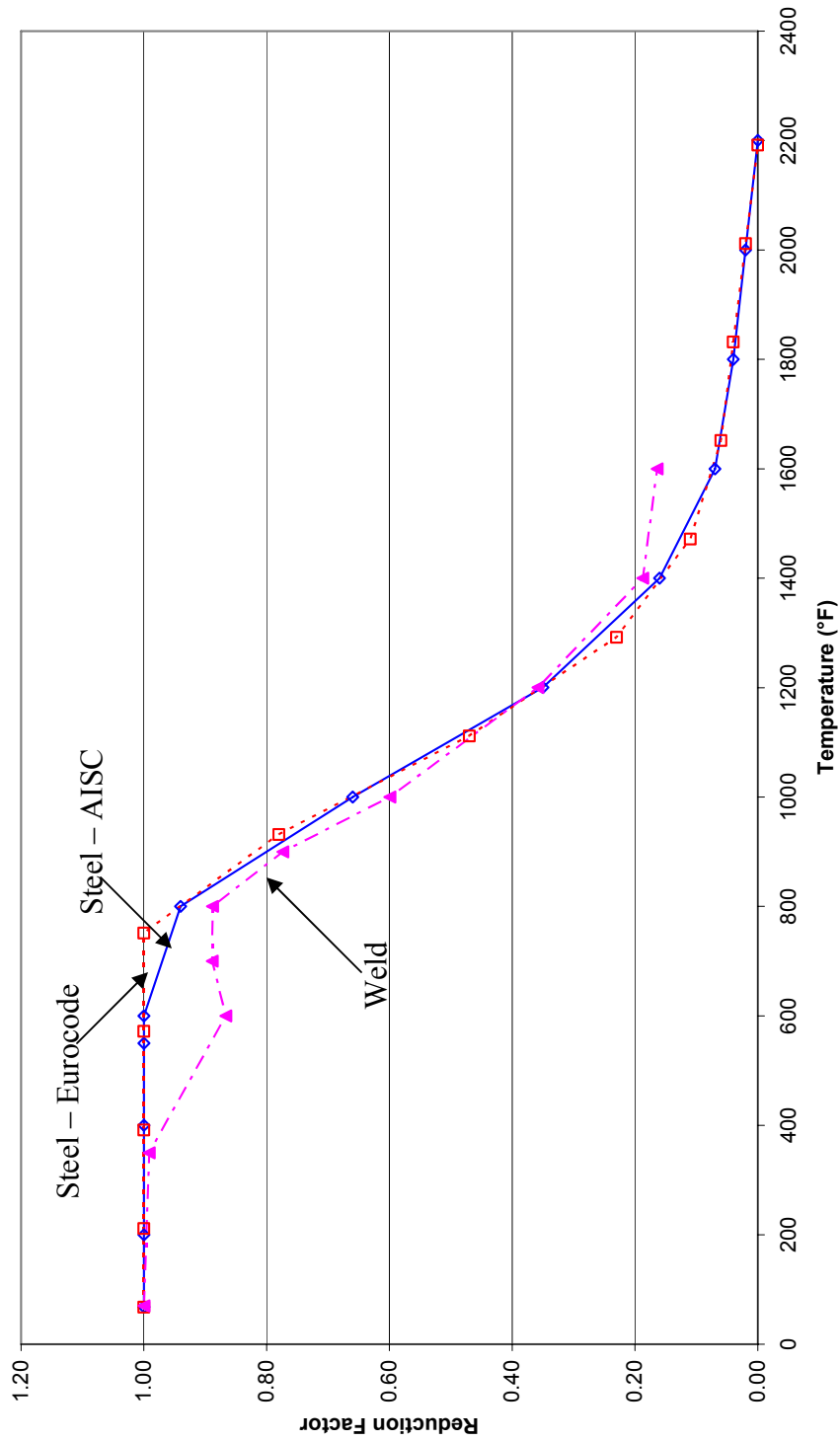
Figure 5.16  Comparison of the reduction factors of the tensile strength of weld metal at elevated temperatures with steel from AISC (2005) and Eurocode (1995)
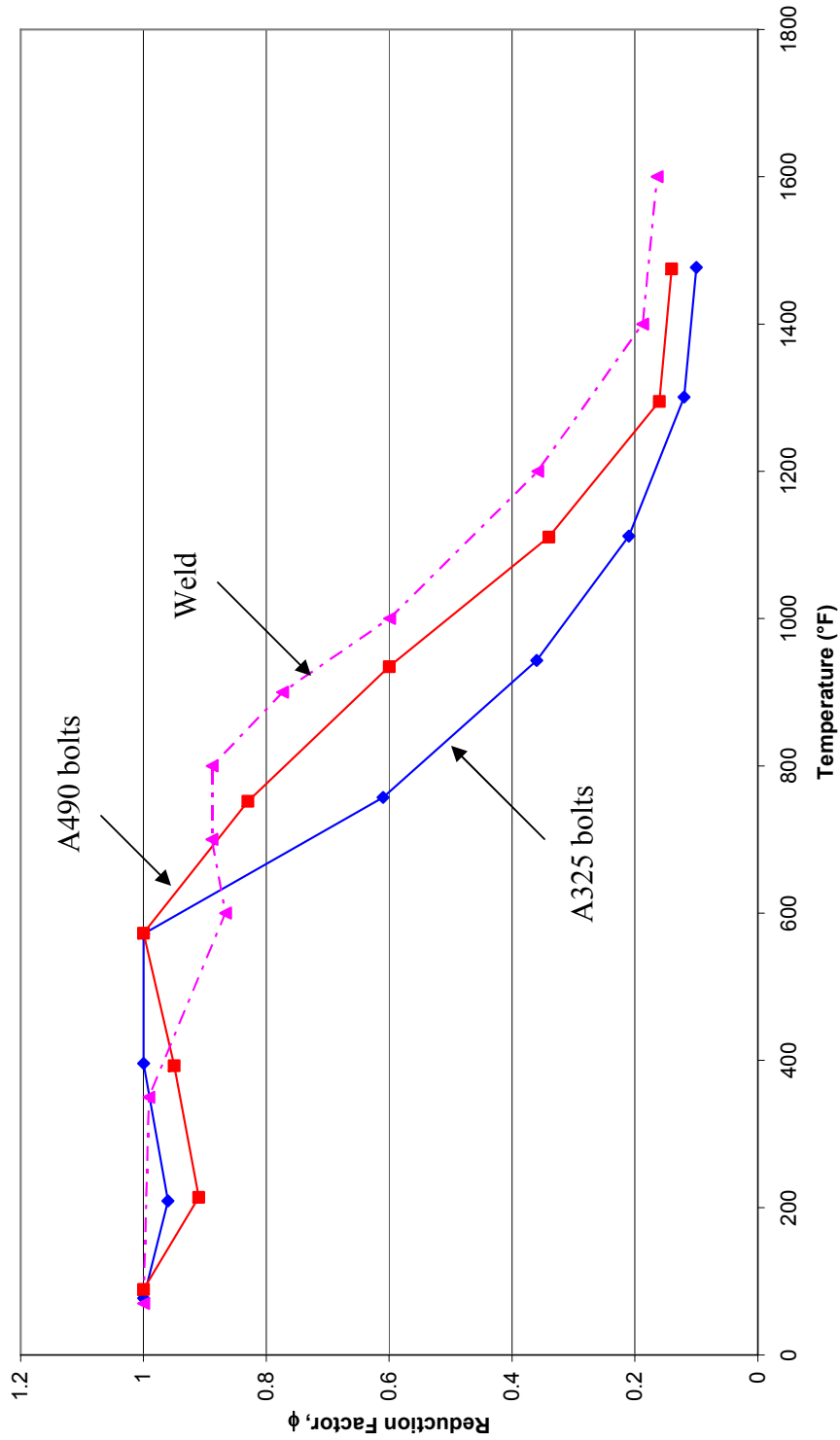
Figure 5.17  Comparison of the reduction factors of the strength of weld metal with bolts from research done by Yu (2006)
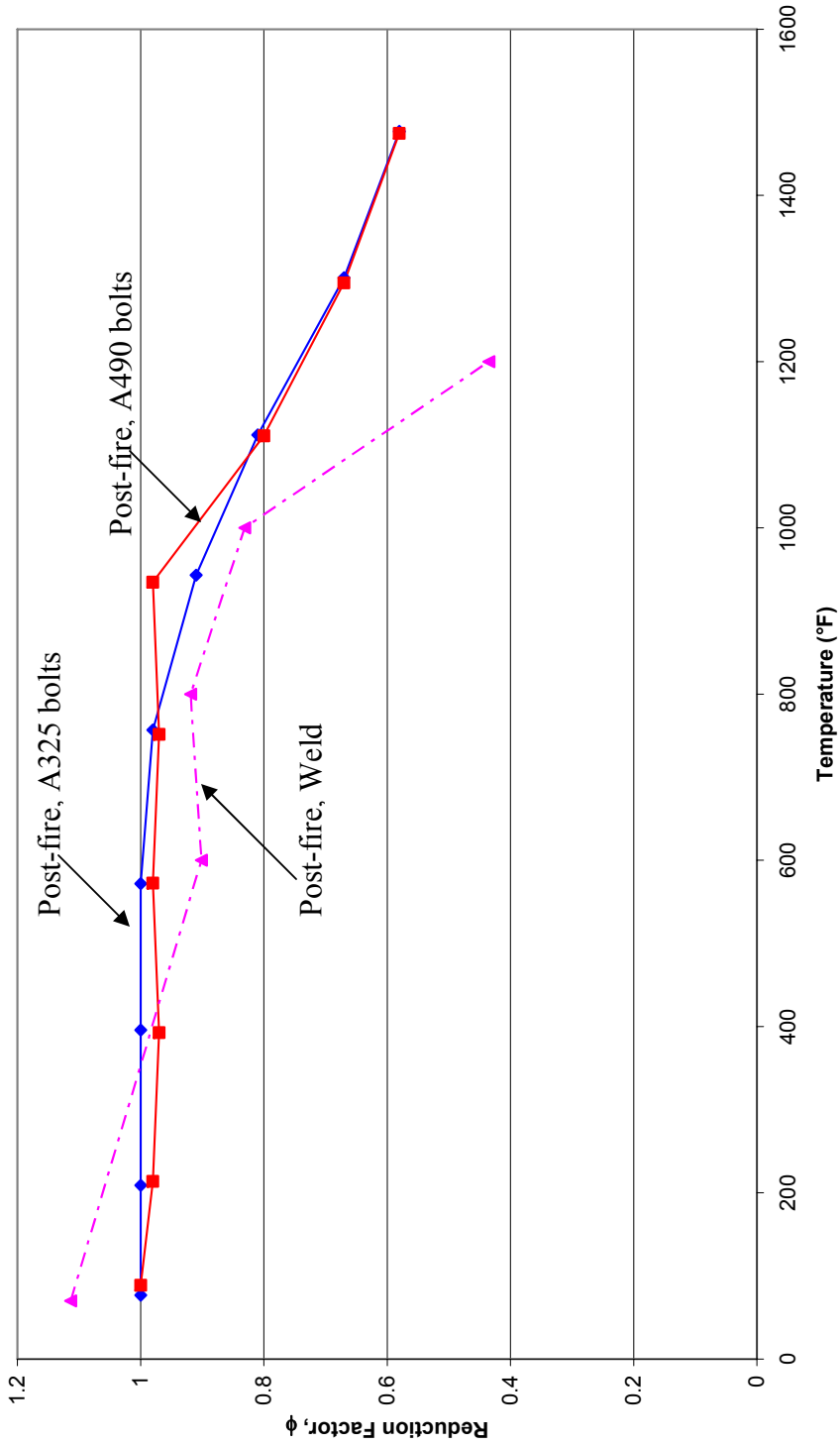
Figure 5.18  Comparison of the reduction factors of the post-fire strength of weld metal with bolts from research done by Yu (2006)

## Chapter 6    Summary, Conclusions, and Recommendations

**6.1    General**

In this chapter a summary of the testing is discussed. Conclusions are presented for the elevated temperature and post-fire scenario tests. Recommendations are made for future research.

**6.2    Summary**

The objectives of this research were to: 1) determine the effect of elevated temperature and post-fire conditions on the strength of transversely loaded fillet welds; and, 2) to develop design recommendations for transversely loaded fillet welds under elevated temperature and elevated temperature-cooling conditions. A review of past research was presented that included studies on steel connections and the behavior of structural systems at elevated temperatures and in post-fire conditions, design criteria from AISC (2005) and Eurocode (1995) for the effect of elevated temperature on the material properties of steel, heat treatment processes, past research on welded connections, and AISC design criteria for transverse welds.

This study consisted of elevated temperature tests and post-fire scenario tests. The test specimens consisted of two pull plates that were welded together by overlapping lap plates fillet welded to the pull plates. At the end of each lap plate a 1.5-inch long transverse fillet weld was placed. These welds were the focus of the study. The base metal used for the lap and pull plates was A588 steel. The transverse welds on the test specimens were performed using the flux core arc welding (FCAW) procedure, which is a field welding process. Type E71-T8 electrode was used, which is commonly used with the FCAW process. Field welding is commonly performed for a shear tab to column connection.

Each specimen was loaded in tension in a SATEC universal testing machine until failure. The elevated temperature tests were performed by heating the test specimen in an electric furnace to the specified test temperature, holding the test temperature for 40 minutes, and applying monotonically increasing tension load until failure. Ten elevated temperature tests were performed at specified test temperatures, including a test at an ambient temperature of 72°F. The post-fire scenario tests were performed by heating the test specimen to 1600°F, allowing the specimen to cool inside the furnace to a specified test temperature, and then applying monotonically increasing tension load to the specimen until failure. Five post-fire scenario tests were performed at specified test temperatures.

For each specimen the time-temperature curves obtained from a CR5000 data acquisition system and load-displacements response obtained from the SATEC testing machine were presented for the elevated temperature and post-fire scenario tests. Observations were made about the temperature data that included discussion about the heating rate, the actual average test temperature, and the temperature above and below the cooling plates. The actual average test temperature was obtained by averaging the test temperature over

the 40 minute time period that the temperature was held at. The stiffness of each specimen at the test temperature was obtained from the slope of the load-displacement response. The angle of the fracture surface of the transverse weld was measured. This was done by taking a photograph of the top lap plate of the specimen after fracture had occurred and the specimen was removed from the furnace. The angle was measured from the photograph using a protractor.

Reduction factors were developed for the strength of the weld metal and the stiffness of the specimen of the elevated temperature tests and post-fire scenario tests. The reduction factors for strength as a function of temperature were developed by determining the tensile strength of the specimen from the data at a selected test temperature and dividing it by the tensile strength at the ambient temperature. The reduction factor for stiffness was developed by dividing the stiffness of the specimen from the slope of the load-displacement response at a selected test temperature by the stiffness of the specimen at the ambient temperature. The reduction factors for strength of the weld metal were compared to the reduction factors of steel per AISC (2005) and Eurocode (1995). The reduction factors for strength of the weld were also compared to the reduction factor for bolts developed in past research.

## 6.3    Conclusions
Conclusions from the elevated temperature tests and the post-fire scenario tests from this research are presented below.

### 6.3.1    Elevated Temperature Tests
(1) The strength of weld metal decreases with increasing temperature. Weld metal begins to develop a significant reduction in strength at the temperature of 800°F.
(2) The stiffness of the specimen decreases with increasing temperature. The load-displacement response becomes flatter near the peak load as the temperature increases, resulting in a more ductile response and a lower stiffness for specimens tested at higher temperatures. The specimen experienced a significant reduction in stiffness at 1000°F.
(3) The fracture angle of the weld was measured and it appears that there is not a well defined trend. The average angle appears to begin to decrease at 1400°F, while at temperatures below 1400°F the angle stays within 15% of the fracture angle of 45° at ambient temperature.
(4) The strength of the weld metal was compared to that of steel per AISC (2005) and Eurocode (1995) at elevated temperatures. Similar to steel, the weld metal begins to develop a significant reduction in strength at the temperature of 800°F. In the temperature range below 800°F, the strength reduction of the weld metal is greater than that of the steel. Between 800°F and 1400°F, the strength reduction factor of the weld metal and the steel are similar. Above 1400°F, the strength reduction of the steel is greater than that of the weld metal.
(5)  The strength of the weld metal was compared to that of bolts from previous research. Between 400°F and 700°F, the strength reduction of the weld metal is

greater than that of the bolts. Between 700°F and 1400°F, the strength reduction of the bolts is greater than that of the welds, with the strength reduction of the A325 bolts greater than that of the A490 bolts. When the temperature is greater than 1400°F, the strength reduction of the bolts remains greater than that of the welds; however at this temperature, they all begin to level off.

### 6.3.2  Post-Fire Scenario Tests

(1) Similar to the elevated temperature tests, the strength of the weld metal during post-fire conditions decreased with increasing temperature. However, the strength of the weld metal was greater during post-fire conditions than the strength found during the elevated temperature tests. At temperatures above 800°F, the specimens tested during the post-fire scenario tests had a smaller reduction in strength than those tested during the elevated temperature tests. At ambient temperature, there was an increase in strength due to the effect of annealing from the heat treatment process.

(2) Similar to the elevated temperature tests, the stiffness of the specimen decreased during post-fire conditions with increasing temperature. The load-displacement response becomes flatter near the peak load as temperature increases, resulting in a lower stiffness as temperature increases. The specimen experienced a significant reduction in stiffness at 1000°F. The load-displacement response was more ductile than that of the specimens from the elevated temperature tests, resulting in a more gradual reduction of the stiffness during post-fire scenario tests.

(3)  The fracture angle of the weld was measured and found to be greater than 45° for all specimens tested between 600°F and 1000°F. At 1200°F the fracture angle of the weld decreases to below 45°. Similar to the elevated temperature tests, there is not a well defined trend for the fracture angle of the weld with increasing temperature.

(4) The strength of the weld metal was compared to that of bolts from previous research under post-fire conditions. With the exception of the post-fire scenario test performed at ambient temperature, the strength reduction of the weld metal is greater than that of the A490 and A325 bolts at all test temperatures. At 1000°F the strength of the weld metal was found to be significantly reduced.

### 6.4  Recommendations

The following recommendations are made for future research:

(1) This research was conducted on transverse fillet welds, oriented 90° to the application of loading. As previously discussed, as a structure is exposed to fire, compressive axial forces develop, followed by tensile axial forces upon cooling to ambient temperature. During heating and cooling, a shear force due to the transverse gravity loading is also present. The resultant of the shear and axial forces is acting at an angle to the weld. Therefore, it would be beneficial to conduct tests at various temperatures with the weld located at selected angles to the direction of loading.

200

(2) Welded connections may be designed with both transverse and longitudinal fillet welds. Tests at elevated temperatures and post-fire conditions should be performed on welded connections that have a combination of longitudinal and transverse fillet welds.

(3) It would be beneficial to research different types of welds, such as groove welds, partial joint penetration welds, and complete joint penetration welds. It would also be beneficial to perform tests on connections fabricated from various types of weld metals. A different weld process, such as a process typical in shop welding should be included in the study.

(4) Further testing should be done on different types of welded connections in addition to the welded lap slice connections that were tested in this research. During the post-fire scenario tests, it would be beneficial to provide restraint to the specimen to evaluate the resistance that would be provided by a welded connection.

(5) Post-fire scenario tests should be performed at lower temperatures and near ambient temperature to populate the data base in the lower temperature region.

# References

AISC (2005), *Manual of Steel Construction, Thirteenth Edition*, American Institute of Steel Construction, Chicago, IL

ASM (2002), *Volume 4: Heat Treating*, American Society for Materials, Materials Park, OH

ASTM E 119 (2005), *Standard Test Methods for Fire Tests of Building Construction and Materials*, American Society for Testing Materials, West Conshohocken, PA

ASTM E 8 (2004), *Standard Test Methods for Tension Testing of Metallic Materials*, American Society for Testing Materials, West Conshohocken, PA

ASTM (2008), *Annual Book of ASTM Standards: Section 1Iron and Steel Products*, American Society for Testing Materials, West Conshohocken, PA

AWS (2002), *Structural Welding Code: Steel, Eighteenth Edition*, American Welding Society, Miami, FL

AWS (2005), *Specification for Low Alloy Steel Electrodes for Flux Core Arc Welding*, American Welding Society, A5.29, Miami, FL

BRE (2003), "Results and observations from full-scale fire test at BRE Cardington," Building Research Establishment, BRE Client report number 215-741, Garston, Watford, UK

British Steel (1982), "The performance of beam/column/beam connections in the BS476: art 8 fire test," *Reports T/RS/1380/33/82D and T/RS/1380/34/82D*, Swinden Labs, Moorgate, Rotherham, UK

British Steel (1998), "The Behaviour of a Multi-Storey Steel Framed Building Subjected to a Fire Attack: Experimental Data," Swinden Labs, Moorgate, Rotherham, UK

British Steel (2003), *Structural use of steelwork in building: Code of practice for fire resistant design*, *BS 5950-8:200*, Swinden Labs, Moorgate, Rotherham, UK

Brockenbrough, R.L. and Johnston, B.G. (1981), *Steel Design Manual*, United States Steel Corporation, Pittsburgh, PA

Bulter, L.J. and Kulak, G.L. (1971), "Strength of Fillet Welds as a Function of Direction of Load," *Welding Journal*, Welding Research Council, Vol. 35, No. 5, pp. 231s-234s

Catella, Nicholas (2008), "The Development of a Modular Furnace for Structural Fire Testing and a Study of a Steel Shear Tab Connection in Fire", M.S. Thesis, Department of Civil and Environmental Engineering, Lehigh University, Bethlehem, PA

EC3 (1995), *Eurocode 3: Design of Steel Structures*, ENV 1993-1-2: General Rules - Structural Fire Design, European Committee for Standardisation, Brussels

Fisher, J.W. (1995), "Behavior of Fasteners and Plates with Holes," Journal of the Structural Division, ASCE, Vol. 91, No. ST6

IBC (2003), *2003 International Building Code*, International Code Council, Washington, DC

Kato, B. and Morita, K. (1974), "Strength of Transverse Fillet Welded Joints," *Welding Journal*, Welding Research Supplement, pp. 59s-64s

Kruppa, J. (1979) "Resistance au feu des assemblages par boulons haute resistance", St. Remy-les-Chevreuse, Centre Technique Industriel de la Construction Metalique, France

Lawson, R.M. (1990), "Behaviour of steel beam-to-column connections in fire," *The Structural Engineer*, Vol. 68, No. 14, London, pp. 263-271

Liu, T.C.H., Fahad, M.K., Davies, J.M. (2002), "Experimental investigation of behaviour of axially restrained steel beams in fire," *Journal of Constructional Steel Research*, Vol. 58, pp. 1211-1230

Newman, G.M., Robinson, J.T., Bailey, C.G. (2000), *Fire Safe Design: A New Approach to Multi-Storey Steel-Framed Buildings (1st edition)*, The Steel Construction Institute, Berkshire, UK

Yu, Liang (2006), "Behavior of Bolted Connections During and After a Fire", Ph.D. Dissertation, Department of Civil and Environmental Engineering, University of Texas at Austin, Austin, TX